

Structural characterisation of biotin protein ligase and its interacting partners: A novel antibiotic

Min Yin Yap

PhD

2014

Copyright notice

Notice 1

Under the Copyright Act 1968, this thesis must be used only under the normal conditions of scholarly fair dealing.

In particular no results or conclusions should be extracted from it, nor should it be copied or closely paraphrased in whole or in part without the written consent of the author. Proper written acknowledgment should be made for any assistance obtained from this thesis.

Notice 2

I certify that I have made all reasonable efforts to secure copyright permissions for third-party content included in this thesis and have not knowingly added copyright content to my work without the owner's permission.

Index

Declaration	3
Acknowledgement.....	4
Summary.....	5
Chapter 1 Introduction to biotin protein ligase.....	6
1.1. Biotin and its role in metabolism	6
1.2. Biotin protein ligase: A multifunctional enzyme.....	7
1.3. Classification of BPLs	7
1.4. The structure of BPL	8
1.4.1. Catalytic domain	10
1.4.2. C-terminal cap domain	13
1.4.3. The N-terminal DNA-binding domain of class II BPLs	13
1.4.4. The N-terminal domain of class III eukaryotic BPLs	14
1.5. Biotinylation of BCCP by BPL	14
1.5.1. BCCP domain in biotin-dependent metabolic carboxylases	14
1.5.2. Structural cues to the biotinylation of BCCP	16
1.6. The transcriptional repression of biotin biosynthetic genes by Class II BPL	18
1.6.1. Class II BPLs form a homodimer to regulate biotin synthesis	19
1.7. Homodimerization of class I BPL	22
1.8. Human BPL	23
1.8.1. Three isoforms of HCS	23
1.8.2. Multiple carboxylase deficiency	24
1.8.3. Role of the N-terminal domain	27
1.9. Project aims	28
1.9.1. Structure-based drug design	28
1.9.2. Investigating the interaction between <i>Sa</i> BPL and the BioO operator	28
1.9.3. Structurally characterize HCS	28
Chapter 2 General materials and methods	30
2.1. Protein expression and purification	30
2.1.1. Protein expression and purification of <i>Sa</i> BPL.....	30
2.1.2. Production of Holo and Apo- <i>Sa</i> BPL	30
2.1.3. Determination of Apo or Holo- <i>Sa</i> BPL using BCCP	31
2.1.4. Protein expression of <i>Ac</i> BPL, <i>Kp</i> BPL and <i>Pc</i> BPL	31
2.2. Cloning of Met58-HCS and Cat-HCS	33
2.2.1. Expression.....	34
2.2.2. Purification of Met 58-HCS.....	34
2.2.3. Purification of Cat-HCS-GST.....	35
2.3. SaBCCP purification	35
2.4. SDS-gel electrophoresis	36
2.5. Western Blotting	36
2.5.1. Western transfer.....	36
2.5.2. Immunodetection	36
2.6. Analysis of DNA binding	37
2.6.1. Annealing double stranded DNA.....	37
2.6.2. DIG (Digoxigenin)-labelled DNA	37
2.6.3. EMSA	38
2.6.4. K_d determination	39
2.7. In vitro Biotinylation assay	39
2.8. Multi angle light scattering (MALS) and Dynamic light scattering (DLS).	40
2.9. Small angle X-ray scattering.....	41
2.10. X-ray crystallography	44

Chapter 3 Biotin analogues with antibacterial activity as potent inhibitors for biotin protein ligase	48
3.1. Contribution of publication:	49
Chapter 4 Selective inhibition of biotin protein ligase from <i>Staphylococcus aureus</i>....	50
4.1. Contribution of publication.....	50
Chapter 5 Characterising biotin protein ligases from ESKAPE pathogens	51
5.1. Introduction	51
5.2. Results	52
5.2.1. <i>Ac</i> BPL protein purification.....	52
5.2.2. <i>Kp</i> BPL purification.....	54
5.2.3. Expression and purification of <i>Pa</i> BPL	56
5.2.4. Oligomerisation states of <i>Kp</i> BPL and <i>Ac</i> BPL	58
5.2.5. Biotinylation kinetics.....	60
5.2.6. Crystallization studies.....	62
5.2.7. Modelling of <i>Ac</i> BPL and <i>Ph</i> BPL	65
Discussion	66
Chapter 6 Structural characterization of <i>Sa</i>BPL in complex with DNA	72
6.1. Contribution of publication.....	72
6.2. Results	73
6.2.1. DNA-binding studies	73
6.2.2. SAXS analysis of <i>Sa</i> BPL-bioO complex	75
6.2.3. Crystallization studies.....	78
6.3. Discussion.....	82
Chapter 7 Eukaryotic Biotin Protein Ligase.....	85
7.1. Introduction	85
7.2. Results	87
7.2.1. Purification of FL-HCS	87
7.2.2. Expression and purification of Met58-HCS	88
7.2.3. Expression and purification of CAT-GST	91
7.3. Discussion.....	93
Chapter 8 Final Discussion	96
References.....	103
Appendix I - Abbreviations	114
Appendix II - List of buffers and media	116
Appendix III - Publications	119

Monash University

Declaration for thesis based or partially based on conjointly published or unpublished work

General Declaration

In accordance with Monash University Doctorate Regulation 17 Doctor of Philosophy and Research Master's regulations the following declarations are made:

I hereby declare that this thesis contains no material which has been accepted for the award of any other degree or diploma at any university or equivalent institution and that, to the best of my knowledge and belief, this thesis contains no material previously published or written by another person, except where due reference is made in the text of the thesis.

This thesis includes **3** original papers published in peer-reviewed journals. The core theme of the thesis is **the characterization of prokaryotic and eukaryotic biotin protein ligase**. The ideas, development and writing up of all the papers in the thesis were the principal responsibility of myself, the candidate, working within the **Department of Biochemistry and Molecular Biology** under the supervision of **Prof. Matthew Wilce**

The inclusion of co-authors reflects the fact that the work came from active collaboration between researchers and acknowledges input into team-based research.

Thesis chapter	Publication title	Publication status
3	Selective inhibition of biotin protein ligase from <i>Staphylococcus aureus</i> .	Published
4	Biotin analogues with antibacterial activity are potent inhibitors of biotin protein ligase.	Published
6	Structural characterization of <i>Staphylococcus aureus</i> biotin protein ligase and interaction partners: an antibiotic target	Published

I have not renumbered sections of submitted or published papers in order to generate a consistent presentation within the thesis.

Signed:

Date:

Acknowledgments

First and foremost I'd like to thank Prof. Matthew Wilce for his supervision of my PhD project, and for proof reading the manuscript. I am especially grateful for his crash courses in crystallography and SAXS, and his patience and humor in dealing with me on a regular basis over the past 4.5 years.

I would also like to thank our collaborators at the University of Adelaide: Dr. Steven Polyak, Dr. Tatiana Soares Da Costa for performing SPR, antimicrobial assays, and AUC on SaBPL; Dr. William Tieu and Prof. Andrew Abell for designing the inhibitors used for crystallographic experiments; Prof. Grant Booker for hosting me for two weeks in his lab whilst I performed biotinylation kinetic experiments. The kind advice and help provided by my collaborators has been extremely useful and much appreciated. I am especially grateful to Dr. Steven Polyak, for his patience in answering a constant barrage of questions and providing plasmids and proteins when required during the course of my PhD.

For the strenuous task of proof reading various parts of my thesis: thanks goes to Dr. Steven Polyak and Assoc. Prof. Jackie Wilce.

I'd like to thank past and present members of the Wilce Lab for making it a happy and interesting place to learn, and for putting up with my moments of randomness. Special thanks goes to Dr. Daouda Traore for his lessons in crystallography, Dr. Simone Beckham and Dr. Andrew Sivakumaran for their help in cloning, Dr. Nicole Pardini for her advice on the BPL project, and Gabrielle Watson for providing endless entertainment (but mainly because she asked to be put on the list).

Lastly I'd like to thank my family for being sensible and pulling me back to earth whenever I needed it; The Lius, for being my family away from home and feeding me on a regular basis; to my favourite flogs Steph and Gordie, for making the past 6 years better than it would have been; and Pei, Jess, Bixia, KCP, Sherlyn and HT, just for being there.

Summary

Biotin protein ligase (BPL) is an enzyme found in all organisms, and is required for the attachment of biotin to a specific lysine residue located on the biotin carboxyl carrier protein (BCCP) domain of biotin-dependent metabolic carboxylases which are involved in a variety of metabolic processes which include lipogenesis, amino acid catabolism and gluconeogenesis.

BPL can be divided into three main classes: the first 2 classes consist of BPLs found in bacteria, class I bacterial BPLs consist of a C-terminal cap domain and catalytic domain, but not a DNA-binding domain, whilst class II bacterial BPLs have an extra N-terminal DNA-binding domain which is used to repress the transcription of biotin biosynthetic genes. Eukaryotic BPLs fall into class III, and whilst their C-terminal cap domain and catalytic domain have sequence similarity to their bacterial counterparts, they also contain a N-terminal domain which does not bind to DNA, and to date its function and structure is still under investigation.

Bacterial BPL is a novel target as an antibacterial, due to it being essential for bacterial cell survival. Chapters 3 and 4 of this thesis consist of two published journal articles, and focus on the design of antibacterials that specifically target the BPL from *S. aureus* (SaBPL), a pathogen which is one of the main causes of mortality in hospitals and in the community, and has rapidly gained resistance to many modern antibiotics. In chapter 5, the expression, purification and preliminary characterization of *K. pneumoniae* and *A. calcoaceticus* BPL was performed, as an initial step for future drug design studies.

Class II BPLs have to regulate two vastly different roles, the biotinylation of biotin-dependent enzymes, as well as binding to the *bioO* operator to repress biotin synthesis. The work in chapter 6 uses a combination of X-ray crystallography and small angle X-ray scattering (SAXS) to provide structural information of how the class II BPL, SaBPL binds to its binding partners, BCCP and *bioO*. This chapter includes a recently published paper as well as further experiments done to obtain a protein crystals of the SaBPL:*bioO* complex.

As the structure of eukaryotic BPLs have not yet been determined, the final chapter of this thesis focuses on the expression and purification of the human BPL, holocarboxylase synthetase (HCS) for use in future structural studies. Structural information not only provides information into the function of HCS, but would also aid in our drug design studies as outlined in chapters 3 to 5.

Introduction to biotin protein ligase

1.1. Biotin and its role in metabolism

In 1901, a growth factor that was required by several yeast strains was discovered by E. Wildiers who called it bioS (Wildiers, 1901). Later, “protective factor X” or vitamin H was found to cure dermatitis and hair loss in rats fed with high doses of egg white (Boas, 1927, du Vigneaud et al., 1940). In 1933, Allison *et al* isolated a respiratory coenzyme in *Rhizobium* and termed it coenzyme R (Allison and Minor, 1938). However, it was 5 years after Kögl and Tönnis extracted biotin from dried egg yolk that researchers came to the conclusion that bioS, protective factor X, coenzyme R, and biotin were one and the same (du Vigneaud et al., 1940, Gyorgy et al., 1940, Kogl and Tönnis, 1936). In 1940, Du Vigneaud and colleagues had determined the structure of biotin and found that biotin is comprised of a fused ureido and tetrahydrothiophene ring attached to a valeric acid tail (du Vigneaud et al., 1942, Chakravartty and Cronan, 2012) (**Figure 1.1**).

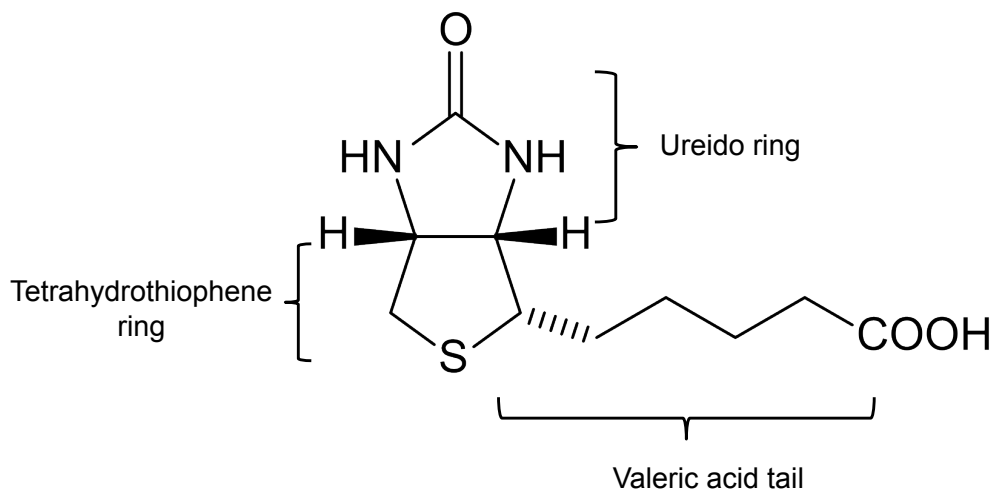


Figure 1.1 Structure of biotin. Biotin is made up of a fused ureido and tetrahydrothiophene ring connected to a valeric acid side chain.

Biotin's role in metabolism was established when it was found to be required as a cofactor in biotin-dependent carboxylases (Lynen et al., 1961). Biotin protein ligase (BPL, also known as holocarboxylase synthetase in humans) covalently ligates biotin onto biotin-dependent metabolic carboxylases, where it acts as a mobile carboxyl carrier to transfer carbon dioxide from bicarbonate to organic acid metabolites. As the biotin-dependent carboxylases are turned over, biotinidase aids in breaking the covalent bond between biotin and the carboxylase and recycles biotin for further use (DeTitta et al., 1976). In the 70s, it was discovered that a lack of biotin was potentially linked to multiple carboxylase deficiencies

(James and Cronan, 2004), and in the 80s, the cause of multiple carboxylase deficiency was noted to be due to mutations located in the enzymes holocarboxylase synthetase and biotinidase (Wolf et al., 1983, Burri et al., 1985).

1.2. Biotin protein ligase: A multifunctional enzyme

Biotin protein ligase (BPL) is the enzyme responsible for facilitating biotin's role in metabolism by attaching it to the **biotin carboxyl carrier protein (BCCP)** domain of biotin-dependent metabolic carboxylases. BPL is found in all organisms, and the biotinylation of BCCP is a highly conserved reaction throughout, as has been shown through studies where BPLs and BCCPs from divergent species such as bacteria and humans cross-react with each other (Cronan, 1990, McAllister and Coon, 1966, Samols et al., 1988, Tissot et al., 1998). The biotinylation reaction occurs in a highly conserved two-step process (**Figure 1.2**). In the first step, biotin and ATP bind within their respective binding sites of BPL to form the reaction intermediate biotinyl-5'-AMP (Btyl). After Btyl formation has occurred, biotin is transferred onto the ϵ -amino group of a specific lysine located in the target BCCP (Lane et al., 1964). The biotinylation reaction is similar to that involving amino acyl-tRNA synthetases and lipoyl ligases where the formation of an adenylate intermediate is required for the enzymatic reaction to occur (Artymiuk et al., 1994, Reche, 2000).

1. $\text{ATP} + \text{Biotin} \rightarrow \text{Biotinyl-5'-AMP} + \text{PPi}$
2. $\text{Biotinyl-5'-AMP} + \text{Apo-BCCP} \rightarrow \text{Holo-BCCP} + \text{AMP}$

Figure 1.2 The two-step biotinylation reaction. In the first step, biotin and ATP bind within the catalytic active site and form biotinyl-5'-AMP and the release of phosphate. Apo-BCCP then comes into contact with BPL, where biotinyl-5'-AMP is hydrolysed, and biotin is covalently bound onto BCCP together with the release of AMP.

In addition to its role in transferring biotin onto BCCP, some bacterial BPLs have also evolved an additional function in the transcriptional regulation of biotin synthesis (Rodionov et al., 2002). This function is dependent on the concentration of biotin and BCCP within the cell, and will be discussed in further detail below.

1.3. Classification of BPLs

BPLs can be divided into 3 distinct classes (**Figure 1.3**). The BPLs from prokaryotes belong to either class I or class II, whilst eukaryotic BPLs fall into class III. All BPLs contain a C-terminal cap domain and a catalytic domain, and BPLs that consist of only these two

domains are classified as class I BPLs. Class II BPLs play a role in the regulation of biotin synthesis, and form a homodimer that can bind to DNA via a DNA-binding domain located on the N-terminus. Class III eukaryotic BPLs have a large N-terminal domain that differs from the DNA-binding domain of class II enzymes, and to date has no known structure or function. Our knowledge of the mechanism and structure of BPLs has been provided mainly through mutational and structural studies done on class I and class II BPLs due to the relative ease of expression and purification, with the *E. coli* BPL, BirA, being the best-characterized enzyme.

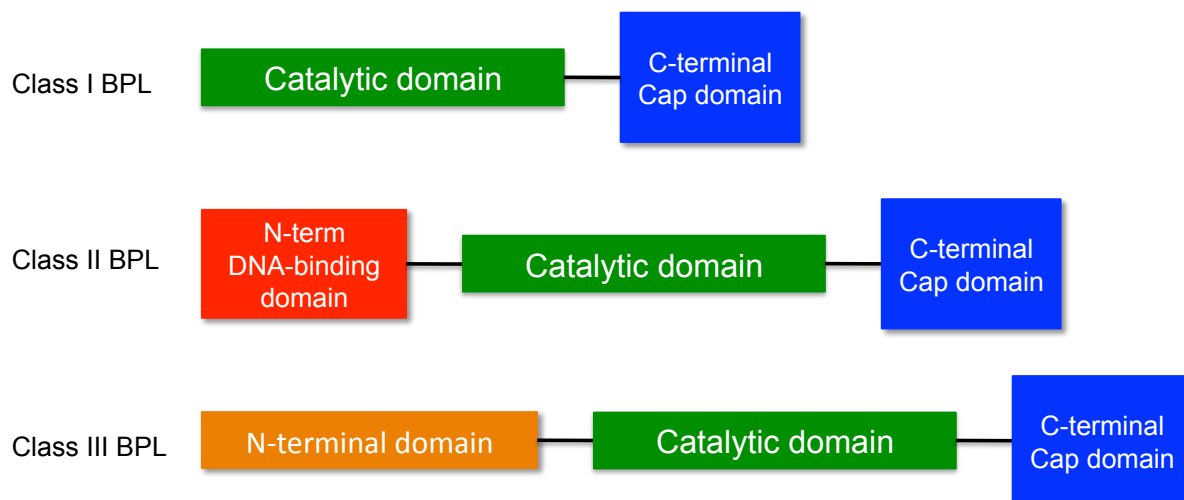
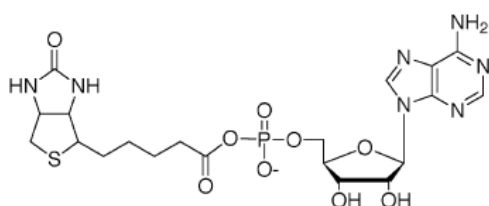


Figure 1.3 The three classes of BPL. All BPLs consist of a catalytic domain and a cap domain. Class II BPLs have an N-terminal DNA-binding domain, whilst the N-terminal domain of class III BPLs have an undetermined function.

1.4. The structure of BPL

Biotinyl-5'-AMP



Biotinol-5'-AMP

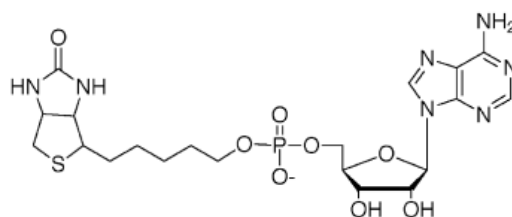


Figure 1.4 The structure of biotinyl-5'-AMP (Btyl) and biotinol-5'-AMP (BtOH). Btyl is formed within the active site of BPL upon biotin and ATP binding. Its non-hydrolysable analogue BtOH has been a useful tool in structural, thermodynamic and functional studies.

The crystal structure of the non-ligand bound apo form of BirA was first determined in 1992 (Wilson et al., 1992), while the holo form in complex with biotin and the non-hydrolysable Btyl analog, biotinol-5'-AMP (BtOH) was determined a few years later (**Figure 1.5**), and provided further structural information on class II BPLs (Wood et al., 2006, Weaver et al., 2001b). Like Btyl, BtOH (**Figure 1.4**) can bind tightly to BirA but is unable to biotinylate

BCCP (Brown et al., 2004), and hence provides a useful tool in structural, thermodynamic and functional studies. Since then, the crystal structures of both the ligand bound and non-ligand bound forms of class I BPLs from *Aquifex aeolicus*, *Mycobacterium tuberculosis*, *Pyrococcus horikoshii* have been reported (Tron et al., 2009, Bagautdinov et al., 2005b, Purushothaman et al., 2008).

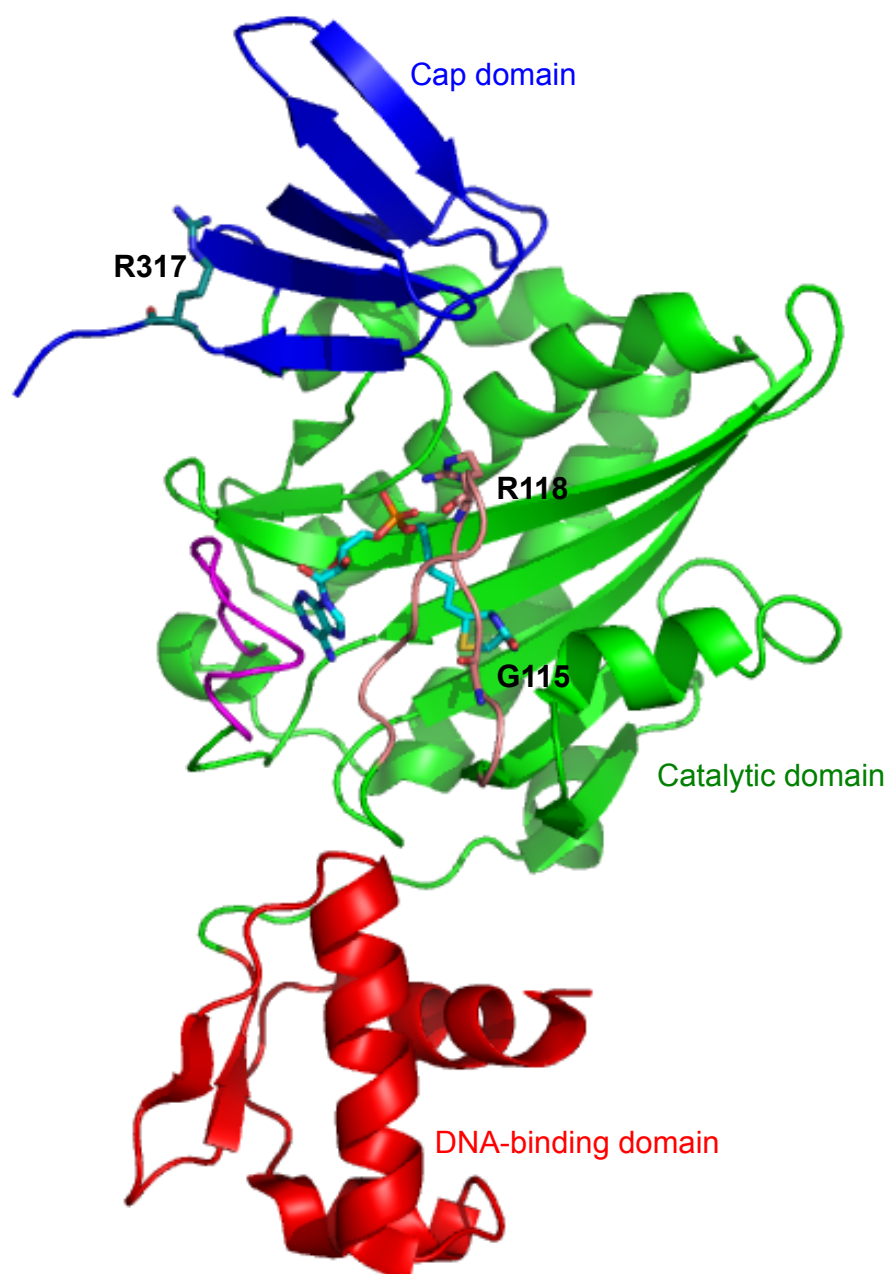


Figure 1.5 Structure of a Class II BPL, BirA (PDB:2EWN). Apart from a cap (blue) and catalytic domain (green), class II BPLs also contain an N-terminal DNA-binding domain (red). ABL and BBL (magenta and orange respectively) aid in ligand binding. Mutational studies have showed that R317 in BirA is involved in ATP-binding despite a lack of contact with the ligand binding site. R118 and G115 are strictly conserved residues located on the BBL of BPLs, and are important for ligand binding and biotinyl-5'-AMP formation.

1.4.1. Catalytic domain

The C-terminal cap and catalytic domains of BPLs across organisms are highly conserved, and show between 20 – 25 % sequence similarity. Based on mutational studies done mainly on BirA, conserved sequences located in the catalytic domain of BPLs are known to be involved in biotin and ATP binding, formation of Btyl, binding to BCCP or, in the case of class II BPLs, homodimer formation (Kwon and Beckett, 2000, Polyak et al., 2001, Xu and Beckett, 1994, Choi-Rhee et al., 2004, Bagautdinov et al., 2008, Tron et al., 2009, Naganathan and Beckett, 2007). Known crystal structures of the catalytic domain of different BPLs show high structural similarity: a mixed β -sheet packed between several α -helices, as well as several surface loops (Bagautdinov et al., 2005b, Tron et al., 2009, Wilson et al., 1992) (**Figure 1.5**). The main difference between the structures of class I and class II BPLs are the mobility of several surface loops: In apo BirA, four of the five surface loops are disordered, whilst in the case of apo *Pyrococcus horikoshii* BPL (*PhBPL*) and *AaBPL* however, only one of the five surface loops is disordered (**Figure 1.6**). In chemical protection studies done on BirA, the 5 surface loops were protected from cleavage in the presence of Btyl, showing that they underwent a disorder-to-order transition upon ligand binding to the active site (Streaker and Beckett, 1999).

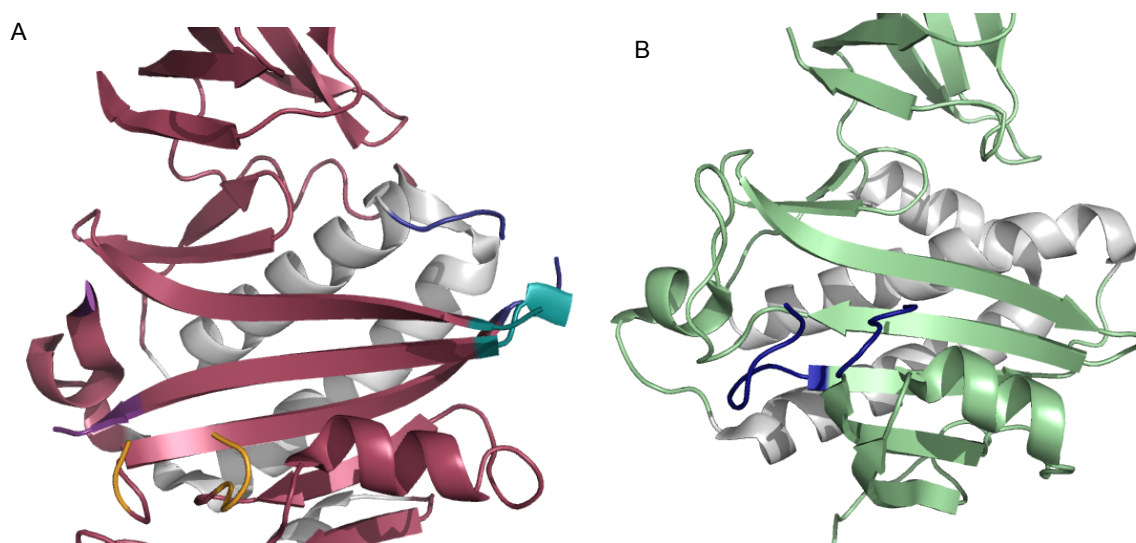


Figure 1.6 The surface loops of class I and class II BPLs. There are four disordered surface loops (highlighted in different colors) in the catalytic domain of (A) apo-BirA (PDB : 1BiA), whilst only the biotin-binding loop in (B) apo-*PhBPL* (PDB : 1WQ7) is disordered.

The catalytic domain of BPL contains the active site in which biotin and ATP bind to form the substrate Btyl. The biotin-binding site of BPL is located on the surface of the mixed β -sheet in the catalytic domain. It is a large pocket made out of a hydrophobic wall and a glycine rich hydrophilic bottom. The carboxyl group of biotin and its ureido nitrogens bind to the bottom via hydrogen bonding, whilst the hydrophobic carbon tail and thiophene ring interact with the

wall (Volkov and Svergun, 2003, Bagautdinov et al., 2005a). Glycine residues found on the hydrophilic bottom are important for accommodating the ureido and thiophene side chains of biotin. Upon biotin binding within this active site, the disordered biotin binding loop (BBL) folds over biotin to form a lid and becomes ordered. It contributes 2 additional hydrogen bonds through an arginine residue found on the BBL to which the ureido ring binds to, and further stabilizes the biotin within the biotin-binding pocket (**Figure 1.7**) (Tron et al., 2009, Wood et al., 2006). Mutations that affect the stability of BBL also reduce the rate of Btyl synthesis (Kwon and Beckett, 2000).

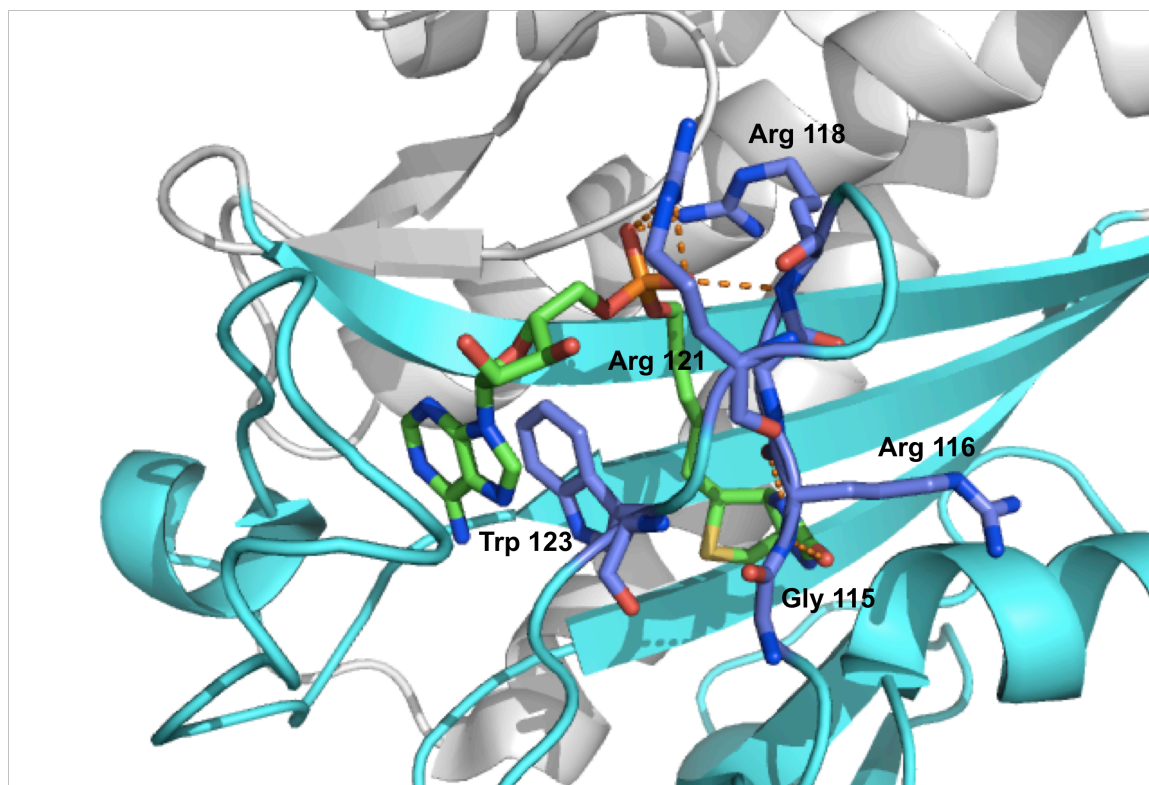


Figure 1.7 Crystal structure of BirA in complex with biotinol-5'-AMP. BirA BBL residues that form hydrogen bonds with the biotin component aid in stabilizing biotin within the biotin-binding pocket and are shown as purple sticks. The adenylate is stabilized in the adenylate-binding pocket by valine residues which fold over the adenylate (not shown), and tryptophan 123 that forms π - π interactions with the adenylate.

The apo form of BirA also contains a disordered adenylate-binding loop (ABL). After biotin binding, an ATP-binding site is created which allows ATP to bind followed by Btyl formation and the ABL undergoes a disordered-to-ordered transition. Residues on the BirA ABL do not interact directly with the adenylate; however, several valines fold over the adenylate base of Btyl, which is further buttressed by a tryptophan which forms π - π interactions with adenine (**Figure 1.7**) (Naganathan and Beckett, 2007). The BPLs of *A. aeolicus* and *P. horikoshii* have a somewhat ordered ABL, and unlike BirA in which biotin and ATP binding is an ordered process, AaBPL binds to biotin and ATP in a random manner, however, binding of

one substrate to AaBPL greatly increases the binding of the other (Tron et al., 2009, Bagautdinov et al., 2005a).

There are three very short segments which are highly conserved among bacterial BPLs, one of these being the “GRGRXX” sequence located on the BBL (**Figure 1.8**). Based on kinetic and thermodynamic studies done on several BirA mutants, the ₁₁₅GRGRXX₁₂₀ motif is essential for both biotin and Btyl binding, but is not essential for the binding of ATP (Barker and Campbell, 1981b, Wilson et al., 2011, Kwon and Beckett, 2000). Despite being conserved, this same motif in the class I BPLs *PhBPL* (₄₅GRGRXX₅₀) and AaBPL (₃₇GRGRXX₄₂) is not only important for biotin and Btyl binding, but also with ATP (Bagautdinov et al., 2005a, Tron et al., 2009). This difference in binding mechanisms between bacterial BPLs may be due to the fact that class II BPLs have to control two different roles and hence need tighter regulation of ligand binding compared to class I BPLs. After both biotin and ATP bind within the active site, the formation of Btyl occurs, and BPL must then form a complex with its target BCCP in order for successful biotinylation to occur. Mutational studies done on residues located in the BBL of BirA (G115 and R118) also showed that despite reduced biotin and Btyl binding, the ability to catalyse the biotinylation of BCCP was not affected (Kwon and Beckett, 2000, Weaver et al., 2001a). It was also shown that the R118G mutant was also promiscuous: not only was it able to biotinylate BCCP, it could also self-biotinylate, as well as biotinylate non-specific substrates such as bovine serum albumin and RNase A in a proximity dependent manner (Cronan, 2005, Choi-Rhee et al., 2004).

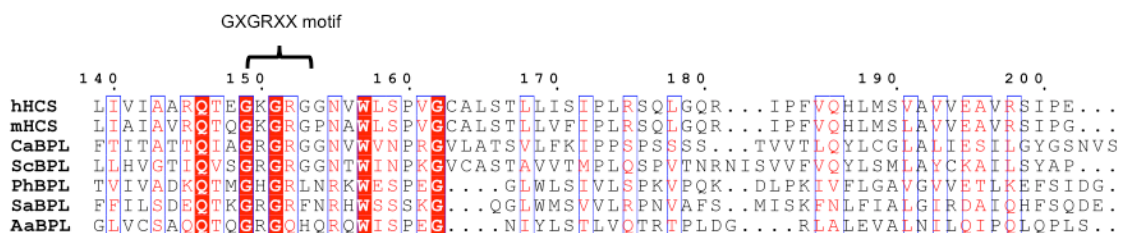


Figure 1.8 Sequence alignment of BPLs from different organisms show that there is a conserved GXGRXX motif located in the catalytic domain of BPLs, which is important for ligand binding. hHCS: human BPL, mHCS: mouse BPL, ScBPL: *Saccharomyces cerevisiae* BPL, CaBPL: *Candida albicans* BPL, SaBPL: *S. aureus* BPL, PhBPL: *Pyrococcus horikoshii* BPL, AaBPL: *Aquifex aeolicus* BPL. Numbers above sequence indicate SaBPL residue number. Red boxes are strictly conserved sequences, whilst white boxes are semi-conserved sequences. Sequence alignment constructed with CLUSTALW (www.ebi.ac.uk/Tools/msa/clustalw2/) and formatted with ESPrInt (esprint.ibcp.fr/).

The catalytic domain of BPLs also contains residues required for forming a heterodimer with the target protein BCCP, and in the case of class II BPLs, for forming a homodimer in order to regulate the transcription of biotin biosynthetic genes. The formation of these dimers is discussed in further detail below (**SECTION 1.6 and 1.7**).

1.4.2. C-terminal cap domain

The cap domains of BPLs of known structures are formed by 5 – 6 strands of mixed β -sheets and structurally resemble SH3 domains (Noble et al., 1993, Tron et al., 2009, Wilson et al., 1992) (**Figure 1.5**). SH3 domains are small β -modules containing a peptide-binding site composed of a non-polar patch surrounded by RT-Src and n-Src loops (Noble et al., 1993, Boucher et al., 2009), which is common in proteins involved in signaling.

Genetic screens have been unable to isolate mutants in the C-terminal region, and a C-terminal truncated BirA was insoluble and lack activity, which indicates that the C-terminal domain is required for bacterial cell survival (Wood et al., 2006, Chapman-Smith et al., 2001). Structural studies done on *PhBPL* show that the C-terminal domain undergoes large structural changes when ligands are bound in the active site (Bagautdinov et al., 2008). A point mutation of residue R317 located in the C-terminal domain of BirA showed a decrease in ATP-binding despite not forming any contacts with residues located in the catalytic active site (Chapman-Smith et al., 2001), whilst Tron *et al.* reported that long range hydrogen bonds are formed between the oxygen atoms of the ATP γ -phosphate bound within the ATP-binding site and residues Ser 229, Leu 230 and Arg 231 located on the C-terminal domain of *Aquifex aeolicus* BPL (*AaBPL*) (Tron et al., 2009). These results and other mutational studies done on BirA suggest that its C-terminal domain may function to correctly align BCCP within the active site of BPL, and aid in binding to ATP and biotin (Weaver et al., 2001a, Chapman-Smith et al., 2001).

1.4.3. The N-terminal DNA-binding domain of class II BPLs

Apart from the C-terminal and catalytic domain, class II BPLs have an extra N-terminal domain, which has a winged helix-turn-helix (wHTH) motif associated with DNA-binding (**Figure 1.5**) (Wilson et al., 1992). The X-ray crystal structures of BirA suggest there is little interaction between the DNA-binding and the catalytic domains but despite this lack of interaction, an N-terminal truncated mutant BirA was found to have decreased affinity for biotin and Btyl, even though its ability to synthesise the reaction intermediate Btyl and transfer biotin onto BCCP was not compromised (Franke and Svergun, 2009). This same mutant also showed that the N-terminal domain is crucial for the kinetic stability of the BirA-Btyl complex (Franke and Svergun, 2009). The orientation of the DNA-binding domain of BirA relative to the catalytic domain differs as much as 19° between the apo-BirA, biotin-BirA and BtOH-BirA, suggesting that the DNA-binding domain is relatively mobile compared to the rest of the protein (Wood et al., 2006), and may interact with the other domains upon substrate binding.

1.4.4. The N-terminal domain of class III eukaryotic BPLs

The cap and catalytic domain of class III BPLs has high sequence similarity compared to the class I and class II enzymes. However, class III BPLs also contain a large N-terminal domain that does not resemble the DNA-binding domain of class II BPLs. To date, studies have been done on the BPLs of humans, *S. cerevisiae* and *C. albicans* (Pendini et al., 2008a, Polyak et al., 1999, Whitten and Trehwella, 2009). Removal of the N-terminus results in enzymes that have reduced activity, and NMR studies done on the human BPL have showed that the N-terminus is required for associating with the BCCP domain (Polyak et al., 1999, Whitten and Trehwella, 2009). Further discussion of this N-terminal domain is presented in **section 1.8** of this chapter.

1.5. Biotinylation of BCCP by BPL

BPL facilitates biotin's role in metabolism by ligating biotin onto the biotin carboxyl carrier protein (BCCP) domain of biotin-dependent metabolic carboxylases. The biotin-dependent enzymes play key roles in important metabolic pathways such as fatty acid synthesis, gluconeogenesis, and amino acid catabolism (Wolf and Feldman, 1982, Wolf, 1995). The number of different biotin-dependent carboxylases found in organisms can range from a single acetyl CoA carboxylase in *E. coli*, to up to five enzymes in humans.

1.5.1. BCCP domain in biotin-dependent metabolic carboxylases

Biotin-dependent metabolic carboxylases all employ a conserved reaction mechanism to perform the carboxylation of organic substrates using three different domains. Biotin is first covalently attached through its carboxyl group onto the BCCP domain (Lane et al., 1964) (**Figure 1.9B**). By binding to the BCCP through its valeric acid tail, the bicyclic ring of biotin protrudes out from BCCP where it is necessary to bind and transfer biotin. The BCCP itself resides on a "swinging arm" that allows this domain to oscillate between two partial reaction sites. The biotin carboxylase domain is first required for the carboxylation of biotin via an ATP-dependent reaction. N1-carboxybiotin subsequently moves across to the carboxyl transferase domain where CO₂ is transferred onto the acceptor substrate (Whitten and Trehwella, 2009, Knowles, 1989). In this mechanism, the biotin cofactor is essential for catalysis. Likewise, the covalent attachment of biotin onto BCCP, performed by BPL, is vitally important for the biotin-dependent enzymes to fulfill their important metabolic functions.

The structure of the BCCP domain across different species is highly conserved throughout organisms (**Figure 1.9A**). It consists of two anti-parallel β -sheets that form a flattened β -barrel structure. A core of conserved glycine and hydrophobic residues stabilize BCCP, with mutations in these conserved residues impairing the biotinylation reaction (Schneidman-Duhovny et al., 2010, Cronan, 1990, Polyak et al., 2001). The lysine amino acid targeted for biotinylation is located within a hairpin turn between the $\beta 3$ and $\beta 4$ strands, and is located within a Met-Lys-Met motif that is conserved within all BCCP domains. NMR spectroscopy has revealed that biotinylation stabilizes this hairpin turn and aids in the biotin-carboxylation reaction (Kondo et al., 1984, Svergun et al., 1995, Yao et al., 1999). Some bacterial BCCP domains also possess a thumb-like loop between the $\beta 2$ and $\beta 3$ strands, which is important for interacting with the biotinyl group of the carboxylase and burying biotin with the surface of the protein. Therefore the thumb functions as a flexible lid to prevent solvation of the active site and transfer of CO_2 between carboxybiotin and acetyl-CoA (Athappilly and Hendrickson, 1995, Roberts et al., 1999, Cronan, 2001).

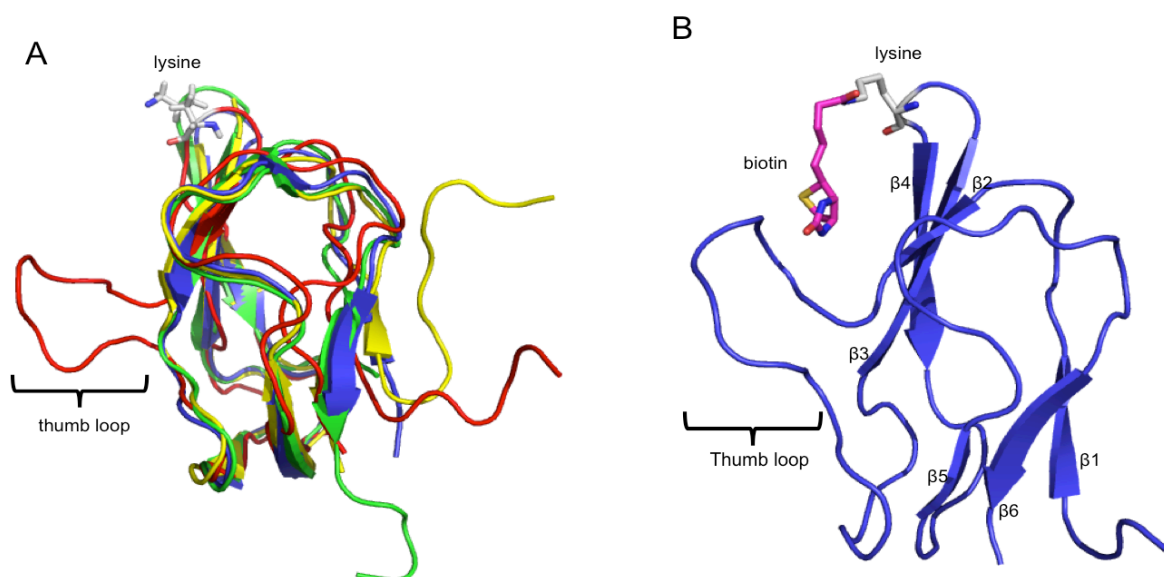


Figure 1.9 A) Structural conservation of the apo-BCCP domain. Co-ordinates deposited in the PDB were downloaded and superimposed on other biotin domains to demonstrate the structural conservation across species (PDB: 3BDO, 1DCZ, 1Z7T, 2D5D). The target lysine chain is shown as a ball and stick model, located within a hairpin loop found between β -strands 3 and 4. *E. coli* BCCP (PDB: 3BDO) is shown in red with a thumb loop between $\beta 2$ and $\beta 3$. **(B) Structure of Holo *E. coli* BCCP with β -strands labeled.** Biotin binds the lysine located within an MKM motif and forms a swinging arm structure.

The acetyl CoA carboxylase complex in *E. coli* (Cronan, 2001) is able to biotinylate BCCP from humans, a vastly different organism from *E. coli* but is unable to biotinylate BCCP from the thermophilic archaeon *Sulfolobus tokodaii*. Likewise, the *S. tokodaii* BPL is unable to biotinylate *EcBCCP*. *S. tokodaii* BCCP has a serine in place of the methionine on the C-terminal side of the conserved lysine, thus abolishing recognition by BirA (Sueda et al.,

2006). Lipoyl ligases also have a similar domain, which contains a target lysine, but found within a Asp-Lys-Ala motif (Brocklehurst and Perham, 1993, Dardel et al., 1993). The location of lysine and the surrounding methionines are important for biotinylation: replacement of the methionine residues flanking the target lysine with aspartate and alanine abolishes biotinylation, and moving lysine away from its position within the loop also prevents biotinylation (Polyak et al., 2001, Shenoy and Wood, 1988, Kondo et al., 1984, Reche et al., 1998). Recognition of the biotin domain or lipoyl domain by their respective ligases is also based on their respective structures: even though both are similar, the loop on which the lysine residue is recognized on the lipoyl domain has variable length, and has an effect on the surface topography of lipoyl domains, and so is not recognized by BPL (Konarev et al., 2003). Removal of the previously mentioned “thumb” loop on *E. coli* BCCP also prevents biotinylation by BPL but increases its ability to be lipoylated (Reche and Perham, 1999). Hence, the biotinylation of BCCP by BPL relies on BCCP adopting an appropriate structure, and the correct positioning of the lysine residue on the BCCP domain.

1.5.2. Structural cues to the biotinylation of BCCP

The recent elucidation of the structure of mutant *P. horikoshii* BPL (*PhBPL*) in association with *P. horikoshii* BCCP (*PhBCCP*) provides structural information as to how BPL and BCCP interact (**Figure 1.10**). The structure of the *PhBPL:PhBCCP* complex was found to be a *PhBPL* dimer bound to two separate *PhBCCP* substrates. The association of *PhBPL* and *PhBCCP* involves interactions occurring between the $\beta 2$ strand of *PhBCCP* and $\beta 7$ strand of *PhBPL*, forming an intermolecular β -sheet that is solvent exposed on one side to accommodate Btyl. The intermolecular surface is mainly hydrophobic, and is stabilized by a number of hydrogen bonds. *PhBCCP* also interacts with BPL with the loop region between strands $\beta 3$ and $\beta 4$, which includes the target lysine residue (Bagautdinov et al., 2008). The structure of *PhBCCP* in its free and complex states is generally similar, suggesting that the binding of *PhBCCP* to *PhBPL* and its subsequent biotinylation cause few significant structural changes. *PhBPL* however, undergoes more extensive structural changes. Although the catalytic domain in the free and complex state stays relatively similar, the C-terminal domain shows large structural variations (**Figure 1.10**) (Bagautdinov et al., 2008) suggesting that it has an important functional role.

The structural data has provided powerful new insights into the BPL reaction mechanism. The first step of the biotinylation reaction requires BPL to catalyse the nucleophilic attack of the oxygen atom on the biotin carboxylate group with the α -phosphate group of ATP to form

Btyl. The substrates biotin and ATP are bound within the active site in a fixed configuration that places the ligands spatially close to facilitate the reaction (Bagautdinov et al., 2005a). After Btyl is formed, biotin has to be ligated onto BCCP. Structural studies done by Bagautdinov *et al.* on *PhBPL* mutants which are unable to release *PhBCCP* after biotinylation has occurred have suggested a possible scenario for the transfer mechanism of biotin onto BCCP, in which correct positioning of the substrate lysine of BCCP near the BPL active site is essential for the biotinylation reaction of BCCP to occur (Ingaramo and Beckett, 2011).

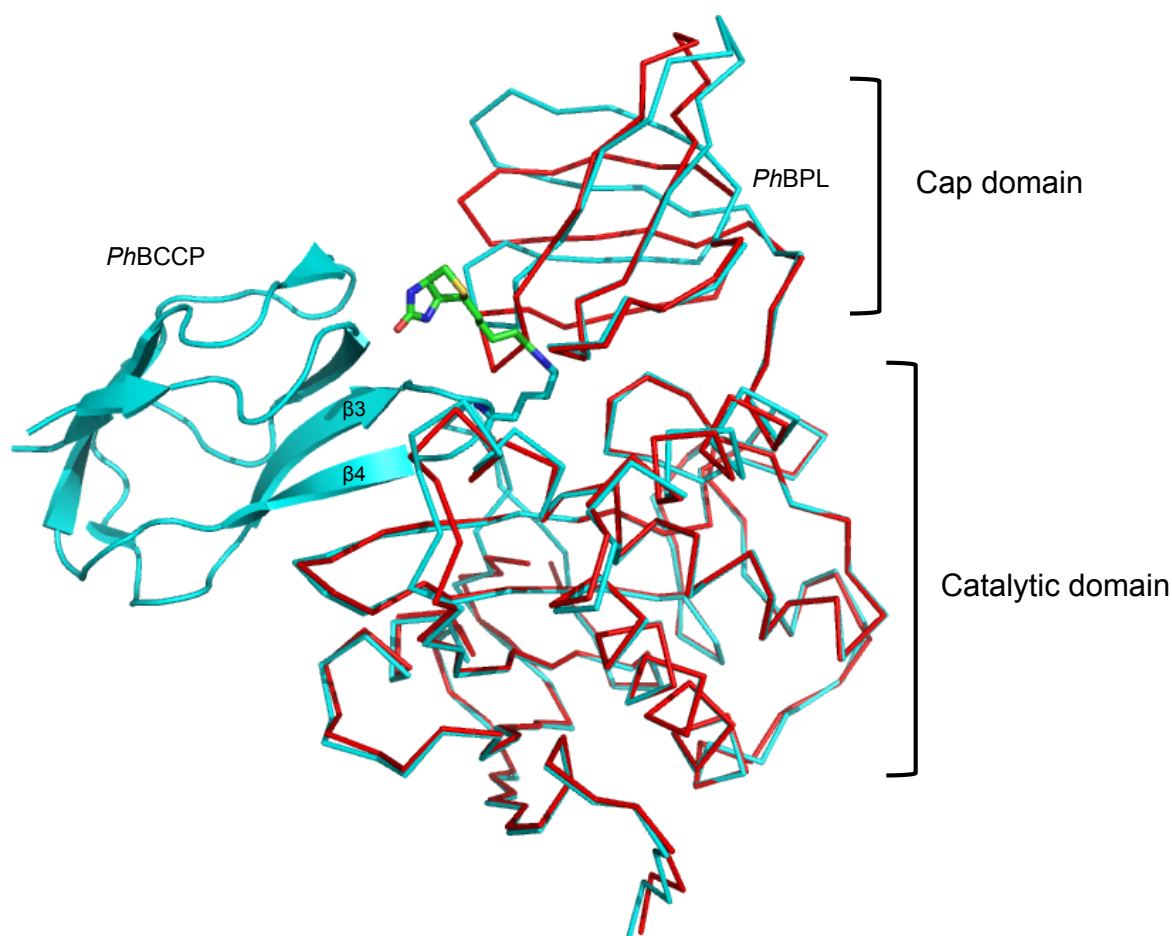


Figure 1.10 Apo *PhBCCP* (red ribbon, PDB: 1WQ7) and Holo *PhBCCP* (cyan ribbon) in complex with *PhBCCP* (cyan cartoon) (PDB: 2EJF). The substrate lysine located on the loop between $\beta 3$ and $\beta 4$ facilitates a nucleophilic attack on Btyl which results in the transfer of biotin (green stick) and the release of AMP. The structural changes undergone by the cap domain suggest that it plays a role in heterodimerisation formation.

During the first stage, or the “formation stage”, the side chain of the target lysine enters the active site and binds to BPL. There are two different formation stages, indicating a degree of flexibility in which BCCP can enter the active site of BPL. In the second stage, after apo-BCCP is bound to BPL, the ϵ -amino of the substrate lysine provides a positive charge that facilitates a nucleophilic attack on the carbonyl group of Btyl, resulting in the transfer of

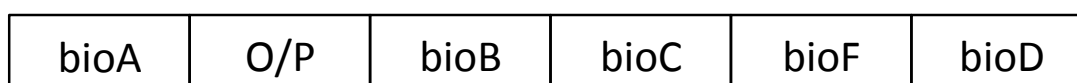
biotin onto apo-BCCP and the release of AMP (**Figure 1.8**). This second catalytic step is known as the “reaction stage”. The third and last stage is the “product stage”, where holo-BCCP is released from BPL (Bagautdinov et al., 2008)

The biotinylation of *Ph*BCCP by *Ph*BPL is a complex process, requiring several steps for successful catalytic activity to occur. *Ph*BPL is a class I BPL, and is only involved in biotinylation. The biotinylation of BCCP by class II and class III BPLs although likely to be similar, may require further methods of regulating biotinylation due to the presence of an N-terminal domain is required for other functions of BPL, for example, the transcriptional repression of biotin biosynthetic genes by class II BPLs.

1.6. The transcriptional repression of biotin biosynthetic genes by Class II BPL

Some bacteria are biotin autotrophs and hence can synthesis biotin for their own metabolic needs, and thus require a way to regulate biotin synthesis. The biosynthetic pathway of biotin in bacteria is divided into two components: the initial synthesis of a pimelate moiety and assembly of the bicyclic rings. The synthesis of the pimelate moiety is not conserved in bacteria, and is catalysed by several different pathways, of which the bioH-bioC pathway of *E. coli* is the most understood (Lin and Cronan, 2011). The biotin operon operator (*bioO*) of *E. coli* is located between the divergent bioBFCD operon and *bioA* gene, and functions to regulate the synthesis of these biotin biosynthetic genes (**Figure 1.11**). The operator sequence is an imperfect palindrome, and two divergent promoters, P_a and P_b can be seen in the sequence (Lee et al., 2010), which partially overlap the *bioO* operator (**Figure 1.11**). Class II BPLs contain a DNA-binding domain and can also act as a transcriptional repressor of biotin biosynthetic genes. In situations where the concentration of apo-BCCP is low in the cell, Btyl acts as a co-repressor of biotin biosynthetic genes by promoting BPL homodimerisation and binding to *bioO* and transcription is repressed in both directions through both promoters (Rodionov et al., 2002, Streaker and Beckett, 2003, Eisenstein and Beckett, 1999, Barker and Campbell, 1981a, Mayende et al., 2012). Regulation of biotin biosynthesis by BirA has been extensively characterized in *E. coli*. To date, no investigations of other examples have been reported.

A



B

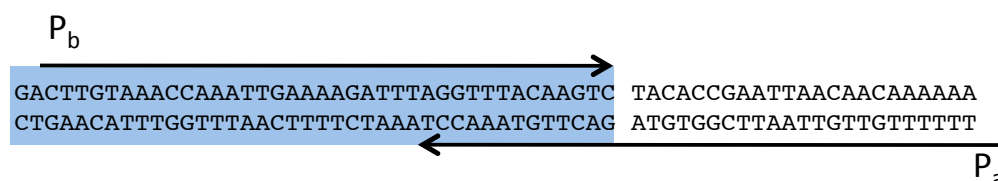


Figure 1.11 (A) Schematic representation of the *E. coli* biotin biosynthetic operon. BioA, B, C, F and D encode enzymes required for biotin synthesis, whilst O/P is the control region of the operon. **(B)** The sequence of the biotin operon operator transcriptional region. P_a and P_b are the promoters for leftward and rightward transcription. Boxed region represents the biotin operator sequence, *bioO* to which holo-BirA binds to in order to regulate transcription.

1.6.1. Class II BPLs form a homodimer to regulate biotin synthesis

In order to regulate the transcription of biotin biosynthetic genes, class II BPLs must first bind to the target *bioO* operator sequence (Streaker and Beckett, 1998). The N-terminal domain of class II BPLs contains a winged helix-turn-helix motif that is a common DNA-binding motif, which is used to bind to *bioO* (Streaker and Beckett, 1998). Kinetic measurements of *bioO* binding by holo-BirA have indicated that BirA must first form a homodimer prior to *bioO* binding (Streaker and Beckett, 2003). The BirA homodimer is formed via the β -sheets located in the catalytic domain, with each monomer arranged side by side, forming a large, continuous β -sheet (**Figure 1.12**), with Btyl-bound BirA forming a tighter dimer compared to the biotin-bound form (Wood et al., 2006, Weaver et al., 2001a).

Btyl-bound holo BirA forms a dimer at micromolar concentration, which is in contrast to the apo form that has little tendency to self-associate (Hassan et al., 2009). The kinetics of holo BirA homodimerization is slow, and is thus thought to provide a long window for heterodimerization with BCCP to occur and pushes the system towards metabolism (Zhao and Beckett, 2008). However, when concentrations of apo-BCCP in the cell are low, homodimerisation occurs instead, allowing binding of *bioO* to occur. The binding of holo-BirA to *bioO* occurs at nanomolar concentrations, suggesting that homodimerization is driven not only by the binding of Btyl but may also be induced by DNA (Hassan et al., 2009, Zhao and Beckett, 2008). BirA homodimer has a half-life of 30 minutes, and is a moderately stable complex with little spontaneous dissociation occurring. The BirA:biotin complex homodimer

can also bind to *bioO*, however the concentrations of biotin required for this reaction to occur are significantly higher, due to biotin being a very weak activator of homodimer formation (Prakash and Eisenberg, 1979).

Early studies focusing on mutant BirA first showed that repressional activity and biotin transfer were closely linked (Brunger, 1992). The biotin-induced disorder-to-order transition of the surface loops is not only important for the biotinylation activity of BirA, but is also a prerequisite to dimerization and important in controlling biotin transcription (Weaver et al., 2001b). Three surface loops in BirA, whilst not conserved across bacteria, are important in homodimer formation and aid the two conserved loops in regulating the dual roles of BirA (Adikaram and Beckett, 2012). Mutations located on the highly conserved ¹¹⁵GRGRXX₁₂₀ biotin binding loop motif (**Figure 1.12**) result in BirA enzymes which are monomeric despite the addition of Btyl, and hence defective in DNA-binding and transcriptional repression due to the inability of the protein to form a homodimer (Kwon et al., 2000). The other conserved ¹⁷⁰RVKWPND₁₇₆ loop of BirA is also required for the dual roles of BirA. Mutations in this loop affect homodimerisation, heterodimerisation with BCCP, as well as biotin transfer (Adikaram and Beckett, 2012). A recent study which isolated several strains of BirA with super repressor activity found that the majority of these proteins bound with a stronger affinity to the *bioO* operator compared to the wildtype protein, but still maintained the same biotinylation activity. One mutant (G154D) had the same super repressor phenotype, but was lethal to cells and lacked the ability to biotinylate its substrate (Chakravartty and Cronan, 2012). The communication between the catalytic and DNA-binding domains of class II BPLs is more complex than previously thought, and regulation of both roles is still not fully understood.

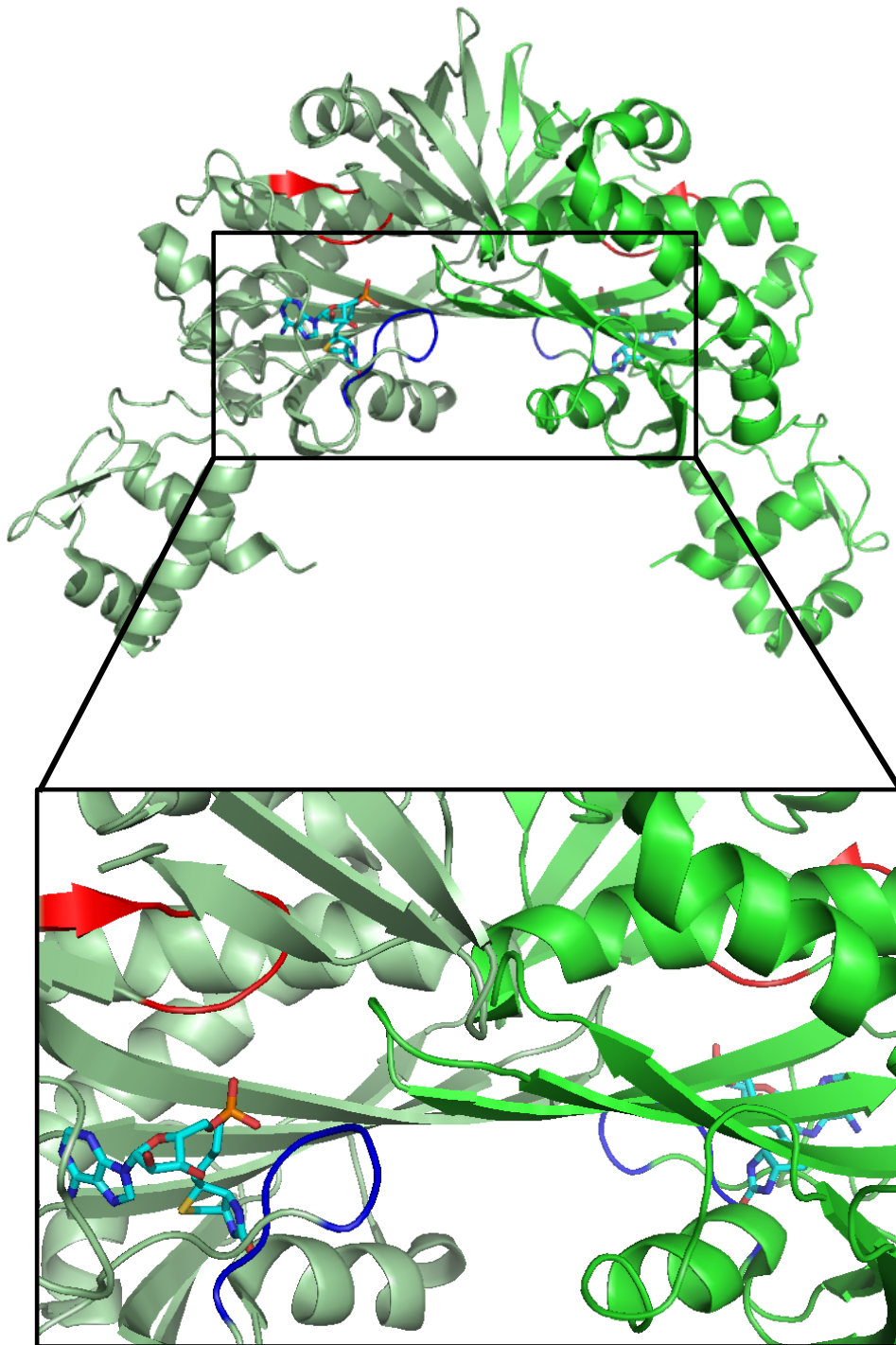


Figure 1.12 BirA BtOH homodimer. Insert shows the dimerisation interface formed through a continuous β -sheet between two BirA molecules. Conserved GRGRXX loop shown in blue, whilst RKWPND loop showed in red.

Most dimeric proteins with a winged helix-turn-helix motif bind to DNA target sites that are around 20 to 30bp in length. The *bioO* operator, however, is longer at 40bp in length (Otsuka, 1978). It is known that the dimeric holo-BirA binds to the operator site, dispelling the theory that holo BirA forms an oligomer larger than a dimer when bound to the operator (Abbott and Beckett, 1993). DNA-footprinting studies suggest that each BirA monomer binds to a binding site located at each termini of the operator sequence, comprising of a DNA

sequence of approximately 12bp in length, whilst gel mobility shift assays show that the DNA is distorted when BirA binds to the 12bp termini (Streaker and Beckett, 1998). To date, there is no crystallographic data to show how BPL binds to DNA at the molecular level. The change in structural confirmation of the DNA and the homodimeric BPL when complex formation occurs will be discussed in chapter 6.

1.7. Homodimerization of class I BPL

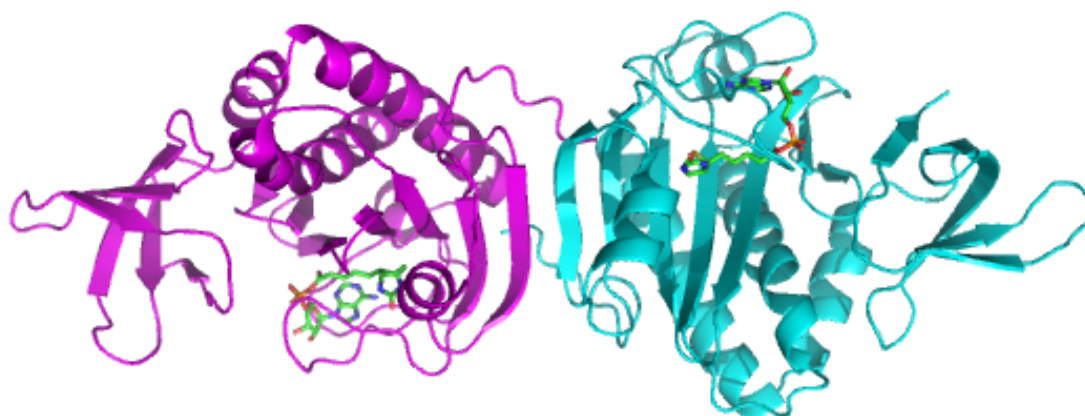


Figure 1.13 Structure of PhBPL homodimer. Unlike class II BPLs where the dimerisation interface is located near the ligand-binding site, the dimerisation interface of the class II PhBPL is formed by β -strands located at its N-terminus.

Class I BPLs do not act as transcriptional repressors, and in general do not form homodimers. Gel filtration studies of *Aquifex aeolicus* and *Mycobacterium tuberculosis* BPL show that they are monomeric in both their apo- and holo- forms (Tron et al., 2009, Purushothaman et al., 2008). On the other hand, the apo and holo forms of *PhBPL* are both dimeric. Although the catalytic domains of *PhBPL* has high sequence identity with BirA, the homodimers of *PhBPL* and BirA are vastly different. The crystal structure of *PhBPL* shows that the dimerization interface formed between two *PhBPL* molecules is formed at the N-terminus of the protein, located away from the active site (**Figure 1.13**). The two subunits are linked via hydrogen bonds between their respective β 1 strands to form an inter-subunit continuous β -sheet. The surface area that is buried at the interface accounts for 19% of the total area of each monomer, hence forming stable intermolecular interactions. Upon ligand binding to the apo-protein, orientational differences of up to 14Å are observed between the apo and holo forms (Bagautdinov et al., 2005a, Bagautdinov et al., 2007). *P. horikoshii* is a thermophile, and it is possible that the dimeric structure of its BPL may be linked to structural

stability, as in the case of the dimeric/tetrameric 2-deoxyribose-5-phosphate aldolase (Lokanath et al., 2004).

1.8. Human BPL

Unlike bacterial BPL that biotinylates between 1 – 3 biotin-dependent carboxylases, there are five biotin-dependent enzymes in mammals that are targets for mammalian BPL. These include: acetyl-CoA carboxylase (ACC1 and ACC2), pyruvate carboxylase (PC), 3-methylcrotonyl-CoA carboxylase (MCC) and propionyl carboxylase (PCC) (Wood and Barden, 1977). The full-length human BPL, or holocarboxylase synthetase (HCS) as it is more commonly referred to in the literature, is a large protein consisting of 726 amino acids with a molecular weight of 81kDa. Residues 448-701 of HCS form the catalytic and cap domains that are homologous to the catalytic and cap domains of bacterial BPL and catalyse the same conserved biotinylation reaction. However HCS also has a large N-terminal domain that only has homology with the N-terminal of other mammalian holocarboxylase synthetases but does not resemble the N-terminal DNA-binding domain of class II BPLs, and to date has no known structure or function.

Apart from its role in metabolism, it has also been proposed that HCS may also play a part in gene regulation by biotinylating histones H1, H3, H4 and H2A (Stanley et al., 2001, Cronan and Lin, 2011, Chew et al., 2006). Histone biotinylation is a rare event in humans, where only <0.1% of histones are biotinylated (Kuroishi et al., 2011), but has a role in the transcriptional repression of genes and repeat sequences (Pestinger et al., 2011). The majority of HCS is located in the cytoplasm, however small amounts can also be found in the cell nucleus (Bailey et al., 2010) and can bind to chromatin through physical interactions of histone H3 and H4 (Narang et al., 2004, Camporeale et al., 2007).

1.8.1. Three isoforms of HCS

Although there is only one copy of the human HCS gene present per haploid genome, characterization of HCS cDNA identified an mRNA in which the initiator codon was at position 58 (Met58) of the full-length protein coding sequence (Met1) (Leon-Del-Rio et al., 1995). A western-blot assay of HCS purified from human placenta revealed the presence of a third HCS isoform where the initiator codon was at position 7 (Met7) (**Figure 1.14**) (Hiratsuka et al., 1998). It is known that the alternative splicing of exon 5 and 6 results in the Met58-HCS (Yang et al., 2001), however the regulation of the molecular mechanisms that

govern the production of each isoform is unclear. Splice variants have been detected in different tissue types, suggesting that mRNA processing may be cell specific (Yang et al., 2001). Full length HCS is able to biotinylate p67, a 67 residue long polypeptide based on the PCC BCCP known to be recognized by HCS, at a 2-fold faster rate than the Met58 isoform, suggesting that the three isoforms have different activity (Ingaramo and Beckett, 2009, Leon-Del-Rio and Gravel, 1994). The three isoforms reside in different areas of the cell: Met1 and Met7 are located predominantly in the cytoplasm, whilst Met58 is present in both the cytoplasm and nucleus, leading to the suggestion that the first 58 residues may prevent nuclear translocation or be required for a protein-protein interaction that anchors the protein within the cytoplasm (Bailey et al., 2010). FL-HCS is able to biotinylate BCCPs from human carboxylases, as well as the BCCP from the *E. coli* pyruvate carboxylase, albeit at a slower rate. However, it is unable to biotinylate BCCP from an archaeal organism, showing that it can discriminate between BCCP substrates from different species (Lin and Cronan, 2011). Biotinylation of the 5 different human carboxylases by FL-HCS vary depending on cellular location: full length HCS has a kinetic preference for mitochondrial carboxylases (PC, PCC and MCC) over their cytosolic counterparts (ACC1 and ACC2) (Cheng et al., 2012). The majority of FL-HCS is located in the cytosol, and may need to biotinylate the mitochondrial carboxylases quickly prior to them being transported into the mitochondria, which may explain the difference in biotinylation rate between mitochondrial and cytosolic carboxylases (Cheng et al., 2012). The biotinylation activity of the truncated HCS isoforms against the carboxylases has not been fully explored, and it is possible that the three isoforms may have different biotinylation activity against all five carboxylases.

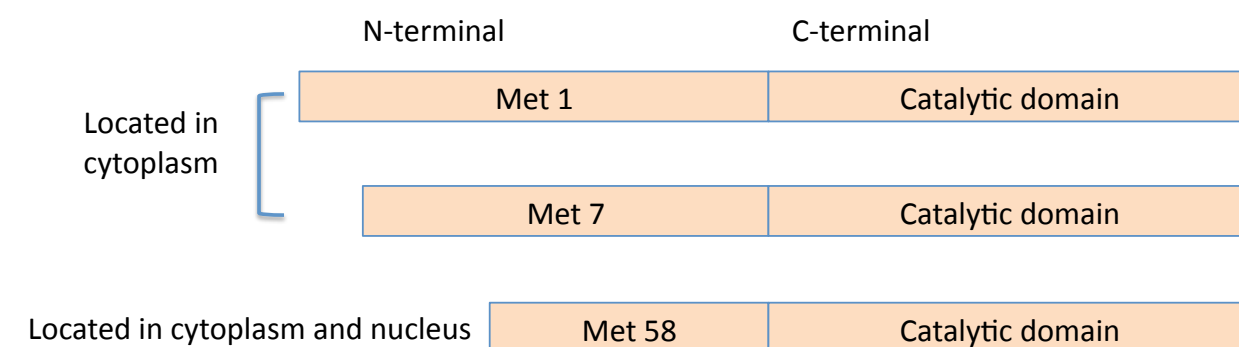


Figure 1.14 The three HCS isoforms and their location in the cell.

1.8.2. Multiple carboxylase deficiency

Mutations in HCS cause an autosomal recessive metabolic disorder known as multiple carboxylase deficiency (MCD) (Sweetman et al., 1981), due to an inability of HCS to

biotinylate its target proteins and hence result in reduced activity of the carboxylases. Apart from HCS deficiency, biotinidase (enzyme required for biotin recycling) deficiency can cause MCD, and both forms usually present themselves early on in life. Symptoms of MCD include acidosis, ketosis, dermatitis, seizures, convulsions and hypotonia, and is lethal if left undiagnosed, but can usually be treated with up to 1.2 mg of biotin supplemented in the diet (Nyhan, 1987, Pendini et al., 2013). However, there are several reported cases of patients with mutations in HCS who respond poorly to oral biotin therapy, even with doses as high as 200 mg (Dupuis et al., 1996, Aoki et al., 1995, Wilson et al., 2005, Morrone et al., 2002).

Table 1.1 List of human mutations in the catalytic domain and the corresponding residue in *E. coli* BirA. * indicates strictly conserved residues.

Human Mutation	<i>E. coli</i> BirA	Ref
Y456C	A69	(Yang et al., 2001)
T462I	Q75	(Yang et al., 2001, Aoki et al., 1999)
L470S	V83	(Yang et al., 2001)
G505R*	G115*	(Pendini et al., 2013)
R508W*	R118*	(Yang et al., 2001, Sakamoto et al., 1998, Dupuis et al., 1996, Morrone et al., 2002)
N511K	R121	(Morrone et al., 2002)
G518E*	G128*	(Dupuis et al., 1996)
L529RfsX15	F136	(Aoki et al., 1999)
V547G	V152	(Yang et al., 2001)
V550M	I155	(Aoki et al., 1999, Morrone et al., 2002)
R565X*	R170*	(Yang et al., 2001, Sakamoto et al., 1999)
D571N*	D176*	(Suzuki et al., 2005, Aoki et al., 1999, Dupuis et al., 1996)
G581S*	G186*	(Fuchshuber et al., 1993, Morrone et al., 2002, Suormala et al., 1997)
G582R	I187	(Morrone et al., 2002)
T610del	E215	(Aoki et al., 1999, Touma et al., 1999)
D615Y	N220	(Suzuki et al., 2005)
D634Y	-	(Suormala et al., 1997)
D634N	-	(Suzuki et al., 2005)
R665DfsX41	D269	(Suormala et al., 1997)
R665X		(Suzuki et al., 2005)
D715G	R317	(Suzuki et al., 2005)
780delG	-	(Yokoi et al., 2009)

MCD can be caused by mutations located in both the catalytic domain and DNA-binding domain. Experiments using a transient expression system in HCS-deficient fibroblasts showed that mutations located in the catalytic region (**Table 1.1**) were low K_m mutations, ie, they had a lower affinity for biotin. The residues G505, R508 and G518 are located on the

highly conserved biotin-binding loop and mutations in the corresponding residues in BirA result in mutants which have a low affinity for biotin, but have normal enzymatic activity (Choi-Rhee et al., 2004, Cronan, 2005, Kwon and Beckett, 2000) (**Figure 1.15**).

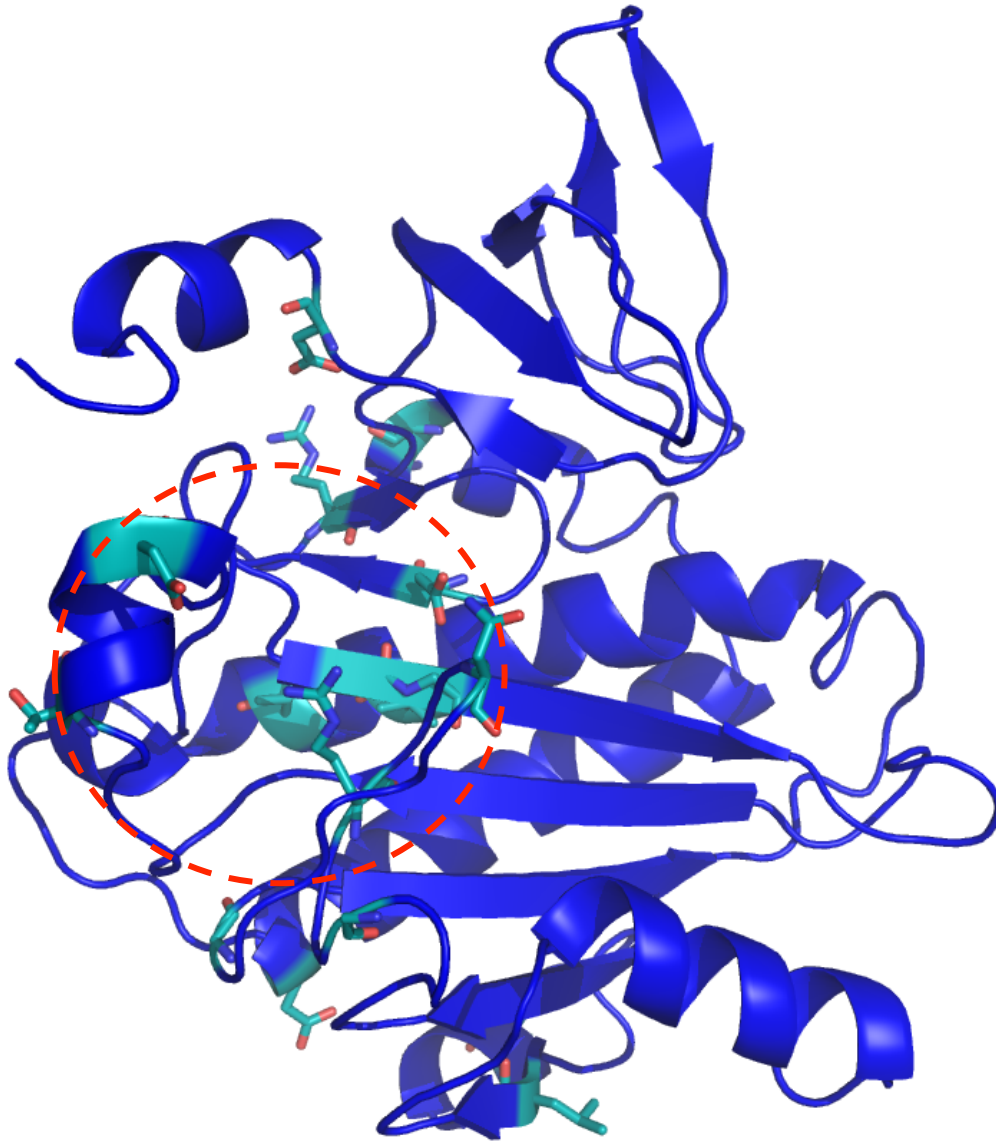


Figure 1.15 Model of HCS with residues corresponding to known mutations in cyan sticks. Red circle indicates the Btyl binding site, where most of the mutations are located. Model created with Phyre2 (<http://www.sbg.bio.ic.ac.uk/phyre2/>), with BirA as a template.

Other conserved residues such as D571 resides within the highly conserved KWPND motif, and is required for making contact with a lysine residue near the adenylate binding site, whilst G581 is located near the biotin-binding site. On the other hand, N-terminal mutants had normal or higher affinity for biotin but a lowered V_{\max} (Aoki et al., 1995, Sakamoto et al., 2000). Patients who had catalytic domain mutations were more responsive to biotin treatment, and tended to have a later onset of disease, however patients with an N-terminal mutation was less responsive to biotin, and onset of disease happened very soon after birth

(Suzuki et al., 2005). Hence further investigation of the N-terminal domain of HCS is essential in aiding the treatment of this disease.

1.8.3. Role of the N-terminal domain

To date, the structure of the N-terminal domain of HCS has not yet been elucidated but several recent studies have provided new insight into the function of the N-terminal domain. One of the proposed roles for the N-terminal domain of HCS is homodimerization, however, equilibrium sedimentation studies show that it is a monomer in both its apo and holo form thereby ruling out self-association (Ingaramo and Beckett, 2009). Functional studies have revealed that the N-terminal domain of HCS is involved in BCCP recognition (Campeau and Gravel, 2001, Hassan et al., 2009). The first 159 amino acids of HCS have high mobility and are sensitive to protease treatment, indicative of an open conformation (Campeau and Gravel, 2001, Oliva et al., 2004). Limited proteolytic studies suggested that there is a structured domain present between residues 160 – 315 in HCS, and truncations in this domain abolish HCS activity, suggesting that this domain is important for catalysis (Campeau and Gravel, 2001, Oliva et al., 2004, Bailey et al., 2010). Using surface plasmon resonance analysis, Mayende *et al.* found that two N-terminal mutations L216R and L237P reduced the stability of enzyme in complex with BCCP, hence biotin transfer between mutant HCS and substrate were unable to occur (Oliva et al., 2004). Likewise, N-terminally truncated HCS variants were able to biotinylate both *E. coli* and human BCCP, although with different affinities (Campeau and Gravel, 2001). Kinetic analysis of full length HCS and the Met58 isoform showed although both had similar rates for synthesizing Btyl, the full length protein was able to associate with its target substrate at twice the rate of the shorter isoform (Ingaramo and Beckett, 2009). And finally, a yeast-2-hybrid assay showed that the N-terminal could bind to the BCCP from propionyl CoA carboxylase (Hassan et al., 2009). The N-terminal domain of HCS can interact with different surfaces of its target substrate BCCP as well as the catalytic domain, which suggests that both the N-terminal and catalytic domain need to interact cooperatively to recruit the substrate protein (Whitten and Trehwella, 2009). Apart from substrate recognition, the N-terminal is also important for the catalytic activity of HCS: when anti-HCS antibodies were tested for their ability to inhibit HCS enzymatic activity, antibodies targeted to the region between Ile128 and Pro398 of the N-terminal inhibited HCS activity (Hiratsuka et al., 1998). To date, there is no known structure of the HCS, or that of other eukaryotic BPLs. Elucidating the structure of a eukaryotic BPL would hopefully provide more clues to the function of the N-terminal domain.

1.9. Project aims

1.9.1. Structure-based drug design

Multi-drug resistant bacteria (collectively termed the ESKAPE pathogens by the Center for Disease Control in the United States, and includes *E. faecium*, *Staphylococcus aureus*, *Klebsiella pneumoniae*, *Acinetobacter baumannii*, *Pseudomonas aeruginosa*, and *Enterobacter* spp (Boucher et al., 2009) have become increasingly problematic, and are responsible for the majority of hospitalization in the US. Hence there is a need to design a drug that can target a molecule within the cell which is critical for bacterial cell survival. BPL is one such molecule: it is essential for bacterial cell metabolism, and although it is ubiquitous in nature, there are enough differences between eukaryotic and bacterial BPL to make it a potential drug target. There have been inhibitors designed against the BPL from *Mycobacterium tuberculosis*, most of which mimic the structure of Btyl. The structure of SaBPL was previously solved in our lab, and provided the basis for structure-based drug design. Together with our collaborators in Adelaide University, we aim to design inhibitors that can selectively target SaBPL in order to combat infections caused by MRSA. The BPLs from other ESKAPE pathogens will also be investigated and characterized using both functional and structural methods, in order for future drug design studies.

1.9.2. Investigating the interaction between SaBPL and the BioO operator

To date, a lot of work has been done on the BirA enzyme and its target BioO operator sequence. However, although SaBPL and BirA are both class II BPLs, and are structurally similar, there are more interactions between the homodimer formed between two SaBPL molecules compared to the BirA structure, causing the position of both the DNA-binding domains in the SaBPL dimer to be in much closer proximity. The physiological relevance of the different structures is unknown, and hence the aim of this part of the project is to investigate the interaction between SaBPL and its target BioO operator, using a combination of both kinetic and structural methods.

1.9.3. Structurally characterize HCS

The structure and function of the N-terminal domain of HCS is still largely unknown, and we are interested in solving the structure of HCS to further understand its role in the biotinylation of biotin-dependent carboxylases, as well as to elucidate other probable functions. The structure of HCS would also aid in the design of antibacterials specifically targeted to

SaBPL. The expression and purification of HCS will be performed and a combination of X-ray crystallography and SAXS will be used to solve the structure of HCS.

Chapter 2 General materials and methods

2.1. Protein expression and purification

2.1.1. Protein expression and purification of SaBPL

SaBPL was previously cloned, expressed and purified as outlined in a published paper by Pendini *et al* (Pendini et al., 2008b). Briefly, SaBPL was cloned into a pET16b His-tagged plasmid, which was subsequently transformed into BL21 (DE3) *E. coli* bacterial cells (Sambrook and Russell, 2001), grown at 37 °C in 2YT medium supplemented with 100 µg/mL ampicillin until the optical density measured at an absorbance of 600 nm (OD₆₀₀) was 0.6, and induced with 1 mM IPTG to express recombinant SaBPL. Cells were harvested by centrifugation at 3,000 g for 15 minutes and stored at -80 °C.

BL21 (DE3) *E. coli* bacterial cells were lysed in lysis buffer (50 mM Tris-HCl, 500 mM NaCl, 1 mM DTT) with the addition of 10 mM imidazole using a French press. After filtering through a 0.22 µ filter (Milipore), the crude protein extract was loaded onto a 5 mL HisTrap column (GE Healthcare) which had been pre-equilibrated with lysis buffer and 10 mM imidazole. The loaded column was then washed with 10 column volumes of lysis buffer. Column was then washed with lysis buffer and 50 mM imidazole. SaBPL was eluted using 100 mM imidazole in lysis buffer. After dialyzing the protein into cation buffer (A) (50 mM sodium phosphate, 50 mM NaCl, 5 % glycerol), protein was loaded onto an Sulphonate-sepharose (S-sepharose) column and eluted with a 50 mM to 500 mM NaCl gradient using a GE AKTA Purifier 100 FPLC. Purified protein was snap frozen in 1 mL aliquots and stored at -80 °C until required.

2.1.2. Production of Holo and Apo-SaBPL

As SaBPL is purified with biotin bound within the active site, Apo-SaBPL was produced by adding the protein substrate BCCP to the crude protein extract and incubating at 37 °C for an hour with shaking prior to loading it onto the HisTrap column.

When performing experiments that require Holo-SaBPL, 10 x molar excess biotin and ATP was added to the purified protein and incubated at room temperature for 30 minutes to ensure that all the protein had biotinyl-5'-AMP in the active site.

2.1.3. Determination of Apo or Holo-SaBPL using BCCP

For the experiments outlined here, it was important to determine if recombinant SaBPL purified from *E. coli* was in its apo (ie unliganded) or holo (in complex with Btyl) form. Purified SaBPL was incubated in the presence of the target substrate, non-biotinylated BCCP for 10 minutes at room temperature, in 50 mM Tris-HCl, 100 mM NaCl, 1mM DTT, 10 % glycerol. Biotinylated BCCP, which could be generated in the presence of holo-SaBPL was then detected by Streptavidin blot. First the above products of the above reaction were fractionated on a 18 % SDS-PAGE and transferred onto a 0.2 μ M nitrocellulose membrane. The membrane was incubated at room temperature for 1 hour in 1 % skim milk powder in 1 x PBS, and a further 1 hour with streptavidin-HRP (Sigma-Aldrich), washed twice with 1 x PBS for 15 minutes and detected with ECL reagent (GE Healthcare). The presence of biotinylated BCCP indicated that SaBPL was in its holo form, whilst the absence of biotinylated BCCP indicated that apo-SaBPL was purified.

2.1.4. Protein expression of AcBPL, KpBPL and PcBPL

2.1.4.1. Cloning

Table 2.1: Forward and reverse primers used for the cloning of AcBPL, KpBPL and PaBPL, with restriction enzyme sites underlined.

	Forward primer (5' – 3')	Reverse primer (5' – 3')
AcBPL	TATATACATATGGATTAGAGACTCGCCAAC TACAACAA	TTATTACTCGAGGGTTTGTGGTCTTAGACGACC
KpBPL	TATATACATATGAAAGACCATACTATTCCCTTAACGTTG	TCATCACTCGAGGCTGCGCAATGATATTTACCC
PaBPL	TATATACATATGCAGACCTTGCTGAACTACTTCAAGAC	TCATCACTCGAGCAACCTCAAAC TAAGCTCCCC

Due to the difficulty of obtaining *A. baumannii* cells for our purposes, *A. calcoaceticus* was used instead as the sequence of BPL from both species have 98.8% sequence similarity. Cultures of *Acinetobacter calcoaceticus*, *Klebsiella pneumoniae* and *Pseudomonas aeruginosa* were kindly provided by Dr. Kylie Wilson, Department of Microbiology, Monash University. Liquid cultures of these bacteria were grown overnight at 37 °C and genomic DNA extracted using a genomic DNA extraction kit (Sigma-Aldrich). Forward and reverse primers were designed based on sequence information obtained from Genbank (Table 2.1). The forward and reverse primers had *Nde*I and *Xho*I restriction enzyme sites designed into them, respectively, to facilitate cloning. PCR amplification was carried out with *Pfu* polymerase (Promega) to generate the PCR products. The PCR products were then

digested with *Nde*I and *Xho*I restriction enzymes (NEB) and ligated with T4 DNA ligase (NEB) into a C-terminal His₆-tag pET22b vector. After generation of the plasmid, it was transformed into DH5 α *E. coli* cells to generate larger amounts of plasmid, and the final plasmid extracted from the bacterial cells with a miniprep kit (Qiagen). The final plasmid sequence was verified at the Micromon DNA sequencing facility.

2.1.4.2. Small scale over-expression

pET22b vectors containing *KpBPL*, *AcBPL* or *PaBPL* were transformed into BL21 (DE3) *E. coli* competent cells, and plated onto 2YT-Ampicillin agar plates and grown at 37 °C overnight. A single colony was then grown overnight in 2YT-Ampicillin media, and diluted 1 : 100 the next day into fresh 2YT-Ampicillin media and grown at 37 °C until the cells had reached an OD₆₀₀ ~ 0.6. At this stage cells were induced with 0.1 mM, 0.5 mM or 1 mM IPTG and grown at 25 °C for 4.5 hours, or 16 °C overnight. 500 μ L of the post induction sample was harvested and resuspended in 100 μ L SDS-loading dye prior to loading onto a 15 % SDS-PAGE gel. Another 500 μ L of the post induction sample was also harvested at max speed, and the cell pellet resuspended in 200 μ L lysis buffer and sonicated for 10 minutes. The lysed cells were centrifuged at maximum speed for 5 minutes and the resulting supernatant (soluble protein) and pellet (insoluble debris) were separated and loaded onto a 15 % SDS-PAGE gel.

2.1.4.3. Expression and protein purification

E. coli BL21 (DE3) cells harbouring pET22b-*KpBPL*, pET22b-*AcBPL* and pET22b-*PaBPL* plasmids were grown overnight in 2 YT media at 37 °C, and diluted 1 : 100 the next day into 1 L of 2 YT media. After the cells had reached an OD₆₀₀ ~ 0.6, they were induced with 0.5 mM IPTG and further incubated for 18 hours at 16 °C. The next day, cell pellets were harvested at 3,000 x g and stored at – 80 °C until further use.

Bacterial cell pellets were resuspended in cold lysis buffer and disrupted using a French press. The cell lysate was centrifuged at 15,000 rpm for 30 minutes to remove the insoluble debris. After equilibrating a 5 mL Ni HiTrap column (GE Healthcare) with lysis buffer (50 mM Tris-HCl, pH 7.5, 500 mM NaCl, 10 mM imidazole), the supernatant was applied to the nickel resin using a flow rate of 2.5 mL/min. The column was then washed with 10 column volumes of lysis buffer to remove unbound protein. BPL subsequently eluted with 50 mM imidazole, 100 mM imidazole and 150 mM imidazole in the presence of lysis buffer. *KpBPL* and *AcBPL* were then dialysed into SE buffer (50 mM Tris-HCl pH 7.5, 100 mM NaCl, 10 % glycerol) for

3 hours and overnight at 4 °C. *KpBPL* was purified further via anion exchange chromatography using a Quaternary amine sepharose (Q-sepharose) 16/60 column (GE Healthcare) and size exclusion with a Superdex 200 16/60 column (S200 16/60) (GE Healthcare), whilst further purification of *AcBPL* was performed using a S-sepharose 16/60 column (GE Healthcare) equilibrated in cation exchange buffer (A) (50 mM Sodium phosphate pH 7.5, 10 % glycerol) and eluted using a salt gradient of 0 - 500 mM NaCl on a GE AKTA FPLC. Protein purity was assessed following separation on a 15% SDS-PAGE gel, and protein concentration determined spectrophotometrically by absorbance at 280 nm (*KpBPL* theoretical $\epsilon = 50420 \text{ M}^{-1}\text{cm}^{-1}$; *AcBPL* theoretical $\epsilon = 33728 \text{ M}^{-1}\text{cm}^{-1}$). Presence of hexahistidine tagged *KpBPL* or *AcBPL* was determined by Western blot using an anti-His-tag antibody conjugated to HRP, as well as N-terminal sequencing.

2.2. Cloning of Met58-HCS and Cat-HCS

As the catalytic domains of eukaryotic BPL and bacterial BPL have high sequence homology, we determined the boundaries of the catalytic domain of human HCS (cat-HCS) based on a sequence alignment with the catalytic domain of BirA and the full length *PhBPL* (Fig 1). It was proposed that cat-HCS would reside between residues 464 – 720 of the full length HCS.

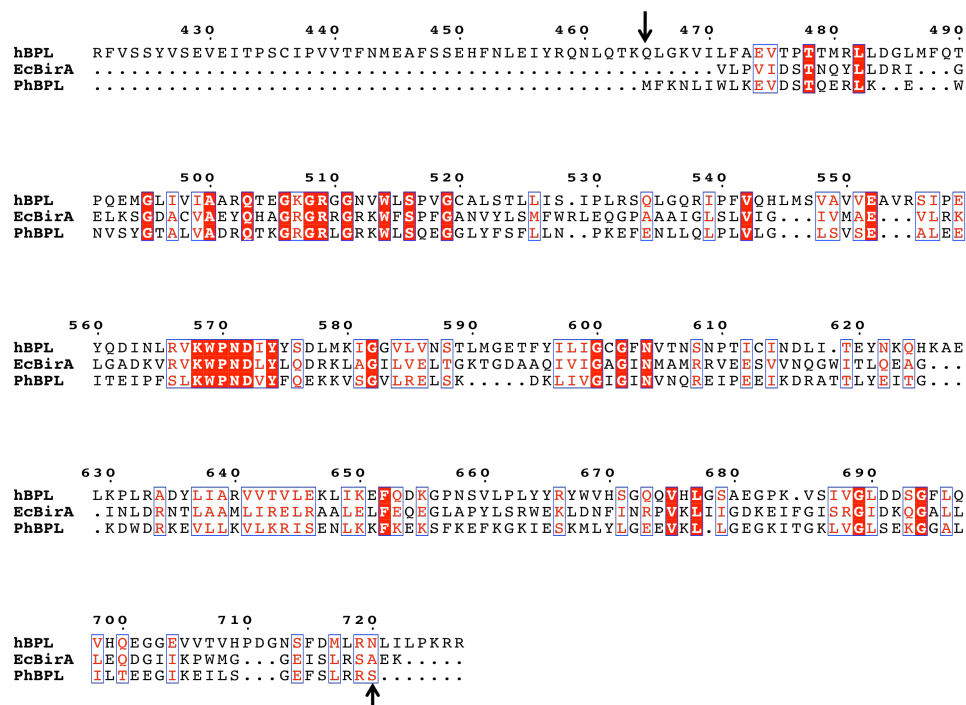


Figure 2.1 sequence alignment of HCS, BirA and *PhBPL*. *PhBPL* and the catalytic domain of BirA aligns with residues 464-720 of full length HCS, and was assigned as the boundaries of cat-HCS. Arrows indicate position 464 and 720.

Plasmids suitable for the recombinant expression of HCS in *E. coli* were designed and cloned based on sequence information obtained from Genbank (Accession no: BAB68550) (table 2.2). The DNA sequence was amplified by PCR with *Pfu* polymerase (Promega) to generate the BPL PCR products using oligonucleotide primers containing restriction enzyme sites to facilitate cloning into either a C-terminal His-tag pET15b vector, or a pGEX4T-2 vector that produces a protein with a N-terminal GST-tag that can be cleaved off with thrombin. Restriction enzymes that were used for cloning are listed in table 2.2.

Table 2.2 (A) List of restriction enzymes used to digest PCR products for cloning. (B) List of primers used to clone Met58-HCS and Cat-HCS, with restriction sites underlined.

	Restriction enzyme 1	Restriction enzyme 2
(1) Met58-HCS (pET15b)	NcoI	XhoI
(2) Cat-HCS (pET15b)	NdeI	XhoI
(3) Cat-HCS (pGEX4T2)	BamHI	EcoRI

	Forward primer (5' – 3')	Reverse primer (5' – 3')
1	CTGAGCAGGACACCATGGAGCATGTTGGCAG	GGGGAGGATCTCGAGTCACAGCATGTTCGAA
2	GAGATCTATCATATGAATCTGCAGACCAAGCAG	GGGGAGGATCTCGAGTCACAGCATGTTCGAA
3	AACTTAGAGGGATCCCGCCAAAATCTGCAGACC	CTAATGATGATGAATTCCTTACCGCCGTTGGGGAG

2.2.1.Expression

BL21 (DE3) *E. coli* competent cells containing plasmids were grown overnight in 2 YT media at 37 °C, and diluted 1 : 100 the next day into 1 L of 2 YT media. The cells were grown at 37 °C until an OD₆₀₀ of 0.6 was reached, and induced with 0.5 mM IPTG and further incubated for 18 hours at 16 °C. The following day, cell pellets were spun down at 3,000 x g and stored at – 80 °C until further use.

2.2.2.Purification of Met 58-HCS

The first step of Met58-HCS purification was performed as per bacterial BPL purification where cell lysate was loaded onto a Ni HiTrap column and subsequently eluted with 50 mM, 100 mM and 150 mM imidazole. Met58-HCS was dialysed into SE buffer (appendix II) once for 3 hours, then overnight at 4 °C. A cation step was included as a final clean up step. The dialysed material was loaded onto a S-sepharose 16/60 column (GE Healthcare) and eluted with a gradient of 0 – 1M NaCl over 5 column volumes.

2.2.3. Purification of Cat-HCS-GST

After resuspending frozen bacterial cell pellets in cold 1 x PBS and lysis by French press, the disrupted cells were centrifuged at 15,000 rpm for 30 minutes to remove the insoluble debris. After equilibrating a 5 mL GSTrap FF (GE Healthcare) with 1 x PBS, the cleared cell lysate was then applied to the column using a flow rate of 2.5 mL/min. The column was then washed with 10 column volumes of 1 x PBS, and protein eluted with 10 mM reduced GSH, pH 7.5 in 1 x PBS. The column was then washed again with 3 column volumes of 1 x PBS, and the supernatant re-loaded and re-eluted a further 2 times to increase the total yield. The three elutions were pooled, and 50 U thrombin was added. This was then dialysed into 50 mM Mes pH 6.5, 50 mM NaCl and 10 % glycerol overnight and 3 hours at 4 °C. The cleaved Cat-HCS was then separated from GST using GSTrap FF column again, and collecting the flow through.

2.3. SaBCCP purification

The plasmid containing GST-SaBCCP was a gift from our collaborators at the University of Adelaide. BL21 (DE3) plysS *E. coli* cells containing the GST-SaBCCP plasmid was grown overnight in 2 YT media at 37 °C and diluted 1 : 100 the next day into 4 L of 2 YT media. After the cells had reached an OD600 ~ 0.6, they were induced with 0.5 mM IPTG and further incubated for 4.5 hours at 37 °C. The cell culture was spun down at 3,000 x g and the resulting cell pellet stored at – 80 °C until further use.

The cell pellet was resuspended in PBS, pH 7.5 and passed through a French press 3 times to lyse the cells. The lysed cells were then centrifuged at 15, 000 rpm for 30 minutes to separate the supernatant and insoluble debris. After equilibrating a 5 mL GSTrap FF Column (GE Healthcare) with PBS, the supernatant was bound to the column at a flow rate of 2.5 mL/min, and the flow through collected. The column was then washed with 10 column volumes of PBS to remove unbound protein. 10 mM GSH in PBS, pH 7.5 was then used to elute the protein. After washing the column thoroughly with PBS, the flow through was rebound to the column, and the elution step repeated again. Altogether, the supernatant was bound and eluted from the column 3 times. The eluted protein was pooled and thrombin added. The pooled protein and thrombin was dialysed at 4 °C for 3 hours and overnight into 50 mM HEPES pH 7, 10 % glycerol. The next day, the dialysed sample was loaded onto a MonoQ column (GE Healthcare) and eluted with a 0 -1 M NaCl gradient to separate GST,

apo-SaBCCP and holo-SaBCCP. The presence of apo or holo SaBCCP was determined by doing a western blot with streptavidin-HRP.

2.4. SDS-gel electrophoresis

Sodium dodecyl sulphate polyacrylamide gel electrophoresis (SDS-PAGE) was used to detect the presence of protein after purification through separation according to their size via electrophoretic mobility. 1.5 mm thick stacking and resolving SDS-PAGE gels were made according to the method in appendix II and electrophoresis carried out using a Mini-Protean Tetra Cell apparatus (Bio-Rad). 3 μ L of Dual-color Precision Plus Protein Standards (Bio-Rad) was run in each gel as a reference standard. 10 μ L protein sample was mixed with 2 μ L 5 x loading dye and denatured for 5 minutes at 95 °C. After centrifuging at maximum speed for 10 seconds, the samples were loaded onto the gels and separated using electrophoresis at 200 V for 45 minutes. The gels were then stained with coomassie blue for 20 minutes at room temperature and destained until bands could be seen on the gel.

2.5. Western Blotting

2.5.1. Western transfer

After electrophoresis of protein samples down a 1.5 mm thick SDS polyacrylamide gel, the protein samples were transferred onto a 0.45 μ m nitrocellulose membrane (BioRad) using an electro-transfer apparatus (Mini-trans-Blot, Bio-Rad), assembled with fibre pads, filter paper and the SDS gel which had been pre-soaked in ice cold Towbin transfer buffer (refer to appendix II). Transfer was performed at 4 °C in Towbin transfer buffer at 100V for 60 minutes.

2.5.2. Immunodetection

After transferring the protein onto the nitrocellulose membrane, the membrane was blocked with PBS containing 5 % (w/v) skim milk powder for an hour at room temperature. 1:1000 dilution of ultrasensitive streptavidin-peroxidase polymer (Sigma) was used to detect biotinylated protein, whilst 1:5000 dilution of anti-His₆ tag antibody HRP (Abcam) was used to detect His-tagged BPL. Detection was done by diluting the antibody in PBS and incubating the nitrocellulose PBS-antibody mixture at room temperature for 2 hours. The membrane was then washed 2 times with PBS for 10 minutes at room temperature. Development of the membrane was done by incubating with 1.5 mL West-Zol ® Plus

Western Blot Detection System (Intron Bio) for 1 min, and exposing the membrane to an X-ray film from between 10 seconds to 5 minutes until there was sufficient detection of the protein bands.

2.6. Analysis of DNA binding

2.6.1. Annealing double stranded DNA

Single stranded DNA primers (**table 2.3**) were purchased from Geneworks. Complementary forward and reverse single-stranded DNA primers were placed on a heating block at 95 °C for 5 minutes, and then removed and left to anneal at room temperature for 15 minutes. Double-stranded DNA was confirmed through a 10 % TBE-page gel. Concentration of DNA was determined using a nanodrop (Thermo-fischer scientific). Molecular weight used to calculate molar concentration of each double-stranded DNA is listed in table 1.

2.6.2. DIG (Digoxigenin)-labelled DNA

The labeling and detection of double-stranded DNA using DIG and DIG-antibody was done using the DIG Gel Shift Kit, and performed according to manufacturer's instructions (Roche Applied Science). Briefly, after annealing the double stranded DNA, 155 fmol/ μ L of *bioO* was labeled with DIG-ddUTP in the presence of terminal transferase. CoCl_2 , and 5 x labeling buffer provided. DIG-labeled *bioO* was stored at -20 °C until required.

Table 2.3 Sequences used to construct double stranded *bioO*, with molecular weight used to calculate molar concentration also listed. Binding sites are underlined in bold.

	5' – 3'	3' – 5'	MW of double strand
44-mer	CCTTAAAT <u>GTA</u> AACTTATTAAATTATAAA <u>AGT</u> TTACATTGGAT	GGAATTACATT <u>TGA</u> ATAATTAATATTTCA <u>AA</u> TGTAAACCTAA	27050 Da
42-mer	CTTAAAT <u>GTA</u> AACTTATTAAATTATAAA <u>AGT</u> TTACATTGGAT	GAATTACATT <u>TGA</u> ATAATTAATATTTCA <u>AA</u> TGTAAACCTA	25813 Da
40-mer	TTAAAT <u>GTA</u> AACTTATTAAATTATAAA <u>AGT</u> TTACATTGGA	AATTACATT <u>TGA</u> ATAATTAATATTTCA <u>AA</u> TGTAAACCT	24578 Da
31-mer	AT <u>GTA</u> AACTTATTAAATTATAAA <u>AGT</u> TTACAT	CATT <u>TGA</u> ATAATTAATATTTCA <u>AA</u> TGTAAAC	19028 Da
OH1	CCTTAAAT <u>GTA</u> AACTTATTAAATTATAAA <u>AGT</u> TTACATTGGAT	GAATTACATT <u>TGA</u> ATAATTAATATTTCA <u>AA</u> TGTAAACCTAG	26103 Da
OH2	CCTTAAAT <u>GTA</u> AACTTATTAAATTATAAA <u>AGT</u> TTACATTGGAT	AATTACATT <u>TGA</u> ATAATTAATATTTCA <u>AA</u> TGTAAACCTAGG	26433 Da
HS1	CCTTAAAT <u>GTA</u> AACTTATTAAT	GGAATTACATT <u>TGA</u> ATAATTA	13525 Da
HS2	TATAAA <u>AGT</u> TTACATTGGATT	ATATTTCA <u>AA</u> TGTAAACCTAA	13525 Da

2.6.3. EMSA

In order to determine the formation of SaBPL-BioO complex, unlabelled BioO was incubated in the presence of 10 x molar excess SaBPL in 50 mM Tris-HCl pH 7.5, 50 mM NaCl, 10 mM MgCl₂, 10 % glycerol and 1 mM DTT for 10 minutes at room temperature. The mixture was then run down a 10 % TBE-PAGE gel for 200 V, 30 minutes. The gel was soaked in Gel-red nucleic acid stain (Biotium) for 5 minutes before visualizing the gel using an Alphaimager.

To determine the binding affinity of both holo and apo SaBPL, DIG-labelled DNA was used. 15.5 nM DNA was incubated with increasing concentrations of protein in SE buffer (50 mM Tris-HCl pH 7.5, 100 mM NaCl, 5 % glycerol). In the case of Holo-SaBPL, the protein-DNA complex was also incubated in the presence of 1 mM biotin and 1 mM ATP. After separating the unbound DNA and SaBPL-DNA complex down a 10 % TBE-PAGE gel, the detection of DIG-labelled DNA was performed according to manufacturer's instructions. Briefly, the DNA was transferred to a positively charged nylon membrane (Roche Applied Science) by contact-blotting for an hour at room temperature, and the DNA fixed onto the membrane by cross-linking with a transilluminator for 5 minutes. The membrane was then incubated with blocking solution (1 % blocking reagent (provided in kit) in 0.1 M Maleic acid pH 7.5, 0.15 M NaCl) for an hour with shaking, and further incubated with 1:10,000 anti-digoxigenin-AP in the presence of the blocking solution, and washed twice for 15 minutes with wash buffer (0.1 M Maleic acid pH 7.5, 0.15 M NaCl, 0.3 % (v/v) Tween 20). The membrane was then equilibrated with detection buffer (0.1 M Tris HCl pH 9.5, 0.1 M NaCl), and then incubated with CSPD working solution (CSPD provided in kit diluted 1:100 in detection buffer)

overnight at room temperature, and exposed for 20 minutes to an X-ray film. The intensity of unbound and bound DNA bands was quantitated using ImageJ.

2.6.4. K_d determination

The amount of bound DNA was determined by summing the intensities of both unbound and bound bands in each lane, and calculating the percentage the intensities of bound DNA against the total DNA. The binding affinity was then analysed using the Michaelis-Menten analysis program on Graphpad Prism version 6.0b. Each experiment was repeated 3 times, in triplicate.

2.7. In vitro Biotinylation assay

The incorporation of ^3H -biotin into BCCP was performed based on the method described by Chapman-Smith *et al.* (Chapman-Smith *et al.*, 1999). Briefly, the reaction mixture contained 50 mM Tris-HCl pH 8.0, 3 mM ATP, 4.5 μM biotin, 0.5 μM ^3H -biotin, 5.5 mM MgCl_2 , 100 mM KCl, 0.1 mg/mL BSA and 10 μM SaBCCP. The reaction was initiated with the addition of either 175 nM *Kp*BPL or 500 nM *Ac*BPL as these concentrations were found to saturate SaBCCP with Btyl, and incubated for 10 minutes at 37 °C, during which time the reaction was linear at saturating substrate concentrations. 4 μL of the reaction mix was spotted onto Whatman filter paper pre-treated with biotin and trichloroacetic acid. The filters were washed twice with 10 % (v/v) ice-cold trichloroacetic acid and once with 100 % ethanol before air-drying. Quantitation of ^3H -biotin labeled BCCP was performed using a liquid scintillation counter. One unit of enzyme activity was defined by the amount of BPL required to incorporate 1 nmol of biotin per minute.

The binding kinetics of biotin or ATP was measured by varying concentrations of one substrate in the reaction mixture above whilst keeping the other substrates at saturating concentrations. Values for K_m and V_{max} were determined by fitting a plot of substrate concentration against rate directly to the Michaelis-Menten equation using GraphPad Prism.

To measure the potency of the BPL inhibitor biotinol-5'-AMP, BPL activity was measured in the presence of varying concentrations of compound. The IC_{50} value was obtained from a dose-response curve generated in GraphPad Prism using a non-linear fit of \log_{10} (inhibitor) vs. normalized response. The absolute inhibition constant for a compound (K_i) was determined using the equation:

$$K_i = \frac{IC_{50}}{1 + \frac{[S]}{K_m}}$$

where K_m is the affinity of biotin for each respective enzyme and $[S]$ is the biotin concentration (5 μ M).

2.8. Multi angle light scattering (MALS) and Dynamic light scattering (DLS).

In order to ensure the protein sample was monodisperse and of the correct molecular weight prior to SAXS analysis, multi angle light scattering (MALS) was performed on the samples. In a MALS experiment, a monochromatic light is used to illuminate a solution containing the macromolecule of interest, the excess light scattered by the molecule through an angle to the incident beam over the scattered light by the solvent alone is directly proportional to the molar mass. The molecular weight of the macromolecule can be calculated by the Rayleigh-Gans-Debye (RGD) approximation (Oliva et al., 2004):

$$\frac{K^*C}{R(\theta)} = \frac{1}{M_w P(\theta)} + 2A_2C, \text{ where:}$$

K^* is the constant $4\pi^2(dn/dc)^2/N_A\lambda_0^4$

$R(\theta)$ is the excess intensity of the light scattered by an angle θ

$P(\theta)$ is the form factor of the light scattered at angle θ

C is the sample concentration (g/mL)

M_w is the weight-average molecular weight (molar mass)

A_2 is the second virial coefficient in the virial expansion of the osmotic pressure

N_A is Avogadro's number

dn/dc is the solution's refractive index (dn) with respect to the molecular concentration change (dc), and can be obtained using a differential refractometer (Optilab rEX)

The RGD approximation can also be used to calculate the root mean square (RMS) radius, and provide information of the size of the molecule.

Apart from using MALS to measure the RMS radius and molecular weight of the macromolecule, dynamic light scattering (DLS), also known as quasi-elastic light scattering,

(QELS) was also performed concurrently with the static light scattering experiment. When light scatters through macromolecules moving in solvent, the motion of the molecules impart a randomness to the phase of the scattered light, and causes a destructive or constructive interference when the scattered light of two or more particles are added together, which leads to time-dependent fluctuations in the intensity of the scattered light. A fast photon counter used in DLS measurement can be used to measure this fluctuation, which is directly related to the rate of diffusion of the molecule through solvent, and can be used to determine the hydrodynamic radius of a sample, as well as to further check the homogeneity of the sample.

In a typical MALS experiment performed to obtain results in this thesis, 100 μ L of protein at a concentration of 2 mg/mL was dialysed into SE buffer for 3 hours and overnight at 4 °C. To test the effects that biotin and ATP had on the dimerisation of holo-BPL, the protein was incubated with 10 x molar excess of both ligands prior to dialysis. After dialysis, the protein was injected and separated on a Superdex 200 10/300 size exclusion column (GE Healthcare) which had been equilibrated with the same buffer. MALS data was recorded on an in-line Dawn Heleos II 18-angle light scattering detector with an inline Optilab rEX refractive index monitor, while WyattQELS instrument was used for DLS (Wyatt Technology). Data was analysed with the ASTRA software and fitted to the Zimm model with an estimated dn/dc value of 0.183 mL/g.

2.9. Small angle X-ray scattering

Protein-protein complexes or protein-DNA complexes were subjected to small angle X-ray scattering (SAXS) experiments. Small angle X-ray scattering (SAXS) is a technique that is able to provide information of a molecule in regards to its size and shape (Neylon, 2008). SAXS is a contrast method, in which the scattering signal is derived from the difference in the average electron density of solute molecules and the bulk solvent (Jacques and Trewella, 2010).

In a typical SAXS experiment, a highly collimated X-ray beam is used to illuminate a sample in which the particles are monodisperse and identical, to produce scattering radiation that is recorded on a detector (Jacques and Trewella, 2010). The subsequent scattering pattern is usually described by intensity, $I(q)$, as a function of the amplitude of the scattering vector $q = (4\pi \sin \theta) / \lambda$, where λ is the wavelength of the radiation, and θ is half the angle between the incident and scattered radiation.

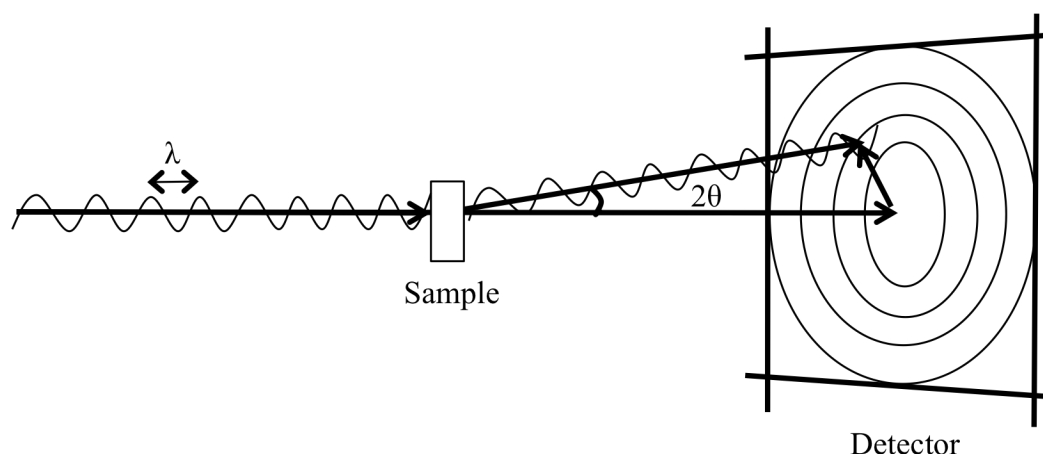


Figure 2.2 The setup of a typical SAXS experiment. An incident X-ray beam of wavelength λ is used to illuminate a monodisperse sample, which scatters light at an angle of 2θ , and the scattering pattern is recorded on a detector.

$I(q)$ versus q can provide information of the shape of a molecule in solution, but in order to obtain further details about the structure, an indirect Fourier transform of the scattering profile is used to calculate the pair-distribution function, $P(r)$, of the scattering particle.

$$I(q) = 4\pi \int_0^{D_{max}} P(r) \frac{\sin(qr)}{qr} dr$$

The $P(r)$ provides information of the distances between electrons in the scattering particles in the sample. $P(r)$ calculations are based on assumptions, such as $P(r) = 0$ when $r = 0$ and at the maximum distance present in the scattering particle, D_{max} . The $P(r)$ plot can also be used to estimate the radius of gyration (R_G), which is the square root of the average squared distance of each scatterer from the particle center, and provides information of the mass distribution within a particle. Two different molecules with the same molecular weight but different shapes will have different R_G values (Jacques and Trehwella, 2010). A useful method of calculating R_G is through the Guinier approximation, in which at small values of q :

$$I(q) = I(0)e^{\frac{-q^2 R_G^2}{3}}$$

and is measured via the slope of the plot $\log(I(q))$ versus q^2 . Typically for a small globular molecule, qR_G is less than 1.3, whilst for an elongated molecule, $qR_G < 0.8$. Lack of linearity in the Guinier plot can indicate problems with the sample, such as aggregation. The Guinier plot is also able to provide information of the intensity measured at $q=0$, $I(0)$. On an absolute

scale, $I(0)$ is the square of the number of the electrons in the scatterer, and can be used for molecular weight determination. $I(0)$ can also be calculated from $P(r)$, where,

$$I(0) = 4\pi \int_0^{D_{max}} P(r) dr$$

This is considered to be more advantageous as the $P(r)$ plot is calculated from the entire scattering curve, as opposed to the Guinier plot which only uses a few points in the low resolution region (Putnam et al., 2007).

SAXS data can be calculated from any sample, regardless of purity, presence of aggregate or homogeneity, hence much care must be taken during sample preparation to minimise ambiguity of the data. Firstly, the sample must be of high purity. The scattering signal is proportional to the square of the molecular weight, and hence samples with even small amounts of high molecular weight contaminants or aggregation are susceptible to data bias. The purity of the samples prior to SAXS experiments was analysed using SDS-PAGE analysis, and the presence of aggregation and monodispersity of the sample determined using MALS.

Due to SAXS being a contrast method, the buffer blank and the sample buffer must be perfectly matched for buffer subtraction from the sample in order to obtain accurate absorbance measurements and scattering data (Jacques and Trewhella, 2010). After protein purification, protein samples that were prepared for SAXS experiments were first dialysed into 1000 times excess of the buffer of choice at 4 °C for 3 hours, and again overnight with fresh buffer. After washing a 0.5 mL, 3000 MWCO centrifugal unit (Millipore) thoroughly once with milliQ water and 3 times with the overnight buffer, the protein was then concentrated to anywhere between 0.2 – 2 mg/mL. SAXS data collection was performed at the SAXS/WAXS beamline at the Australian Synchrotron, and data reduction was executed by the scatterBrain software developed by the Australian Synchrotron.

The subsequent reduced data was analysed using the ATSAS suite of software. PRIMUS was initially used to average and merge the data, calculate the R_G from the Guinier plot and $P(r)$, as well as to estimate D_{max} and the molecular weight of the sample (Konarev et al., 2003). 20 *ab initio* dummy atom models were created using DAMMIF with a 2-fold symmetry (Franke and Svergun, 2009). The *ab initio* models were averaged, merged and superposed with DAMAVER (Volkov and Svergun, 2003). The final *ab initio* model was superimposed with a Apo-BPL-BioO model built based on a previously solved crystal structure using

SUPCOMB (Kozin and Svergun, 2001). Theoretical scattering curves were calculated from the crystal structures coordinates and compared to the experimental data using CRY SOL (Svergun et al., 1995).

2.10. X-ray crystallography

X-ray crystallography is a technique used to determine the 3-dimensional structures of proteins or protein complexes, and was used to determine the structures of SaBPL in complex with its inhibitors. An attempt to crystallize other bacterial BPLs was also performed in this thesis. The crystals produced in these experiments were produced via the hanging drop method, in which 1 μ L of protein was mixed with 1 μ L of crystallization solution (comprised of precipitant, salts and buffer), and placed on a cover slip. The cover slip with the drop on it is suspended above a well containing the crystallization solution, and incubated at room temperature or 4°C for a period of time, from days to weeks, during which the water in the drop slowly vaporises and the precipitant concentration in the drop slowly increases until the optimal protein crystallization condition is obtained and a crystal is formed.

A protein crystal is a 3-dimensional array of a repetition of identical unit cells, with each unit cell containing one or more molecules. Once a crystal is produced, it is placed in front of a finely focused X-ray beam exposed to X-ray. Each exposure causes the molecules in the protein crystal to scatter the X-ray, and produces a diffraction pattern comprised of diffraction spots known as reflections. These reflections are caused by X-rays diffracting off the Bragg planes located in each unit cell (**Figure 2.3**), and can be described by Bragg's Law:

$2d \sin\theta = n\lambda$, where θ is the angle of diffraction and λ is the wavelength of the X-ray, and n is an integer.

Constructive interference of X-ray waves in different planes appears as spots (reflections) on the diffraction pattern, and in each diffraction experiment the intensities and position of each reflection can be measured. The position of each reflection can be used to determine its reciprocal lattice index hkl (integers that define a lattice plane), and an appropriate intensity assigned to it. The structure factor F_{hkl} , is proportional to the square root of the observed intensity of a reflection with hkl , and is the sum of the scattering caused by all the atoms in a unit cell.

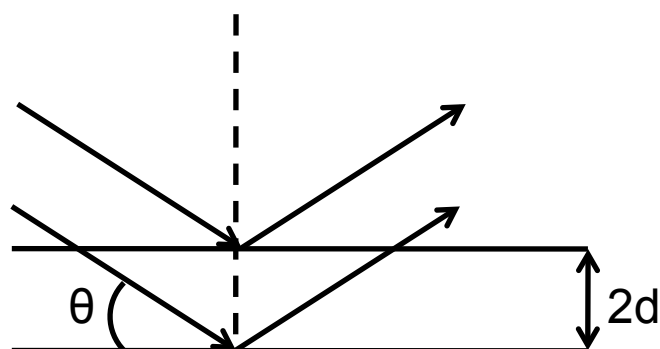


Figure 2.3 Incoming X-rays diffract (reflect) off the Bragg planes located in each unit cell. When the reflected waves from different planes are in phase with each other, they appear as a reflection spot on the diffraction pattern.

One set of reflections is insufficient to construct the whole structure, and in order to collect all the necessary data, the crystal must be rotated in small steps up to 180°, with a different diffraction image collected at each step. Prior to collecting a full data set, a small number of images are initially collected, and the reflections of these images are "indexed", in order to determine the symmetry or "space group" of the crystal, and can be used to decide the number of images to collect. After a full data set has been collected and indexed, the data is then compiled into a single file through integration, and merged to ensure that each reflection appearing in each data set has a consistent intensity scale.

The electron density of a crystal and the diffraction patterns are related through the Fourier transformation of the structure factors. The structure factor F_{hkl} can be expressed as

$$F(hkl) = \int_{\text{cell}} \rho(\mathbf{x}) e^{2\pi i(\mathbf{h}\cdot\mathbf{x})} d\mathbf{v}$$

, where $\rho(\mathbf{x})$ is the electron density, \mathbf{v} is the volume of the unit cell, and $\mathbf{h}\cdot\mathbf{x}$ is an integral multiple of the reciprocal axes.

Inverse transformation of the structure factor equation can produce the electron density equation:

$$\rho(\mathbf{x}) = 1/V \sum F(hkl) \exp(-2\pi i\mathbf{h}\cdot\mathbf{x})$$

, and can then be used to calculate an electron density map to fit a model of the protein structure.

To ensure that the final crystallographic model and experimental diffraction data were in agreement with each other, the R-factor was calculated during each round of refinement, in which

$$R = \frac{\sum ||F_{\text{obs}}| - |F_{\text{calc}}||}{\sum |F_{\text{obs}}|}$$

where F_{obs} is the observed structure factor, and F_{calc} is the calculated structure factor.

Each round of refinement improves the fit, and lowers the R-value, however, it is possible to over-fit the model and experimental data, but this problem is circumvented by using most of the data (or working set) to calculate the R-value, and the remaining data (test set) to calculate R-free, which is calculated in the same manner as the R-value but uses less data (Brunger, 1992). Models that are not over-interpreted generally have similar R-free and R-values, with R-free being slightly higher.

Crystallization of SaBPL in complex with its inhibitors is outlined in the corresponding chapters. In order to crystallize SaBPL in complex with *bioO*, 1.5 x molar excess of the 44-mer *bioO* was added to SaBPL in the presence of biotin, ATP and 10 mM MgCl_2 , and buffer exchanged into SE buffer with 10 mM MgCl_2 using an Amicon Ultra-15 Centrifugal Filter Units (Millipore). The resulting SaBPL-*bioO* complex was concentrated to an estimated protein concentration of 2.5, 5, 7.5 or 10 mg/mL. Protein crystallization trials were performed at the Monash Macromolecular Crystallization facility using broad screen crystallization kits, which included the Sigma Basic Crystallography Kit, Sigma Basic Extension Kit, Hampton PEG/ION, Hampton SaltRX, Hampton Index, Qiagen JCSG+ Suite, Qiagen PACT Suite and Emerald Bio Wizard I and II screens. Sitting drop crystallization trays were set up and subsequent drops visualised using the Rigaku CrystalMation system. Trays were stored at 4 °C, after which crystals appeared after several days. These conditions were further fine-tuned by varying both pH and precipitations concentration in order to create larger crystals for X-ray diffraction experiments.

Crystallographic data was collected at the macromolecular crystallography beamline at the Australian synchrotron using an ADSC Quantum 210r Detector. After a full data set had been collected, it was indexed, integrated and merged using XDS (Kabsch, 2010). XDS was also used to produce MTZ files required for structure refinement. Co-crystallization of SaBPL in complex with its inhibitors generated data sets that had the same space group and symmetry as a previously solved structure of SaBPL with its natural ligand biotin or biotinyl-

5'-AMP, and were isomorphous with these previously solved structures. Hence SaBPL in complex with biotin / biotinyl-5'-AMP was used as a starting model to refine the structures of SaBPL in complex with its inhibitors. PDB (www.rcsb.org) (Berman et al., 2000) and CIF (Hall et al., 1991) files for inhibitors were constructed using the PRODRG web interface (Schüttelkopf and van Aalten, 2004). PDB, CIF and MTZ files were loaded onto REFMAC for rigid body refinement (Murshudov et al., 1997). Holo SaBPL with waters and ligand removed from the PDB file was used as a starting model for refinement (PDB ID: 3V8K and 3V8L). After the initial refinement, models were then built using cycles of manual modeling with COOT (Emsley et al., 2010) and were further refined again using REFMAC. The quality of the final models was evaluated using MOLPROBITY (Chen et al., 2010)

Chapter 3 Biotin analogues with antibacterial activity as potent inhibitors for biotin protein ligase

The increasing rate of *Staphylococcus aureus* bacterial infections is a major threat in hospitals worldwide. In the United States alone, hospital acquired infections has tripled in the past 20 years, with more than half of these caused by methicillin-resistant strains (MRSA) (Deleo et al., 2010). Of considerable concern is the rapid emergence of community-associated MRSA, in which previously healthy young people are infected despite not being exposed to a healthcare setting (David and Daum, 2010). Across Australia and New Zealand, community-associated MRSA account for nearly 30% of MRSA infections (Turnidge et al., 2009). There are few antibiotics to treat MRSA infections, and the limitations of older glycopeptides and emergence of vancomycin-resistant MRSA strains, together with the lack of development in new antibiotics presents a future in which there is a high risk of untreatable for MRSA infections (David and Daum, 2010, Gould et al., 2012).

Essential enzymes required for the survival of bacterial cells thus provide an attractive target for drug design. One such enzyme is biotin protein ligase. Despite being found in all organisms, sequence comparison between human and bacterial BPL show there is enough difference to ensure that bacterial BPLs can be a potential drug target. More importantly, genetic studies have shown that the *Staphylococcus aureus* BPL (SaBPL) is an important enzyme required for cell survival (Chaudhuri et al., 2009, Forsyth et al., 2002, Ji et al., 2001).

SaBPL is a Class II BPL, and apart from its role in metabolism, it also serves to regulate the transcription of biotin biosynthetic genes. The structure of SaBPL in its apo, biotin, and biotinyl-5'-AMP (Btyl) bound form was previously solved in our lab. Apo-SaBPL is monomeric, with several disordered surface loops which undergo an disordered to ordered transition when biotin or Btyl is bound within their respective binding sites. Like the well-documented BirA, holo-SaBPL forms a homodimer.

In a bid to design a new antibiotic which targets SaBPL, the structure of biotin in complex with SaBPL had been determined by Pardini *et al.* (Pardini et al., 2013), and hence used as a starting point to design biotin analogues which had inhibitory activity against SaBPL. Biotin analogues with activity against SaBPL were designed and synthesized, and showed to have

selective activity against SaBPL. The mode of binding of these analogues with SaBPL was structurally determined using X-ray crystallography to pave way for future drug design.

3.1. Contribution of publication:

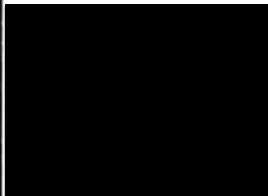
My contribution towards the publication which forms this chapter (Soares da Costa et al., 2012b) first includes the expression and purification of SaBPL for crystallography studies based on a method that has been previously described (Pendini et al., 2008b). I then crystallized SaBPL with biotin alcohol (compound 6, **PDB: 3RKY**) and biotin acetylene (compound 14 in publication by Soares da Costa et al. **PDB: 4HA8**) to which a group of readily available azides could be easily linked to. I collected X-ray data at the Australian Synchrotron, and analysed the data and solved the structures of SaBPL in complex with the inhibitors through several cycles of manual modeling using COOT and restrained refinement with REFMAC. I also analysed the protein-ligand interaction to support the further development of new SaBPL inhibitors. I was also involved in writing and editing the manuscript.

Monash University

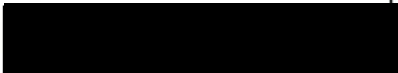



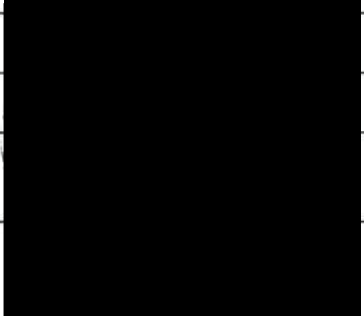
Declaration for Thesis **Chapter 3: Biotin analogues with antibacterial activity as potent inhibitors for biotin protein ligase**

Declaration by candidate:

In the case of **Chapter 3**, the nature and extent of my contribution to the work was the following:

Nature of contribution	Extent of contribution	Signature
1. Expression and purification of SaBPL for protein crystallography 2. Crystallization of SaBPL in complex with biotin analogue alcohol 6 and acetylene 14 3. Collection of crystallographic data, analysis of data and solving structures of SaBPL in complex with biotin acetylene 4. Analysis of protein-ligand interaction to support development of new ligands 5. Contributed to manuscript preparation	30 %	

The following co-authors contributed to the work. Co-authors who are students at Monash University must also indicate the extent of their contribution in percentage terms:

Name	Nature of contribution	Signature
Tatiana P. Soares da Costa ²	1. Expression and purification of SaBPL. 2. Performed biological assays with SaBPL (in vitro inhibition assays, SPR) 3. Contributed to manuscript preparation	
William Tieu ³	1. Design, synthesis and characterization of SaBPL inhibitors 2. Contributed to manuscript preparation	
Ondrej Zvarec ³	Design, synthesis and characterization of SaBPL inhibitors	
Jan M. Bell ⁴	Performed antibacterial susceptibility assays with clinical isolates of bacteria.	
John D. Turnidge ^{2,4}	Supervised antibacterial assays and interpretation of data.	
John C. Wallace ²	Contributed to manuscript preparation	
Grant W. Booker ²	Supervised biochemical assays and contributed to manuscript preparation	
Matthew C. J. Wilce ¹	1. Supervised X-ray crystallization studies, data collection and analysis. 2. Contributed to manuscript	

	preparation. 3. Overall project direction	
Andrew D. Abell ⁵	1. Supervised the design, synthesis and characterization of BPL inhibitors. 2. Contributed to manuscript preparation 3. Overall project direction	
Steven W. Polyak ²	1. Supervised the biochemical assays and data analysis. 2. Contributed to manuscript preparation. 3. Corresponding author on both manuscripts. 4. Overall project direction	

1. School of Biomedical science, Monash University, VIC 3800, Australia
2. School of Molecular and Biomedical Science, University of Adelaide, Adelaide, South Australia, 5005, Australia
3. School of Chemistry and Physics, University of Adelaide, Adelaide, South Australia 5005, Australia
4. SA Pathology at Women's and Children's Hospital, South Australia 5006, Australia

Declaration by co-authors:

- (1) the above declaration correctly reflects the nature and extent of the candidate's contribution to this work, and the nature of the contribution of each of the co-authors.
- (2) they meet the criteria for authorship in that they have participated in the conception, execution, or interpretation, of at least that part of the publication in their field of expertise;
- (3) they take public responsibility for their part of the publication, except for the responsible author who accepts overall responsibility for the publication;
- (4) there are no other authors of the publication according to these criteria;
- (5) potential conflicts of interest have been disclosed to (a) granting bodies, (b) the editor or publisher of journals or other publications, and (c) the head of the responsible academic unit; and
- (6) the original data are stored at the following location(s) and will be held for at least five years from the date indicated below:

Biotin Analogues with Antibacterial Activity Are Potent Inhibitors of Biotin Protein Ligase

Tatiana P. Soares da Costa,^{†,‡} William Tieu,^{‡,§} Min Y. Yap,[§] Ondrej Zvarec,^{‡,⊥} Jan M. Bell,^{||} John D. Turnidge,^{†,||} John C. Wallace,[†] Grant W. Booker,[†] Matthew C. J. Wilce,^{*,§} Andrew D. Abell,^{*,‡} and Steven W. Polyak^{*,†}

[†]School of Molecular and Biomedical Science and [‡]School of Chemistry and Physics, University of Adelaide, South Australia 5005, Australia

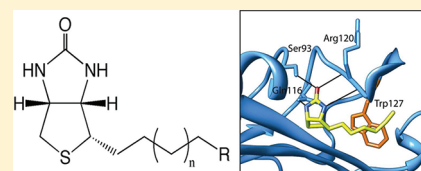
[§]School of Biomedical Science, Monash University, Victoria, 3800, Australia

^{||}Microbiology and Infectious Diseases Directorate, SA Pathology, Women's and Children's Hospital, South Australia 5006, Australia

S Supporting Information

ABSTRACT: There is a desperate need to develop new antibiotic agents to combat the rise of drug-resistant bacteria, such as clinically important *Staphylococcus aureus*. The essential multifunctional enzyme, biotin protein ligase (BPL), is one potential drug target for new antibiotics. We report the synthesis and characterization of a series of biotin analogues with activity against BPLs from *S. aureus*, *Escherichia coli*, and *Homo sapiens*. Two potent inhibitors with $K_i < 100$ nM were identified with antibacterial activity against a panel of clinical isolates of *S. aureus* (MIC 2–16 $\mu\text{g/mL}$). Compounds with high ligand efficiency and >20 -fold selectivity between the isozymes were identified and characterized. The antibacterial mode of action was shown to be via inhibition of BPL. The bimolecular interactions between the BPL and the inhibitors were defined by surface plasmon resonance studies and X-ray crystallography. These findings pave the way for second-generation inhibitors and antibiotics with greater potency and selectivity.

KEYWORDS: biotin protein ligase, enzyme, enzyme inhibitor, antibiotic, medicinal chemistry



It is imperative that we identify new antibiotics to combat drug-resistant bacteria.¹ One clinically important pathogen, *Staphylococcus aureus* (*S. aureus*), is responsible for more than half of all life-threatening bloodstream infections. *S. aureus* is challenging to control as it has the ability to rapidly acquire drug-resistance mechanisms in both hospitals and the community, making treatment increasingly difficult and costly.^{2,3} An important strategy to combat drug resistance is to develop novel antibiotic classes for which there are no pre-existing resistance mechanisms. This is becoming increasingly difficult, as most of the known chemical classes and obvious drug targets have been well explored, leaving the more challenging targets as a new frontier for antibacterial research. For example, little work has been done on essential bacterial enzymes that have mammalian paralogues due to perceived fears of possible toxicity.⁴ For these targets, selective inhibition is critical.

The ubiquitous enzyme biotin protein ligase (BPL) is one potential antibacterial target that has not yet been comprehensively investigated.⁵ BPL is responsible for the attachment of the cofactor biotin onto biotin-dependent enzymes. This proceeds in two partial reactions. Initially, the adenylated reaction intermediate biotinyl-5'-AMP is produced from biotin and ATP. Subsequently, the biotin moiety is covalently attached to the ϵ -amino group of a single target lysine residue present in the active site of biotin-dependent enzymes.⁶ Here, biotin is required to facilitate the carboxylation of metabolites.

Without the attached cofactor, biotin-dependent enzymes are catalytically inactive and unable to fulfill their critical metabolic roles. As all organisms possess between one and five biotin-dependent enzymes, all organisms require a BPL, as there are no alternative enzymes to perform protein biotinylation. One important biotin-dependent enzyme is acetyl CoA carboxylase, which catalyzes the first committed step in the fatty acid biosynthetic pathway.⁴ As this pathway is essential for bacterial cell membrane maintenance and biogenesis, they are a potential source of new antibiotic targets in certain Gram-positive bacteria such as *S. aureus*.⁷ *S. aureus* expresses a second biotin-dependent enzyme, pyruvate carboxylase, which catalyzes the conversion of pyruvate to oxaloacetate, thereby replenishing the TCA cycle.⁸ In addition to its biotin ligase activity, certain bacterial BPLs also function as transcriptional repressors, making them bifunctional proteins.⁹ BPL recognition sites in the *S. aureus* genome suggest that *S. aureus* BPL regulates expression of the enzymes in the biotin biosynthesis operon, as well as the biotin transport protein BioY.¹⁰ Thus, BPL is the master regulator protein of all biotin-mediated events in bacteria and, therefore, an attractive new antibiotic drug target.

In this paper, we present a novel series of biotin analogues with potent inhibitory activity against SaBPL and antibacterial

Received: May 1, 2012

Accepted: May 23, 2012

Published: May 23, 2012



activity against clinical strains of *S. aureus*. The mode of small molecule binding to SaBPL was defined by X-ray crystallography and surface plasmon resonance studies. A few examples of biotin analogues with antibacterial activity do appear in the literature, including the natural product α -dehydrobiotin¹¹ and an analogue chemically modified at the N1 position required for binding carbon dioxide (Figure 1).¹² These function by first

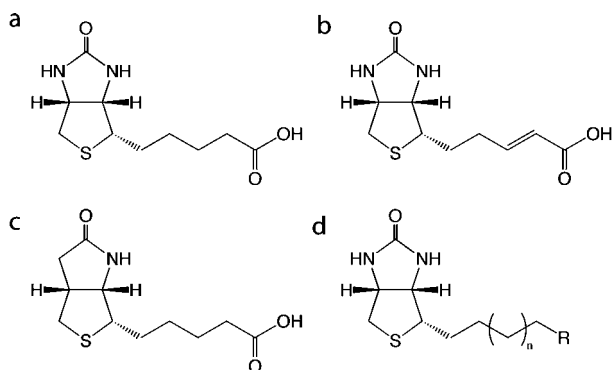


Figure 1. Chemical structures of (a) biotin **1** and its analogues (b) α -dehydrobiotin, (c) N1 substituted biotin, and (d) the pharmacophore investigated in this study.

being incorporated into a biotin-dependent enzyme where they abolish catalytic activity by preventing the binding or transfer of carbon dioxide.^{13–15} Importantly, these analogues are either not specific or loose broad-spectrum antibacterial activity when assayed in rich growth media containing biotin.^{11,14} Moreover, their activity has not been linked to the inhibition of BPL as they only transiently occupy the active site of this enzyme. A more effective approach for antibiotic discovery requires high-affinity inhibitors that bind directly and specifically to the bacterial BPL target, thereby preventing all protein biotinylation. A proof of concept for this approach to antibiotic discovery has been reported recently, targeting the BPLs from *Mycobacterium tuberculosis* and *S. aureus*.^{5,16} In this current paper, we investigated biotin analogues with a view to

identifying BPL inhibitors with improved ligand efficiency (LE). Our findings provide new lead structures for further optimization, for example, **5** and **16**.

We began our search by screening analogues of biotin for their inhibitory properties. The compounds were assayed in an *in vitro* biotinylation assay measuring the incorporation of radiolabeled biotin into protein.¹⁷ Purified recombinant BPLs from the Gram-positive bacterium *S. aureus* (SaBPL¹⁸), the Gram-negative bacterium *Escherichia coli* (EcBPL¹⁹), and *Homo sapiens* (HsBPL²⁰) were all assessed to investigate potency and species selectivity (Table 1). K_i values were calculated assuming that the mechanism of action was competitive with biotin, in agreement with Lineweaver–Burk analysis (Supporting Information, Figure S1).²¹ This identified biotinol (**6**) as a pan inhibitor with K_i values of 3.4–4 μ M for all three BPLs (Table 1). The binding mechanism was confirmed by solving the X-ray crystal structure of SaBPL in complex with **6** (Figure 2a).

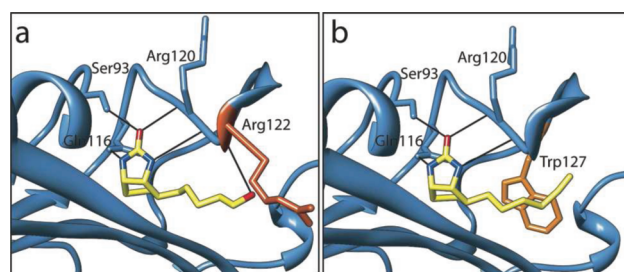


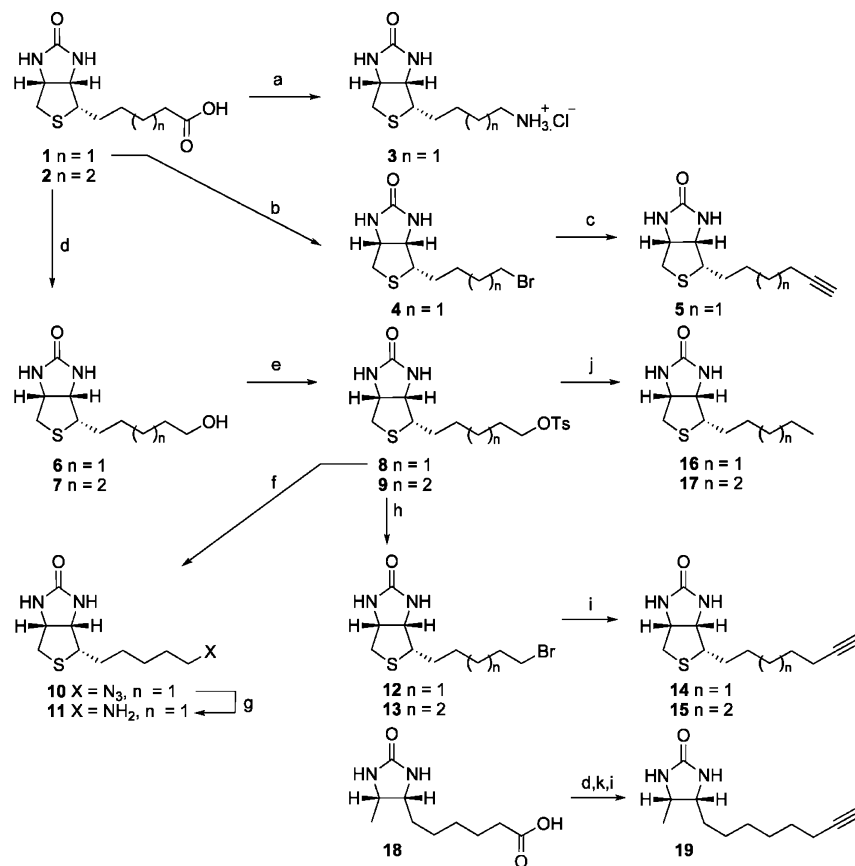
Figure 2. X-ray structures of inhibitors in complex with BPL. *S. aureus* BPL was crystallized in complex with biotin analogues alcohol **6** (a) and acetylene **14** (b). The hydrogen-bonding interactions with the inhibitors are shown.

Consistent with other BPL crystal structures that appear in the protein database, our data revealed the biotin-binding pocket of SaBPL to be relatively small (187 Å³) with a hydrophobic cavity encasing the polar ureido and thiophene rings of biotin. This suggested limited opportunity for chemical modification of the biotin heterocycle in our inhibitor design. A narrow

Table 1. SAR Data for the Biotin Analogue Series^a

ID	<i>n</i>	R	<i>S. aureus</i>		<i>E. coli</i>		<i>H. sapiens</i>	selectivity ^c
			K_i (μ M)	LE ^b	K_i (μ M)	LE ^b	K_i (μ M)	
6	2	OH	3.37 \pm 0.3	0.52	3.96 \pm 0.4	0.51	3.85 \pm 0.3	1.1/1.0/1.2
7	3	OH	>20	ND	>20	ND	>20	ND
3	1	NH ₂	>20	ND	>20	ND	>20	ND
11	2	NH ₂	>20	ND	>20	ND	>20	ND
16	1	CH ₃	0.05 \pm 0.01	0.69	1.10 \pm 0.12	0.56	0.14 \pm 0.02	2.8/7.9/22
17	2	CH ₃	0.52 \pm 0.06	0.56	7.30 \pm 1.9	0.46	6.43 \pm 1.4	12.4/1.1/14
5	1	C \equiv CH	0.08 \pm 0.01	0.67	0.90 \pm 0.1	0.57	0.2 \pm 0.03	2.5/4.5/11.3
14	2	C \equiv CH	0.3 \pm 0.05	0.58	7.33 \pm 1.0	0.46	3.50 \pm 0.5	11.7/2.1/24.4
15	3	C \equiv CH	2.40 \pm 0.02	0.47	20.0 \pm 0.3	0.39	12.0 \pm 1.83	5/1.7/8.3

^aA SAR series was investigated based upon the pharmacophore shown above. Compounds were assayed against BPLs from three species and where inhibition was observed K_i values are reported. Each K_i value is the mean (\pm standard error) of three independent experiments. ^bLE is ligand efficiency in kcal K^{−1} mol^{−1} per heavy atom. ^cSelectivity is expressed as ratios of K_i values. Sa is *S. aureus* BPL, Ec is *E. coli* BPL, and Hs is *H. sapiens* BPL.

Scheme 1^a

^aConditions and reagents: (a) (i) DPPA, Et₃N, THF; (ii) 6 N HCl. (b) (i) (COCl)₂, DCM (ii) 2-pyridione, 1:9 (BrCCl₃:DMF), 80 °C. (c) Li-acetylide EDA complex, DMSO, 15 °C. (d) (i) SOCl₂, MeOH; (ii) LiAlH₄, THF. (e) TsCl, py. (f) NaN₃, DMF. (g) (i) PPh₃, THF; (ii) H₂O. (h) LiBr, 2-butanone. (i) Li-acetylide EDA complex, DMSO, 15 °C. (j) LiAlH₄, THF.

hydrophobic tunnel accommodates the valeric acid side chain with the carboxyl group being solvent exposed to provide a prime target for derivitisation. The protein:ligand interaction is stabilized through hydrogen bonding between the hydroxyl group (present on biotin and alcohol **6**) and an NH backbone amide of Arg 122 (Figure 2a). A series of analogues were proposed to further explore inhibition of BPL as a route to novel antibacterial agents. Our hypothesis was that derivatization of the carboxyl moiety of biotin would produce tight-binding inhibitors with increased potency and selectivity. Thus, to establish optimal binding, modifications of biotin were investigated that either replaced the carboxyl functionality with motifs capable of forming direct contacts with BPL as in compounds **3**, **16**, and **5**, and/or modified the length of the carbon chain (compounds **7**, **11**, **17**, **14**, and **15**).

The syntheses of all of the derivatives are shown in Scheme 1. Biotin **1** and homobiotin **2**⁵ were first esterified, and the resulting methyl esters reduced with LiAlH₄ to give the alcohols **6** and **7**, respectively. Tosylation followed by bromination then gave **12** and **13**, respectively, which were separately reacted with lithium-acetylide EDA complex to give the two acetylenes **14** and **15**.⁵ The tosylate **8** was also reacted with NaN₃ to give the azide **10**, which then gave the amine **11** using Staudinger reduction with PPh₃ followed by hydrolysis of the aza-ylide intermediate. The two tosylates **8** and **9** were also reduced with LiAlH₄ to give the alkyl derivatives **16** and **17**, respectively. Curtius rearrangement of biotin **1**, on reaction with diphenylphosphoryl azide in *tert*-butanol, followed by treatment

with 6 N aqueous HCl, gave amine **3**.²² Finally, bromide **4** was prepared by Barton decarboxylation of **1** using 2-pyridione, which on treatment with lithium-acetylide EDA complex gave acetylene **5**.⁵

The biotin derivatives were tested against the three BPLs using an *in vitro* biotinylation assay (Table 1) to reveal potent and selective inhibitors of SaBPL. Interestingly, increasing the chain length of **6** by one carbon resulted in an inactive compound (**7**). The crystallographic data for SaBPL bound to **6** as discussed earlier supports this observation, where the key hydrogen bond between the hydroxyl group of **6** and the enzyme is incompatible with the longer chain length. Replacement of the hydroxyl group of **6** with an amine, as in **3** and **11**, removed all inhibitory activity. This was somewhat surprising given that the amine would be expected to have similar polarity and hydrogen-bonding properties to the hydroxyl group of **6**. This observation may simply reflect the relative pK_a values of the two groups. We also assayed the synthetic intermediate bromides (**4**, **12**, and **13**), and these were all devoid of activity, presumably due to the steric bulk of the halides.

We next investigated hydrophobic groups (alkyl and acetylene) at the terminus of the carbon chain of biotin (see **5** and **14–17**) that we anticipated might be accommodated by the hydrophobic nature of the biotin pocket. Most notably **5**, **14**, **16**, and **17** exhibited up to a 20-fold selectivity for SaBPL over EcBPL and HsBPL. Interestingly, removal of the tetrahydrothiophane ring in **14** removed all activity (see **18**

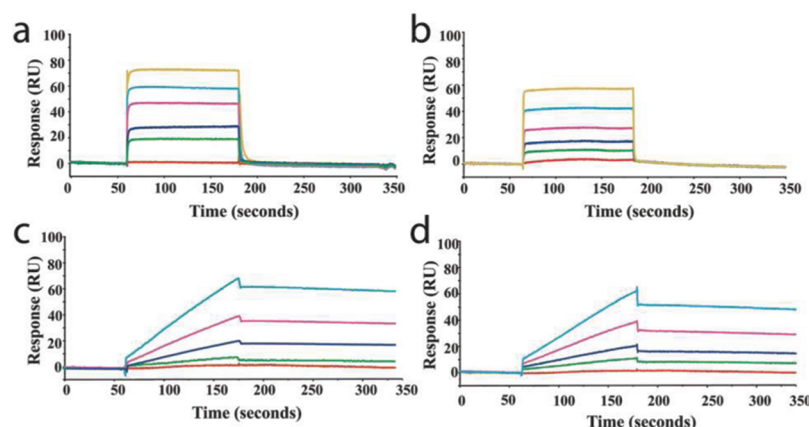


Figure 3. SPR analysis of BPL inhibitor binding. Surface plasmon resonance sensorgrams are shown for the binding of (a) biotin, (b) **6**, (c) **16**, and (d) **5** to immobilized *S. aureus* BPL. Varying concentrations of the inhibitors were included in the running buffer, and analysis was performed as described in the Supporting Information.

and **19**), highlighting the importance of the fused bicyclic ring of biotin. In the alkyl series, **16** was the most potent inhibitor for all three enzymes (*SaBPL*, $K_i = 0.05 \mu\text{M}$) and displayed the greatest LE ($0.69 \text{ kcal K}^{-1} \text{ mol}^{-1}$ per heavy atom). Again, a longer chain length (see **17**) decreased potency by ≈ 10 -fold for the two bacterial enzymes and by 45-fold for the human enzyme. However, significant improvement in selectivity was apparent (see Table 1). The most potent compound in the acetylene series was again that with the shortest carbon chain (see **5**, $K_i = 0.08 \mu\text{M}$ and LE $0.67 \text{ kcal K}^{-1} \text{ mol}^{-1}$ per heavy atom for *SaBPL*) with an observed decrease in potency and LE on increasing the chain length from $n = 1$ to 3 (see compounds **14** and **15** in Table 1). Once again, the most selective compound was where $n = 2$ (see **14**; with 20- and 10-fold selectivity for *SaBPL* against *E. coli* and *H. sapiens* BPL, respectively). The acetylene **5** retained significant potency against the target *SaBPL* with a $K_i = 0.30 \mu\text{M}$. The structure of biotin acetylene (**14**) in complex with *SaBPL* was determined to confirm both the mode of binding and our proposal that substitution of the carboxyl group of biotin with hydrophobic functionalities would promote binding to the target. In agreement with the hypothesis, the complex was stabilized through a direct hydrophobic interaction between the acetylene and the Trp 127 (Figure 2b). Given that we observed selectivity in this series, we propose that this interaction should be further explored in inhibitor design. Our data strongly suggest that the biotin pockets of the three BPLs are not as structurally conserved as previously proposed, and this could be explored to improve potency and selectivity.

Ideally, our antibacterial compounds should have a relatively high affinity for BPL through slow dissociation from the binding pocket. To study this, *SaBPL* was immobilized on a sensor chip for subsequent binding studies by surface plasmon resonance. Biotin and analogues **6**, **16**, and **5** were then separately passed across the surface, providing quantitative analysis of association and dissociation rates. The binding of biotin to *SaBPL* (Figure 3a) was found to exhibit rapid on and off rates outside the range for quantitative evaluation. Hence, the K_D ($9.2 \pm 1.4 \mu\text{M}$) was calculated using steady-state affinity. This observation is consistent with a two-step binding mechanism that has been reported for *E. coli* BPL.²³ Initially, the enzyme and biotin rapidly form a "collision complex" that is followed by a slower conformational change to BPL that is both rate-limiting in the binding mechanism and necessary to

stabilize the enzyme–biotin complex. Alcohol analogue **6** showed similar kinetics of binding as biotin (Figure 3b, $K_D = 2.5 \pm 0.3 \mu\text{M}$), representative of a dynamic equilibrium between the free enzyme and the collision complex but unable to overcome the rate-limiting conformational change. In contrast, **16** and **5** displayed slower association ($k_a = 43.2 \pm 2.3 \times 10^3 \text{ M}^{-1} \text{ s}^{-1}$ and $41.2 \pm 2.3 \times 10^3 \text{ M}^{-1} \text{ s}^{-1}$, respectively) and dissociation rates relative to both biotin and **6** (**16** $k_d = 2.80 \pm 0.20 \times 10^{-3} \text{ s}^{-1}$ and **5** $3.40 \pm 0.30 \times 10^{-3} \text{ s}^{-1}$), thereby contributing to their significantly higher affinities (**16** $K_D = 0.06 \pm 0.01 \mu\text{M}$, Figure 3c, and **5** $K_D = 0.08 \pm 0.01$, Figure 3d). The different association and dissociation kinetics displayed by **16** and **5** as compared to biotin and **6** imply that the modes of binding are mechanistically different. We propose that unlike biotin, **16** and **5** do indeed induce the conformational changes to *SaBPL* that are necessary to retard the inhibitors from vacating their binding pockets. For antibacterial discovery, inhibitors that possess high occupancy rates on their bacterial targets are desirable.

Finally, the antibacterial activity of the most potent biotin analogues was determined using antimicrobial growth assays. These studies revealed significant bacteriostatic activity against both Gram-positive and Gram-negative bacteria. Compounds **16** and **5** were the most potent against clinical isolates of *S. aureus* with MICs in the range of 2–16 $\mu\text{g/mL}$, including methicillin-susceptible and -resistant strains (Table 2). This is consistent with the fact that these two derivatives were the most potent inhibitors of *SaBPL* (Table 1). Derivative **17**, containing an extra carbon in the side chain relative to **16**, was less active against MSSA and MRSA, but interestingly, it was weakly active against vancomycin-resistant *Enterococcus* (MIC 32 $\mu\text{g/mL}$).

Table 2. Antibacterial Susceptibility Testing^a

strain	range ($\mu\text{g/mL}$)	MIC ₅₀ ($\mu\text{g/mL}$)		MIC ₉₀ ($\mu\text{g/mL}$)	
		16	5	16	5
MSSA ($n = 8$)	4–16	8	8	16	16
MRSA ($n = 8$)	4–16	8	8	16	16
coagulase negative <i>Staphylococci</i> ($n = 7$)	2–>64	2	4	8	8

^aMICs are shown for a library of *S. aureus* clinical isolates of coagulase negative and positive strains, including methicillin-sensitive (MSSA) and -resistant (MRSA) subtypes.

Compounds **16** and **5** were also active against coagulase negative *Staphylococci* strains. The mechanism of antibacterial action was assessed with a complementation assay using **5** with an *E. coli* K12 strain engineered to overexpress the BPL target. Bacterial growth was monitored over 14 h in the absence or presence of **5** at 32 $\mu\text{g/mL}$ (Figure S2 in the Supporting Information). Overexpression of *EcBPL* completely alleviated antibacterial activity, strongly implying that the drug target is indeed BPL. Finally, the toxicity of the compounds was addressed in a mammalian cell culture model using HepG2 cells. These studies showed that the metabolic activity of the cells was unaffected when treated with 64 $\mu\text{g/mL}$ of **7**, **16**, **17**, **5**, **14**, and **15**.

Here, we report new data that supports the hypothesis that BPL is a druggable antibacterial target in vitro. Our data demonstrate that BPL inhibitors with favorable in vitro properties also show significant antibacterial activity against clinical isolates of methicillin-sensitive and -resistant *S. aureus*. It is noteworthy that there was a positive correlation between slow enzyme:inhibitor dissociation kinetics and potent antibacterial activity. The quantitative data reported here help to define the target product profile necessary for future chemical optimization. Our biotin alkyl and acetylene series represent new chemical scaffolds with high LE for chemical development toward new antibacterial agents, a point that we have begun to address as reported in our earlier publication.⁵

■ ASSOCIATED CONTENT

Supporting Information

Assay and synthetic procedures and data for selected compounds. This material is available free of charge via the Internet at <http://pubs.acs.org>.

■ AUTHOR INFORMATION

Corresponding Author

*Tel: +61 3 9902 9244. E-mail: [REDACTED] (M.C.J.W.). Tel: +61 8 8313 5652. Fax: +61 8 8313 4358. E-mail: [REDACTED] (A.D.A.). [REDACTED] (S.W.P.).

Present Address

[REDACTED]

Author Contributions

[#]These authors contributed equally. The manuscript was written through contributions of all authors. All authors have given approval to the final version of the manuscript.

Funding

We acknowledge funding from the Australian Research Council and National Health and Medical Research Council of Australia (application number 1011806), BioInnovationSA, and the University of Adelaide's Commercial Accelerator Scheme.

Notes

The authors declare no competing financial interest. M.C.J.W. is a National Health and Medical Research Council Senior Research Fellow.

■ ACKNOWLEDGMENTS

Diffraction data were collected on the MX1 beamline at the Australian Synchrotron, Victoria, Australia.

■ ABBREVIATIONS

BPL, biotin protein ligase; *Ec*, *Escherichia coli*; *Hs*, *Homo sapiens*; LE, ligand efficiency; MIC, minimal inhibitory concentration; *Sa*, *Staphylococcus aureus*

■ REFERENCES

- (1) Cooper, M. A.; Shlaes, D. Fix the antibiotics pipeline. *Nature* **2011**, 472 (7341), 32.
- (2) Allegranzi, B.; Bagheri Nejad, S.; Combescure, C.; Graafmans, W.; Attar, H.; Donaldson, L.; Pittet, D. Burden of endemic health-care-associated infection in developing countries: Systematic review and meta-analysis. *Lancet* **2011**, 377 (9761), 228–241.
- (3) Jean, S. S.; Hsueh, P. R. High burden of antimicrobial resistance in Asia. *Int. J. Antimicrob. Agents* **2011**, 37 (4), 291–295.
- (4) Polyak, S. W.; Abell, A. D.; Wilce, M. C.; Zhang, L.; Booker, G. W. Structure, function and selective inhibition of bacterial acetyl-CoA carboxylase. *Appl. Microbiol. Biotechnol.* **2012**, 93 (3), 983–992.
- (5) Soares da Costa, T. P.; Tieu, W.; Yap, M. Y.; Pendini, N. R.; Polyak, S. W.; Sejer Pedersen, D.; Morona, R.; Turnidge, J. D.; Wallace, J. C.; Wilce, M. C.; Booker, G. W.; Abell, A. D. Selective inhibition of biotin protein ligase from *Staphylococcus aureus*. *J. Biol. Chem.* **2012**, 287, 17823–17832.
- (6) Pendini, N. R.; Bailey, L. M.; Booker, G. W.; Wilce, M. C.; Wallace, J. C.; Polyak, S. W. Microbial biotin protein ligases aid in understanding holocarboxylase synthetase deficiency. *Biochim. Biophys. Acta* **2008**, 1784 (7–8), 973–982.
- (7) Parsons, J. B.; Rock, C. O. Is bacterial fatty acid synthesis a valid target for antibacterial drug discovery? *Curr. Opin. Microbiol.* **2011**, 14 (5), 544–549.
- (8) Jitrapakdee, S.; St. Maurice, M.; Rayment, I.; Cleland, W. W.; Wallace, J. C.; Attwood, P. V. Structure, mechanism and regulation of pyruvate carboxylase. *Biochem. J.* **2008**, 413 (3), 369–387.
- (9) Beckett, D. Biotin sensing at the molecular level. *J. Nutr.* **2009**, 139 (1), 167–170.
- (10) Rodionov, D. A.; Mironov, A. A.; Gelfand, M. S. Conservation of the biotin regulon and the BirA regulatory signal in Eubacteria and Archaea. *Genome Res.* **2002**, 12 (10), 1507–1516.
- (11) Hanka, L. J.; Bergy, M. E.; Kelly, R. B. Naturally occurring antimetabolite antibiotic related to biotin. *Science* **1966**, 154 (757), 1667–1668.
- (12) Ampacher, D. R.; Blanchard, C. Z.; Fronczek, F. R.; Saraiva, M. C.; Waldrop, G. L.; Strongin, R. M. Synthesis of a reaction intermediate analogue of biotin-dependent carboxylases via a selective derivatization of biotin. *Org. Lett.* **1999**, 1 (1), 99–102.
- (13) Blanchard, C. Z.; Ampacher, D.; Strongin, R.; Waldrop, G. L. Inhibition of biotin carboxylase by a reaction intermediate analog: Implications for the kinetic mechanism. *Biochem. Biophys. Res. Commun.* **1999**, 266 (2), 466–471.
- (14) Levert, K. L.; Waldrop, G. L.; Stephens, J. M. A biotin analog inhibits acetyl-CoA carboxylase activity and adipogenesis. *J. Biol. Chem.* **2002**, 277 (19), 16347–16350.
- (15) Piffeteau, A.; Dufour, M. N.; Zamboni, M.; Gaudry, M.; Marquet, A. Mechanism of the antibiotic action of alpha-dehydrobiotin. *Biochemistry* **1980**, 19 (13), 3069–3073.
- (16) Duckworth, B. P.; Geders, T. W.; Tiwari, D.; Boshoff, H. I.; Sibbald, P. A.; Barry, C. E., 3rd; Schnappinger, D.; Finzel, B. C.; Aldrich, C. C. Bisubstrate adenylation inhibitors of biotin protein ligase from *Mycobacterium tuberculosis*. *Chem. Biol.* **2011**, 18 (11), 1432–1441.
- (17) Polyak, S. W.; Chapman-Smith, A.; Brautigan, P. J.; Wallace, J. C. Biotin protein ligase from *Saccharomyces cerevisiae*. The N-terminal domain is required for complete activity. *J. Biol. Chem.* **1999**, 274 (46), 32847–32854.
- (18) Pendini, N. R.; Polyak, S. W.; Booker, G. W.; Wallace, J. C.; Wilce, M. C. Purification, crystallization and preliminary crystallographic analysis of biotin protein ligase from *Staphylococcus aureus*. *Acta Crystallogr., Sect. F: Struct. Biol. Cryst. Commun.* **2008**, 64 (Part 6), 520–523.

- (19) Chapman-Smith, A.; Mulhern, T. D.; Whelan, F.; Cronan, J. E., Jr.; Wallace, J. C. The C-terminal domain of biotin protein ligase from *E. coli* is required for catalytic activity. *Protein Sci.* **2001**, *10* (12), 2608–2617.
- (20) Mayende, L.; Swift, R. D.; Bailey, L. M.; Soares da Costa, T. P.; Wallace, J. C.; Booker, G. W.; Polyak, S. W. A novel molecular mechanism to explain biotin-unresponsive holocarboxylase synthetase deficiency. *J. Mol. Med. (Berlin)* **2012**, *90* (1), 81–88.
- (21) Cleland, W. W. Steady State Kinetics. *The Enzymes* **1970**, *2*, 1.
- (22) Szalecki, W. Synthesis of norbiotinamine and its derivatives. *Bioconjugate Chem.* **1996**, *7* (2), 271–273.
- (23) Xu, Y.; Nenortas, E.; Beckett, D. Evidence for distinct ligand-bound conformational states of the multifunctional *Escherichia coli* repressor of biotin biosynthesis. *Biochemistry* **1995**, *34* (51), 16624–16631.

BIOTIN ANALOGUES WITH ANTIBACTERIAL ACTIVITY ARE POTENT INHIBITORS OF BIOTIN PROTEIN LIGASE

Tatiana P. Soares da Costa †, William Tieu ‡, Min Y. Yap", Ondrej Zvarec ‡, Jan Bell §, John D. Turnidge †§, John C. Wallace †, Grant W. Booker †, Matthew C. J. Wilce", Andrew D. Abell ‡, Steven W. Polyak †.

† School of Molecular and Biomedical Science, University of Adelaide, South Australia 5005, Australia.

‡ School of Chemistry and Physics, University of Adelaide, South Australia 5005, Australia.

" School of Biomedical Science, Monash University, Victoria, Australia.

§ Microbiology and Infectious Diseases Directorate, SA Pathology, Women's and Children's Hospital, South Australia 5006, Australia.

Supporting information

Contents

Supporting Experimental Methods	S2
<i>General synthetic chemistry methods</i>	S2
<i>Specific chemical synthesis and characterisation methods</i>	S2
<i>Protein Expression and purification</i>	S7
<i>Nucleic acid manipulations</i>	S7
<i>X ray crystallography</i>	S7
<i>In vitro biotinylation assays</i>	S8
<i>Surface plasmon resonance</i>	S9
<i>Antibacterial activity evaluation</i>	S10
<i>Assay for cytotoxicity</i>	S10
Supporting References	S11
Supporting Figures	S13
Supporting Table 1	S15

Supporting Experimental Methods

General synthetic chemistry methods

All reagents were from standard commercial sources and of reagent grade or as specified. Solvents were from standard commercial sources and used without further treatment, except for anhydrous THF and anhydrous dichloromethane that were dried and distilled according to reported procedures.¹ Reactions were monitored by ascending TLC using precoated plates (silica gel 60 F₂₅₄, 250 µm, Merck, Darmstadt, Germany), spots were visualised under ultraviolet light at 254 nm and with basic potassium permanganate dip. Column chromatography was performed with silica gel (40-63 µm 60 Å, Davisil, Grace, Germany). RP-HPLC was performed on HP Series 1100 with Phenomenex Gemini C18 5 µm (250 x 4.60 mm). ¹H and ¹³C NMR spectra were recorded on a Varian Gemini 2000 (300 MHz) or a Varian Inova 600 MHz. Chemical shifts are given in ppm (δ) relative to the residue signals (DMSO-d₆ was 2.50 ppm for ¹H and 39.55 ppm for ¹³C and CDCl₃ was 7.26 ppm for ¹H and 77.23 ppm for ¹³C. High-resolution mass spectra (HRMS) were recorded on a Thermo Fisher Scientific LTQ orbitrap FT MS equipment (Δ < 2 ppm) at Adelaide Proteomics Centre, the University of Adelaide. Purity of biologically assayed compounds were determined using ¹H NMR or analytical RP-HPLC (>90%). Compounds **2** – **7** and **12** - **15** were synthesized as previously reported.²⁻⁴

Specific chemical synthesis and characterisation methods

(3aS,6aR)-4-(5-Azidopentyl)-1,3,3a,4,6,6a-hexahydrothieno[3,4-d]imidazol-2-one (Compound 10).

To a solution of biotin tosylate **8**⁵ (151 mg, 0.39 mmol) in DMF (2 mL) was added sodium azide (32 mg, 0.48 mmol) and solution was stirred overnight under nitrogen atmosphere. The reaction mixture was poured into water (20 mL) and extracted with dichloromethane (3 x 25 mL). The organic layers were pooled and washed with brine (1 x 75 mL), dried over Na₂SO₄, filtered and concentrated *in vacuo*. The residue was purified by silica gel chromatography eluting with 5% methanol in dichloromethane

to give a white solid (86 mg, 86%). ¹H NMR (300 MHz, CDCl₃): 6.57 (1H, bs), 6.46 (1H, bs), 4.38-4.42 (1H, m), 4.20-4.24 (1H, m), 3.40 (2H, t, *J* = 6.9 Hz), 3.16-3.22 (1H, m), 2.91 (1H, dd, *J* = 5.1, 12.6 Hz), 2.66 (1H, d, *J* = 12.6 Hz), 1.37-1.78 (8H, m); ¹³C NMR (300 MHz, DMSO-*d*₆): δ 164.30, 62.31, 60.35, 55.91, 51.56, 40.62, 28.93, 28.87, 28.71, 26.85.

(3a*S*,6a*R*)-4-(5-Aminopentyl)-1,3,3a,4,6,6a-hexahydrothieno[3,4-*d*]imidazol-2-one (Compound 11)

To a solution of biotin azide **10**⁶ (80 mg, 0.31 mmol) in THF (2 mL) was added triphenylphosphine (106 mg, 0.41 mmol) and the solution was stirred at ambient temperature for 1 h, followed by addition of water (2 mL) and stirred for a further 3 h at 60 °C. The reaction mixture was filtered and the filtrand was diluted with water (20 mL) and extracted with dichloromethane (3 x 25 mL). The organic layer were pooled, dried over Na₂SO₄, filtered and concentrated *in vacuo*. The residue was purified by silica gel chromatography eluting with 10% methanol in dichloromethane to give a white solid (13 mg, 18%). ¹H NMR (300 MHz, CDCl₃): 6.51 (0.5H, bs, C(O)NH), 6.41 (0.5H, bs), 4.33-4.38 (1H, m), 4.15-4.20 (1H, m), 3.59 (2H, bs), 3.14-3.16 (1H, m), 2.87 (1H, dd, *J* = 7.5, 12.6 Hz), 2.56-2.64 (3H, m), 1.25-1.74 (8H, m); ¹³C NMR (300 MHz, DMSO-*d*₆): 163.14, 79.61, 61.47, 59.64, 55.94, 41.35, 32.35, 28.87, 28.70, 26.74. HRMS calcd. for (M⁺ + H) C₁₁H₂₀N₂OSNa: requires 230.1322, found 230.1319.

(3a*S*,6a*R*)-4-Hexyl-1,3,3a,4,6,6a-hexahydrothieno[3,4-*d*]imidazol-2-one (Compound 16)

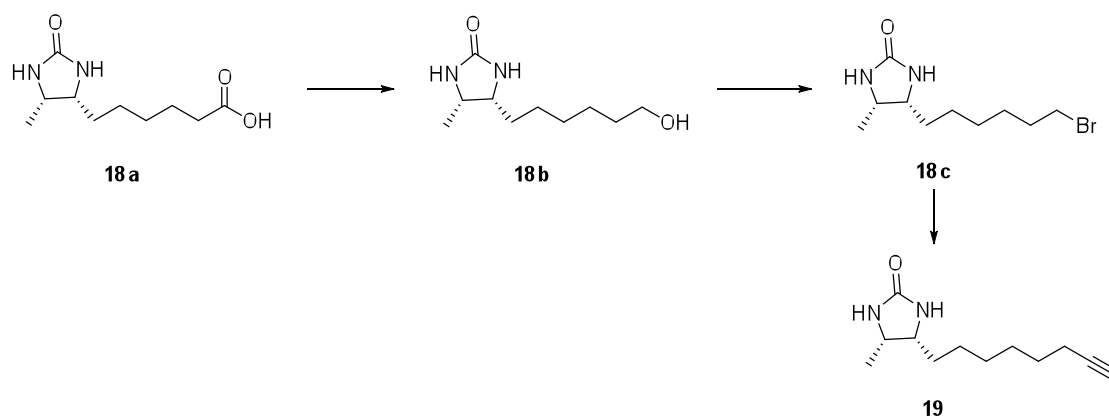
To a solution of biotin tosylate **8**⁵ (52 mg, 0.14 mmol) in anhydrous THF (2 mL) was added lithium aluminium hydride (15 mg, 0.41 mmol) and the solution was stirred under reflux for 3 h. The reaction mixture was cooled to ambient temperature and were added methanol (1 mL) and saturated aqueous sodium sulphate (2 mL), followed by concentration *in vacuo* and dissolving with 1:1 dichloromethane and methanol (15 mL) and stirring for 30 min. The solution was filtered and the filtrate was concentrated *in vacuo* and purified by silica gel chromatography eluting with 3%

methanol in dichloromethane to give an off white solid (16 mg, 56%). **¹H NMR** (300 MHz, CDCl₃): δ 5.27 (1H, bs), 5.16 (1H, bs), 4.49-4.53 (1H, m); 4.29-4.33 (1H, m), 3.14-3.20 (1H, m), 2.94 (1H, dd, *J* = 4.8, 12.6 Hz), 2.73(1H, d, *J* = 12.6 Hz), 1.62-1.70 (2H, m), 1.28-1.45 (4H, m), 0.89 (3H, t, *J* = 6.6 Hz); **¹³C NMR** (300 MHz, DMSO-*d*₆): δ 163.16, 62.23, 60.41, 55.81, 40.92, 31.93, 29.52, 29.34, 28.98, 22.90, 14.39. **HRMS** calcd. for (M + H) C₁₀H₁₉N₂OS: requires 215.1218, found 215.1217.

(3a*S*,6a*R*)-4-Heptyl-1,3,3a,4,6,6a-hexahydrothieno[3,4-*d*]imidazol-2-one
(Compound 17)

To a solution of homobiotin tosylate **9**³ (5 mg, 0.013mmol) in anhydrous THF (1 mL) was added lithium aluminium hydride (3 mg, 0.079 mmol) and the solution was stirred under reflux for 3 h. The reaction mixture was cooled to ambient temperature and were added methanol (1 mL) and saturated aqueous sodium sulphate (2 mL), followed by concentration *in vacuo* and dissolving with 1:1 dichloromethane and methanol (15 mL) and stirring for 30 min. The solution was filtered and the filtrate was concentrated *in vacuo* and purified by silica gel chromatography eluting with 3% methanol in dichloromethane to give an off white solid (2 mg, 69%). **¹H NMR** (300 MHz, CDCl₃): δ 4.93 (1H, bs), 4.86 (1H, bs), 4.50-4.54 (1H, m); 4.32 (1H, ddd, *J* = 1.5, 4.5, 7.5 Hz), 3.19 (1H, dt, *J* = 4.5, 7.5 Hz), 2.94 (1H, dd, *J* = 5.1, 12.9 Hz), 2.73 (1H, d, *J* = 12.9 Hz), 1.63-1.68 (2H, m), 1.26-1.45 (6H, m), 0.89 (3H, t, *J* = 6.9 Hz); **¹³C NMR** (75 MHz, DMSO-*d*₆): δ 163.16, 62.23, 60.41, 55.81, 40.92, 31.93, 29.52, 29.34, 28.98, 22.90, 14.39. **HRMS** calcd. for (M + H) C₁₁H₂₁N₂OS: requires 229.1374 found 229.1369.

(4*S*,5*R*)-4-methyl-5-(oct-7-ynyl)imidazolidin-2-one (Compound 19)



Compound **18b** was prepared from desthiobiotin **18a** (200 mg, 0.93 mmol) and according to the procedure outlined for compound **7**.³ Yield (153 mg, 82%); ¹H NMR (300 MHz, CDCl₃): δ 1.33 (3H, d, *J* = 6.6 Hz), 1.25-1.77 (11H, m), 3.62-3.71 (3H, m), 3.84 (1H, ddd, *J* = 13.5, 6.6, 6.6 Hz), 4.69 (1H, s), 5.11 (1H, s); ¹³C NMR (75 MHz, DMSO-*d*₆): δ 163.47, 62.65, 56.00, 51.38, 32.45, 29.50, 29.09, 26.38, 25.52, 15.74; HRMS calcd. for (M + Na) C₁₀H₂₀O₂N₂Na: requires 223.1422, found 223.1432.

To a stirred solution of triphenylphosphine (152 mg, 0.58 mmol) and 2,3-dichloro-5,6-dicyano-*p*-benzoquinone (DDQ) (130 mg, 0.58 mmol) in dry dichloromethane (10 mL) under a stream of nitrogen at ambient temperature was added tetrabutylammonium bromide (186 mg, 0.58 mmol) followed by addition of the compound **18b** (97 mg, 0.48 mmol) and stirred for 1 h. Volatiles were removed *in vacuo* and the crude residue purified by silica gel chromatography to give compound **18c** as an orange powder (113 mg, 89%). ¹H NMR (300 MHz, CDCl₃): δ 1.46 (3H, d, *J* = 6.3 Hz), 1.29-1.47 (8H, m), 1.86 (2H, ddd, *J* = 14.25, 6.9, 6.9 Hz), 3.41 (1H, t, *J* = 6.9 Hz), 3.67-3.74 (1H, m), 3.86 (1H, ddd, *J* = 13.65, 6.6, 6.6 Hz), 4.44 (1H, s), 4.64 (1H, s); ¹³C NMR (300 MHz, DMSO-*d*₆): δ 163.06, 56.27, 51.37, 33.78, 32.58, 29.57, 28.71, 27.95, 26.34, 15.77; HRMS calcd. for (M + Na) C₁₀H₁₉O₂N₂Na: requires 285.0578, found 285.0584.

Compound **18c** (86 mg, 0.32 mmol) was reacted according to the procedure outlined for compound **14**.³ The residue was purified by silica gel chromatography eluting with 5% methanol in dichloromethane to give the title compound (**19**) as an orange

powder (34 mg, 50%) **¹H NMR** (300 MHz, CDCl₃): δ 1.14 (3H, d, *J* = 6.3 Hz), 1.25-1.59 (10H, m), 1.95 (1H, dt, *J* = 2.55, 0.9 Hz), 2.19 (1H, ddd, *J* = 6.9, 6.9, 2.7 Hz), 3.67-3.73 (1H, m), 3.85 (1H, ddd, *J* = 13.8, 6.6, 6.6 Hz), 4.36 (1H, s), 4.54 (1H, s); **¹³C NMR** (300 MHz, DMSO-d₆): δ 163.75, 84.45, 68.16, 55.96, 51.23, 40.77, 29.52, 28.93, 28.36, 28.17, 26.20, 18.19, 15.57; **HRMS** calcd. for (M + Na) C₁₂H₂₀ON₂Na: requires 231.1473, found 231.1470.

Protein expression and purification

The expression and purification of recombinant *Sa*BPL⁷, *Ec*BPL⁸ and *Hs*BPL⁹ were performed as previously described.

Nucleic acid manipulation

To generate a construct for over-expression of *Ec*BPL in *E. coli*, the *birA* gene was placed under control of the IPTG-inducible, strong tac promoter. The gene was amplified by PCR using oligonucleotides B130 [5'-TCATGAAGGATAACACCGTGCCAC-3'] and B131 [5'-AAGCTTAATGATGATGATGATGATGTCCTTTTCTGCACTACGCAGGG-3'] upon template pCY216 containing the *birA*.¹⁰ The resulting PCR product was digested with *Bsp*H1 and *Hind*III and ligated into *Nco*I and *Hind*III treated pC104¹¹, a derivative of pK223-3 (Amersham). This yielded the vector pK(*Ec*BPL-H6) that was confirmed by DNA sequence analysis (DNA Sequencing Service, SA Pathology, South Australia). *E. coli* K12 was transformed with pK (*Ec*BPL-H6) to address the mechanism of antibiotic action.

X-ray crystallography

Apo-*Sa*BPL was buffer exchanged into 50 mM Tris HCl pH 7.5, 50 mM NaCl, 1 mM DTT and 5% (v/v) glycerol, and concentrated to 5 mg/mL. Each compound was then added to BPL in a 10:1 molar ratio. The complex was crystallized using the hanging drop method at 4°C in 8 – 12% Peg 8000 in 0.1 M Tris pH 7.5 or 8.0, and 10% (v/v) glycerol as the reservoir. A single crystal was picked using a Hampton cryo-loop (Hampton Research, USA) and streaked through cryo-protectant containing 25% (v/v) glycerol in the reservoir buffer prior to cryo-cooling. X-ray diffraction data was collected using the macromolecular crystallography beamline (MX1) at the Australian Synchrotron using an ADSC Quantum 210r Detector. 90 images were collected with a 1 second exposure each and an oscillation angle of 1° for each frame. Data was integrated and scaled using XDS.¹² PDB and cif files for the compounds were obtained using the PRODRG web interface.¹³ The co-ordinates from the *Sa*BPL –

biotinol-5-AMP (PDBID = 4DQ2)³, with all water and ligands removed were used as a starting model. After rigid body refinement using REFMAC,¹⁴ the models were built using cycles of manual modelling using COOT¹⁵ and refinement with REFMAC.¹⁴ The electron density clearly defined the positions of the ligands. The quality of the final models was evaluated using MOLPROBITY.¹⁶ Data collection and refinement statistics are summarized in Supplementary Table S1.

In vitro biotinylation assays

Quantitation of BPL catalysed ³H-biotin incorporation into the biotin domain substrate was performed as previously described^{11, 17}. Briefly, the reaction mixture contained: 50 mM Tris HCl pH 8.0, 3 mM ATP, 4.5 μM biotin, 0.5 μM ³H-biotin, 5.5 mM MgCl₂, 100 mM KCl, 0.1 mg/mL BSA and 10 μM biotin domain of *S. aureus* pyruvate carboxylase. The reaction was initiated by the addition of BPL to a final concentration of 4 nM. After 20 minutes at 37° C, 4 μL aliquots of the reaction were spotted onto Whatman paper pre-treated with biotin and trichloroacetic acid. The filters were washed twice with 10% v/v ice-cold trichloroacetic acid and once with ethanol before air-drying. Quantitation of protein-bound radiolabelled biotin was performed by liquid scintillation. One unit of enzyme activity was defined by the amount of BPL required to incorporate 1 nmol of biotin per minute. The IC₅₀ value of each compound was determined from a dose-response curve by varying the concentration of the inhibitor under the same enzyme concentration. The data was analysed with GraphPad Prism using a non-linear fit of log₁₀ (inhibitor) vs. normalized response. The K_i, the absolute inhibition constant for a compound, was determined using Eq 1:¹⁸

$$\text{Eq 1. } K_i = \frac{IC_{50}}{1 + \frac{[S]}{K_m}}$$

where [S] is the substrate concentration ([biotin] = 5 μM) and K_m is the affinity of the enzyme for biotin (*S. aureus* BPL = 1 μM³, *E. coli* BPL = 0.3 μM⁸ and human BPL = 1 μM¹⁹). The mode of inhibition was investigated by varying the concentrations of inhibitor alongside varying the concentrations of ³H-biotin. The data was plotted as

double reciprocal plots and assessed using Lineweaver-Burk analysis. Ligand efficiency was calculated using Eq2: ²⁰

$$\text{Eq 2. } LE = -RT \ln K_i / \text{number of heavy atoms}$$

where R is the gas constant and T is the temperature (° Kelvin).

Surface Plasmon Resonance

SPR was performed using a Biacore™ T100 (GE Healthcare). BPL was immobilised on a CM5 sensor chip following the manufacturer's instructions. Typically, 6500 resonance units of *Sa*BPL were immobilised on the sensor chip. One channel was left blank which was subtracted from sample channel to allow analysis methods to distinguish between actual and non-specific binding. All experiments were conducted at 25° C at a flow rate of 30 µL/minute with running buffer containing 10 mM HEPES pH 7.4, 150 mM NaCl, 3 mM EDTA and 0.005% (v/v) surfactant. Regeneration of the surface was carried out by injecting 10 mM sodium acetate pH 5.8 at a flow rate of 30 µL/minute for 10 seconds. Zero concentration samples were used as blanks. Biotin and compound **6** showed fast on and off rates outside the range of kinetic quantification hence only K_D values could be estimated from equilibrium responses using compounds of different concentrations. In contrast, the association and dissociate rate constants for compounds **16** and **5** could be determined from the sensorgrams. The data were fitted to a 1:1 ligand binding model using the Biacore™ evaluation software. Buffers for experiments conducted with non-water soluble compounds contained 4% (v/v) DMSO.

The sensorgrams for the SPR experiments are shown in Figure 3. The concentrations of ligands employed were as follows: For biotin (Figure 1a) the concentrations used were 0 (-), 0.98 (-), 3.9 (-), 7.8 (-), 31.3 (-), 62.5 (-) and 125 µM. For compound **6** (Figure 1b), the concentrations used were: 0 (-), 0.68 (-), 2.7 (-), 5.5 (-), 10.9 (-) and 43.8 (-) µM. For compounds **16** and **5** (Figure 1c and d), the concentrations used were: 0 (-), 0.4 (-), 0.8 (-), 1.6 (-) and 3.2 (-) µM.

Antibacterial Activity Evaluation

Minimal Inhibitory Concentrations (MICs) were determined by a microdilution broth method as recommended by the CLSI (Clinical and Laboratory Standards Institute, Document M07-A8, 2009, Wayne, Pa.) with cation-adjusted Mueller-Hinton broth (Trek Diagnostics Systems, U.K.). Compounds were dissolved using DMSO. Serial two-fold dilutions of each compound were made using DMSO as the diluent. Trays were inoculated with 5×10^4 CFU of each strain in a volume of 100 μ L (final concentration of DMSO was 5% (v/v)), and incubated at 35° C for 16-20 hours when MICs were determined.

To address the antibiotic mechanism of action, a complementation assay was performed using *E. coli* K12 cells. Cells harbouring the *EcBPL* over-expression vector pK(*EcBPL*-H6) was employed. Bacteria, 5×10^4 CFU, were seeded in each well of a 96-well plate and treated either with compound **16** (final concentration 32 μ g/mL) or DMSO control (final concentration 3.2% (v/v)) for 20 hours at 37° C. The final optical density of the culture was measured on a Thermo Multiskan Ascent plate reader at 620 nm.

Assay of cytotoxicity

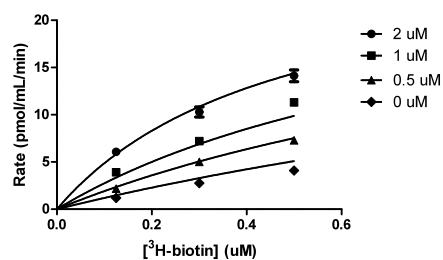
HepG2 cells were suspended in Dulbecco-modified Eagle's medium containing 10% fetal bovine serum, and then seeded in 96-well tissue culture plates at either 5 000, 10 000 or 20 000 cells per well. After 24 hours, cells were treated with varying concentrations of compound, such that the DMSO concentration was consistent at 4% (v/v) in all wells. After treatment for 24 or 48 hours, WST-1 cell proliferation reagent (Roche) was added to each well and incubated for 0.5 hours at 37° C. The WST-1 assay quantitatively monitors the metabolic activity of cells by measuring the hydrolysis of the WST-1 reagent, the products of which are detectable at absorbance 450 nm.

Supporting References

1. Armarego, W. L. F.; Perrin, D. D., *Purification of laboratory chemicals*. 1997; Vol. 4, p 529.
2. Liu, F.-T.; Leonard, N. J., Avidin-biotin interaction. Synthesis, oxidation and spectroscopic properties of linked models. *J. Am. Chem. Soc.* **1979**, *101* (4), 996 - 1005.
3. Soares da Costa, T. P.; Tieu, W.; Yap, M. Y.; Pendini, N. R.; Polyak, S. W.; Sejer Pedersen, D.; Morona, R.; Turnidge, J. D.; Wallace, J. C.; Wilce, M. C.; Booker, G. W.; Abell, A. D., Selective inhibition of Biotin Protein Ligase from *Staphylococcus aureus*. *J Biol Chem* **2012**.
4. Szalecki, W., Synthesis of norbiotinamine and its derivatives. *Bioconjug Chem* **1996**, *7* (2), 271-3.
5. Corona, C.; Bryant, B. K.; Arterburn, J. B., Synthesis of a biotin-derived alkyne for pd-catalyzed coupling reactions. *Org Lett* **2006**, *8* (9), 1883-6.
6. Umeda, N.; Ueno, T.; Pohlmeier, C.; Nagano, T.; Inoue, T., A photocleavable rapamycin conjugate for spatiotemporal control of small GTPase activity. *J Am Chem Soc* **2010**, *133* (1), 12-4.
7. Pendini, N. R.; Polyak, S. W.; Booker, G. W.; Wallace, J. C.; Wilce, M. C., Purification, crystallization and preliminary crystallographic analysis of biotin protein ligase from *Staphylococcus aureus*. *Acta Crystallogr Sect F Struct Biol Cryst Commun* **2008**, *64* (Pt 6), 520-3.
8. Chapman-Smith, A.; Mulhern, T. D.; Whelan, F.; Cronan, J. E., Jr.; Wallace, J. C., The C-terminal domain of biotin protein ligase from *E. coli* is required for catalytic activity. *Protein Sci* **2001**, *10* (12), 2608-17.
9. Mayende, L.; Swift, R. D.; Bailey, L. M.; Soares da Costa, T. P.; Wallace, J. C.; Booker, G. W.; Polyak, S. W., A novel molecular mechanism to explain biotin-unresponsive holocarboxylase synthetase deficiency. *J Mol Med (Berl)* **2012**, *90* (1), 81-8.
10. Chapman-Smith, A.; Turner, D. L.; Cronan, J. E.; Morris, T. W.; Wallace, J. C., Expression, biotinylation and purification of a biotin-domain peptide from the biotin carboxy carrier protein of *Escherichia coli* acetyl-CoA carboxylase. *Biochem. J.* **1994**, *302* (3), 881-887.
11. Polyak, S. W.; Chapman-Smith, A.; Mulhern, T. D.; Cronan, J. E., Jr.; Wallace, J. C., Mutational analysis of protein substrate presentation in the post-translational attachment of biotin to biotin domains. *J Biol Chem* **2001**, *276* (5), 3037-45.
12. Kabsch, W., Xds. *Acta Crystallogr D Biol Crystallogr* **2010**, *66* (Pt 2), 125-32.
13. Schuttelkopf, A. W.; van Aalten, D. M., PRODRG: a tool for high-throughput crystallography of protein-ligand complexes. *Acta Crystallogr D Biol Crystallogr* **2004**, *60* (Pt 8), 1355-63.
14. Winn, M. D.; Murshudov, G. N.; Papiz, M. Z., Macromolecular TLS refinement in REFMAC at moderate resolutions. *Methods Enzymol* **2003**, *374*, 300-21.
15. Emsley, P.; Cowtan, K., Coot: model-building tools for molecular graphics. *Acta Crystallogr D Biol Crystallogr* **2004**, *60* (Pt 12 Pt 1), 2126-32.

16. Chen, V. B.; Arendall, W. B., 3rd; Headd, J. J.; Keedy, D. A.; Immormino, R. M.; Kapral, G. J.; Murray, L. W.; Richardson, J. S.; Richardson, D. C., MolProbity: all-atom structure validation for macromolecular crystallography. *Acta Crystallogr D Biol Crystallogr* **2010**, *66* (Pt 1), 12-21.
17. Polyak, S. W.; Chapman-Smith, A.; Brautigan, P. J.; Wallace, J. C., Biotin protein ligase from *Saccharomyces cerevisiae*. The N-terminal domain is required for complete activity. *J Biol Chem* **1999**, *274* (46), 32847-54.
18. Cheng, Y.; Prusoff, W. H., Relationship between the inhibition constant (K_i) and the concentration of inhibitor which causes 50 per cent inhibition (I₅₀) of an enzymatic reaction. *Biochem Pharmacol* **1973**, *22* (23), 3099-108.
19. Bailey, L. M.; Ivanov, R. A.; Jitrapakdee, S.; Wilson, C. J.; Wallace, J. C.; Polyak, S. W., Reduced half-life of holocarboxylase synthetase from patients with severe multiple carboxylase deficiency. *Hum Mutat* **2008**, *29* (6), E47-57.
20. Kuntz, I. D.; Chen, K.; Sharp, K. A.; Kollman, P. A., The maximal affinity of ligands. *Proc Natl Acad Sci U S A* **1999**, *96* (18), 9997-10002.
21. Weiss, M. S., Global indicators of X-ray quality. *Journal of Applied Crystallography* **2001**, *34* (2), 130-135.

(a)



(b)

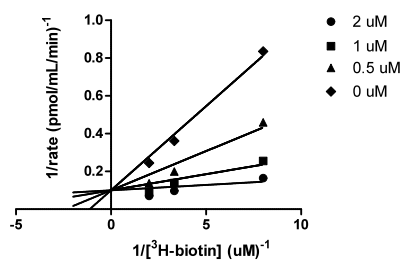


Figure S1. Mechanism of inhibition is via competition with biotin.

Concentration dependent inhibition of *S. aureus* BPL by compound **16** and associated double reciprocal Lineweaver-Burk plot show that this compound is a competitive inhibitor of biotin. (a) Rate plot with different fixed concentrations of inhibitor and varying concentrations of ^3H -biotin, b) Double reciprocal Lineweaver-Burke plot of initial velocity curves against varying concentrations of ^3H -biotin.

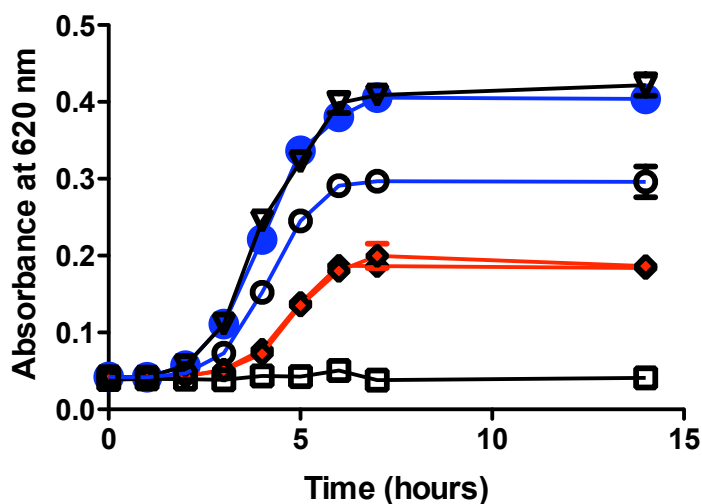


Figure S2. Mechanism of antibacterial activity is via inhibition of BPL.

E. coli K12 cells were transformed with either the parent vector pKK-223-3 (diamonds with red lines) or pK(*Ec*BPL-H6) (circles with blue lines) for the over-expression of *E. coli* BPL. Cells were grown for 14 hours at 37°C in the presence or absence of 32 µg/ml compound **5** when the absorbance of the culture was measured at 600 nm. Protein expression was induced by the addition of IPTG into the growth media (solid symbols contain IPTG vs open symbols with no IPTG). A control with no compound was included (▽), as was a control with no bacteria (□).

Supporting Table S1. X-ray data collection and refinement. Data collection and refinement statistics for holo *SaBPL* structures with compounds **6** and **14** bound.

	Compound 6	Compound 14
Data collection		
Space group	<i>P4₂2₁2</i>	<i>P4₂2₁2</i>
Unit cell (<i>a,b,c</i>)	93.6, 93.6, 130.4	93.1, 93.1, 129.9
Resolution	50.00 -2.60 (2.67- 2.60)	50.00 - 2.65 (2.72-2.65)
Number of unique reflections	18454 (1329)	17103 (1234)
Multiplicity	6.9 (7.1)	5.4 (5.6)
Completeness	99.3% (99.6%)	99.3% (97.4%)
I/σ	13.9 (4.5)	17.4 (2.5)
<i>R</i> _{merge}	12.5% (70.5%)	8.1% (83.1%)
<i>R</i> _{pim}	2.8% (26.4%)	2.2 % (27.0%)
Refinement		
<i>R</i> _{factor}	19.7	19.7
<i>R</i> _{free}	26.8	24.2
<i>r.m.s. deviations</i>		
Bond lengths	0.022	0.022
Bond angles	1.96	2.05
<i>Ramachandran plot</i>		
Allowed regions	99.4%	98.7%
Outliers	0.7%	1.3%

^a Values in parentheses refer to the highest resolution shell.

^b $R_{\text{merge}} = \sum |I - \langle I \rangle| / \sum \langle I \rangle$ where *I* is the intensity of individual reflections.

^c $R_{\text{pim}} = \sum [1/(N-1)]^{1/2} \sum |I - \langle I \rangle| / \sum \langle I \rangle$ ²¹

^d $R_{\text{factor}} = \sum_h |F_o - F_c| / \sum_h |F_o|$, where *F_o* and *F_c* are the observed and calculated structure-factor amplitudes for each reflection "h".

^e *R*_{free} was calculated with 5% of the diffraction data selected randomly and excluded from refinement.

Chapter 4 Selective inhibition of biotin protein ligase from *Staphylococcus aureus*

In a continuation from the previous chapter, the structure of biotinyl-5'-AMP (Btyl) in complex with SaBPL (Pendini et al., 2013) was used as a starting point to design Btyl analogues that had inhibitory activity against SaBPL. The non-hydrolysable Btyl analogue, biotinol-5'-AMP (BtOH) (Brown et al., 2004) was crystallized in complex with SaBPL as a first step in drug design. Based on these two SaBPL-ligand structures, further inhibitors were designed by linking azide groups onto biotin acetylene with improved stability, species selectivity and ease of synthesis kept in mind (Soares da Costa et al., 2012a). These new inhibitors were crystallized in complex with SaBPL and the structure determined to analyze mode of binding and for further drug design down the track.

4.1. Contribution of publication

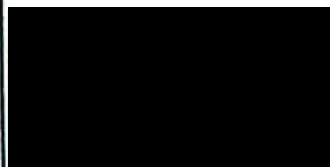
My contribution towards the publication which forms this chapter (Brown et al., 2004) first includes the expression and purification of SaBPL for crystallography studies based on a method that has been previously described (Pendini et al., 2008b). I then crystallized SaBPL in complex with BtOH (**PDB: 4DQ2**) and determined the structure that acted as a starting template for drug design. After the compounds had been designed and tested for binding affinity with surface plasmon resonance (SPR) by our collaborators, I crystallized SaBPL in complex with the biotin triazoles 7 and 14 (**PDB: 3V7C** and **3V7S**). After collecting X-ray data at the Australian Synchrotron, I analysed the data and solved the structures of SaBPL in complex with the inhibitors through several cycles of manual modeling using COOT and restrained refinement with REFMAC. I also analysed the structure to determine protein-ligand interaction and support further development of new SaBPL inhibitors. I was also involved in writing and editing the manuscript.

Monash University


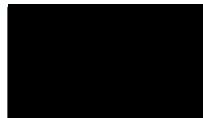
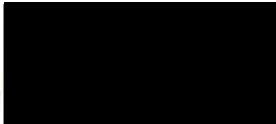
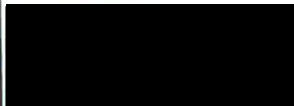
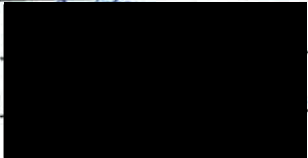
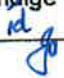
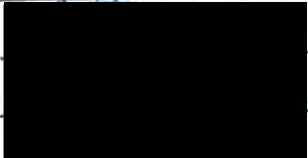
Declaration for Thesis Chapter 4: Selective inhibition of biotin protein ligase from Staphylococcus aureus

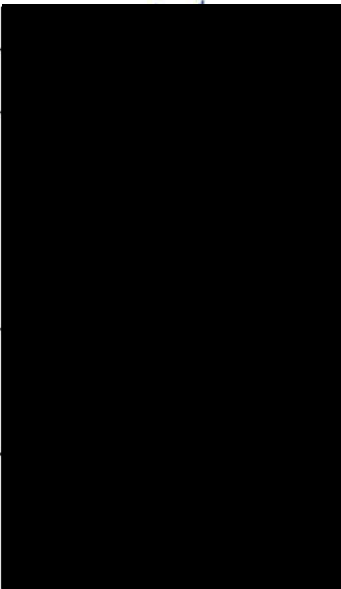
Declaration by candidate:

In the case of Chapter 4, the nature and extent of my contribution to the work was the following:

Nature of contribution	Extent of contribution	Signature
<ol style="list-style-type: none"> 1. Expression and purification of SaBPL for protein crystallography 2. Crystallization of SaBPL in complex with biotin analogue alcohol 6 and acetylene 14 3. Collection of crystallographic data and analyzing and solving the structures of SaBPL in complex with biotin acetylene 4. Analysis of protein-ligand interaction to support development of new ligands 5. Contributed to manuscript preparation 	30%	

The following co-authors contributed to the work. Co-authors who are students at Monash University must also indicate the extent of their contribution in percentage terms:

Name	Nature of contribution	Signature
Tatiana P. Soares da Costa ²	<ol style="list-style-type: none"> 1. Expression and purification of SaBPL. 2. Performed biological assays with SaBPL (in vitro inhibition assays, SPR) 3. Contributed to manuscript preparation 	
William Tieu ³	<ol style="list-style-type: none"> 1. Design, synthesis and characterization of SaBPL inhibitors 2. Contributed to manuscript preparation 	
Nicole R. Pendini ^{1,2}	Contributed to manuscript preparation	
Steven W. Polyak ²	<ol style="list-style-type: none"> 1. Supervised the biochemical assays and data analysis. 2. Contributed to manuscript preparation. 3. Corresponding author on both manuscripts. 4. Overall project direction 	
Daniel S. Pederson ³	Design, synthesis and characterization of SaBPL inhibitors.	
Renato Morona ²	Contributed to manuscript preparation	
John D. Turnidge ^{2,4} 	Supervised antibacterial assays and interpretation of data	

John C. Wallace ²	Contributed to manuscript preparation	
Matthew C. J. Wilce ¹	1. Supervised X-ray crystallization studies, data collection and analysis. 2. Contributed to manuscript preparation. 3. Overall project direction	
Grant W. Booker ²	1. Supervised biochemical assays . 2. Contributed to manuscript preparation.	
Andrew D. Abell ³	1. Supervised the design, synthesis and characterization of BPL inhibitors. 2. Contributed to manuscript preparation 3. Overall project direction	

1. School of Biomedical science, Monash University, VIC 3800, Australia
2. School of Molecular and Biomedical Science, University of Adelaide, Adelaide, South Australia, 5005, Australia
3. School of Chemistry and Physics, University of Adelaide, Adelaide, South Australia 5005, Australia
4. SA Pathology at Women's and Children's Hospital, South Australia 5006, Australia

Declaration by co-authors:

- (1) the above declaration correctly reflects the nature and extent of the candidate's contribution to this work, and the nature of the contribution of each of the co-authors.
- (2) they meet the criteria for authorship in that they have participated in the conception, execution, or interpretation, of at least that part of the publication in their field of expertise;
- (3) they take public responsibility for their part of the publication, except for the responsible author who accepts overall responsibility for the publication;
- (4) there are no other authors of the publication according to these criteria;
- (5) potential conflicts of interest have been disclosed to (a) granting bodies, (b) the editor or publisher of journals or other publications, and (c) the head of the responsible academic unit; and
- (6) the original data are stored at the following location(s) and will be held for at least five years from the date indicated below:

Selective inhibition of Biotin Protein Ligase from *Staphylococcus aureus*^{*[5]}

Received for publication, February 26, 2012. Published, JBC Papers in Press, March 21, 2012, DOI 10.1074/jbc.M112.356576

Tatiana P. Soares da Costa^{†1}, William Tieu^{§1}, Min Y. Yap^{¶1}, Nicole R. Pendini^{‡¶}, Steven W. Polyak^{‡2}, Daniel Sejer Pedersen^{§3}, Renato Morona[‡], John D. Turnidge^{¶||}, John C. Wallace[‡], Matthew C. J. Wilce^{¶4,5}, Grant W. Booker^{‡4}, and Andrew D. Abell^{§4}

From the [†]School of Molecular and Biomedical Science, University of Adelaide, Adelaide, South Australia 5005, Australia, [§]School of Chemistry and Physics, University of Adelaide, Adelaide, South Australia 5005, Australia, [¶]School of Biomedical Science, Monash University, Victoria 3800, Australia, and ^{||}SA Pathology at Women's and Children's Hospital, South Australia 5006, Australia

Background: Inhibitors of biotin protein ligase potentially represent a new antibiotic class.

Results: Biotin triazoles inhibit the BPL from *Staphylococcus aureus* but not the human homologue.

Conclusion: Our most potent inhibitor shows cytotoxicity against *S. aureus* but not cultured mammalian cells.

Significance: This is the first report demonstrating selective inhibition of BPL.

There is a well documented need to replenish the antibiotic pipeline with new agents to combat the rise of drug resistant bacteria. One strategy to combat resistance is to discover new chemical classes immune to current resistance mechanisms that inhibit essential metabolic enzymes. Many of the obvious drug targets that have no homologous isozyme in the human host have now been investigated. Bacterial drug targets that have a closely related human homologue represent a new frontier in antibiotic discovery. However, to avoid potential toxicity to the host, these inhibitors must have very high selectivity for the bacterial enzyme over the human homolog. We have demonstrated that the essential enzyme biotin protein ligase (BPL) from the clinically important pathogen *Staphylococcus aureus* could be selectively inhibited. Linking biotin to adenosine via a 1,2,3 triazole yielded the first BPL inhibitor selective for *S. aureus* BPL over the human equivalent. The synthesis of new biotin 1,2,3-triazole analogues using click chemistry yielded our most potent structure (K_i 90 nM) with a >1100-fold selectivity for the *S. aureus* BPL over the human homologue. X-ray crystallography confirmed the mechanism of inhibitor binding. Importantly, the inhibitor showed cytotoxicity against *S. aureus* but not cultured mammalian cells. The biotin 1,2,3-triazole provides a novel pharmacophore for future medicinal chemistry programs to develop this new antibiotic class.

Since the discovery and development of penicillin more than 70 years ago, society has grown accustomed to rapid and effective treatment of bacterial infections. Although a range of antibiotics has since been developed to target a wide diversity of infectious agents, resistance to these compounds is an inevitable and relentless process. The combination of over-prescription and the waning interest of the pharmaceutical industry in this area over the last 30 years has contributed to the emergence of wide spread life-threatening infections with strains that are resistant to most if not all antibiotics in current clinical use (1, 2). For example, *Staphylococcus aureus* bacteremia in the United States has almost trebled in the past 20 years, with 50–60% of hospital-acquired infections now due to methicillin-resistant strains (MRSA) (3, 4). More disturbingly, although the public profile of serious *S. aureus* infections is that they are hospital-acquired, it is important to recognize that 60% of such infections are now thought to begin in the community (3, 4).

Screening for antimicrobial activity in natural product extracts identified the majority of the currently prescribed classes of antibiotics. The molecular targets for these agents, where known, are generally an essential protein or enzyme that is unique to the prokaryotic pathogen. These obvious drug targets have now been extensively investigated. Because only three new classes of antibiotic have been developed for the clinic in the last 35 years, it is clear that alternative avenues to antibiotic discovery must be considered. One such approach is to target essential proteins and enzymes even if they have homologues in humans. This greatly increases the opportunity to identify new classes of antibiotics with novel modes of action. Importantly, this absolutely necessitates that very high selectivity for the bacterial enzyme is achieved over the human equivalent. A number of antivirals have been identified using this approach, with multiple neuraminidase inhibitors available that have a therapeutic window of >5 orders of magnitude (5, 6).

Biotin protein ligase (BPL)⁶ presents one such antibacterial drug target. Although it is ubiquitously found throughout the

^{*} This work was supported by the National Health and Medical Research Council of Australia (applications 565506 and 1011806) and Adelaide Research and Innovation's Commercial Accelerator Scheme.

^[5] This article contains supplemental Experimental Procedures, Figs S1–S5, and Tables S1 and S2.

The atomic coordinates and structure factors (codes 4DQ2, 3V7C, and 3V7S) have been deposited in the Protein Data Bank, Research Collaboratory for Structural Bioinformatics, Rutgers University, New Brunswick, NJ (<http://www.rcsb.org/>).

¹ These authors were equal contributors.

² To whom correspondence should be addressed. Tel.: 61-8-8303-5289; Fax: 61-8-8303-4362; E-mail: [REDACTED]

³ Supported by the Carlsberg Foundation. Present address: Dept. of Medicinal Chemistry, University of Copenhagen, Universitetsparken 2, Copenhagen, 2100 Denmark.

⁴ These authors contributed equally as senior authors.

⁵ An Australian National Health and Medical Research Council of Australia Senior Research Fellow.

⁶ The abbreviations used are: BPL, biotin protein ligase; SaBPL, *S. aureus*; BBL, biotin binding loop; ABL, ATP binding loop.

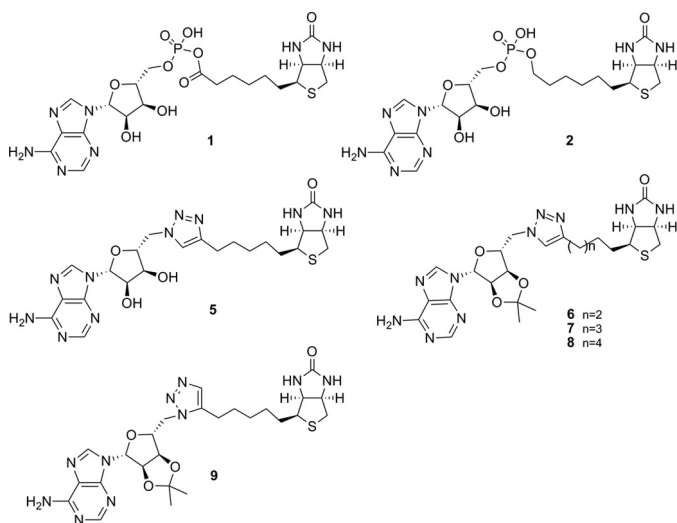


FIGURE 1. Chemical structures of key compounds in this study.

living world, protein sequence comparisons show that this enzyme family is segregated into three structural classes. Importantly, the Gram-negative and Gram-positive pathogenic bacteria fall into class I or II, whereas the enzymes from mammals are in a separate class (III) with a large N-terminal extension required for catalysis that is not present in the bacterial enzymes (7, 8). BPL catalyzes the ATP-dependent addition of biotin onto specific carboxylases that require the cofactor for activity. The BPL in *S. aureus* (SaBPL) has two such substrates, acetyl-CoA carboxylase and pyruvate carboxylase, that without biotinylation are totally inactive. We and others have proposed BPL as a potential antibacterial target, as acetyl-CoA carboxylase is required for membrane lipid biosynthesis (9–11). This metabolic pathway is important in *S. aureus*, as the bacteria can only derive 50% of their membrane phospholipids from exogenous fatty acids (12). Inhibitors of bacterial acetyl-CoA carboxylase have demonstrated *in vivo* efficacy in an *S. aureus* infection model of mice (13). Pyruvate carboxylase plays an anaplerotic role in central carbon metabolism where it replenishes the tricarboxylic acid cycle with oxaloacetate (14). The inhibition of BPL, therefore, targets both fatty acid biosynthesis and the tricarboxylic acid cycle pathways. Genetic studies support the observation that SaBPL is an essential gene product in *S. aureus* (15–17).

BPL performs protein biotinylation via the synthesis of a reaction intermediate, biotinyl-5'-AMP (1, Fig. 1), where a labile phosphoanhydride linker joins biotin with AMP. An enzymatic mechanism involving an adenylated intermediate is employed by other organic acid ligases, such as aminoacyl-tRNA synthetases, *o*-succinylbenzoyl-CoA synthetase, and phosphopantothoenoylcysteine synthetase, among others. Using an adenylated intermediate as a basis for developing ligase inhibitors is problematic because of the hydrolytic and enzymatic instability of the component phosphoanhydride linkage and difficulties of synthesis (18). Nonetheless, several of these enzymes have been the subjects of antibacterial drug discovery studies using inhibitors designed to replace the labile phosphoanhydride with more stable functionalities (19–24). Non-hydrolysable phosphate bioisosteres, such as sulfonyl,

phosphodiester, hydroxylamine, and di-keto-ester, have been reported. However, there has been limited success in developing inhibitors that show the required selectivity over the mammalian homologues. This was highlighted in a recent study targeting the BPL from *Mycobacterium tuberculosis* (11) using a simple analog of the reaction intermediate 1 where the phosphate linker was replaced with a sulfamate group. Although the acylsulfamate analog was a potent inhibitor of *M. tuberculosis* BPL (K_D 0.5 nM), it was not tested for its selectivity *in vitro* with human BPL. However, observed toxicity in a cell culture model suggested poor selectivity. Thus the development of antibiotics based on the inhibition of BPL requires compounds with improved stability, species selectivity, and versatility of synthesis.

It is important to note that BPL was one of 70 molecular targets investigated by GSK in an antibacterial discovery program using high throughput screening (9). The reported lack of success using this approach highlights the need for a more sophisticated approach to inhibitor discovery and the importance of combining structural biology, enzymology, and biophysical characterization to direct medicinal chemistry. As an important first step we determined the x-ray crystal structures of SaBPL alone and in complex with a chemical analog of 1, biotinol-5'-AMP (2, Fig. 1), that contains a non-hydrolysable phosphodiester linker (25). The challenge is to now incorporate structural biology into the design of potent and selective inhibitors of SaBPL. With this in mind, we report a rational structure-guided design to obtain and characterize potent and selective BPL inhibitors containing a triazole bioisostere of the phosphate group of 1 that possess narrow-spectrum antimicrobial activity.

EXPERIMENTAL PROCEDURES

Protein Methods—The expression and purification of recombinant SaBPL (10), *Escherichia coli* BPL (26), and *Homo sapiens* BPL (8) have been previously described. SaBPL and *H. sapiens* BPL were obtained with a C-terminal hexahistidine tag. Quantitation of BPL activity was performed as previously described (27, 28) and in the supplemental Experimental Procedures. Methodologies for surface plasmon resonance and circular dichroism are also described in the supplemental Experimental Procedures.

X-ray Crystallography—ApoSaBPL was buffer-exchanged into 50 mM Tris HCl, pH 7.5, 50 mM NaCl, 1 mM DTT, and 5% (v/v) glycerol and concentrated to 5 mg/ml. Each compound was then added to BPL in a 10:1 molar ratio. The complex was crystallized using the hanging drop method at 4 °C in 8–12% (w/v) PEG 8000 in 0.1 M Tris pH 7.5 or 8.0 and 10% (v/v) glycerol as the reservoir. A single crystal was picked using a Hampton silicon loop and streaked through cryoprotectant containing 25% (v/v) glycerol in the reservoir buffer before data collection. X-ray diffraction data were collected at the macromolecular crystallography beamline at the Australian Synchrotron using an ADSC Quantum 210r Detector. 90 images were collected for 1 s each at an oscillation angle of 1° for each frame. Data were integrated using HKL and refined using the CCP4 suite of programs (29). PDB and cif files for the compounds were obtained using the PRODRG web interface. The models were built using

cycles of manual modeling using COOT (30) and refinement with REFMAC (29). The quality of the final models was evaluated using MOLPROBITY. Composite omit maps were inspected for each crystal structure and statistics for the data and refinement reported (supplemental Table S1). The crystallography, atomic coordinates, and structure factors have been deposited in the Protein Data Bank, codes 4DQ2 (*Sa*BPL with 2), 3V7C (*Sa*BPL with 7), and 3V7S (*Sa*BPL with 14).

Antibacterial Activity Evaluation—Antimicrobial activity of the compounds was determined by a microdilution broth method as recommended by the Clinical and Laboratory Standards Institute (Document M07-A8, 2009, Wayne, PA) with cation-adjusted Mueller-Hinton broth (Trek Diagnostics Systems). Compounds were dissolved using DMSO. Serial 2-fold dilutions of each compound were made using DMSO as the diluent. Trays were inoculated with 5×10^4 colony-forming units of each strain in a volume of 100 μ L (final concentration of DMSO was 3.2% (v/v)) and incubated at 35 °C for 16–20 h. Growth of the bacterium was quantitated by measuring the absorbance at 620 nm.

Assay of Cell Culture Cytotoxicity—HepG2 cells were suspended in Dulbecco-modified Eagle's medium containing 10% fetal bovine serum and then seeded in 96-well tissue culture plates at either 5,000, 10,000, or 20,000 cells per well. After 24 h, cells were treated with varying concentrations of compound, such that the DMSO concentration was consistent at 4% (v/v) in all wells. After treatment for 24 or 48 h, WST-1 cell proliferation reagent (Roche Applied Science) was added to each well and incubated for 0.5 h at 37 °C. The WST-1 assay quantitatively monitors the metabolic activity of cells by measuring the hydrolysis of the WST-1 reagent, the products of which are detectable at absorbance 450 nm.

Synthetic Chemistry Methods—All reagents were from standard commercial sources and of reagent grade or as specified. Solvents were from standard commercial sources. Reactions were monitored by ascending TLC using precoated plates (silica gel 60 F₂₅₄, 250 μ m, Merck), and spots were visualized under ultraviolet light at 254 nm and with either sulfuric acid-vanillin spray, potassium permanganate dip, or Hanessian's stain. Flash chromatography was performed with silica gel (40–63 μ m 60 Å, Davisil, Grace, Germany). Melting points were recorded uncorrected on a Reichert Thermovar Kofler microscope. ¹H and ¹³C NMR spectra were recorded on a Varian Gemini (200 MHz) Varian Gemini 2000 (300 MHz) or a Varian Inova 600 MHz. Chemical shifts are given in ppm (δ) relative to the residue signals, which in the case of DMSO-*d*₆ were 2.50 ppm for ¹H and 39.55 ppm for ¹³C and in the case of CDCl₃ were 7.26 ppm for ¹H and 77.23 ppm for ¹³C. Structural assignment was confirmed with COSY, rotating-frame overhauser effect spectroscopy (ROESY), HMQC (heteronuclear multiple quantum coherence), and HMBC (heteronuclear multiple bond coherence). High resolution mass spectra (HRMS) were recorded on a Thermo Fisher Scientific LTQ orbitrap FT MS equipment ($\Delta < 2$ ppm) at Adelaide Proteomics, University of Adelaide, and Bruker micro TOF-Q at The Australia Wine Research Institute. Purity for assayed compounds was determined by ¹H NMR (>95%). Compounds 2 (25), 3 (31), and 4 (32) were prepared according to literature procedures.

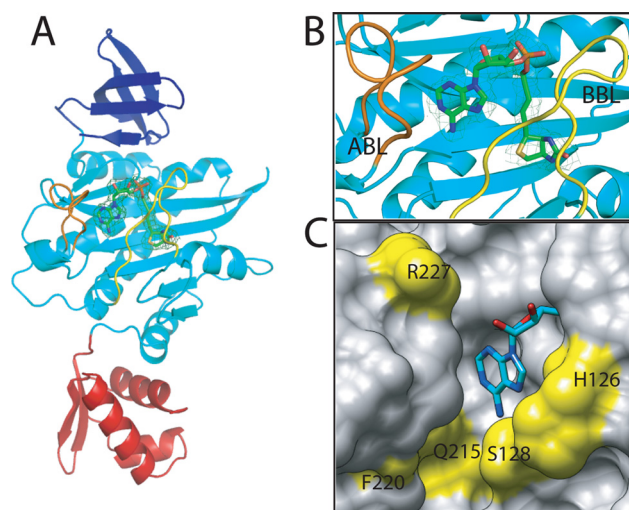


FIGURE 2. *S. aureus* BPL in complex with biotinol-5'-AMP. A, *Sa*BPL consists of three structured domains, an N-terminal DNA binding domain (red), a central domain (cyan), and C-terminal domain (dark blue). B, a close-up of the inhibitor binding site shows the relative positions of the ABL (orange) and BBL (yellow). The final $2F_o - 2F_c$ map is contoured at the 1σ level is shown on inhibitor 2 in ball and stick representation. C, the ATP pocket of *Sa*BPL in complex with 2 is shown in space-filled mode with the adenine portion shown in ball and stick representation. Amino acid residues that line the pocket and that are not conserved between *Sa*BPL and human BPL are highlighted in yellow.

RESULTS

Molecular Basis for Inhibitor Binding—To assist with inhibitor design, the structure of *Sa*BPL in complex with inhibitor biotinol-5'-AMP 2 was determined by x-ray crystallography to 2.5 Å resolution. This revealed that the enzyme contains three domains (Fig. 2A). A helix-turn-helix motif at the N terminus facilitates DNA binding activity. The central and C-terminal domains contain amino acids required for ligand binding and catalysis and adopt SH2- and SH3-like folds, respectively. The overall structures are consistent with the class II enzyme from *E. coli* (33) (root mean square (r.m.s.d.) of α 1.89 Å over 249 amino acids) and with the catalytic region of class I enzymes from *Pyrococcus horikoshii* (r.m.s.d. 1.89 Å), *Aquifex aeolicus* (r.m.s.d. 1.8 Å), and *M. tuberculosis* (r.m.s.d. 1.89 Å) (11, 34–36). The high degree of structural conservation observed in all available BPL structures highlights the challenge in designing selective inhibitors.

The α backbone could be traced from residues Ser-2 to Phe-323, indicating all amino acids were observed in the x-ray diffraction data with the exception of Met 1. Noteworthy were residues Thr-117–Lys-131 and Phe-220–Ala-228 (Fig. 2, A and B). In other BPLs these features, known as the biotin binding loop (BBL) and ATP binding loop (ABL), are not visible in the unliganded form of the enzyme but are observed when ligand is bound. The disordered-to-ordered transition that accompanies ligand binding has been previously reported (33–36). In the complex of *Sa*BPL with 2, the BBL folds against the central β -sheet in the central domain to cover the active site and maintain the reaction intermediate *in situ* (Fig. 2, A and B). The side chain of Trp-127 in the BBL becomes buried and forms a barrier over which the biotin and adenosine halves of 2 must bend (supplemental Fig. S1), thereby forming distinct biotin and ATP binding pockets. The ribose moiety in 2 assists the inhib-

itor to bridge the two binding pockets and forms a hydrogen bond through its 2' hydroxyl group with the side chain of Arg-227 (supplemental Fig. S1). As for other BPLs, the phosphodiester in **2** permits the inhibitor to adopt the same V-shaped geometry observed for **1** binding. The complex with **2** is further stabilized through hydrogen-bonding interactions between the phosphate in the linker with residues in the BBL, namely Arg-122 and Arg-125 (supplemental Fig. S1). The ATP pocket is dominated by the side chain of Trp-127, which is required for a π - π stacking interaction with adenine. The side chains of hydrophobic residues Phe-220, Ile-224, and Ala-228 in the ABL present in the same plane as the purine ring provide a hydrophobic surface for binding. Hydrogen bonding with the side chain of Asn-212 and the backbone nitrogen of Ser-128 within the pocket also stabilize the complex. These key structural features were considered in the design of a chemical mimic of **1** that could function as a selective BPL inhibitor.

An analysis of primary structures reveals that the amino acids involved in binding biotin are highly conserved among all species (supplemental Fig. S2 and Ref. 37). In addition, the x-ray crystal structures show the biotin pocket to be relatively small and hydrophobic, as required to accommodate the ureido and thiophane rings of biotin. This is consistent with reported literature that showed chemical modifications to these heterocycles produced biotin analogues that were unable to be used as substrates by the BPLs from a wide range of species (38). Hence, targeting the biotin site alone is an unattractive approach for inhibitor design. We propose that targeting the ATP binding pocket would provide significant opportunity for introducing selectivity. A comparison of our *Sa*BPL crystal structure with others available in the PDB and also a model of the human BPL active site (7) revealed the amino acid residues in the ATP binding sites to be far more divergent. For example, five of the residues that define the nucleotide binding pocket for *Sa*BPL are not conserved with the sequence of the human BPL. These residues are located immediately around the adenine binding site (Gln-125, Phe-220, and Arg-227) and in the BBL (His-126 and Ser-128). The position of these residues is shown in Fig. 2C (yellow) relative to the adenosine portion of **2** bound in the *Sa*BPL structure.

Biotin Binding Induces Nucleotide Binding Pocket—An understanding of the ligand binding mechanism provided important information for inhibitor design. Biophysical analysis of the class II BPL from *E. coli* has shown that the enzyme possesses an ordered binding mechanism during catalysis with biotin binding first, triggering the disorder-to-order transition that forms the nucleotide binding pocket (33, 39). This ordered binding mechanism was confirmed for *Sa*BPL using surface plasmon resonance. The addition of MgATP to *Sa*BPL that was covalently attached to the matrix did not result in binding (Fig. 3, A and B). In contrast, biotin binds in a concentration-dependent manner with fast association and dissociation kinetics (Fig. 3A). Importantly, when biotin and MgATP were co-administered, a larger magnitude response was observed with the generation of a product that remained on the surface of the sensorchip (Fig. 3A). This is consistent with the immobilized enzyme retaining biotinyl-5'-AMP synthetase activity and the formation of a stable holoenzyme complex. The addition of

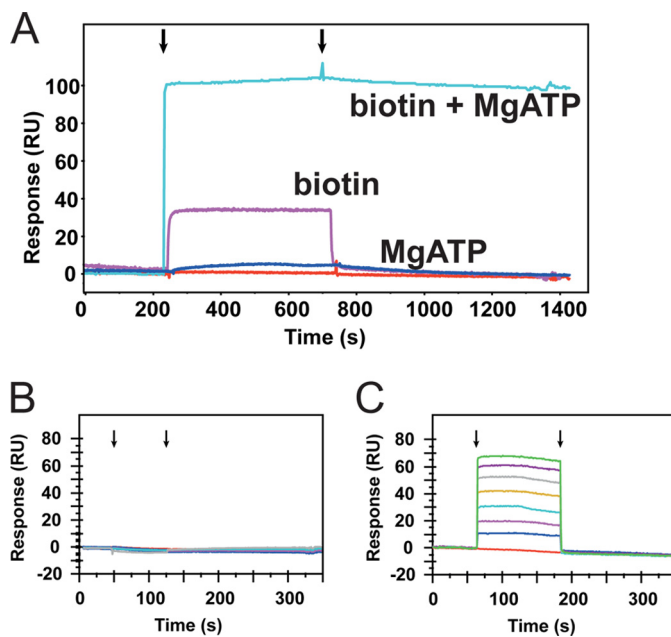
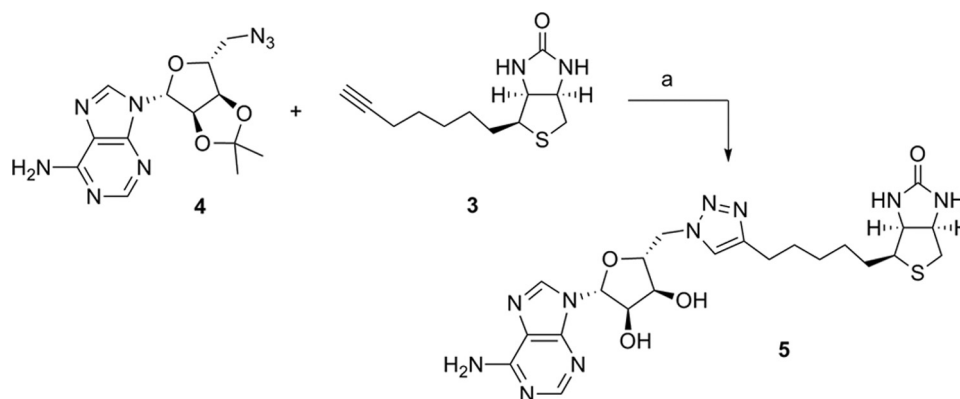


FIGURE 3. Binding at the ATP-site is biotin-dependent. The mechanism of ligand binding was monitored using surface plasmon resonance with immobilized *Sa*BPL. A, overlaid are the surface plasmon resonance traces that resulted from the inclusion of either biotin (pink) or MgATP (dark blue) in the running buffer or both ligands co-injected together (cyan). Arrows indicate the start and end of the ligand injection phase. B and C. ATP binding is dependent upon the formation of a biotin-enzyme complex. The surface plasmon resonance traces are shown when increasing concentrations of MgATP were applied to apo*Sa*BPL (B) or *Sa*BPL (C) in a preformed complex with biotin analog **3**.

protein substrate in the running buffer induced a decrease in response of the surface plasmon, as would be expected when *Sa*BPL discharges the reaction intermediate **1** during protein biotinylation (data not shown). This finding agrees with studies on *E. coli* BPL that demonstrated the holoenzyme complex is stable with a half-life of 30 min (40, 41). This result has a significant impact on inhibitor design. To target the ATP pocket, a successful inhibitor must induce the conformational changes required to form this pocket. We thus chose to incorporate a biotinyl moiety into our inhibitor design. In support of this, surface plasmon resonance analysis showed that MgATP could bind to *Sa*BPL but only after the formation of an enzyme complex with biotin analog **3** (Fig. 3, B and C). It is important that an inhibitor competes with biotin binding because once the ligand occupies the enzyme, the saturating concentration of ATP in the bacterial cell (~ 3 mM, versus the K_m of *Sa*BPL for ATP at $180 \mu\text{M}$; see supplemental Table S2) will drive the formation of intermediate **1** and subsequent biotinylation of the protein substrates.

Triazole Linker as Phosphate Isostere—Currently, there are no reports of selective BPL inhibitors in the literature. Biotinyl-5'-AMP (**2**) (25) and the sulfamate analog 5'-amino-5'-N-(biotinyl)sulfamoyl-5'-deoxyadenosine (**11**) are close mimics of the reaction intermediate (**1**) that contain non-hydrolysable linkers. We demonstrated that **2** inhibited *Sa*BPL with a $K_i = 0.03 \pm 0.01 \mu\text{M}$ in *in vitro* BPL enzyme assays. However, it was also a potent inhibitor of the human BPL with a $K_i = 0.21 \pm 0.03 \mu\text{M}$. Alternative bioisosteres were considered as a means to link biotin and adenine components identified in our inhibitor



SCHEME 1. Conditions and reagents: a, (i) copper nano-powder, 2:1 MeCN/H₂O, 35 °C; (ii) 90% TFA_(aq), dichloro-methane (CH₂Cl₂).

design to access selective inhibitors. The 1,2,3-triazole motif is a versatile heterocycle with a number of desirable attributes that made it a good candidate. It is stable to acid/base hydrolysis and reductive and oxidative conditions, rendering it resistant to metabolic degradation. A 1,2,3-triazole ring has three potential hydrogen bond acceptor sites (nitrogens) and a polarized proton and can also participate in π - π interactions. In addition, a 1,2,3-triazole is readily synthesized by an azide alkyne Huisgen cycloaddition reaction under chemically benign conditions (42, 43). As a result, the 1,2,3-triazole has found some applicability as bioisosteric analogues for phosphomonoesters (44), pyrophosphate (45), phosphodiester linkers (46), and phosphoanhydrides (47).

Our first example of this new class of BPL inhibitors was prepared by Huisgen cycloaddition of biotin acetylene (**3**) with adenosine azide (**4**) in the presence of copper nanopowder followed by removal of the isopropylidene diol-protecting group, which gave the biotin 1,4-disubstituted triazole-adenosine (**5**), as shown in Scheme 1. The related triazoles (**6**, **7**, and **8**, see Fig. 1) were similarly prepared by reaction of the appropriate azide and acetylene as described in the [supplemental Experimental Procedures](#). *In vitro* enzyme inhibition studies demonstrated that the triazole (**5**) was a competitive inhibitor of SaBPL with a K_i of $1.17 \pm 0.3 \mu\text{M}$. The ribose 2',3'-diol was deemed not important for activity as the isopropylidene-protected analog of **5** (see **7**, Fig. 1) was as equally potent as the unprotected analog (K_i $1.83 \pm 0.33 \mu\text{M}$, $p = 0.2$, **5** versus **7**). Significantly, it was also observed that shortening or lengthening the valeric acid chain on the biotinyl moiety of **7** by one carbon (see **6** and **8** respectively) abolished inhibitory activity. Similarly, the 1,5-disubstituted triazole-adenosine isomer of **7** (see **9**, Fig. 1) was also inactive against SaBPL, presumably because this moiety does not provide the appropriate V-shaped geometry required for active site binding as discussed earlier. This was supported by a crystal structure of **7** bound to SaBPL that revealed the expected mode of binding (discussed later). These data highlight the need for the precise positioning of the isostere in the inhibitor.

The biotin triazoles **5** and **7** were next tested for inhibitory activity against recombinant *E. coli* and human BPLs, with both being inactive at the highest concentration achievable without precipitation in the assay medium (typically $200 \mu\text{M}$). These are the first compounds that show significant selectivity for SaBPL.

The biotin-triazole pharmacophore thus provides a scaffold for further development of selective inhibitors of SaBPL.

Improving Inhibitor Potency and Selectivity—In addition to providing a phosphodiester bioisostere, the triazole linkage provides an ideal opportunity to rationally advance the inhibitor design. A selection of readily available azides, the side chains of which might occupy the ATP pocket, were linked to the acetylene **3** under standard Huisgen cyclo-addition conditions to give a second series of triazole-based inhibitors (see the [supplemental Experimental Procedures](#)). Key features of the earlier inhibitors were considered in this stage of the design: (i) the 1,4-disubstituted triazole was retained to allow the inhibitor to adopt the desired V-shape for binding with BPL, (ii) the ribose sugar of **1** was removed as the kinetic data with inhibitors **5** (with unprotected diol) and **7** (protected diol) demonstrated it was not essential for binding, and (iii) the optimum five-carbon linker length between the triazole and biotin groups of **5** and **7** was retained. Two linker lengths between the triazole and potential adenine replacements were investigated, with the choice of analog guided by the hydrophobicity of the ATP binding pocket, defined by the side chains of Phe-220, Ile-224, and Ala-228, and the potential for π interactions with Trp-127. Thus we chose to target triazoles containing aliphatic and aromatic groups (see R group in Table 1) that might be predicted to substitute for adenine and bind in the hydrophobic ATP pocket. A privileged 2-benzoxazolone scaffold (**48**, **49**) was also included in this series (see structures **14** and **16** in Table 1).

The triazole with the appended aliphatic tertiary butyl ester (**10**) was inactive against SaBPL, as were the phenyl and 1-naphthyl analogues **11** and **12**, respectively. Interestingly, the analogous 2-naphthyl derivative **13** showed encouraging activity with a $K_i = 1.17 \pm 0.17 \mu\text{M}$. The triazole with the appended 2-benzoxazolone (**14**) proved to be particularly potent with a K_i of $0.09 \pm 0.02 \mu\text{M}$ (Fig. 4A). Of particular significance was the observation that both compounds **15** and **16** were inactive despite containing the favored aryl groups but a linker reduced by one carbon. This suggests that the correct nature and positioning of the aryl group in the ATP pocket is critical for optimal π stacking and hydrophobic-hydrophobic interactions (see the discussion below on the x-ray crystal structures of complexes with **7** and **14**).

Biotin triazole **14** was confirmed as a competitive inhibitor versus biotin using Lineweaver-Burke analysis. Critically for

Inhibition of *S. aureus* Biotin Protein Ligase

this study, the biotin triazoles **13** and **14** were inactive against both human and *E. coli* BPLs *in vitro* at concentrations limited by solubility. For biotin triazole **14** the selectivity for SaBPL was

TABLE 1
Structure Activity Relationship series of biotin triazoles

ID	R	K_i SaBPL (uM)	Selectivity*
10		> 10	N/D
11		> 10	N/D
12		> 10	N/D
13		1.17 ± 0.17	>77-fold
14		0.09 ± 0.01	>1100
15		> 10	N/D
16		> 10	N/D

* Selectivity is calculated by K_i human BPL/ K_i SaBPL, where the K_i for human BPL is the maximum concentration of compound possible in assay medium due to solubility restraints (90 μ M). ND, not determined.

>1100-fold over the human isozyme (Fig. 4A), making this compound by far the most significant example of a selective BPL inhibitor reported to date.

Anti-microbial Activity of Biotin-triazoles—The anti-microbial activity of selected SaBPL inhibitors was measured against *S. aureus* ATCC strain 49775 using a microbroth dilution assay. Bacteriostatic activity was observed with the pan inhibitor **2**, demonstrating for the first time that the BPL target is indeed drug-receptive in *S. aureus* in an *in vitro* setting (minimal inhibitory concentration 8–32 μ g/ml). The most potent of the triazole inhibitors (**14**) also reduced cell growth by 80% when 8 μ g/ml was included in the growth medium (Fig. 4B). Interestingly, triazole **13** did not show anti-microbial activity even though it is only 13-fold less potent than **14** in an *in vitro* enzyme inhibition assay. This suggests that additional factors such as uptake across the bacterial membrane impact on the utility of this class of compounds. Biotin triazoles **13** and **14** were both inactive against *E. coli* ATCC strain 25922 in the micro-broth dilution assay. This is consistent with the fact that both were inactive against *E. coli* BPL. Importantly, **5**, **7**, **13**, and **14** did not show any toxicity in a cell culture model using HepG2 cells (Fig. 4C). Cells seeded at three different densities were treated with 64 μ g/ml in the growth media for 48 h with no inhibition of cell growth, consistent with the lack of inhibitory activity against human BPL *in vitro*.

X-ray Structures of Biotin-triazoles Bound to SaBPL—The x-ray crystal structures of SaBPL in complex with this new class

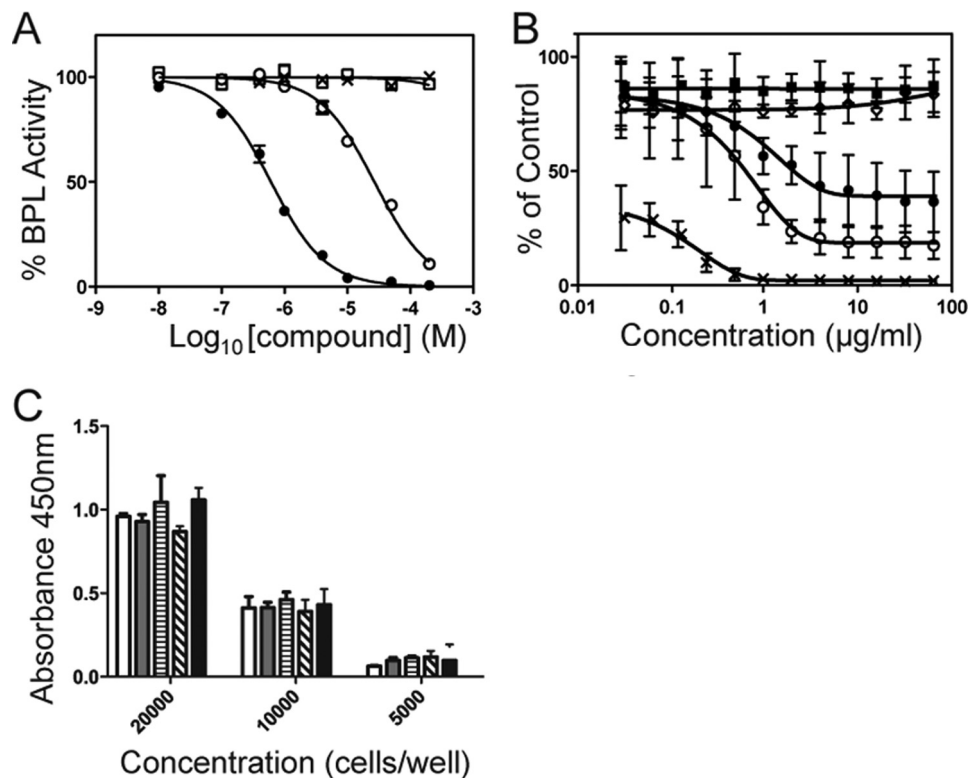


FIGURE 4. Biological assays. A, differential inhibition is shown. BPL activity was measured *in vitro* with varying concentrations of **14**. The assays were performed using recombinant BPL from *S. aureus* (●), *E. coli* (□), and *H. sapiens* (×). The mutant Arg-125→Asn was also included (○). B, anti-*Staphylococcus* activity is shown. Inhibition of the growth of *S. aureus* ATCC 49775 was measured using a microbroth dilution assay with varying concentrations of **2** (○), **13** (◇) and **14** (●). No inhibitor (■) and erythromycin (×) served as negative and positive controls, respectively. C, the cytotoxicity of the biotin triazole series was assessed on HepG2 cells using an assay for metabolic activity. Cells were seeded at either 20,000, 10,000, or 5,000 cells per well and treated for 48 h with media containing 64 μ g/ml of compound and 4% (v/v) DMSO. The treatments in this series were the DMSO vehicle control (white bar), **5** (gray bar), **7** (horizontal stripe), **13** (diagonal stripe), and **14** (black bar).

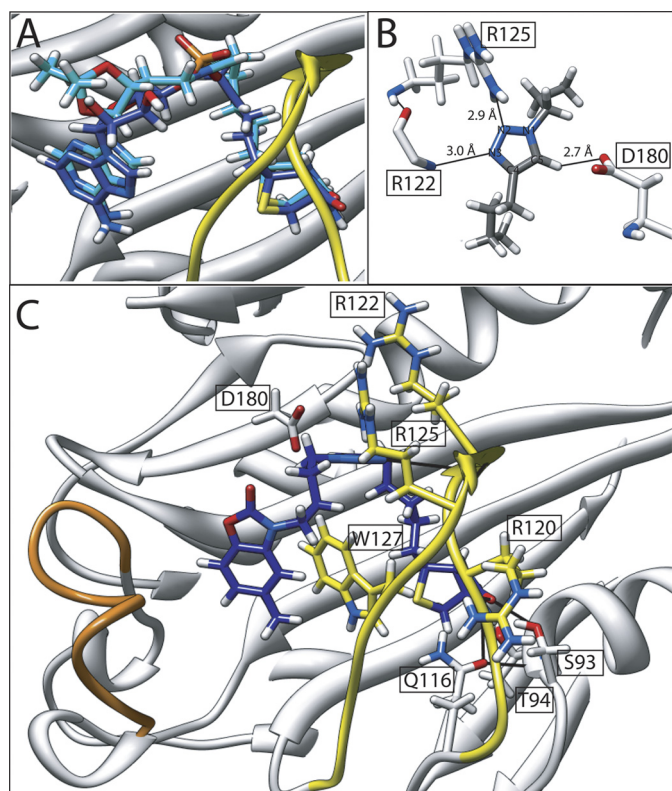


FIGURE 5. **Mode of inhibitor binding.** A, the backbone atoms of SaBPL in complex with inhibitor **2** (dark blue) and inhibitor **7** (cyan) were superimposed to reveal the remarkable overlap in the conformations imparted by the triazole bioisostere. B, hydrogen bonding interactions between SaBPL and the triazole ring are shown. C, the crystal structure of biotin triazole **14** (dark blue) bound in the active site of SaBPL. Hydrogen bonding contacts with the amino acids of SaBPL are shown. The BBL is highlighted in yellow, and the ABL is in orange.

of BPL inhibitor (**7** and **14**) were determined to define their mode of binding (Fig. 5). A comparison of these structures with the enzyme complex of **2** revealed the biotin triazole inhibitors adopted the same V-shaped geometry in the active site as the inhibitor **2**. Indeed, a superimposition of the backbone atoms for SaBPL from the holo and **7**-bound structures showed an almost perfect overlay highlighting the isosteric nature of the triazole relative to the phosphate moiety (Fig. 5A). Additionally, many of the hydrogen-bonding interactions were retained in all structures. The isopropylidene protecting group on inhibitor **7** caused the displacement of the Arg-227 side chain away from its position noted in our other x-ray structures, thereby disrupting a potential hydrogen bond (supplemental Fig. S3). However, the fact that the protecting group showed no effect on inhibitor potency (see **5** versus **7** above) suggests that the ribose ring in **1** is dispensable, consistent with inhibitor design principles described previously. Importantly, the triazole group assists to stabilize the enzyme: inhibitor complex through hydrogen bonding interactions with residues in the BBL, namely N2 with the guanidinium side chain of Arg-125 and N3 and the backbone amide at Arg-122 (Fig. 5B). The proton at C5 of the triazole ring also formed a hydrogen bond with the carboxylate side chain of Asp-180. In addition, the triazole ring participates in an edge-tilted-T shape interaction with Trp-127 (Fig. 5B).

Crystal structures of **7** and **14** in a co-complex with SaBPL all revealed that the inhibitors occupied both biotin and ATP pockets as per our inhibitor design and again with the expected V-shaped geometry essential for binding (Fig. 5C).

The x-ray crystal structure of SaBPL in complex with **7** reveals the adenine ring adopts an analogous binding mechanism to that observed with the holoenzyme complex with inhibitor **2** (discussed earlier). Hence, the requisite properties necessary for binding in the ATP pocket are maintained, namely π - π stacking interaction with Trp-127, hydrophobic interactions with the ABL, and hydrogen-bonding interactions with Asn-212 and Ser-128 located at the bottom of the ATP pocket (supplemental Fig. S4A). Conversely, the benzoxazolone ring of **14** adopts a displaced π interaction with Trp-127 that places the carbamate ring at the top of the ATP pocket (3.6 Å from the Arg-122 side chain; Fig. 5C). The angular placement of the benzoxazolone is accommodated by the grooved hydrophobic region created by Phe-220, Ile-224, and Ala-228 (supplemental Fig. S4B). Unlike the adenine-containing compounds **1**, **2**, and **7**, the benzoxazolone ring in **14** does not appear to hydrogen-bond with the protein (Fig. 5C), suggesting the interaction with the ATP pocket is primarily through hydrophobic-hydrophobic interactions. To the best of our knowledge this is the first evidence of a so-called privileged 2-benzoxazolone scaffold binding in an ATP pocket.

Arg-125 Contributes to Selectivity of Biotin-triazoles—To further probe the mechanism of selectivity, we addressed the role of Arg-125 in the binding mechanism by mutagenesis. As the equivalent amino acid residue in human BPL is a non-conservative asparagine, we proposed that Arg-125 in SaBPL was likely to be a key determinant in the selective binding mechanism employed by the biotin triazoles. To test this hypothesis, we generated a mutant SaBPL with an arginine-to asparagine-substitution (SaBPL Arg-125 \rightarrow Asn) as well as an alanine substitution (SaBPL Arg-125 \rightarrow Ala). CD analysis demonstrated the amino acid substitutions did not destabilize the SaBPL secondary structure (supplemental Fig. S5). Similarly, kinetic analysis demonstrated that the affinity for biotin was unaltered by the mutation and the K_m for MgATP had a modest increase of only 2-fold (supplemental Table S2). Significantly, the largest difference observed between the enzymes was the turnover rate with the k_{cat} reduced by >500-fold by both amino acid substitutions. This implied a key role for this residue and the BBL in catalysis. As expected, the pan inhibitor **2** also functioned as an inhibitor against Arg-125 \rightarrow Asn ($K_i = 0.199 \pm 0.028 \mu\text{M}$, $p < 0.05$ versus Wt SaBPL, $p < 0.001$ versus human BPL). In contrast the inhibitory activity of biotin triazole **5** was abolished. Although **14** retained inhibitory activity against both muteins (Arg-125 \rightarrow Ala $K_i = 4.38 \pm 0.39 \mu\text{M}$, Arg-125 \rightarrow Asn $K_i = 4.47 \pm 0.47 \mu\text{M}$), it remained significantly more potent against wild type SaBPL (Wt $K_i = 0.09 \pm 0.01 \mu\text{M}$, $p < 0.0001$ Wt versus mutein) (Fig. 4A). Together these data support the hypothesis that Arg-125 plays a key role in the selective inhibition by the biotin triazoles.

DISCUSSION

In this study we present the first selective inhibitors of *S. aureus* biotin protein ligase using an analog of the reaction

intermediate, biotinol-5'-AMP (2), as the starting point for inhibitor design. This new class of inhibitor contains a 1,2,3-triazole-based bioisostere of the chemically unstable phosphate-based linkages found in the native reaction intermediate **1** and inhibitor **2**. We also considered the hypothesis that a close mimic of the reaction intermediate **1** that targets the BPL active site would have a high barrier for developing drug resistance due to spontaneous mutation (6). However, the conserved reaction mechanism employed by all BPLs that utilizes adenylylated biotin coupled with the high degree of homology in the primary and tertiary structures suggested that this would be challenging (50). Here we utilized structural biology to assist in the rational design of inhibitors that overcome this problem. An important consideration was the disordered-to-ordered transition that accompanies catalysis. The BBL that is observed in the crystal structures of holo BPLs, but not apo structures, plays a key role to stabilize the BPL-ligand complex. The reaction intermediate is maintained *in situ* in the active site through interactions with amino acids in this loop, especially with the phosphate-containing linkers in **1** and **2**. We argued that an effective mimic of **1** should also interact with amino acids in the BBL. Indeed, replacement of the phosphate linker with a 1,2,3-triazole bioisostere yielded a series of potent and selective inhibitors of SaBPL. The triazole linker provided selective binding via a key amino acid (Arg-125) present in the BBL of SaBPL. This amino acid is not conserved between BPLs, thereby contributing to the selective inhibition. Mutation studies targeting Arg-125 confirmed the mode of binding and demonstrated that this amino acid is important for BPL activity and selectivity. The mutein displayed a reduced enzyme catalytic turnover rate of >500-fold. This reduction of specific enzyme activity should be a significant barrier for the development of drug resistance to the biotin-triazoles by spontaneous mutation, as we initially proposed.

The triazole linkage provides an opportunity to develop BPL inhibitors using well documented reaction conditions that give rise to both the 1,4- and 1,5-disubstituted triazole isomers. BPL provides an attractive template for a fragment-based approach with the biotin and ATP pockets juxtaposed in the crystal structures. Compounds that reside in the two pockets can be joined via a 1,2,3-triazole that constrains the partners in the same V-shaped geometry naturally observed for enzyme bound **1**. The biotin-dependent ATP binding mechanism employed by BPLs prevents targeting the ATP site alone. However, by incorporating a biotin moiety into the inhibitor, the ATP pocket can be formed and explored as an avenue toward an optimized inhibitor. There have been reports of large pharma repositioning their nucleotide-analog libraries, assembled for screening eukaryotic protein kinase targets, for antibiotic discovery. Successful examples in the literature include acetyl-CoA carboxylase (51), histidine kinase (52), and D-alanine-D-alanine ligase (53). The availability of high resolution crystal structures of SaBPL is necessary to direct future chemical optimization.

The mechanism of selective inhibition reported in this study provides the first approach to antibiotics based on the selective inhibition of BPL. To date, target-based antibiotic discovery has focused upon metabolic enzymes and pathways that are found exclusively in bacterial pathogens (54, 55). As a result, targets

with close equivalents in mammalian hosts have typically been excluded from consideration. We demonstrate an important new approach to antibiotic discovery based on the selective inhibition of a bacterial target (BPL) that has a mammalian homologue. Examples of antibiotics in clinical use that selectively target a bacterial protein include ribosome inhibitors, such as macrolides, aminoglycosides, tetracyclines, and linezolid (56). In this example, however, the differences between the bacterial and eukaryotic ribosomal proteins are large and provide adequate opportunities for selective binding of drugs. More challenging for antibiotic drug discovery are the drug targets that more closely resemble their mammalian counterparts, as addressed in this paper. The implication from work presented in this study refocuses discussion on what constitutes a drug-responsive target for antibiotic discovery. Given the clinical demand for new agents to combat drug resistance across the globe, these studies are timely.

Acknowledgments—We acknowledge Jackie Wilce for constructive critique of the manuscript. Diffraction data were collected at the Australian Synchrotron. We also acknowledge the computer resources of the Victorian Partnership for Advanced Computing. We thank Prof. John Cronan (University of Illinois) for the kind gift of biotinol-5'-AMP.

REFERENCES

- Cooper, M. A., and Shlaes, D. (2011) Fix the antibiotics pipeline. *Nature* **472**, 32
- Boucher, H. W., Talbot, G. H., Bradley, J. S., Edwards, J. E., Gilbert, D., Rice, L. B., Scheld, M., Spellberg, B., and Bartlett, J. (2009) Bad bugs, no drugs: no ESKAPE! An update from the Infectious Diseases Society of America. *Clin. Infect. Dis.* **48**, 1–12
- Deleo, F. R., Otto, M., Kreiswirth, B. N., and Chambers, H. F. (2010) Community-associated methicillin-resistant *Staphylococcus aureus*. *Lancet* **375**, 1557–1568
- Turnidge, J. D., Kotsanas, D., Munckhof, W., Roberts, S., Bennett, C. M., Nimmo, G. R., Coombs, G. W., Murray, R. J., Howden, B., Johnson, P. D., and Dowling, K. (2009) *Staphylococcus aureus* bacteremia. A major cause of mortality in Australia and New Zealand. *Med. J. Aust.* **191**, 368–373
- von Itzstein, M. (2007) The war against influenza. Discovery and development of sialidase inhibitors. *Nat. Rev. Drug Discov.* **6**, 967–974
- Colman, P. M. (2009) New antivirals and drug resistance. *Annu. Rev. Biochem.* **78**, 95–118
- Pendini, N. R., Bailey, L. M., Booker, G. W., Wilce, M. C., Wallace, J. C., and Polyak, S. W. (2008) Microbial biotin protein ligases aid in understanding holocarboxylase synthetase deficiency. *Biochim. Biophys. Acta* **1784**, 973–982
- Mayende, L., Swift, R. D., Bailey, L. M., Soares da Costa, T. P., Wallace, J. C., Booker, G. W., and Polyak, S. W. (2012) A novel molecular mechanism to explain biotin-unresponsive holocarboxylase synthetase deficiency. *J. Mol. Med.* **90**, 81–88
- Payne, D. J., Gwynn, M. N., Holmes, D. J., and Pompliano, D. L. (2007) Drugs for bad bugs. Confronting the challenges of antibacterial discovery. *Nat. Rev. Drug Discov.* **6**, 29–40
- Pendini, N. R., Polyak, S. W., Booker, G. W., Wallace, J. C., and Wilce, M. C. (2008) Purification, crystallization, and preliminary crystallographic analysis of biotin protein ligase from *Staphylococcus aureus*. *Acta Crystallogr Sect F Struct. Biol. Cryst. Commun.* **64**, 520–523
- Duckworth, B. P., Geders, T. W., Tiwari, D., Boshoff, H. I., Sibbald, P. A., Barry, C. E., 3rd, Schnappinger, D., Finzel, B. C., and Aldrich, C. C. (2011) Bisubstrate adenylation inhibitors of biotin protein ligase from *Mycobacterium tuberculosis*. *Chem. Biol.* **18**, 1432–1441
- Parsons, J. B., Frank, M. W., Subramanian, C., Saenkhram, P., and Rock,

- C. O. (2011) Metabolic basis for the differential susceptibility of Gram-positive pathogens to fatty acid synthesis inhibitors. *Proc. Natl. Acad. Sci. U.S.A.* **108**, 15378–15383
13. Freiberg, C., Pohlmann, J., Nell, P. G., Endermann, R., Schuhmacher, J., Newton, B., Otteneder, M., Lampe, T., Häbich, D., and Ziegelbauer, K. (2006) Novel bacterial acetyl-coenzyme A carboxylase inhibitors with antibiotic efficacy *in vivo*. *Antimicrob. Agents Chemother.* **50**, 2707–2712
 14. Jitrapakdee, S., St Maurice, M., Rayment, I., Cleland, W. W., Wallace, J. C., and Attwood, P. V. (2008) Structure, mechanism, and regulation of pyruvate carboxylase. *Biochem. J.* **413**, 369–387
 15. Chaudhuri, R. R., Allen, A. G., Owen, P. J., Shalom, G., Stone, K., Harrison, M., Burgis, T. A., Lockyer, M., Garcia-Lara, J., Foster, S. J., Pleasance, S. J., Peters, S. E., Maskell, D. J., and Charles, I. G. (2009) Comprehensive identification of essential *Staphylococcus aureus* genes using transposon-mediated differential hybridization (TMDH). *BMC Genomics* **10**, 291
 16. Forsyth, R. A., Haselbeck, R. J., Ohlsen, K. L., Yamamoto, R. T., Xu, H., Trawick, J. D., Wall, D., Wang, L., Brown-Driver, V., Froelich, J. M., Keder, G. C., King, P., McCarthy, M., Malone, C., Misiner, B., Robbins, D., Tan, Z., Zhu Zy, Z. Y., Carr, G., Mosca, D. A., Zamudio, C., Foulkes, J. G., and Zyskind, J. W. (2002) A genome-wide strategy for the identification of essential genes in *Staphylococcus aureus*. *Mol. Microbiol.* **43**, 1387–1400
 17. Ji, Y., Zhang, B., Van, S. F., Horn, Warren, P., Woodnutt, G., Burnham, M. K., and Rosenberg, M. (2001) Identification of critical staphylococcal genes using conditional phenotypes generated by antisense RNA. *Science* **293**, 2266–2269
 18. Hurdle, J. G., O'Neill, A. J., and Chopra, I. (2005) Prospects for aminoacyl-tRNA synthetase inhibitors as new antimicrobial agents. *Antimicrob. Agents Chemother.* **49**, 4821–4833
 19. Yu, X. Y., Hill, J. M., Yu, G., Wang, W., Kluge, A. F., Wendler, P., and Gallant, P. (1999) Synthesis and structure-activity relationships of a series of novel thiazoles as inhibitors of aminoacyl-tRNA synthetases. *Bioorg. Med. Chem. Lett.* **9**, 375–380
 20. Forrest, A. K., Jarvest, R. L., Mensah, L. M., O'Hanlon, P. J., Pope, A. J., and Sheppard, R. J. (2000) Aminoalkyl adenylate and aminoacyl sulfamate intermediate analogues differ greatly in affinity for their cognate *Staphylococcus aureus* aminoacyl-tRNA synthetases. *Bioorg. Med. Chem. Lett.* **10**, 1871–1874
 21. Bernier, S., Akochy, P. M., Lapointe, J., and Chênevert, R. (2005) Synthesis and aminoacyl-tRNA synthetase inhibitory activity of aspartyl adenylate analogs. *Bioorg. Med. Chem.* **13**, 69–75
 22. Lee, J., Kang, S. U., Kang, M. K., Chun, M. W., Jo, Y. J., Kwak, J. H., and Kim, S. (1999) Methionyl adenylate analogues as inhibitors of methionyl-tRNA synthetase. *Bioorg. Med. Chem. Lett.* **9**, 1365–1370
 23. Tian, Y., Suk, D. H., Cai, F., Crich, D., and Mesecar, A. D. (2008) *Bacillus anthracis* *o*-succinylbenzoyl-CoA synthetase. Reaction kinetics and a novel inhibitor mimicking its reaction intermediate. *Biochemistry* **47**, 12434–12447
 24. Patrone, J. D., Yao, J., Scott, N. E., and Dotson, G. D. (2009) Selective inhibitors of bacterial phosphopantothentoylcytisine synthetase. *J. Am. Chem. Soc.* **131**, 16340–16341
 25. Brown, P. H., Cronan, J. E., Grotli, M., and Beckett, D. (2004) The biotin repressor. Modulation of allostery by corepressor analogs. *J. Mol. Biol.* **337**, 857–869
 26. Chapman-Smith, A., Mulhern, T. D., Whelan, F., Cronan, J. E., Jr., and Wallace, J. C. (2001) The C-terminal domain of biotin protein ligase from *E. coli* is required for catalytic activity. *Protein Sci.* **10**, 2608–2617
 27. Polyak, S. W., Chapman-Smith, A., Brautigan, P. J., and Wallace, J. C. (1999) Biotin protein ligase from *Saccharomyces cerevisiae*. The N-terminal domain is required for complete activity. *J. Biol. Chem.* **274**, 32847–32854
 28. Polyak, S. W., Chapman-Smith, A., Mulhern, T. D., Cronan, J. E., Jr., and Wallace, J. C. (2001) Mutational analysis of protein substrate presentation in the post-translational attachment of biotin to biotin domains. *J. Biol. Chem.* **276**, 3037–3045
 29. Collaborative Computational Project, Number 4 (1994) The CCP4 suite. Programs for protein crystallography. *Acta Crystallogr. D Biol. Crystallogr.* **50**, 760–763
 30. Emsley, P., and Cowtan, K. (2004) Coot. Model-building tools for molecular graphics. *Acta Crystallogr. D Biol. Crystallogr.* **60**, 2126–2132
 31. Corona, C., Bryant, B. K., and Arterburn, J. B. (2006) Synthesis of a biotin-derived alkyne for Pd-catalyzed coupling reactions. *Org. Lett.* **8**, 1883–1886
 32. Comstock, L. R., and Rajsiki, S. R. (2002) Expedient synthesis of aziridine-based cofactor mimics. *Tetrahedron* **58**, 6019–6026
 33. Wood, Z. A., Weaver, L. H., Brown, P. H., Beckett, D., and Matthews, B. W. (2006) Co-repressor induced order and biotin repressor dimerization. A case for divergent followed by convergent evolution. *J. Mol. Biol.* **357**, 509–523
 34. Bagautdinov, B., Kuroishi, C., Sugahara, M., and Kunishima, N. (2005) Crystal structures of biotin protein ligase from *Pyrococcus horikoshii* OT3 and its complexes. Structural basis of biotin activation. *J. Mol. Biol.* **353**, 322–333
 35. Tron, C. M., McNae, I. W., Nutley, M., Clarke, D. J., Cooper, A., Walkinshaw, M. D., Baxter, R. L., and Campopiano, D. J. (2009) Structural and functional studies of the biotin protein ligase from *Aquifex aeolicus* reveal a critical role for a conserved residue in target specificity. *J. Mol. Biol.* **387**, 129–146
 36. Gupta, V., Gupta, R. K., Khare, G., Salunke, D. M., Suroliya, A., and Tyagi, A. K. (2010) Structural ordering of disordered ligand binding loops of biotin protein ligase into active conformations as a consequence of dehydration. *PLoS One* **5**, e9222
 37. Chapman-Smith, A., and Cronan, J. E. (1999) Molecular biology of biotin attachment to proteins. *J. Nutr.* **129**, 477S–484S
 38. Slavoff, S. A., Chen, I., Choi, Y. A., and Ting, A. Y. (2008) Expanding the substrate tolerance of biotin ligase through exploration of enzymes from diverse species. *J. Am. Chem. Soc.* **130**, 1160–1162
 39. Xu, Y., Nenortas, E., and Beckett, D. (1995) Evidence for distinct ligand-bound conformational states of the multifunctional *Escherichia coli* repressor of biotin biosynthesis. *Biochemistry* **34**, 16624–16631
 40. Naganathan, S., and Beckett, D. (2007) Nucleation of an allosteric response via ligand-induced loop folding. *J. Mol. Biol.* **373**, 96–111
 41. Streaker, E. D., and Beckett, D. (2003) Coupling of protein assembly and DNA binding. Biotin repressor dimerization precedes biotin operator binding. *J. Mol. Biol.* **325**, 937–948
 42. Meldal, M., and Tornøe, C. W. (2008) Copper-catalyzed azide-alkyne cycloaddition. *Chem. Rev.* **108**, 2952–3015
 43. Rostovtsev, V. V., Green, L. G., Fokin, V. V., and Sharpless, K. B. (2002) A stepwise Huisgen cycloaddition process. Copper(I)-catalyzed regioselective “ligation” of azides and terminal alkynes. *Angew. Chem. Int. Ed. Engl.* **41**, 2596–2599
 44. Byun, Y., Vogel, S. R., Phipps, A. J., Carnrot, C., Eriksson, S., Tiwari, R., and Tjarks, W. (2008) Synthesis and biological evaluation of inhibitors of thymidine monophosphate kinase from *Bacillus anthracis*. *Nucleosides Nucleotides Nucleic Acids* **27**, 244–260
 45. Chen, L., Wilson, D. J., Xu, Y., Aldrich, C. C., Felczak, K., Sham, Y. Y., and Pankiewicz, K. W. (2010) Triazole-linked inhibitors of inosine monophosphate dehydrogenase from human and *Mycobacterium tuberculosis*. *J. Med. Chem.* **53**, 4768–4778
 46. El-Sagheer, A. H., and Brown, T. (2010) Click chemistry with DNA. *Chem. Soc. Rev.* **39**, 1388–1405
 47. Somu, R. V., Boshoff, H., Qiao, C., Bennett, E. M., Barry, C. E., 3rd, and Aldrich, C. C. (2006) Rationally designed nucleoside antibiotics that inhibit siderophore biosynthesis of *Mycobacterium tuberculosis*. *J. Med. Chem.* **49**, 31–34
 48. Costantino, L., and Barlocco, D. (2006) Privileged structures as leads in medicinal chemistry. *Curr. Med. Chem.* **13**, 65–85
 49. Poupaert, J., Carato, P., Colacino, E., and Yous, S. (2005) 2(3H)-benzoxazolone and bioisosters as “privileged scaffold” in the design of pharmacological probes. *Curr. Med. Chem.* **12**, 877–885
 50. Campbell, J. W., and Cronan, J. E., Jr. (2001) Bacterial fatty acid biosynthesis. Targets for antibacterial drug discovery. *Annu. Rev. Microbiol.* **55**, 305–332
 51. Polyak, S. W., Abell, A. D., Wilce, M. C., Zhang, L., and Booker, G. W. (2012) Structure, function, and selective inhibition of bacterial acetyl-CoA carboxylase. *Appl. Microbiol. Biotechnol.* **93**, 983–992
 52. Schreiber, M., Res, I., and Matter, A. (2009) Protein kinases as antibacterial

Inhibition of *S. aureus* Biotin Protein Ligase

- targets. *Curr. Opin. Cell Biol.* **21**, 325–330
53. Triola, G., Wetzel, S., Ellinger, B., Koch, M. A., Hübel, K., Rauh, D., and Waldmann, H. (2009) ATP competitive inhibitors of D-alanine-D-alanine ligase based on protein kinase inhibitor scaffolds. *Bioorg. Med. Chem.* **17**, 1079–1087
54. Frearson, J. A., Wyatt, P. G., Gilbert, I. H., and Fairlamb, A. H. (2007) Target assessment for antiparasitic drug discovery. *Trends Parasitol.* **23**, 589–595
55. Raman, K., Yeturu, K., and Chandra, N. (2008) targetTB: a target identification pipeline for *Mycobacterium tuberculosis* through an interactome, reactome, and genome-scale structural analysis. *BMC Syst. Biol.* **2**, 109
56. Yonath, A. (2005) Antibiotics targeting ribosomes. Resistance, selectivity, synergism, and cellular regulation. *Annu. Rev. Biochem.* **74**, 649–679

Selective inhibitors of biotin protein ligase from *Staphylococcus aureus*

Supplementary Information

Tatiana P. Soares da Costa, William Tieu, Nicole R. Pardini, Min Y. Yap, Steven W. Polyak, Daniel Sejer Pedersen, Renato Morona, John D. Turnidge, John C. Wallace, Matthew C. J. Wilce, Grant W. Booker, Andrew D. Abell

Supplementary data

Fig S1: Molecular details of biotinol-5'-AMP (2) binding to SaBPL.

A) 2D depiction of inhibitor **2** bound to SaBPL with hydrogen bonding interactions shown in green dashes and hydrophobic interactions in red. B) The corresponding 3D depiction obtained using Chimera with black dash indicating the hydrogen bonding interactions.

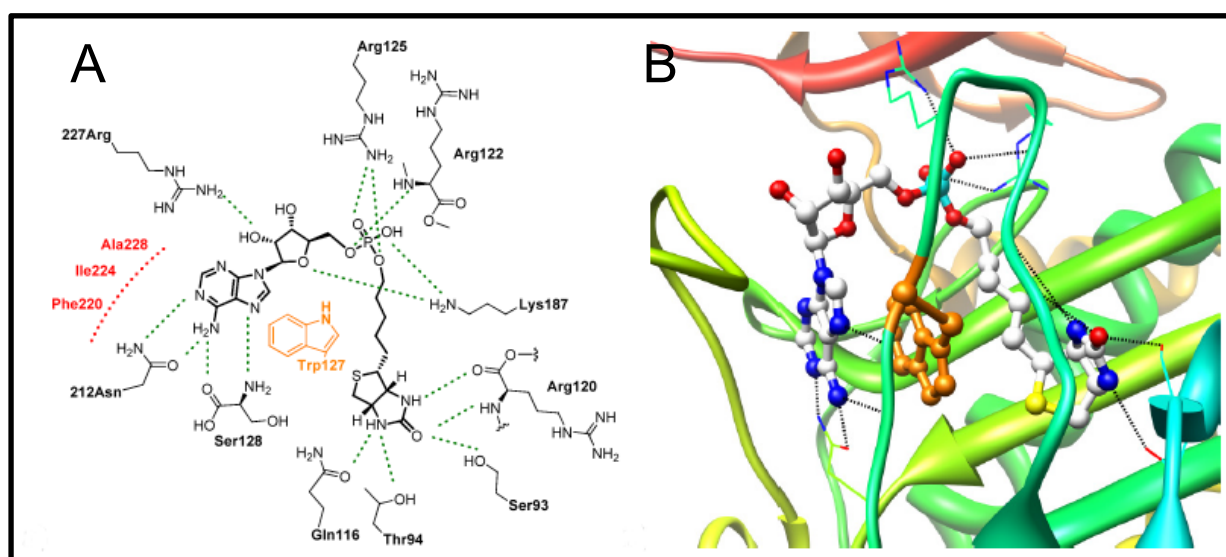


Fig S2: Sequence alignment between structurally determined BPLs and the human homologue.

The amino acid sequences of BPLs for which crystal structures are available in the PDB were aligned using ClustalW. These species are *Staphylococcus aureus* (Sa), *Pyrococcus hirokoshii* (Ph), *Escherichia coli* (Ec), *Mycobacterium tuberculosis* (Mt), *Aquifex aeolicus* (Aa) and *Methanococcus jannaschii* (Mj). Also included in this analysis was the sequence of human BPL, commonly referred to as Holocarboxylase synthetase (HCS). Red triangles indicate hydrogen bonding to biotinol-5'-AMP (**2**), green triangles indicate contact to **2**, orange circles indicate residues involved in salt bridge formation at the dimer interface, black circles indicate dimer hydrogen bonds and blue circles show dimer contact residues for holo-SaBPL.

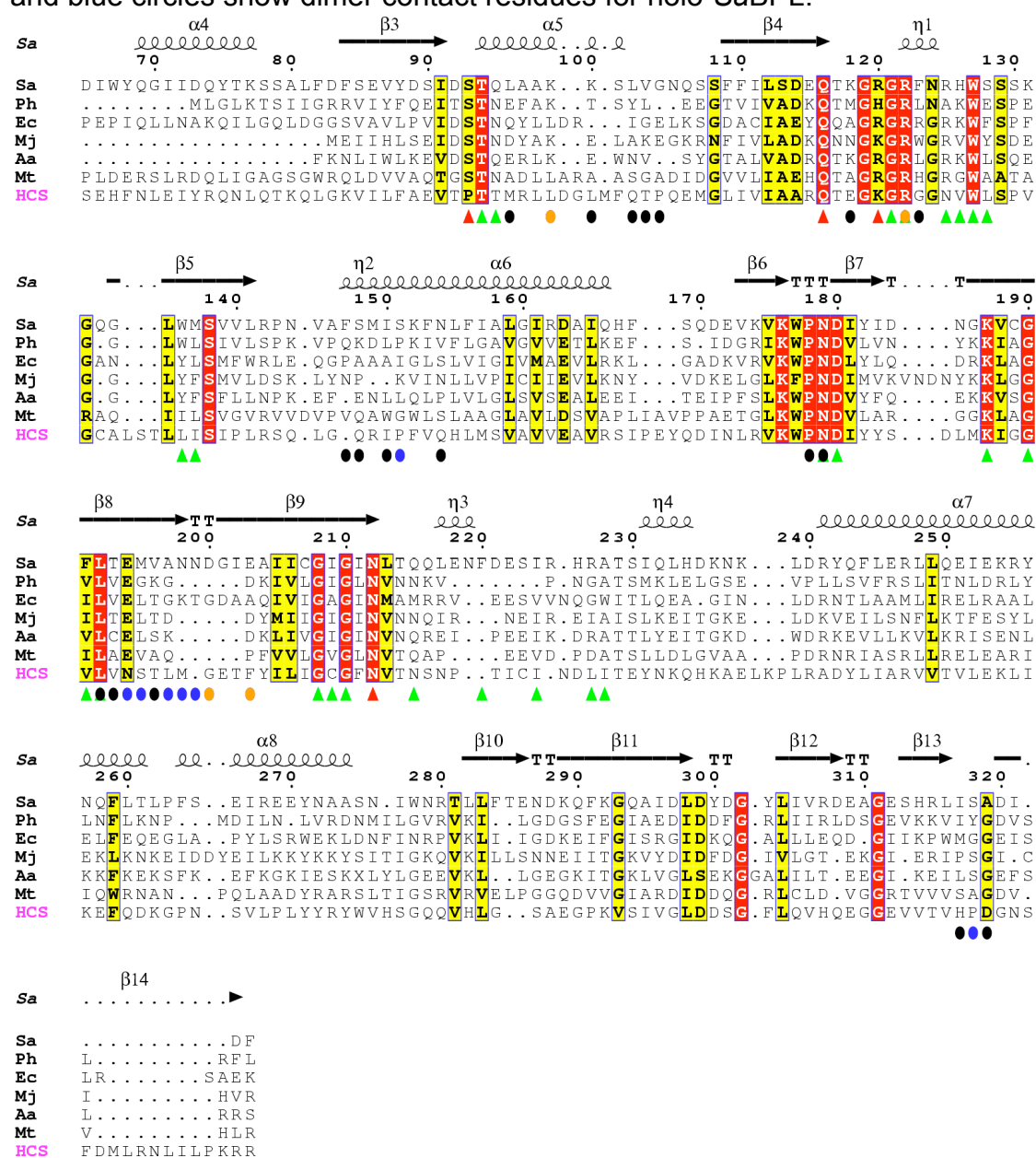


Fig S3: Binding interactions between the ribose ring and Arg 227

The mode of binding of inhibitors (A) biotinol-5'AMP **2** and (B) **7** in the ATP pocket of SaBPL are shown in yellow stick representation. The position of Arg 227 is highlighted in cyan. (A) The 2' hydroxyl group on the ribose ring of **2** hydrogen bonds with the guanidium group on the side chain of Arg 227 (dashed line). (B) An isopropylidene protecting group on the diol of the ribose ring cause the side chain of Arg 227 to reposition itself away from the inhibitor, implying the hydrogen bonding interaction is not essential to stabilise the interaction with the inhibitor.

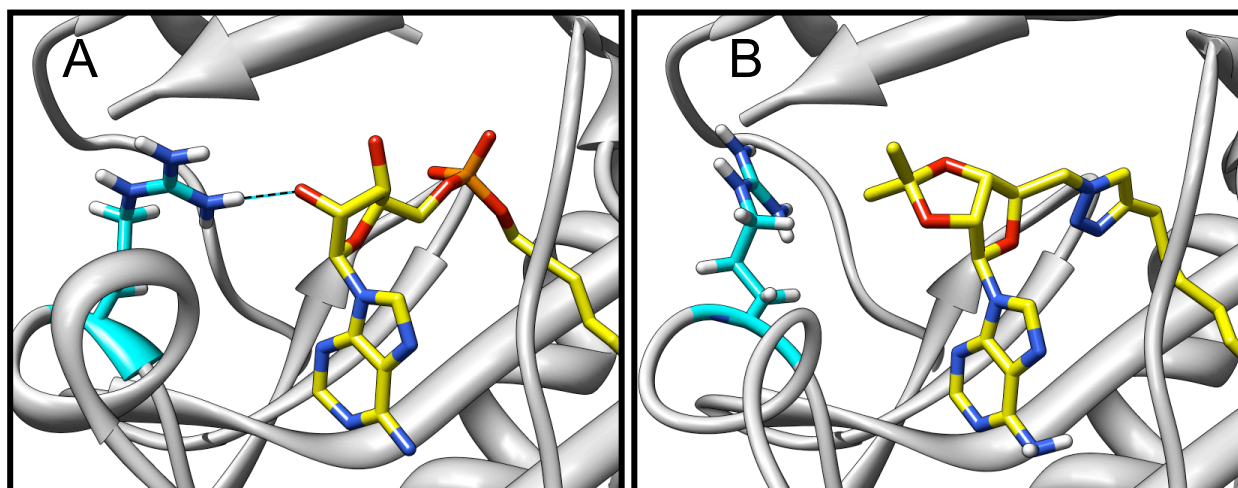


Fig S4: Mechanism of binding for inhibitors 7 and 14.

The figure depicts key residues in the ATP pocket of SaBPL required for binding of inhibitors (A) **7** and (B) **14** (shown in yellow stick mode). Hydrophobic amino acids are highlighted in orange, and other important residues are shown in white stick. The biotin-binding loop (BBL) and ATP-binding loop (ABL) are also shown. A. The adenine moiety buttresses against the side chain of Trp127 for a $\pi - \pi$ stacking interaction, as well as hydrophobic interactions with the ABL and hydrogen bonding interactions with Asn 212 and Ser 128. B. The benzoxazolone moiety adopts a displaced π interaction with Trp 127, and hydrophobic interactions with the ABL.

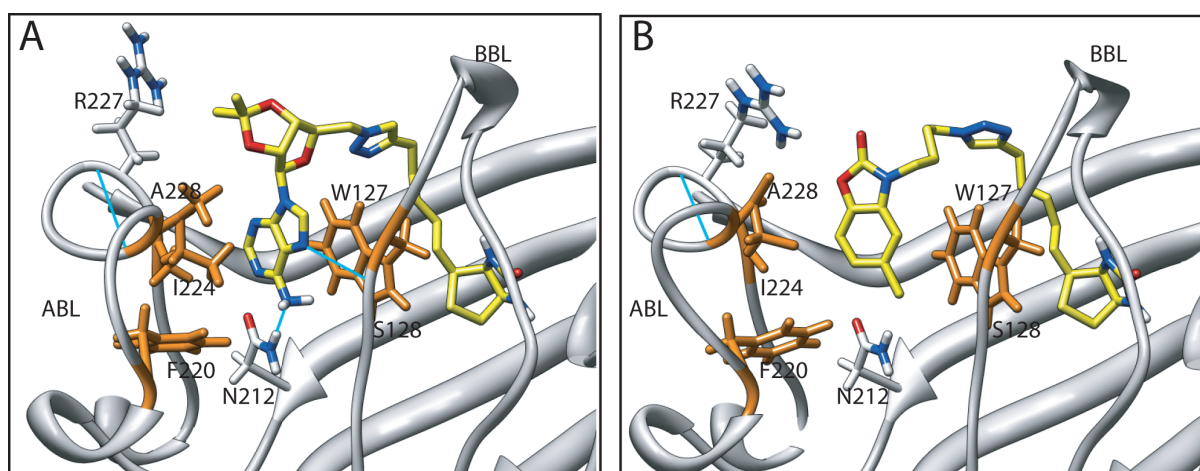


Fig S5: Circular dichroism analysis of SaBPL and Arg 125 muteins.

CD spectra confirmed that wildtype and Arg 125 muteins fold similarly in solution. All three spectra are comprised of double minima at 208 nm and 222 nm, which is characteristic of a predominantly α -helical structure. Therefore, the decrease in catalytic efficiency for the muteins cannot be accounted for by gross perturbations in the secondary structure upon mutation. The chromatographs for wildtype (grey), Arg 125→Ala (red) and Arg 125→Asn (blue) are overlaid.

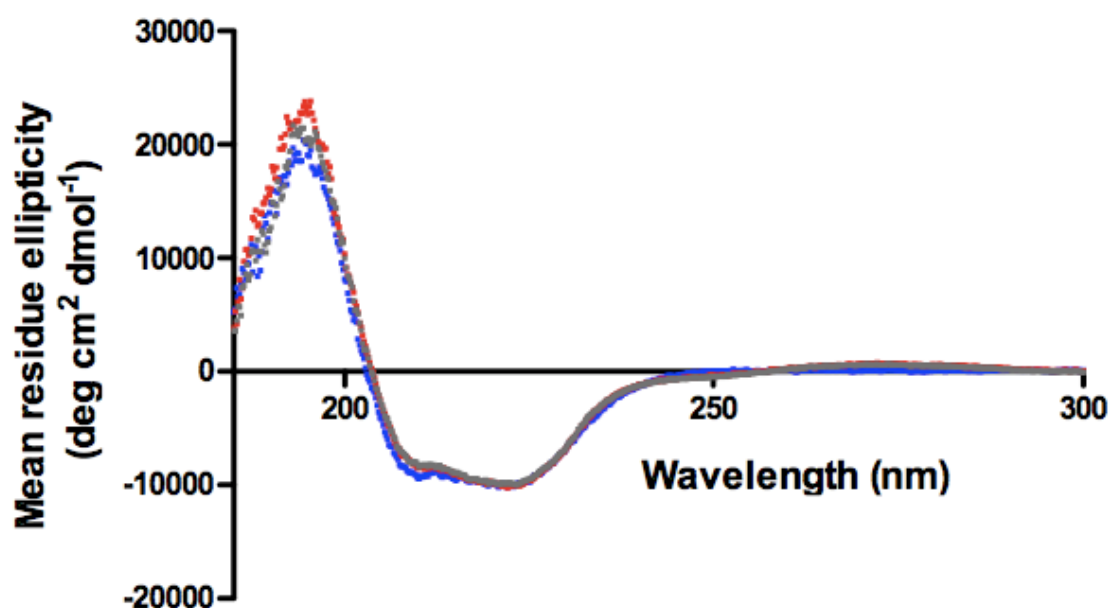


Table S1: Data collection and refinement statistics

	SaBPL with 2	SaBPL with 7	SaBPL with 14
Data collection^a			
Space group	<i>P</i> 4 ₂ 2 ₁ 2	P 4(2) 2(1) 2	P 4(2) 2(1) 2
Cell dimensions			
<i>a</i> , <i>b</i> , <i>c</i> (Å)	94.6,94.6, 130.6	93.06 93.06 130.14	93.5 93.5 130.41
<i>a</i> , <i>b</i> , <i>g</i> (°)	90, 90, 90	90 90 90	90 90 90
Resolution (Å)	49.5-2.5 (2.56-2.5)	50-2.77 (2.94- 2.77)	58.97 - 3.1 (3.185 – 3.1)
<i>R</i> _{sym} or <i>R</i> _{merge}	4.1 (34.7)	11.7 (71.4)	19.0 (77.9)
<i>I</i> / <i>sI</i>	16.6 (2.2)	12.46 (2.60)	7.34 (2.40)
Completeness (%)	99.2 (99.6)	97.9 (99.4)	99.5 (98.0)
Redundancy	11.6 (11.8)	5.46 (5.71)	6.95 (6.94)
Refinement			
Resolution (Å)	49.5-2.5	50 - 2.77	50 - 3.1
No. reflections	20793	14797	10421
<i>R</i> _{work} / <i>R</i> _{free}	21.0/25.5	18.5/22.35	20.284/25.63
No. atoms			
Protein	2614	2602	2613
Ligand/ion	37	39	33
Water	106	85	58
<i>B</i> -factors			
Protein	45.3	46.161	44.183
Ligand/ion	45.1	39.740	33.403
Water	45.2	40.164	32.068
R.m.s. deviations			
Bond lengths (Å)	0.020	0.009	0.0163
Bond angles (°)	1.9	1.543	1.7517

^a Diffraction data was collected from one crystal for each structure

Table S2: Kinetic analysis of wildtype *S. aureus* BPL and the Arg 125 mutant enzymes

Kinetic properties were determined for the ligands biotin and MgATP.

SaBPL	Biotin		MgATP	
	$k_{\text{cat}} (\text{s}^{-1}) \times 10^3$	$K_m (\mu\text{M})$	$k_{\text{cat}} (\text{s}^{-1}) \times 10^3$	$K_m (\text{mM})$
WT	450 ± 90	1.01 ± 0.16	360 ± 70	0.18 ± 0.03
Arg125 Ala	0.81 ± 0.11	1.08 ± 0.12	0.44 ± 0.06	0.42 ± 0.39
Arg125 Asn	0.84 ± 0.12	1.08 ± 0.14	0.52 ± 0.09	0.35 ± 0.05

Supplementary Experimental Procedures

***In vitro* biotinylation assays**

Quantitation of BPL catalysed ³H-biotin incorporation into the biotin domain substrate was performed as previously described (Polyak et al., 1999; Polyak et al., 2001). The *IC*₅₀ value of each compound was determined from a dose-response curve by varying the concentration of the inhibitor under the same enzyme concentration. The data was analysed with GraphPad Prism software using a non-linear fit of log₁₀ (inhibitor) vs. normalized response. The *K*_i, the absolute inhibition constant for a compound, was determined using Eq1 (Cheng and Prusoff, 1973):

$$\text{Eq1. } K_i = IC_{50} / (1 + [S] / K_m)$$

where *K*_m is the affinity of the substrate for the enzyme ([biotin] =1.01 μM, Table S2) and [S] is the substrate concentration ([biotin] =5 μM). The mode of inhibition was investigated by varying the concentrations of inhibitor alongside varying the concentrations of ³H-biotin. The data was plotted as double reciprocal plots and assessed using Lineweaver-Burk analysis. Data reported here are the means of three independent assays (*n* = 3) ± standard error of the mean. Statistical analysis between two data sets was performed using a two-tailed unpaired *t* test using GraphPad Prism.

Surface Plasmon Resonance

SPR was performed using a Biacore™ T100 instrument (GE Healthcare). BPL was immobilised on a CM5 sensor chip by amine coupling, as previously described (Mayende et al., 2012). SaBPL (120 μg/mL) in 10 mM sodium acetate buffer (pH 5.8) was coupled onto the surface and 1 M ethanolamine hydrochloride was injected to block any unreacted sites. Typically, 6,500 resonance units of BPL were immobilised on the sensor chip. One channel was left blank which was subtracted from sample channel to allow analysis methods to distinguish between actual and non-specific binding. Experiment was conducted at 25° C at a flow rate of 30 μL/minute with a running buffer containing 10 mM HEPES pH 7.4, 150 mM NaCl and 0.005% (v/v)

surfactant. The concentration of biotin used was 10 μM and the MgATP concentration used was 500 μM .

Circular Dichroism Analysis

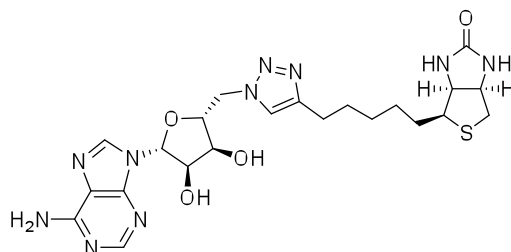
Far UV CD spectra were recorded at 20° C using a Jasco CD J-185 spectrophotometer. Purified wild-type and mutant SaBPL were dialysed overnight against the assay buffer (10 mM NaPO₄ pH 8.0) at 4° C prior to analysis. Final concentrations of the proteins used were 0.25 mg/mL (6.5 μM). CD spectra were recorded from 185 nm to 300 nm at 0.2 nm increments, using a 1 mm path length quartz cell. The reported spectra are the average of five scans that were corrected for buffer blanks.

Synthesis and characterisation of chemicals used in this study

General copper azide alkyne cycloaddition procedure:

To a solution of the appropriate azide (1.0 eq) and alkyne (1.0 eq) in acetonitrile (1 mL per 100 mg of alkyne) were added de-ionised water (0.5 mL per 100 mg of alkyne) and copper nano powder (0.2 eq). The reaction mixture was sonicated for 15 min followed by stirring for 4 h at 35 °C. The reaction mixture was concentrated *in vacuo* and purified by silica gel column chromatography. See individual experiments for details.

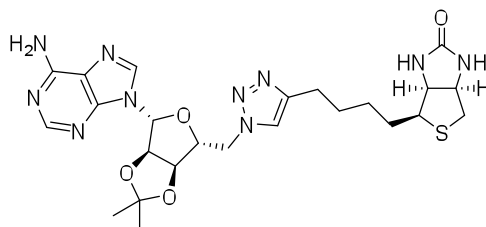
(3a*S*,4*S*,6a*R*)-4-[5-[1-[[[(2*R*,3*S*,4*R*,5*R*)-5-(6-Aminopurin-9-yl)-3,4-dihydroxy-tetrahydrofuran-2-yl]methyl]triazol-4-yl]pentyl]-1,3,3a,4,6,6a-hexahydrothieno[3,4-*d*]imidazol-2-one (Compound 5)



To a solution of compound **7** (15 mg, 0.03 mmol) in dichloromethane (1 mL) was added TFA (0.9 mL) and water (0.1 mL) and stirred for 3 h. The reaction mixture was concentrated *in vacuo* and purified by flash chromatography using 20% methanol in dichloromethane to give a white solid (6 mg, 43%).

¹H NMR (300 MHz, DMSO-*d*₆): δ 8.22 (1H, s, ArH), 8.15 (1H, s, ArH), 7.67 (1H, s, Ar^{tri}H), 7.37 (2H, bs, ArNH₂), 6.54 (1H, bs, C(O)NH), 6.38 (1H, bs, C(O)NH), 5.90 (1H, d, *J* = 5.4 Hz, 1' CH), 5.67 (1H, bs, OH), 5.54 (1H, bs, OH), 4.59-4.73 (3H, m), 4.28-4.33 (1H, m, NHCH), 4.20-4.27 (2H, m, 5' CH₂), 4.11-4.15 (1H, m, NHCH), 3.05-3.11 (1H, m, SCH), 2.81 (1H, dd, *J* = 5.1, 12.3 Hz, SCH_a), 2.50-2.59 (3H, m (under DMSO residual peak), ArC^{tri}CH₂, SCH_b), 1.65-1.211 (8H, m, 4 x CH₂); **¹³C NMR** (150 MHz, DMSO-*d*₆): δ 162.7, 156.1, 152.6, 149.2, 146.7, 139.8, 122.5, 119.2, 87.7, 82.3, 72.5, 71.1, 70.8, 61.1, 59.2, 55.5, 51.0, 40.0, 28.6, 28.3, 28.2, 24.8; **HRMS** calcd. for (M+ H) C₂₂H₃₁N₁₀O₄S: requires 531.2251, found 531.2231.

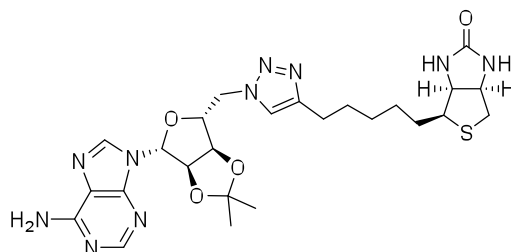
(3a*S*,4*S*,6a*R*)-4-[4-[1-[[[(3a*R*,4*R*,6*R*,6a*R*)-4-(6-Aminopurin-9-yl)-2,2-dimethyl-3a,4,6,6a-tetrahydrofuro[3,4-*d*][1,3]dioxol-6-yl]methyl]triazol-4-yl]butyl]-1,3,3a,4,6,6a-hexa hydrothieno[3,4-*d*]imidazol-2-one (Compound 6)



Norbiotin acetylene **17** (15 mg, 0.05 mmol) was reacted with adenosine azide **4** (16 mg, 0.05 mmol) and Cu nanopowder (1 mg, 0.02 mmol) according to CuAAC general procedure. The crude material was purified by flash chromatography eluting with 9% methanol in dichloromethane to yield a white solid, (15 mg, 60%).

¹H NMR (600 MHz; 1% CD₃OD, CDCl₃): δ 8.17 (1H, s, ArH), 7.81 (1H, s, ArH), 7.12 (1H, s, Ar^{tri}H), 5.93 (1H, d, *J* = 3.0 Hz, 1' CH), 5.48 (1H, dd, *J* = 3.0, 7.2 Hz, 2' CH), 5.02 (0.25H, bs, C(O)NH, exchanged with solvent), 4.88 (1H, dd, *J* = 4.2, 15.0 Hz, 5' CH_a), 4.84 (1H, t, *J* = 6.0 Hz, 3' CH), 4.57 (1H, dd, *J* = 3.0, 15.0 Hz, 5' CH_b), 4.53-4.54 (1H, m, CHNH), 4.43-4.45 (2H, m, 4' CH, CHNH), 3.18-3.21 (1H, m SCH), 2.96 (1H, dd, *J* = 5.4, 13.2 Hz, SCH_a), 2.74 (1H, d, *J* = 13.2 Hz, SCH_b), 2.66-2.70 (2H, m, ArC^{tri}CH₂), 1.70-1.74 (2H, m, CH₂), 1.37 - 1.61 (10H, m); **¹³C NMR** (150 MHz; 1% CD₃OD, CDCl₃): δ 163.9, 156.4, 152.9, 148.7, 148.0, 140.1, 122.9, 115.8, 89.9, 82.8, 82.0, 79.3, 62.2, 59.7, 55.6, 49.9, 49.8, 40.8, 29.6, 28.8, 28.6, 27.2, 25.3, 25.1.

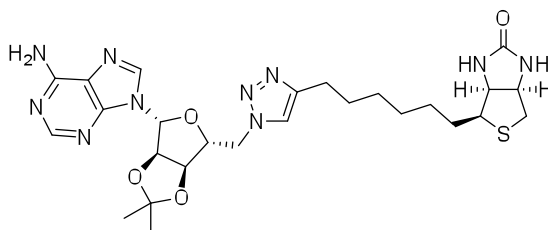
(3a*S*,4*S*,6a*R*)-4-[5-[1-[[[(3a*R*,4*R*,6*R*,6a*R*)-4-(6-Aminopurin-9-yl)-2,2-dimethyl-3a,4,6,6a-tetrahydrofuro[3,4-*d*][1,3]dioxol-6-yl]methyl]triazol-4-yl]pentyl]-1,3,3a,4,6,6a-hexa hydrothieno[3,4-*d*]imidazol-2-one (Compound 7)



Biotin acetylene **3** (Corona et al., 2006) (16 mg, 0.066 mmol) was reacted with adenosine azide **4** (20 mg, 0.06 mmol) and Cu nanopowder (1 mg, 0.02 mmol) according to CuAAC general procedure. The reaction mixture was concentrated *in vacuo* and the resulting residue was purified by flash chromatography eluting with 10% methanol in dichloromethane to give a white solid (25 mg, 73%)

¹H NMR (300 MHz, CDCl₃): δ 8.21 (1H, s, ArH), 7.74 (1H, bs, C(O)NH), 7.53 (1H, s, ArH), 7.07 (1H, s, Ar^{tri}H), 6.93 (2H, bs, ArNH₂), 6.00 (1H, d, *J* = 3.6 Hz, 1' CH), 5.27 (1H, dd, *J* = 3.6, 8.8 Hz, 2' CH), 5.05 (1H, bs, C(O)NH), 5.01 (1H, dd, *J* = 3.9, 8.8 Hz, 3' CH), 4.91 (1H, dd, *J* = 5.4, 14.4 Hz, 5' CH_a), 4.52-4.63 (3H, m, 5' CH_b, 4' CH, NHCH), 4.35-4.40 (1H, NHCH), 3.15-3.22 (1H, SCH), 2.93 (1H, dd, *J* = 4.8, 12.9 Hz, SCH_a), 2.67-2.78 (2H, SCH_b, ArC^{tri}CH_a), 2.48-2.50 (1H, m, ArC^{tri}CH_b), 1.25-1.77 (14H, m); **¹³C NMR** (75 MHz, CDCl₃): δ 164.3, 156.6, 153.4, 149.5, 148.1, 139.5, 123.2, 115.8, 90.1, 83.3, 82.9, 80.6, 63.0, 60.3, 56.3, 50.5, 40.9, 29.5, 29.2, 28.6, 27.5, 25.8, 25.7; **HRMS** calcd. for (M+ H) C₂₅H₃₅N₁₀O₄S: requires 571.2564, found 571.2564.

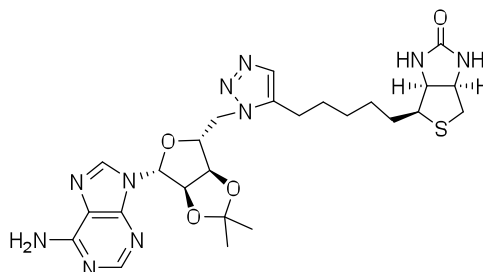
(3a*S*,4*S*,6a*R*)-4-[6-[1-[[[(3a*R*,4*R*,6*R*,6a*R*)-4-(6-Aminopurin-9-yl)-2,2-dimethyl-3a,4,6,6a-tetrahydrofuro[3,4-*d*][1,3]dioxol-6-yl]methyl]triazol-4-yl]hexyl]-1,3,3a,4,6,6a-hexa hydrothieno[3,4-*d*]imidazol-2-one (Compound 8)



Homobiotin acetylene **20** (10 mg, 0.04 mmol) was reacted with adenosine azide **4** (14 mg, 0.04 mmol) and Cu nanopowder (1 mg, 0.02 mmol) according to CuAAC general procedure. The crude material was purified by flash chromatography eluting with 9% methanol in dichloromethane to yield a white solid (16 mg, 69%).

MP: 123 - 128 °C; **¹H NMR** (600 MHz; CDCl₃): δ 8.29 (1H, s, ArH), 7.93 (1H, s, ArH), 7.42 (1H, bs, ArNH), 7.13 (1H, s, Ar^{tri}H), 6.80 (1H, bs, ArNH), 6.06 (1H, bs, C(O)NH), 5.80 (1H, bs, C(O)NH), 5.37 (1H, d, *J* = 4.2 Hz, 1' CH), 5.11 (1H, dd, *J* = 4.8, 6.3 Hz, 3' CH), 4.82 (1H, dd, *J* = 6.0, 14.4 Hz, 5' CH_a), 4.68 (1H, dd, *J* = 3.0, 14.4 Hz, 5' CH_b), 4.58-4.60 (1H, m, 4' CH), 4.53-4.55 (1H, m, NHCH), 4.35-4.37 (1H, m, NHCH), 3.14-3.17 (1H, m, SCH), 2.94 (1H, dd, *J* = 4.8, 12.9 Hz, SCH_a), 2.75 (1H, d, *J* = 12.9 Hz, SCH_b), 2.61 (2H, t, *J* = 7.8 Hz, ArC^{tri}CH₂), 1.46-1.73 (4H, m, 2 x CH₂), 1.60 (3H, s, CCH₃), 1.37 (3H, s, CCH₃), 1.26-1.28 (6H, m, 3 x CH₂); **¹³C NMR** (150 MHz; CDCl₃): δ 164.4, 156.5, 153.4, 149.3, 148.5, 140.1, 122.6, 120.5, 115.4, 90.7, 84.7, 83.3, 81.3, 77.5, 62.5, 60.3, 56.1, 51.1, 40.9, 29.4, 29.2, 28.9, 28.9, 27.5, 25.7, 25.6; **HRMS** calcd. for (M + H) C₂₆H₃₇N₁₀O₄S: requires 585.2720, found 585.2745.

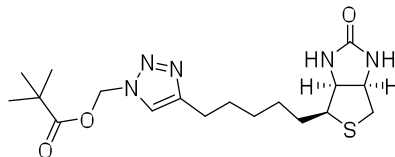
(3a*S*,4*S*,6a*R*)-4-[5-[3-[[[(3a*R*,4*R*,6*R*,6a*R*)-4-(6-Aminopurin-9-yl)-2,2-dimethyl-3a,4,6,6a-tetrahydrofuro[3,4-*d*][1,3]dioxol-6-yl]methyl]triazol-4-yl]pentyl]-1,3,3a,4,6,6a-hexahydro thieno[3,4-*d*]imidazol-2-one (Compound 9)



To a solution of biotin acetylene **3** (Corona et al., 2006) (20 mg, 0.08 mmol) and adenosine azide **4** (31 mg, 0.09 mmol) in THF (2.5 mL) was added Cp*Ru(PPh₃)₂Cl (1 mg, 0.001 mmol) and the solution was refluxed under nitrogen atmosphere for 4h. The reaction mixture was cooled, diluted with dichloromethane (25 mL), washed with water (1 x 25 mL) and brine (1 x 25 mL), dried over Na₂SO₄, filtered and concentrated *in vacuo*. The residue was purified by flash chromatography eluting with 8% methanol in dichloromethane to give a light yellow solid (5 mg, 10%).

¹H NMR (600 MHz, CDCl₃): δ 8.31 (1H, s, ArH), 7.80 (1H, s, ArH), 7.78 (1H, bs, C(O)NH), 7.30 (1H, s, Ar^{tri}H), 7.09 (2H, bs, ArNH₂), 6.04 (1H, s, 1' CH), 5.86 and 5.83 (1H, bd, C(O)NH), 5.42 (1H, d, *J* = 6.0 Hz, 2' CH), 5.33 (1H, dd, *J* = 2.4, 6.0 Hz, 3' CH), 4.69-4.84 (3H, m, 5' CH₂, 4' CH), 4.59-4.61 (1H, m, NHCH), 4.37-4.39 (1H, m, NHCH); 3.12 (1H, m, SCH), 2.95 (1H, dd, *J* = 4.8, 12.6 Hz, SCH_a), 2.71 (1H, d, *J* = 12.6 Hz, SCH_b), 1.76-1.90 (2H, m), 1.60 (3H, s, CCH₃), 1.40 (3H, s, CCH₃), 1.39-1.29 (6H, m, CH₂, ArC^{tri}CH₂), 0.87-0.92 (1H, m), 0.47-0.53 (1H, m); **¹³C NMR** (150 MHz, CDCl₃): 164.5, 156.5, 153.0, 148.6, 143.9, 138.2, 131.7, 120.2, 114.6, 110.0, 91.4, 82.3, 84.5, 82.5, 62.2, 60.1, 56.1, 40.7, 30.3, 29.2, 29.1, 28.1, 27.1, 25.4, 23.0; **HRMS** calcd. for (M + H) C₂₅H₃₅N₁₀O₄S: requires 571.2564, found 571.2586.

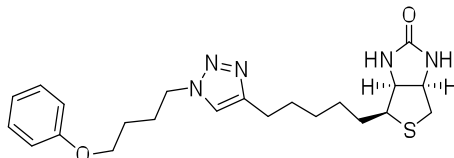
[4-[5-[(3a*S*,4*S*,6a*R*)-2-oxo-1,3,3a,4,6,6a-hexahydrothieno[3,4-*d*]imidazol-4-yl]pentyl]triazol-1-yl]methyl 2,2-dimethylpropanoate (Compound 10)



Biotin acetylene **3** (32 mg, 0.13 mmol) and azidomethylpivalate (Loren et al., 2005) (23 mg, 0.15 mmol) was reacted according to CuAAC general procedure. The residue was purified by flash chromatography eluting with 5% methanol in dichloromethane to give a white solid (25 mg, 48%).

¹H NMR (300 MHz, CDCl₃): δ 7.53 (1H, s, ArH), 6.19 (2H, s, OCH₂), 5.62 (1H, bs, C(O)NH), 5.24 (1H, bs, C(O)NH), 4.49-4.53 (1H, m, NHCH), 4.28-4.33 (1H, m, NHCH), 3.12-3.18 (1H, m, SCH), 2.90 (1H, dd, *J* = 4.8, 12.6 Hz, SCH_a), 2.69-2.74 (3H, m, SCH_b, ArCH₂), 1.67-1.76 (4H, m, 2 x CH₂), 1.34-1.52 (4H, m, 2 x CH₂), 1.18 (9H, s, CCH₃); **¹³C NMR** (75 MHz, CDCl₃): δ 178.2, 163.9, 149.0, 122.4, 69.9, 62.3, 60.4, 56.0, 40.8, 39.1, 29.3, 29.1, 29.0, 28.8, 27.1, 25.6.

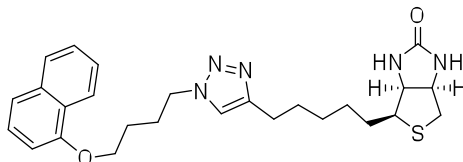
(3a*S*,4*S*,6a*R*)-4-[5-[1-(4-Phenoxybutyl)triazol-4-yl]pentyl]-1,3,3a,4,6,6a-hexahydrothieno[3,4-*d*]imidazol-2-one (Compound 11)



Biotin acetylene **3** (18 mg, 0.075 mmol) was reacted with 4-azidobutoxybenzene (13, 14) (16 mg, 0.083 mmol) and Cu nanopowder (1 mg, 0.015 mmol) according to CuAAC general procedure. The residue was purified by flash chromatography eluting with 7% methanol in dichloromethane to give a white solid, (21 mg, 64%).

MP: 117 - 120 °C; **¹H NMR** (300 MHz, CDCl₃): δ 7.25-7.31 (3H, m, Ar^{tri}H, ArH), 6.86-6.97 (3H, m, ArH), 5.55 (1H, bs, C(O)NH), 5.18 (1H, bs, C(O)NH), 4.47-4.51 (1H, m, NHCH), 4.41 (2H, t, *J* = 7.2 Hz, ArN^{tri}CH₂), 4.27-4.31 (1H, m NHCH), 3.98 (2H, t, *J* = 6.0 Hz, ArOCH₂), 3.11-3.18 (1H, m, SCH), 2.90 (1H, dd, *J* = 5.1, 12.9 Hz, SCH_a), 2.67-2.73 (3H, m, SCH_b, ArC^{tri}CH₂), 2.06-2.16 (2H, m, CH₂), 1.63-1.85 (4H, m, 2 x CH₂), 1.37-1.50 (4H, m, 2 x CH₂); **¹³C NMR** (75 MHz, CDCl₃): δ 163.5, 158.9, 129.7, 121.0, 120.8, 114.6, 67.0, 62.2, 60.3, 55.9, 50.0, 40.8, 29.3, 28.9, 28.8, 27.5, 26.5, 25.7; **HRMS** calcd. for (M + H) C₂₂H₃₂N₅O₂S: requires 430.2277, found 430.2311.

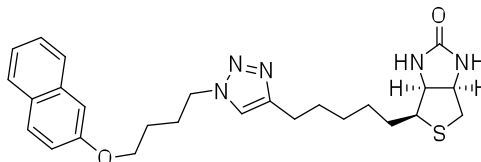
(3a*S*,4*S*,6a*R*)-4-[5-[1-[4-(1-Naphthyloxy)butyl]triazol-4-yl]pentyl]-1,3,3a,4,6,6a-hexahydrothieno[3,4-*d*]imidazol-2-one (Compound 12)



Biotin acetylene **3** (16 mg, 0.07 mmol) was reacted with 1-(4-bromobutoxy)naphthalene (15, **16**) (18 mg, 0.07 mmol) and Cu nanopowder (1 mg, 0.02 mmol) according to CuAAC general procedure. The residue was purified by flash chromatography eluting with 8% methanol in dichloromethane to give a white solid, (14 mg, 41%).

MP: 97 - 98 °C; **¹H NMR** (300 MHz, CDCl₃): δ 8.21-8.24 (1H, m, ArH), 7.78-7.81 (1H, s, ArH), 7.37-7.50 (4H, m, ArH), 7.29 (1H, s, Ar^{tri}H), 6.87 (1H, d, *J* = 7.5 Hz, ArH), 5.63 (1H, bs, C(O)NH), 5.24 (1H, bs, C(O)NH), 4.45 (3H, m, ArN^{tri}CH₂, NHCH), 4.23-4.27 (1H, m, NHCH), 4.15 (2H, t, *J* = 6.0 Hz, ArOCH₂), 3.08-3.14 (1H, m, SCH), 2.87 (1H, dd, *J* = 5.1, 12.6 Hz, SCH_a), 2.67-2.71 (3H, m, SCH_b, ARC^{tri}CH₂), 2.16-2.26 (2H, m, CH₂), 1.90-2.00 (2H, m, CH₂), 1.57-1.71 (2H, m, 2 x CH₂), 1.33-1.48 (2H, m, 2 x CH₂); **¹³C NMR** (75 MHz, CDCl₃): δ 163.6, 154.6, 134.7, 127.7, 126.6, 126.0, 125.7, 125.4, 122.0, 120.8, 120.5, 104.8, 67.2, 62.2, 55.9, 50.1, 40.7, 29.3, 29.2, 28.9, 28.7, 27.8, 26.5, 25.7; **HRMS** calcd. for (M+ H) C₂₆H₃₄N₅O₂S: requires 480.2433, found 480.2458.

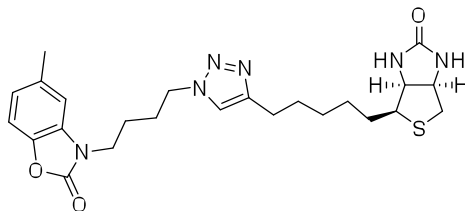
(3a*S*,4*S*,6a*R*)-4-[5-[1-[4-(2-Naphthyloxy)butyl]triazol-4-yl]pentyl]-1,3,3a,4,6,6a-hexahydrothieno[3,4-*d*]imidazol-2-one (Compound 13)



Biotin acetylene **3** (18 mg, 0.07 mmol) was reacted with 2-(4-bromobutoxy)naphthalene (Huang et al., 2010) (20 mg, 0.08 mmol) and Cu nanopowder (1 mg, 0.02 mmol) according to CuAAC general procedure. The residue was purified by flash chromatography eluting with 8% methanol in dichloromethane to give a white solid, (26 mg, 74%).

MP: 96-98 °C; **¹H NMR** (300 MHz, CDCl₃): δ 7.70-7.77 (3H, m, ArH), 7.41-7.46 (1H, m, ArH), 7.31-7.35 (1H, m, ArH), 7.30 (1H, Ar^{tri}H), 7.10-7.14 (2H, m, ArH), 5.39 (1H, bs, C(O)NH), 5.05 (1H, bs, C(O)NH), 4.41-4.50 (3H, m, NHCH, ArN^{tri}CH₂), 4.26-4.30 (1H, m, NHCH), 4.10 (2H, t, *J* = 6.0 Hz, ArOCH₂), 3.10-3.16 (1H, m, SCH), 2.89 (1H, dd, *J* = 5.4, 12.9 Hz, SCH_a), 2.67-2.73 (3H, m, SCH_b, ArC^{tri}CH₂), 2.11-2.20 (2H, m, CH₂), 1.83-1.92 (2H, m, CH₂), 1.63-1.72 (4H, m, 2 x CH₂), 1.37-1.46 (4H, m, 2 x CH₂); **¹³C NMR** (75 MHz, CDCl₃): δ 163.8, 156.8, 148.4, 134.7, 129.6, 129.1, 127.8, 126.9, 126.6, 123.9, 120.8, 118.9, 106.8, 67.1, 62.2, 60.3, 56.0, 50.0, 40.7, 29.3, 29.2, 24.9, 28.7, 27.5, 26.4, 25.7; **HRMS** calcd. for (M+ H) C₂₆H₃₄N₅O₂S: requires 480.2433, found 480.2454.

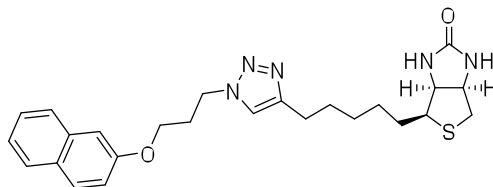
3-[4-[4-[5-[(3a*S*,4*S*,6a*R*)-2-Oxo-1,3,3a,4,6,6a-hexahydrothieno[3,4-*d*]imidazol-4-yl]pentyl]triazol-1-yl]butyl]-5-methyl-1,3-benzoxazol-2-one (Compound 14)



Biotin acetylene **3** (Corona et al., 2006) (21 mg, 0.06 mmol) was reacted with azide **21** (24 mg, 0.06 mmol) and Cu nanopowder (1 mg, 0.02 mmol) according to CuAAC general procedure. The residue was purified by flash chromatography eluting with 8% methanol in dichloromethane to give a white solid, (29 mg, 68%).

MP: 99 - 101 °C; **¹H NMR** (300 MHz, CDCl₃): δ 7.32 (1H, s, Ar^{tri}H), 7.06 (1H, d, *J* = 8.1 Hz, ArH), 6.90 (1H, d, *J* = 8.1 Hz, ArH), 6.77 (1H, m, ArH), 6.22 (1H, bs, C(O)NH), 5.81 (1H, bs, C(O)NH), 4.46-4.50 (1H, m, NHCH), 4.39 (2H, t, *J* = 6.9 Hz, ArN^{tri}CH₂), 4.26-4.31 (1H, m, NHCH), 3.83 (2H, t, *J* = 6.9 Hz, NCH₃), 3.11-3.17 (1H, m, SCH), 2.89 (1H, dd, *J* = 5.1, 12.6 Hz, SCH_a), 2.66-2.73 (3H, m, SCH_b, ArC^{tri}CH₂), 2.39 (3H, s, ArCH₃), 1.93-2.03 (2H, m, CH₂), 1.65-1.84 (6H, m, 3 x CH₂), 1.33-1.43 (4H, m, 2 x CH₂); **¹³C NMR** (300 MHz, CDCl₃): δ 164.0, 155.1, 148.5, 140.8, 134.1, 130.8, 123.1, 121.0, 109.8, 109.0, 62.2, 60.3, 56.0, 49.3, 41.3, 40.7, 29.3, 29.2, 28.9, 28.7, 27.4, 25.7, 24.8, 21.7; **HRMS** calcd. for (M + H) C₂₄H₃₃N₆O₃S: requires 485.2335, found 485.2359.

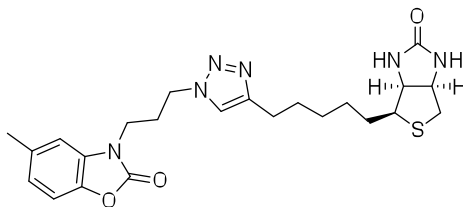
(3a*S*,4*S*,6a*R*)-4-[5-[1-[3-(2-Naphthyloxy)propyl]triazol-4-yl]pentyl]-1,3,3a,4,6,6a-hexahydrothieno[3,4-*d*]imidazol-2-one (Compound 15)



Biotin acetylene **3** (20 mg, 0.08 mmol) was reacted with 2-(3-azidopropoxy)naphthalene (Huang et al., 2010; Shinde et al., 2009) (21 mg, 0.09 mmol) and Cu nanopowder (1 mg, 0.02 mmol) according to CuAAC general procedure. The residue was purified by flash chromatography eluting with 8% methanol in dichloromethane to give a white solid, (20 mg, 51%).

¹H NMR (300 MHz, CDCl₃): δ 7.77 (1H, d, J = 7.5 Hz, ArH), 7.75 (1H, d, J = 8.9 Hz, ArH), 7.71 (1H, d, J = 7.5 Hz, ArH), 7.42-7.47 (1H, m, ArH), 7.32-7.37 (1H, m, ArH), 7.28 (1H, s, Ar^{tri}H), 7.14 (1H, dd, J = 2.7, 8.7 Hz, ArH), 7.09 (1H, d, J = 2.7 Hz, ArH), 5.50 (1H, bs, C(O)NH), 5.15 (1H, bs, C(O)NH), 4.59 (2H, t, J = 6.6 Hz, ArN^{tri}CH₂), 4.44-4.49 (1H, m, NHCH), 4.23-4.27 (1H, m, NHCH), 4.07 (2H, t, J = 6.0 Hz, ArOCH₂), 3.06-3.13 (1H, m, SCH), 2.87 (1H, dd, J = 5.1, 12.6 Hz, SCH_a), 2.65-2.72 (3H, m, SCH_b, ArC^{tri}CH₂), 2.41-2.49 (2H, m, CH₂), 1.62-1.69 (4H, m, 2 x CH₂), 1.34-1.42 (4H, m, 2 x CH₂); **¹³C NMR** (75 MHz, CDCl₃): δ 163.4, 156.6, 148.3, 134.6, 129.8, 129.3, 127.9, 127.0, 126.7, 124.0, 121.5, 118.8, 106.9, 64.3, 62.2, 60.2, 55.9, 47.1, 40.7, 30.1, 29.2, 29.1, 28.9, 25.7; **HRMS** calcd. for (M+ H) C₂₅H₃₂N₅O₂S: requires 466.2277, found 466.2294.

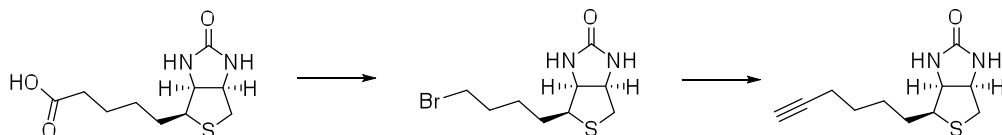
3-[3-[4-[5-[(3a*S*,4*S*,6a*R*)-2-Oxo-1,3,3a,4,6,6a-hexahydrothieno[3,4-*d*]imidazol-4-yl]pentyl]triazol-1-yl]propyl]-5-methyl-1,3-benzoxazol-2-one (Compound 16)



Biotin acetylene **3** (14 mg, 0.06 mmol) was reacted with azide **22** (15 mg, 0.06 mmol) and Cu nanopowder (1 mg, 0.02 mmol) according to CuAAC general procedure. The residue was purified by flash chromatography eluting with 8% methanol in dichloromethane to give a white solid, (17 mg, 61%).

MP: 134-136 °C; **¹H NMR** (300 MHz, CDCl₃): δ 7.48 (1H, s, Ar^{tri}H), 7.08 (1H, d, *J* = 8.1 Hz, ArH), 6.92 (1H, d, *J* = 8.1 Hz, ArH), 6.78 (1H, s, ArH), 5.70 (1H, bs, C(O)NH), 5.30 (1H, bs, C(O)NH), 4.48-4.52 (1H, m, NHCH), 4.40 (2H, t, *J* = 6.6 Hz, ArN^{tri}CH₂), 4.29-4.33 (1H, m, NHCH), 3.87 (2H, t, *J* = 6.6 Hz, NCH₂), 3.12-3.19 (1H, m, SCH), 2.90 (1H, dd, *J* = 5.1, 12.6 Hz, SCH_a), 2.70-2.74 (3H, m, SCH_b, ArC^{tri}CH₂), 2.39-2.47 (5H, m, CH₂, ArCH₃), 1.36-1.78 (8H, m, 4 x CH₂); **¹³C NMR** (75 MHz, CDCl₃): δ 163.6, 155.28, 148.4, 140.9, 134.4, 130.7, 123.4, 121.9, 110.0, 109.1, 62.2, 60.3, 55.9, 47.3, 40.8, 39.5, 29.2, 28.9, 28.7, 28.67, 25.7, 21.8 **HRMS** calcd. for (M + H) C₂₃H₃₁N₆O₃S: requires 471.2178, found 471.2198.

(3a*S*,6a*R*)-4-Hex-5-ynyl-1,3,3a,4,6,6a-hexahydrothieno[3,4-*c*]imidazol-2-one
(Compound 17)



To a suspension of biotin (121 mg, 0.50 mmol) in anhydrous dichloromethane (10 mL) were added thionyl chloride (243 mg, 1.98 mmol) and DMF (1 mL) and the solution was stirred under nitrogen atmosphere for 1 h. The reaction mixture was concentrated *in vacuo* and used as crude. The acid chloride and pyridine sodium salt (82 mg, 0.55 mmol) were suspended in 9:1 DMF and bromotrichloromethane (5 mL) and the mixture was stirred at 80 °C for 4 h. The mixture was cooled and diluted with de-ionized ice water (1 x 20 mL) and extracted with dichloromethane (6 x 25 mL). The organic layer was washed with 0.25 M aqueous NaOH (1 x 100 mL), 0.25 M aqueous HCl (1 x 100 mL), water (1 x 100 mL) and brine (1 x 100 mL), dried over Na₂SO₄ and filtered. Activated carbon was added to the solution and stirred for 30 min, filtered over Celite® and washed with dichloromethane (3 x 100 mL). The filtrate was concentrate *in vacuo* and the residue was purified by flash chromatography eluting with 6% MeOH in DCM to give norbiotin bromide as a white solid (29 mg, 21%).

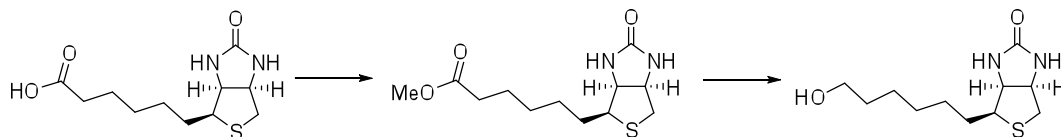
MP: 146 – 148 °C; **¹H NMR** (300 MHz, DMSO-*d*₆): δ 6.49 (1H, bs, NH), 6.42 (1H, bs, NH), 4.33-4.38 (1H, m, CHNH), 4.17-4.21 (1H, m, CHNH), 3.68 (2H, t, *J* = 6.6 Hz, CH₂Br), 3.13-3.19 (1H, m, CHS), 2.89 (1H, dd, *J* = 5.1, 12.6 Hz, CH_aS), 2.70 (1H, d, *J* = 12.6 Hz, CH_bS), 1.46-1.84 (6H, m, CH₂); **¹³C NMR** (75 MHz, DMSO-*d*₆): δ 162.7, 61.0, 59.2, 55.3, 45.2, 39.8, 32.0, 27.6, 25.9.

To a suspension of 90% lithium acetylide ethylene diamine complex (1.5 equiv) in dry DMSO (0.5 mL) cooled at 15 °C was added dropwise a solution of norbiotin bromide (25 mg, 0.09 mmol) in dry DMSO (0.25 mL) and stirred at ambient temperature for 3 h. The reaction mixture was poured into ice-water and extracted with dichloromethane. The organic layer was collected and washed with water and brine, dried over Na₂SO₄, filtered, concentrated *in vacuo* and purified by flash

chromatography eluting with 5% methanol in dichloromethane to give a white solid (9 mg, 44%).

¹H NMR (300 MHz, CDCl₃): δ 5.16 (1H, bs, C(O)NH), 5.11 (1H, bs, C(O)NH), 4.49-4.53 (1H, m, NHCH), 4.30-4.33 (1H, m, NHCH), 3.13-3.20 (1H, m, SCH), 2.94 (1H, dd, *J* = 5.1, 12.9 Hz, SCH_a), 2.73 (1H, d, *J* = 12.9 Hz, SCH_b), 2.21 (2H, dt, *J* = 2.7, 6.75 Hz, CH₂C≡CH), 1.97 (1H, t, *J* = 2.7 Hz, CH₂C≡CH), 1.51-1.70 (6H, m, 3 x CH₂); **¹³C NMR** (300 MHz, DMSO-d₆): δ 163.2, 84.4, 68.9, 62.2, 60.3, 55.5, 40.8, 28.3 (x2), 28.1, 18.4; **HRMS** calcd. for (M + H) C₁₁H₁₇N₂OS: requires 225.1062, found 225.1065.

(3a*S*,6a*R*)-4-(6-Hydroxyhexyl)-1,3,3a,4,6,6a-hexahydrothieno[3,4-*c*]imidazol-2-one (Compound 18)



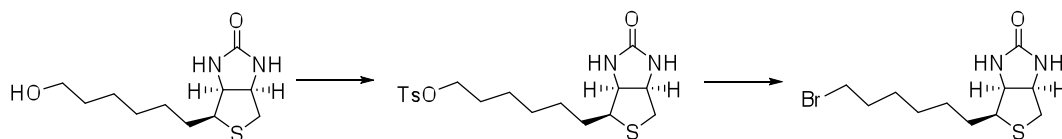
A suspension of homobiotin (Wilbur et al., 2001) (210 mg, 0.81 mmol) in dry methanol (5 mL) was added thionyl chloride (290 mg, 0.211 mL, 2.43 mmol) and stirred for 0.75 h. The reaction mixture was concentrated *in vacuo* and purified by flash chromatography eluting with 5% methanol in dichloromethane to give the methyl ester as a off white solid (221 mg, 100%).

MP: 168 – 170 °C; **¹H NMR** (300 MHz, 2% CD₃OD, CDCl₃): δ 4.46-4.50 (1H, m, CHNH), 4.24-4.30 (1H, m, CHNH), 3.64 (1H, s, COOCH₃), 3.10-3.16 (1H, m, SCH), 2.92 (1H, dd, *J* = 4.8, 12.6 Hz, SCH_a), 2.70 (1H, d, *J* = 12.6 Hz, SCH_b), 2.29 (2H, t, *J* = 7.5 Hz, CH₂COOCH₃), 1.30-1.65 (8H, m, 4 x CH₂); **¹³C NMR** (75 MHz, 2% CD₃OD, CDCl₃): δ 174.5, 164.0, 62.2, 60.3, 56.0, 51.7, 40.8, 34.2, 29.2, 28.9, 28.6, 24.7.

A suspension of the methyl ester (141 mg, 0.52 mmol) in dry THF (5 mL) was added LiAlH₄ (78 mg, 2.04 mmol) and stirred for 8 h under a nitrogen atmosphere. The reaction mixture was slowly quenched with methanol (1 mL) and water (1 mL). To the mixture was added saturated sodium sulphate, stirred for 20 min and concentrated *in vacuo*. The residue was dissolved in 1:4 methanol and dichloromethane (25 mL), stirred for 30 min, filtered and washed with 1:4 methanol and dichloromethane (25 mL). The filtrate was concentrated *in vacuo* and purified by flash chromatography eluting with 8% methanol in dichloromethane to give a white solid (115 mg, 91%).

MP: 158 -161 °C; **¹H NMR** (300 MHz, CD₃OD): δ 4.49 (1H, ddd, *J* = 0.9, 4.8, 6.9 Hz, CHNH), 4.29 (1H, dd, *J* = 4.5, 7.8 Hz, CHNH), 3.55 (2H, t, *J* = 6.6 Hz, CH₂COOCH₃), 3.17-3.24 (1H, m, SCH), 2.93 (1H, dd, *J* = 5.1, 12.8 Hz, SCH_a), 2.70 (1H, d, *J* = 12.8 Hz, SCH_b), 1.29-1.78 (8H, m, 4 x CH₂); **¹³C NMR** (75 MHz, CD₃OD): δ 156.1, 54.0, 53.4, 52.1, 47.7, 31.5, 24.0, 21.0, 20.9, 20.3, 17.3; **HRMS** calcd. for (M + H) C₁₁H₂₁N₂O₂S: requires 245.1324, found 245.1357.

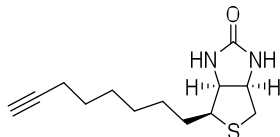
(3a*S*,6a*R*)-4-(6-Bromohexyl)-1,3,3a,4,6,6a-hexahydrothieno[3,4-*d*]imidazol-2-one (Compound 19)



To a suspension of homobiotinol **18** (122 mg, 0.50 mmol) in dry pyridine (1 mL) was added dropwise a solution of tosyl chloride (105 mg, 0.55 mmol) in dry pyridine (1 mL), and the solution was stirred in an ice bath for 1 h and subsequently placed in a 4 °C fridge for 5 h. The reaction mixture was diluted with dichloromethane (25 mL) and washed with 0.5 M aqueous HCl (1 x 25 mL), aqueous saturated sodium bicarbonate (1 x 25 mL), water (1 x 25 mL) and brine (1 x 25 mL). The organic layer was dried over Na₂SO₄, filtered, and concentrated *in vacuo* to give the crude tosylate as a white solid that was used with no further purification. To a suspension of the tosylate in dry methyl ethyl ketone (2 mL) was added lithium bromide (87 mg, 1.00 mmol) and stirred at 80 °C for 3 h. The reaction mixture was cooled, diluted with dichloromethane (1 x 25 mL) and washed with water (1 x 25 mL) and brine (1 x 25 mL). The organic layer was dried over Na₂SO₄, filtered and concentrated *in vacuo* and purified by flash chromatography eluting with 4% methanol in dichloromethane to give a white solid (78 mg, 51% over two steps).

MP: 159 – 161 °C; **¹H NMR** (300 MHz, CDCl₃): δ 5.30 (1H, s, CHNH), 5.15 (1H, s, CHNH), 4.50-4.54 (1H, m, CHNH), 4.30-4.34 (1H, m, CHNH), 3.41 (2H, t, *J* = 6.9 Hz, CH₂Br), 3.14-3.21 (1H, m, SCH), 2.94 (1H, dd, *J* = 5.1, 12.8 Hz, SCH_a), 2.74 (1H, d, *J* = 12.8 Hz, SCH_b), 1.83-1.90 (2H, m, CH₂), 1.30-1.68 (4H, m, 2 x CH₂); **¹³C NMR** (300 MHz, CDCl₃): δ 163.4, 62.2, 60.3, 55.7, 40.8, 34.2, 32.8, 29.1, 28.9, 28.8, 28.1; **HRMS** calcd. for (M + H) C₁₁H₂₀BrN₂OS: requires 307.0480, found 307.0478.

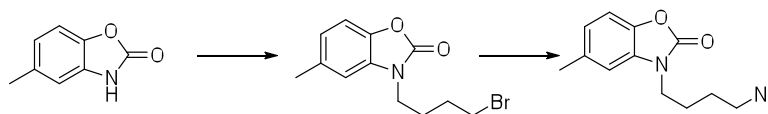
(3a*S*,6a*R*)-4-Oct-7-ynyl-1,3,3a,4,6,6a-hexahydrothieno[3,4-*d*]imidazol-2-one
(Compound 20)



To a suspension of 90% lithium acetylide ethylene diamine complex (23 mg, 23 mmol) in anhydrous DMSO (0.5 mL) cooled at 15 °C was added dropwise a solution of homobiotin bromide **19** (46 g, 0.15 mmol) in dry DMSO (0.25 mL) and the mixture was stirred at ambient temperature for 3 h. The reaction mixture was poured into ice-water and extracted with dichloromethane (1 x 50 mL). The organic layer was collected and washed with water (1 x 50 mL) and brine (1 x 50 mL), dried over Na₂SO₄, filtered, concentrated *in vacuo* and purified by flash chromatography eluting with 3% methanol in dichloromethane to give a white solid (14 mg, 37%).

¹H NMR (300 MHz, CDCl₃): δ 4.79 (2H, bs, 2 x C(O)NH), 4.51-4.55 (1H, m CHNH), 4.30-4.34 (1H, m, CHNH), 3.14-3.20 (1H, m, SCH), 2.94 (1H, dd, *J* = 5.1, 12.9 Hz, SCH_a), 2.73 (1H, d, *J* = 12.6 Hz, SCH_b), 2.19 (2H, dt, *J* = 2.7, 6.9 Hz, CH₂C≡CH), 1.95 (1H, d, *J* = 2.7 Hz, CH₂C≡CH), 1.38 – 1.68 (8H, m, 4 x CH₂); **¹³C NMR** (150 MHz, CDCl₃): δ 162.6, 84.5, 68.3, 61.9, 60.1, 55.4, 40.6, 29.7, 29.4, 28.9, 28.6, 28.4, 18.3; **HRMS** calcd. for (M + H) C₁₃H₂₁N₂OS: requires 253.1375, found 253.1373.

3-(4-Azidobutyl)-5-methyl-1,3-benzoxazol-2-one (Compound 21)



To a dissolved solution of 2-benzoxazolone (Shankaran et al., 1997) (195 mg, 1.31 mmol) in anhydrous DMF (5 mL) was added K_2CO_3 (271 mg, 1.96 mmol) and the reaction mixture was stirred at 50 °C for 1 h under nitrogen atmosphere. The reaction mixture was cooled to ambient temperature and was added 1,4-dibromobutane (420 mg, 1.96 mmol) and stirred at 50 °C for a further 6 h under a nitrogen atmosphere. The reaction mixture was cooled and poured into water (1 x 100 mL) and extracted with ethyl acetate (2 x 100 mL). The organic layers were pooled, washed with brine (1 x 100 mL), dried over Na_2SO_4 , concentrated *in vacuo* and purified by flash chromatography eluting with 20% ethyl acetate in petroleum ether to yield the bromide as an off white solid (310 mg, 88%).

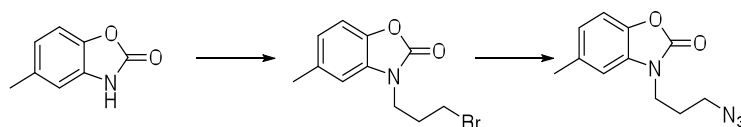
FT-IR (ATR) ν_{max} : 3068, 2931, 1760, 1623, 1383 cm^{-1} ; **1H NMR** (300 MHz; $CDCl_3$): δ 7.04 (1H, d, J = 8.7 Hz, ArH), 6.89 (1H, d, J = 8.7 Hz, ArH), 6.87 (1H, s, ArH), 3.94 (2H, t, J = 6.6 Hz, NCH_2), 3.43 (2H, t, J = 6.6 Hz, CH_2Br), 2.38 (3H, s, $ArCH_3$), 2.32 (2H, tt, J = 6.6, 6.6 Hz, CH_2) **^{13}C NMR** (75 MHz; $CDCl_3$): δ 154.8, 140.7, 134.1, 131.1, 123.0, 109.7, 109.0, 40.6, 30.9, 30.0, 21.6.

To a solution of the bromide (256 mg, 0.90 mmol) in DMF (5 mL) was added sodium azide (74 mg, 1.1 mmol) and stirred under nitrogen for 12 h. The reaction mixture was diluted with ethyl acetate (50 mL) and washed with water (1 x 50 mL) and brine (1 x 50 mL). The organic layer was dried over Na_2SO_4 , filtered, concentrated *in vacuo* and purified by flash chromatography eluting with 15% ethyl acetate in petroleum ether to yield a clear oil (205 mg, 91%).

FT-IR (ATR) ν_{max} : 2937, 2093, 1762, 1622, 1494 cm^{-1} ; **1H NMR** (300 MHz; $CDCl_3$): δ 7.08 (1H, d, J = 8.1 Hz, ArH), 6.91 (1H, d, J = 8.1 Hz, ArH), 6.79 (1H, s, ArH), 3.83 (2H, t, J = 6.9 Hz, NCH_2), 3.36 (2H, t, J = 6.9 Hz, CH_2N_3), 2.40 (3H, s, $ArCH_3$), 1.83-1.93 (2H, m, CH_2), 1.63-1.72 (2H, m, CH_2); **^{13}C NMR** (75 MHz; $CDCl_3$): δ 155.0,

140.9, 134.0, 131.1, 123.0, 109.8, 108.9, 51.0, 41.7, 26.2, 25.2, 21.7; **HRMS** calcd. for (M + Na) C₁₂H₁₄N₄NaO₂: requires 269.1015, found 269.1006.

3-(3-Azidopropyl)-5-methyl-1,3-benzoxazol-2-one (Compound 22)



2-Benzoxazolone (366 mg, 2.46 mmol) was reacted with 1,2-dibromoethane (788 mg, 3.68 mmol) according to procedure outlined for compound **21** and was purified by flash chromatography eluting with 20% ethyl acetate in petroleum ether to yield the bromide as an off white solid (647 mg, 93%)

FT-IR (ATR) ν_{max} : 2946, 1765, 1623, 1493 cm^{-1} ; **¹H NMR** (300 MHz; CDCl_3): δ 7.07 (1H, d, J = 8.1 Hz, ArH), 6.90 (1H, d, J = 8.1 Hz, ArH), 6.78 (1H, s, ArH), 3.84 (2H, t, J = 6.6 Hz, NCH_2), 3.43 (2H, t, J = 6.6 Hz, CH_2Br), 2.39 (3H, s, ArCH_3), 1.92-1.97 (4H, m, CH_2); **¹³C NMR** (75 MHz; CDCl_3): δ 155.0, 140.9, 134.1, 131.0, 123.0, 109.8, 108.9, 41.4, 32.9, 29.6, 26.5, 21.7

The bromide (112 mg, 0.41 mmol) was reacted according to procedure outlined for compound **21** and purified by silica gel chromatography eluting with 20% ethyl acetate in petroleum ether to yield a white solid (81 mg, 83%).

FT-IR (ATR) ν_{max} : 2945, 2100, 1754, 1495, 1240 cm^{-1} ; **¹H NMR** (300 MHz; CDCl_3): δ 7.08 (1H, d, J = 8.4 Hz, ArH), 6.90 (1H, d, J = 8.1 Hz, ArH), 6.83 (1H, s, ArH), 3.90 (2H, t, J = 6.9 Hz, NCH_2), 3.43 (2H, t, J = 6.9 Hz, CH_2N_3), 2.40 (3H, s, ArCH_3), 2.03 (2H, m, CH_2); **¹³C NMR** (75 MHz; CDCl_3): δ 154.9, 140.8, 134.2, 131.1, 123.1, 109.9, 108.2, 48.6, 39.5, 27.4, 21.7; **HRMS** calcd. for $(\text{M}^+ \text{Na}) \text{C}_{11}\text{H}_{12}\text{N}_4\text{NaO}_2$: requires 255.0858, found 255.0851.

Supplementary References

Cheng, Y., and Prusoff, W.H. (1973). Relationship between the inhibition constant (K₁) and the concentration of inhibitor which causes 50 per cent inhibition (I₅₀) of an enzymatic reaction. *Biochem Pharmacol* 22, 3099-3108.

Corona, C., Bryant, B.K., and Arterburn, J.B. (2006). Synthesis of a biotin-derived alkyne for pd-catalyzed coupling reactions. *Org Lett* 8, 1883-1886.

Huang, L., Luo, Z., He, F., Lu, J., and Li, X. (2010). Synthesis and biological evaluation of a new series of berberine derivatives as dual inhibitors of acetylcholinesterase and butyrylcholinesterase. *Bioorg Med Chem* 18, 4475-4484.

Loren, J.C., Kransinski, A., Forkin, V.V., and Sharpless, K.B. (2005). NH-1,2,3-Triazoles from Azidomethyl Pivalate and Carbamates: Base-Labile N-Protecting Groups. *Synlett* 2005, 2847-2850.

Mayende, L., Swift, R.D., Bailey, L.M., Soares da Costa, T.P., Wallace, J.C., Booker, G.W., and Polyak, S.W. (2012). A novel molecular mechanism to explain biotin-unresponsive holocarboxylase synthetase deficiency. *J Mol Med (Berl)* 90, 81-88.

Polyak, S.W., Chapman-Smith, A., Brautigan, P.J., and Wallace, J.C. (1999). Biotin protein ligase from *Saccharomyces cerevisiae*. The N-terminal domain is required for complete activity. *J Biol Chem* 274, 32847-32854.

Polyak, S.W., Chapman-Smith, A., Mulhern, T.D., Cronan, J.E., Jr., and Wallace, J.C. (2001). Mutational analysis of protein substrate presentation in the post-translational attachment of biotin to biotin domains. *J Biol Chem* 276, 3037-3045.

Shankaran, K., Donnelly, K.L., Shan, S.K., Humes, J.L., Pacholok, S.G., Grant, S.K., Green, B.G., and MacCoss, M. (1997). Inhibition of nitric oxide synthase by benzoxazolones *Bioorganic & Medicinal Chemistry Letters* 7, 2887-2892.

Shinde, S.S., Chi, H.M., Lee, B.S., and Chi, D.Y. (2009). tert-Alcohol-functionalized imidazolium ionic liquid: catalyst for mild nucleophilic substitution reactions at room temperature. *Tetrahedron Letters* 50, 6654-6657.

Wilbur, D.S., Hamlin, D.K., Chyan, M.K., Kegley, B.B., and Pathare, P.M. (2001). Biotin reagents for antibody pretargeting. 5. Additional studies of biotin conjugate design to provide biotinidase stability. *Bioconjug Chem* 12, 616-623.

Chapter 5 Characterising biotin protein ligases from ESKAPE pathogens

5.1. Introduction

The continuous emergence of antibiotic-resistant bacteria is a huge and growing problem in both hospital and community settings due to the difficulty and cost of treatment, resulting in high mortality rates (Ingaramo and Beckett, 2012, Konarev et al., 2003). The Infectious Diseases Society of America has highlighted six particularly important bacterial pathogens that are of particular concern due to their resistance to current treatments. These bacteria, known as the ESKAPE pathogens, consisting of *Enterococcus faecalis*, *Staphylococcus aureus*, *Klebsiella pneumoniae*, *Acinetobacter baumannii*, *Pseudomonas aeruginosa* and *Enterobacter* species are able to “escape” the effects of commonly used antimicrobials (Franke and Svergun, 2009).

Of particular relevance in the current study are *K. pneumoniae*, *A. baumannii* and *P. aeruginosa*. All cause a variety of diseases, ranging from pneumonia to blood or wound infections. The incidence of these pathogens in ICUs and high dependency care units are high, and coupled with the widespread use of broad-spectrum antibiotics in these settings, has resulted in the emergence of pathogens which are multi-drug resistant. *K. pneumoniae* is able to acquire and maintain multidrug resistant plasmids, especially the gene which encodes the metallo- β -lactamase, carbapenamase, an enzyme which hydrolyses a large spectrum of β -lactam antibiotics, and hence is highly resistant to the last resort β -lactam antibiotic, carbapenam. The high plasticity of the *A. baumannii* genome has also rendered it resistant to carbapenam and other drugs (Kozin and Svergun, 2001). *P. aeruginosa* is able to acquire multi-drug resistance through imported resistance mechanisms as well as mechanisms encoded within its chromosome (Lister et al., 2009). Carbapenam-resistant strains of *K. pneumoniae*, *A. baumannii* and *P. aeruginosa* are extremely prevalent across Asia, Europe, and the US, where mortality rates amongst infected patients are high (Volkov and Svergun, 2003, Schneidman-Duhovny et al., 2010), hence there is an urgent need to develop a drug which can selectively target these pathogens, and in which gain-of-resistance is unlikely.

In order to create a successful antibiotic that is impervious to bacterial drug resistance, an important step is to identify novel chemical classes that target essential metabolic pathways in the bacteria, and for which there are no pre-existing resistance mechanisms. Traditionally,

macromolecules that were unique to bacteria have been exploited as drug targets to minimise the non-specific binding to a human enzyme. A new frontier for antibacterial discovery is to focus on targets that have a human equivalent, and to identify inhibitors with exceptional specificity for the bacterial homologue. One such example is the enzyme biotin protein ligase (BPL) (Ingaramo and Beckett, 2011, Konarev et al., 2003, Brunger, 1992) that is found in all organisms. Inhibitors targeting the *S. aureus* and *M. tuberculosis* BPLs have been designed through structure-based rational drug design, and were found to inhibit BPL *in vitro* with up to nanomolar affinity, and also showed specificity against other bacterial BPLs and the human enzyme (Konarev et al., 2003, Brunger, 1992), which makes bacterial BPL a promising target for drug design.

The aim of this chapter is to characterize the BPLs from *K. pneumoniae* (KpBPL), *A. calcoaceticus* (AcBPL), and *P. aeruginosa* (PaBPL) using both structural and functional methods, as an initial step for the design of new BPL inhibitors using structure guided principles.

5.2. Results

5.2.1. AcBPL protein purification

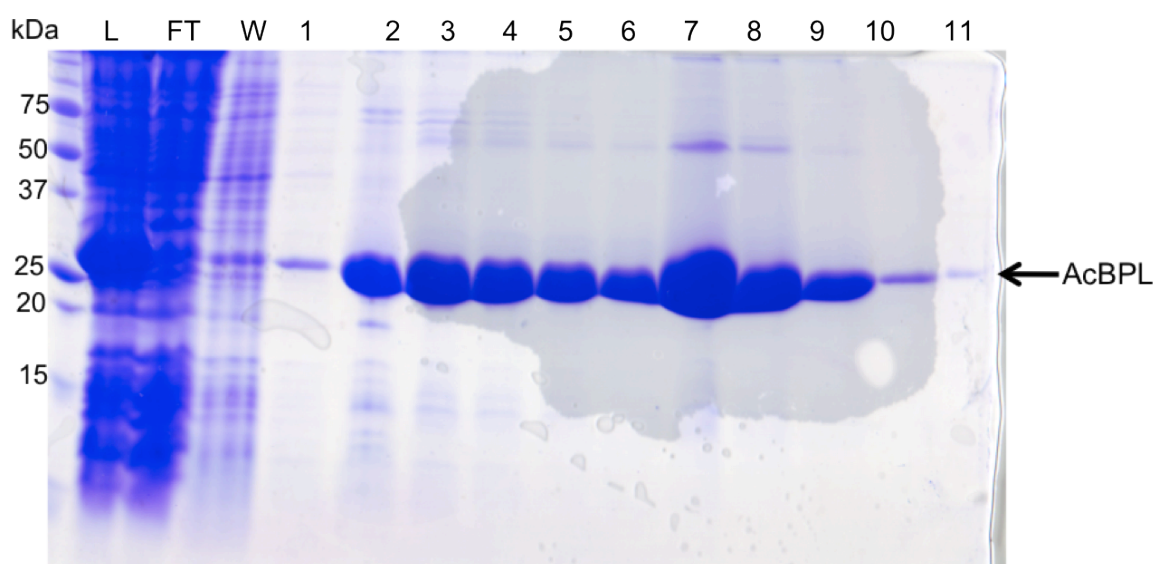


Figure 5.1 SDS-PAGE analysis of nickel purification of AcBPL. L: load; FT: flow through; W1, W2: washed with 10 mM imidazole; lane 1- 5: protein eluted with 50 mM imidazole; lane 6 - 10: protein eluted with 100 mM imidazole.

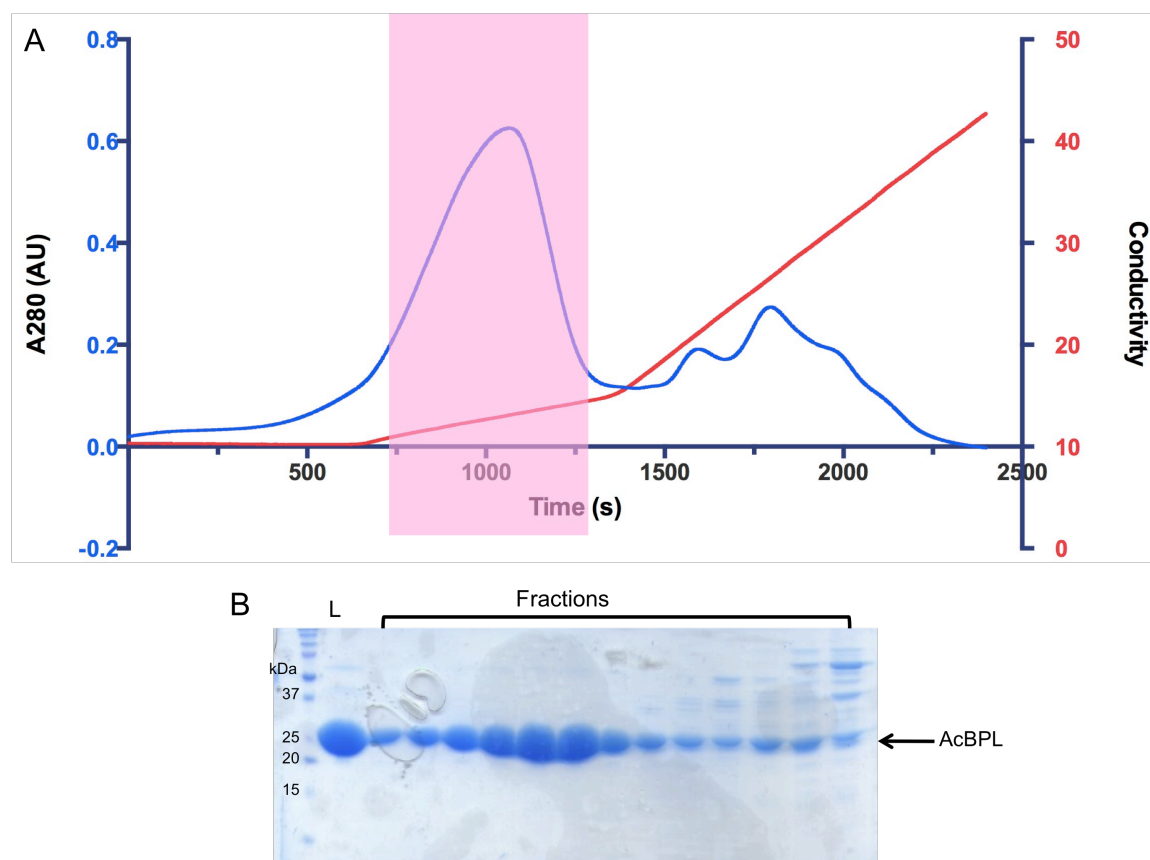


Figure 5.2 (A) Anion exchange chromatography of AcBPL and (B) SDS-page analysis. Peak highlighted in pink indicates point at which AcBPL was eluted (100 mM - 250 mM NaCl), and the subsequent fractions in that peak analysed on SDS-PAGE (L: Load) .

Overexpression of AcBPL at 25 °C produced high levels of soluble C-terminal His-tagged protein. AcBPL was first subjected to nickel-affinity chromatography. After binding to the nickel column and washing off the unbound protein with lysis buffer, AcBPL could be eluted off the column with 50 mM and 100 mM imidazole (**Figure 5.1**). The eluted fractions were pooled and dialysed once into SE buffer for 3 hours and then overnight at 4 °C. AcBPL was further purified by loading onto a Q-sepharose column using a gradient of 50 mM – 1 M NaCl (**Figure 5.2**). Contaminants were further separated from AcBPL using a S200 16/60 size exclusion column at a flow rate of 1.5 mL/min. AcBPL eluted from 60 to 70 minutes (90 – 105 mL) (**Figure 5.3**), and was collected as 1 mL fractions. Fractions corresponding to the sharpest peak were pooled and stored at – 80 °C until further use. Approximately 20 mg of protein was obtained from 500 mL of culture.

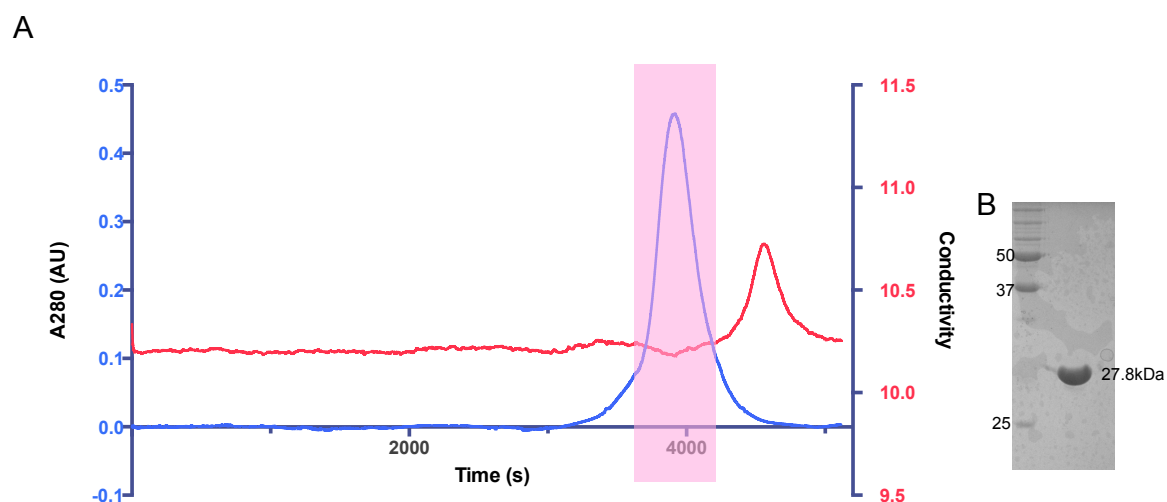


Figure 5.3 (A) Size exclusion chromatography of AcBPL. AcBPL eluted out from 60 to 70 minutes. **(B)** Purified AcBPL used for subsequent experiments.

5.2.2. *KpBPL* purification

Unlike SaBPL and AcBPL, the expression levels of *KpBPL* were lower than other BPLs purified previously. *KpBPL* was also subjected to nickel-affinity chromatography after cell lysis, and was eluted with 50 mM and 100 mM imidazole (**Figure 5.4**). *KpBPL* has a theoretical pI of 5.40, hence after dialyzing protein eluted from the nickel column into 50 mM Tris-HCl, pH 7.5, *KpBPL* was further purified using cation-exchange chromatography, where it eluted out around 200 mM NaCl (**Figure 5.5**). Fractions containing BPL were identified by SDS-page and stored as per AcBPL. 8 mg of protein was obtained from 4 L of 2YT media.

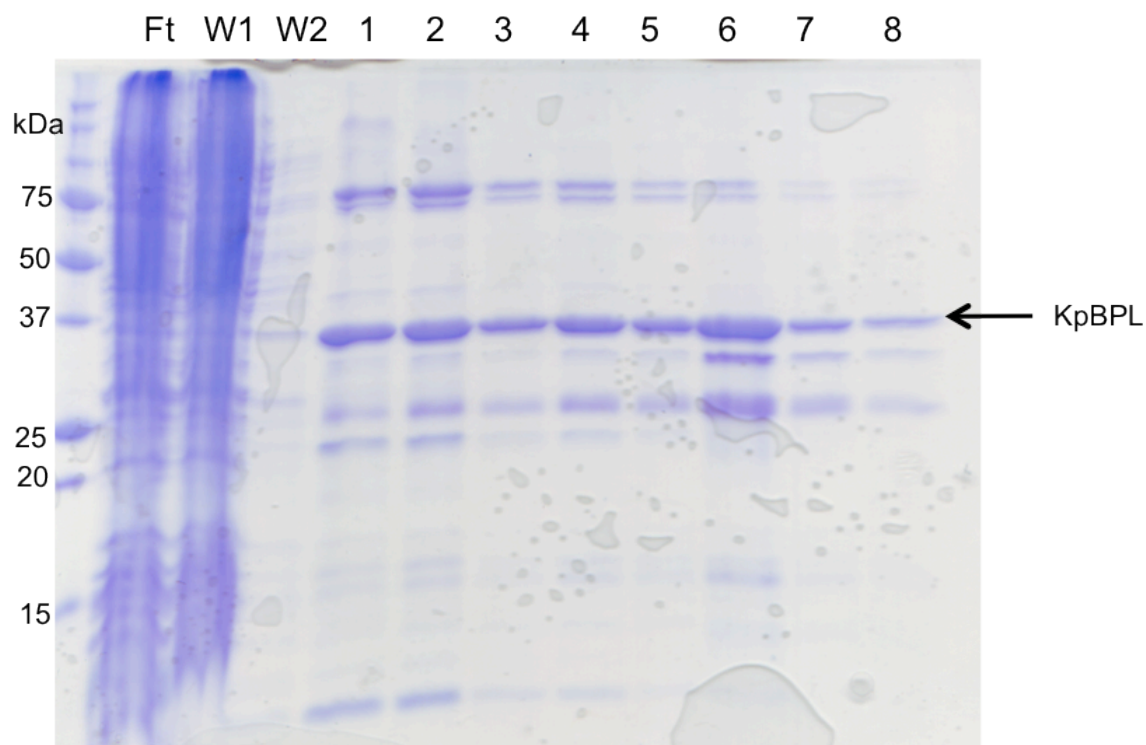


Figure 5.4 SDS-PAGE analysis of *KpBPL* nickel purification. FT: flow through; W1, W2: wash; lane 1- 5; protein eluted with 50 mM imidazole; lane 6 - 8: protein eluted with 100 mM imidazole

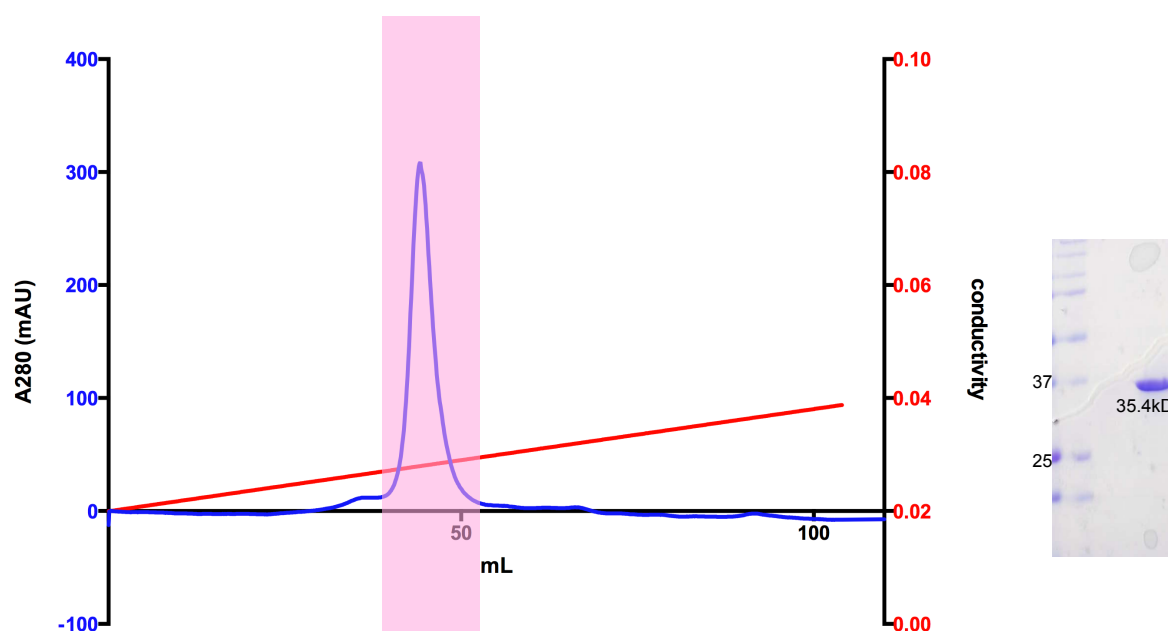


Figure 5.5 Cation exchange chromatography of *KpBPL* and SDS-page analysis. *KpBPL* eluted at 200 mM NaCl.

The purity of AcBPL and *KpBPL* was assessed by loading 10 μ g of protein onto an SDS-PAGE gel that was then stained with Commassie blue. It was estimated that the samples were >90% pure (**Figure 5.6**). Western blot analysis using an Anti-His₆ antibody conjugated

to HRP confirmed the presence of His6-tagged material in the major band. The identity of the protein was further confirmed using N-terminal sequencing.

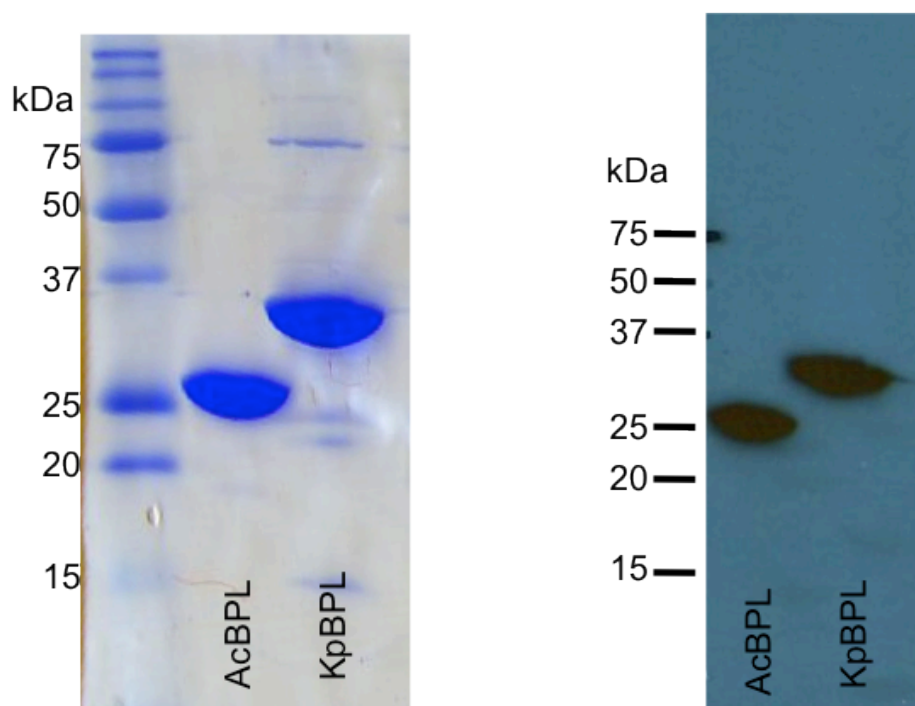


Figure 5.6 Both His6-tagged AcBPL and KpBPL were purified to >95 % purity as indicated by the SDS-PAGE gel on the left. An anti-His Western blot was performed to further confirm the presence of the His6-tagged proteins.

5.2.3. Expression and purification of *PaBPL*

5 mL small-scale expression trials of *PaBPL* showed that this protein could be over-expressed at either 16 °C or 25 °C using varying concentrations of IPTG (0.1 mM - 1 mM IPTG) (**Figure 5.7**). However, when attempting to purify *PaBPL* using the same method as *KpBPL* and *AcBPL*, it was found that *PaBPL* precipitated under the same conditions, and could not be eluted from the nickel resin. An analysis of the pI of *PaBPL* showed that the theoretical pI was 7.05, and hence could be the reason why the protein was unstable at pH 7.5. So the pH of the buffers used for *PaBPL* purification was changed to pH 8.5. This time, small amounts of *PaBPL* was able to be eluted from the nickel resin using 100 mM imidazole and 500 mM imidazole (**Figure 5.8**).

In order to further purify the protein, the fractions containing soluble *PaBPL* was dialysed into 50 mM Tris-HCl pH 8.5, 50 mM NaCl, 10 % glycerol. Unfortunately, the majority of protein precipitated out of solution. Storage of the protein in its original Ni-NTA elution buffer also caused the protein to precipitate. Due to time constraints, purifying *PaBPL* in other buffers at various pH was not attempted, and further work on this protein was not continued.

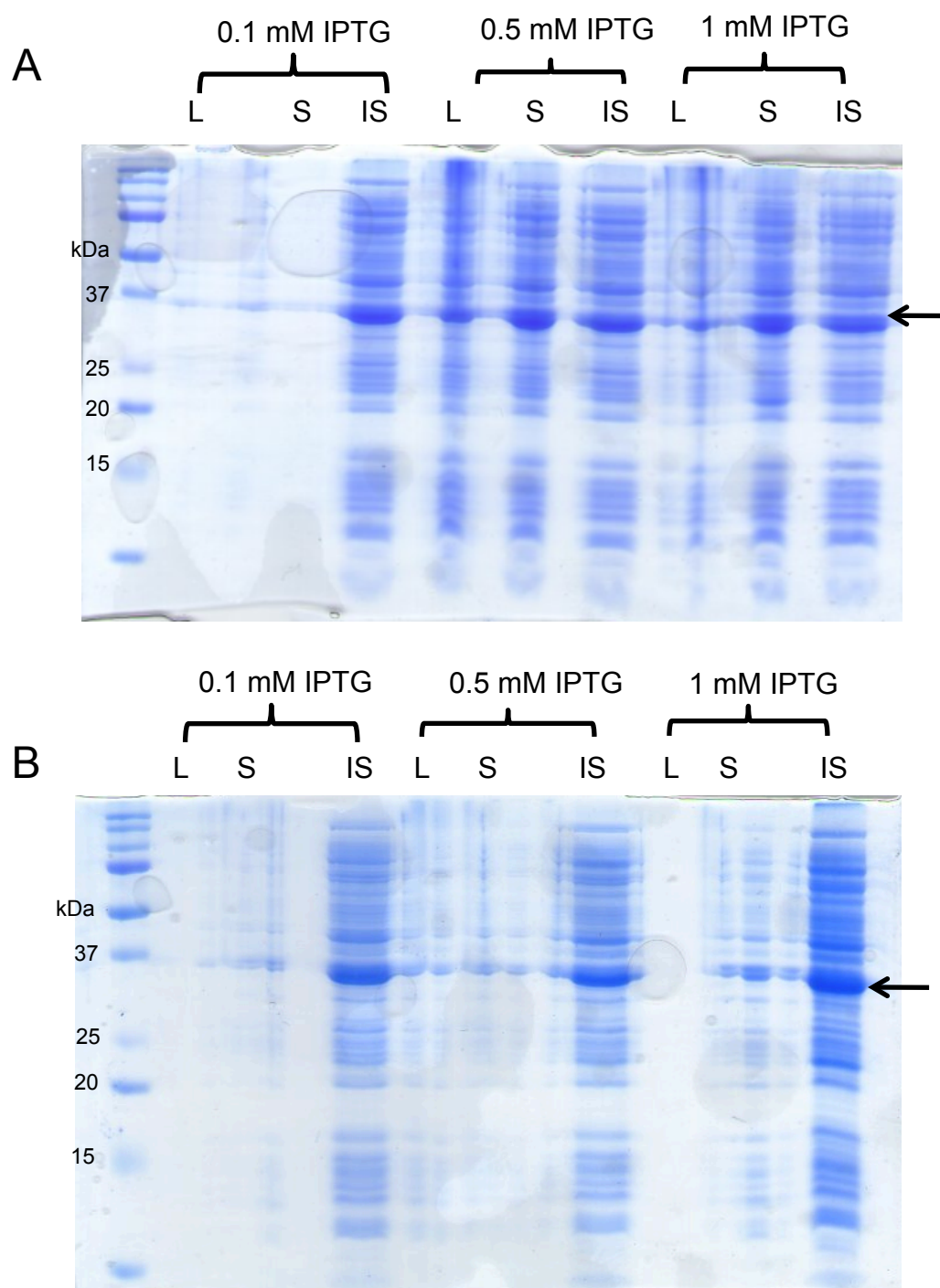


Figure 5.7 SDS-PAGE analysis of small scale over-expression of *PaBPL* at (A) 16°C and (B) 25°C. L: post-IPTG induction sample, S: soluble fraction, IS: insoluble debris. Arrows mark the expected molecular weight of *PaBPL* (35kDa).

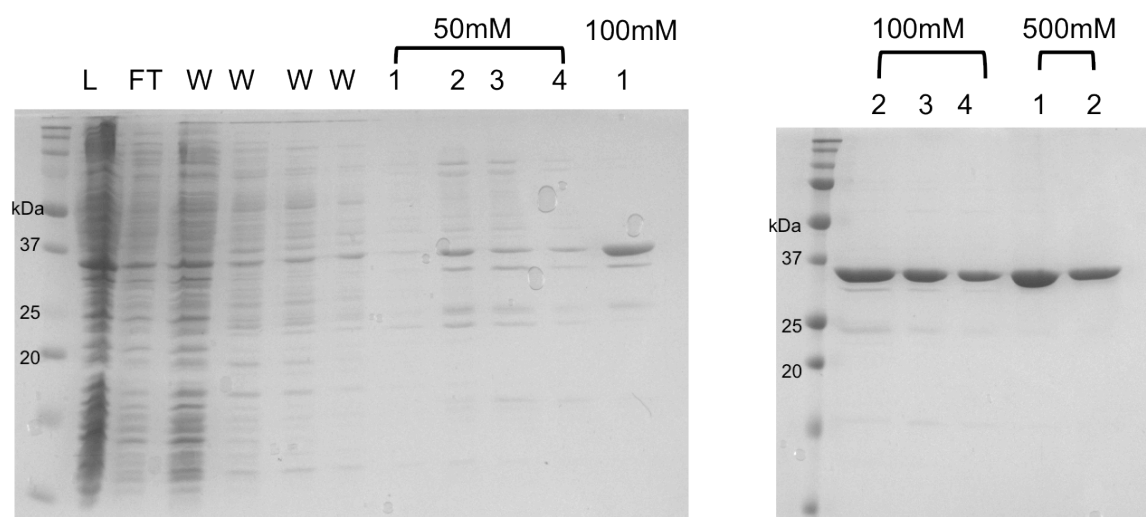


Figure 5.8 SDS-PAGE analysis of nickel purification of *PaBPL*. L: Load, FT: flow through, W: 10 mM imidazole wash of His6-tagged protein bound to nickel resin, and elutions with 50mM, 100 mM and 500 mM imidazole.

5.2.4. Oligomerisation states of *KpBPL* and *AcBPL*

In general, class I bacterial BPLs are monomeric in both its apo and ligand-bound holo forms, whilst class II BPLs form a homodimer when there is ligand bound in the active site. The exception to this rule is *PhBPL* where both the apo and holo forms are homodimeric. In order to determine the oligomerisation states of *KpBPL* and *AcBPL*, SEC-MALLS was performed. MALLS is able to provide very precise measurements of molecular weights, and provides a quick and convenient way of determining the oligomeric states of these BPLs. BPL was concentrated and dialysed into SE buffer before being run down a S200 10/300 column at 0.4 mL/min. Holo BPL was formed by adding 10 x molar excess BtOH after concentrating.

From the chromatograms (**Figure 5.9**), it can be seen there is a large laser light scattering peak which elutes between 10 – 20 minutes, however the absence of a 280 UV trace which measures protein absorbance at this point suggest that the scattering comes from soluble aggregation of the enzymes as larger species are able to scatter light more efficiently. The non-aggregated forms of the proteins elute as a single peak (highlighted in pink), and from the data obtained from MALLS (**Figure 5.9**), both apo and holo *AcBPL* gave a calculated molecular weight of 26.32 kDa and 29.04 kDa, which corresponds to a monomeric protein (Estimated molecular weight = 27.5 kDa). On the other hand, the apo form of *KpBPL* had a calculated molecular weight of 35.4 kDa (estimated molecular weight = 35.6 kDa), whilst holo *KpBPL* had a experimentally determined molecular weight of 71.5 kDa, which is consistent with homodimer formation.

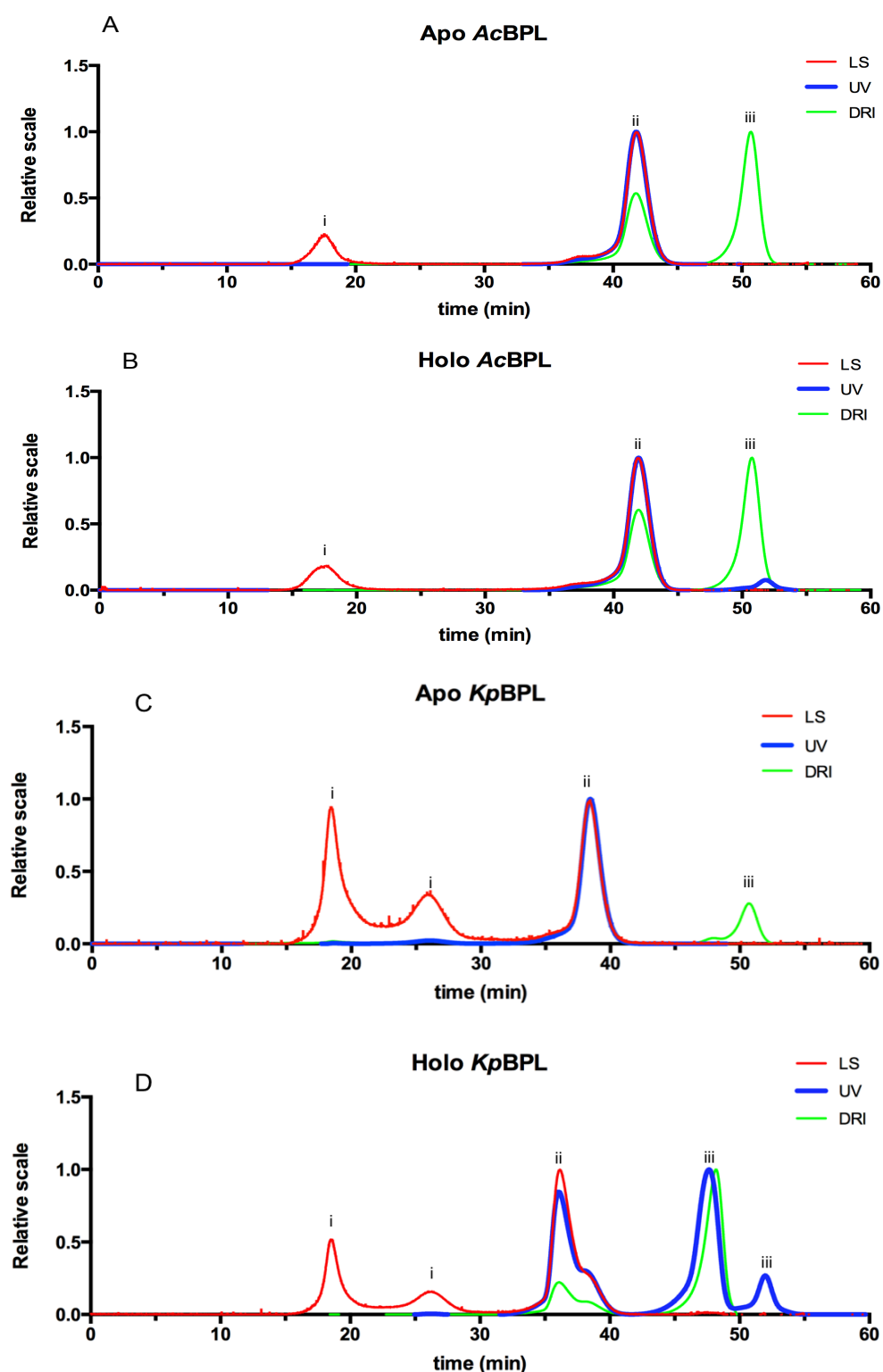


Figure 5.9 SEC-MALLS chromatograms of (A) Apo AcBPL (B) Holo AcBPL (C) Apo KpBPL (D) Holo KpBPL. LS: Light Scattering; UV: Protein absorbance at 280 nm; DRI: Differential Refractive Index. LS is used to measure the molar mass and average size of the protein, whilst DRI can be used to measure protein concentration, and detect changes in buffer. Peak (i) is light scattering from aggregated sample, (ii) UV peak indicates presence of BPL, and molecular weight of protein can be calculated from the light scattering; (iii) DRI peak indicates change in buffer, whilst lack of scattering and presence of UV peak indicates the presence of ATP used to obtain holo-BPL.

5.2.5. Biotinylation kinetics

Experiments performed in our lab routinely use SaBCCP in order to assess the activity of different BPLs. In order to determine that the purified *Kp*BPL and *Ac*BPL were active, the enzymatic activity of *Kp*BPL and *Ac*BPL against SaBCCP was determined. The holo forms of both BPLs were incubated in the presence of SaBCCP, which was then probed with streptavidin-HRP to assess biotinylation. The assumption that *Kp*BPL and *Ac*BPL could react with BCCP from another bacterial species was made as many other studies have showed that BPLs and BCCPs from divergent species could cross react (McAllister and Coon, 1966, Samols et al., 1988, Tissot et al., 1998). The western blot in **Figure 5.10** shows that the purified *Kp*BPL and *Ac*BPL are active, and can biotinylate SaBCCP, as indicated by the bands in lanes 5 and 7 which were detected using streptavidin-HRP.

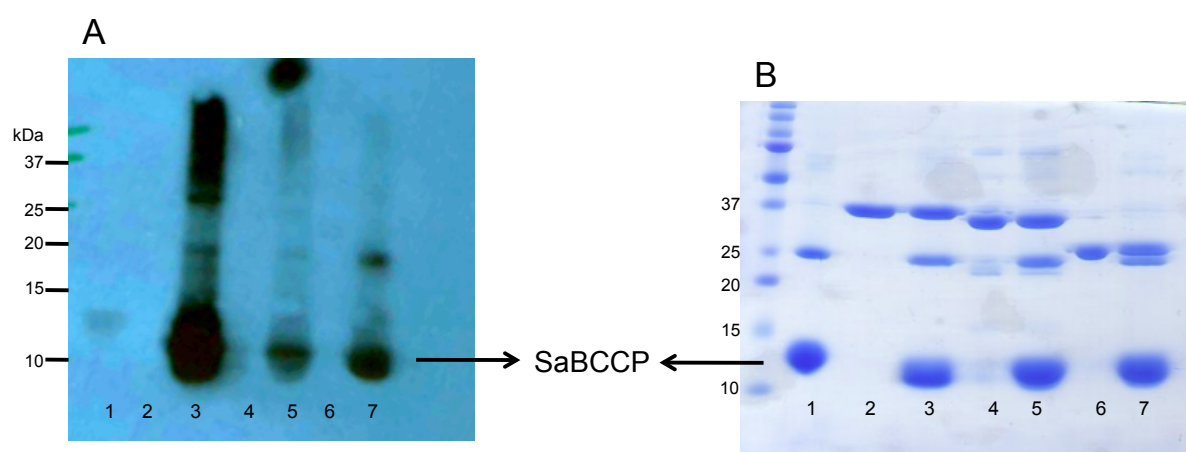


Figure 5.10 (A) Western blot to detect the biotinylation of SaBCCP by different BPLs and (B) the corresponding SDS-PAGE. Lane 1: BCCP, 2: SaBPL, 3: SaBPL + SaBCCP, 4: *Kp*BPL, 5: *Kp*BPL + SaBCCP, 6: *Ac*BPL, 7: *Ac*BPL + SaBCCP

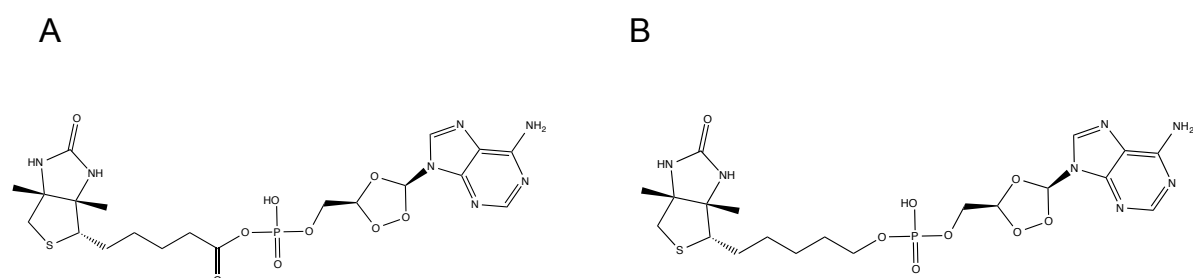
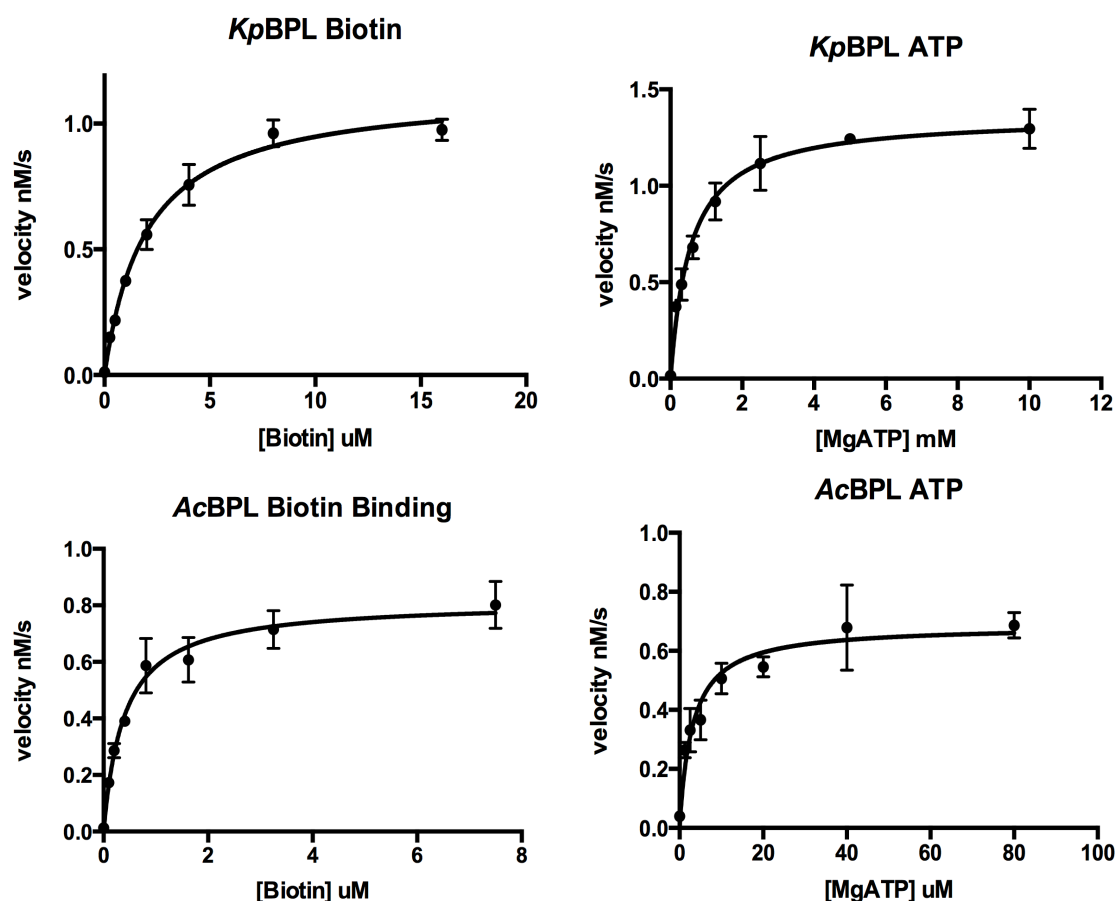


Figure 5.11 Structures of (A) Biotinyl-5'-AMP and the non-hydrolysable analog (B) Biotinol-5'-AMP. Biotinol-5'-AMP can inhibit both *Kp*BPL and *Ac*BPL.

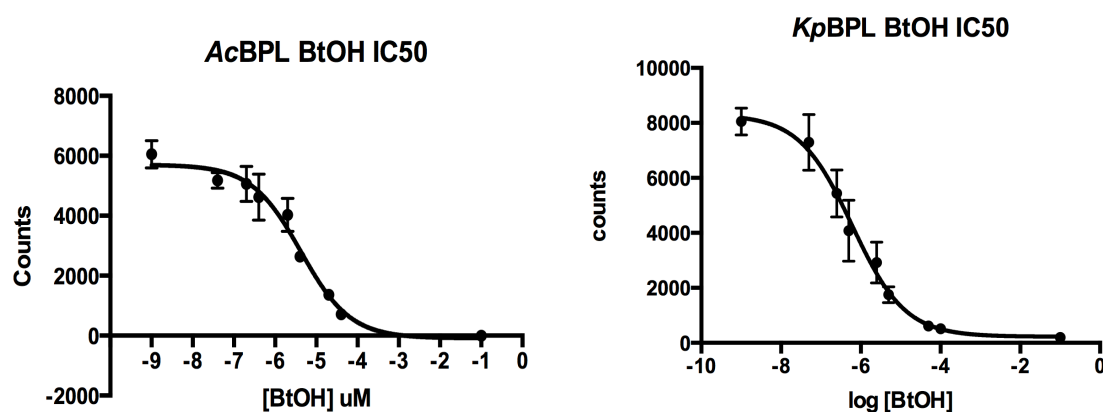
Biotin and ATP binding to either *Kp*BPL or *Ac*BPL were performed through a biotinylation assay based on the incorporation of ^3H -biotin onto SaBCCP by BPL. The binding affinity of *Kp*BPL and *Ac*BPL for biotin was within the normal range of other bacterial BPLs. *Kp*BPL bound to ATP with an affinity of 580 μM , however *Ac*BPL had a 100 fold higher affinity for

ATP. BirA, which is a class II BPL binds with a similar affinity compared to *KpBPL*, raising the possibility that class I and class II BPLs have different modes of binding to the adenylate group (**Figure 5.12**). The difference of affinity however, could also be attributed to differences in substrate specificity.



	K_M Biotin	K_M ATP
<i>AcBPL</i>	335 ± 142 nM	5.728 ± 2.3 μ M
<i>KpBPL</i>	2 ± 0.8 μ M	580.5 ± 193 μ M

Figure 5.12 175 nM *KpBPL* and 500 nM *AcBPL* were respectively used to determine the binding affinity of each protein for biotin or ATP. Reactions were performed in 50 mM Tris-HCL pH 8.0, 3 mM ATP, 4.5 μ M biotin, 0.5 μ M 3 H-biotin, 5.5 mM $MgCl_2$, 100 mM KCl, 0.1 mg/mL BSA and 10 μ M SaBCCP, and incubated at 37 °C for 10 minutes.



	<i>AcBPL</i>	<i>KpBPL</i>
Ki	446.30 nM	386.61 nM

Figure 5.13 Inhibitory curves of BtOH for KpBPL and AcBPL. Dose response curve was obtained by varying BtOH concentration in the presence of biotin and ATP.

As an initial step to see if these BPLs could be inhibited by a biotinyl-5'-AMP like inhibitor, the non-hydrolysable analogue biotinol-5'-AMP (**Figure 5.11**) was used to test its inhibitory effect on these BPLs. As expected, BtOH was able to bind in the active site of *KpBPL* and *AcBPL* with similar inhibitory constants, and can prevent the biotinylation of BCCP (**Figure 5.13**).

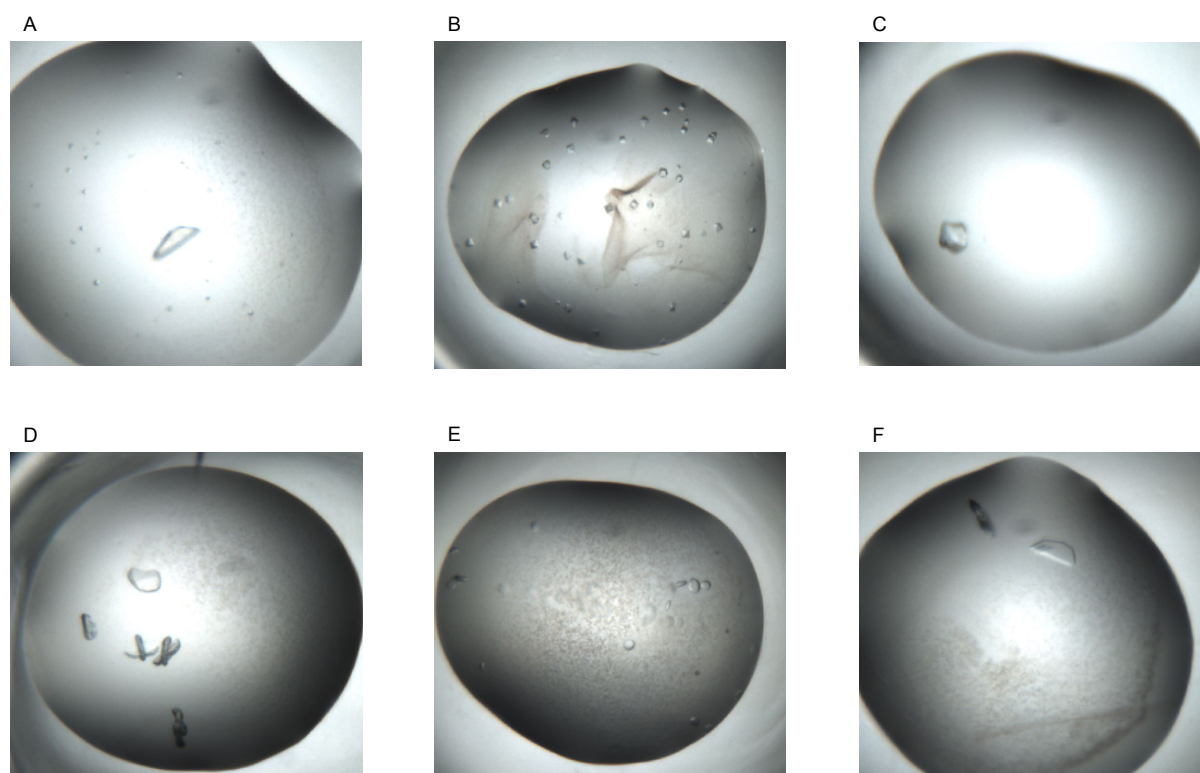
5.2.6. Crystallization studies

Protein crystallization trials were performed on *AcBPL* and *KpBPL* that had been stored in 50mM Tris-HCl pH 7.5, 50 mM NaCl, 5 % glycerol, and concentrated to 10 mg/mL, 5 mg/mL and 2.5 mg/mL. Broad screens were performed at the Macromolecular crystallization facility using crystallization kits, which included the Sigma Basic Crystallography Kit (Sigma-Aldrich), Sigma Basic Extension Kit (Sigma-Aldrich), PEG/ION (Hampton), SaltRX (Hampton), Index (Hampton), JCSG+ Suite (Qiagen), PACT Suite (Qiagen) and Wizard I and II (Emerald Bio) screens. Crystal trays were set up with Rigaku Crystallization system, in which crystals were grown using the sitting-drop method. Protein : crystallization condition was at a 1:1 ratio, and incubated at either room temperature or 4°C. Trays were checked daily using the CrystalTrak software for a week, and weekly thereafter. As no *AcBPL* protein crystals appeared in these conditions, *AcBPL* was dialysed into 50 mM Hepes pH 6.5, 100 mM NaCl, 5 % glycerol, 1 mM DTT prior to setting up the screens in order to see if changing the pH of the buffer would aid in crystallization. To further stabilise the protein, 10 x molar

excess BtOH was added and incubated with the protein for an hour before dialyzing and concentrating.

Attempts to crystallize AcBPL have proved to be unsuccessful, and in many cases the protein precipitates out of the crystallization solution when stored in buffers at pH 7.5 or pH 6.5, suggesting that the protein may be unstable in these conditions. Future experiments to determine the optimal pH and salt concentration in which to store AcBPL at prior to crystallization would need to be performed.

On the other hand, broad screens of KpBPL provided several hits, with the conditions in which crystals grew in listed in **Figure 5.13**. Fine crystallization screens were further performed by varying both pH and precipitant concentration in order to create larger crystals for X-ray diffraction experiments. However, the crystals that were finally used for X-ray diffraction experiments either provided weak or no diffraction.



	Screen name	Conditions
A	Sigma Basic Extension Kit	0.1 M Hepes pH 7.5 5 % MPD 10 % PEG 6000
B	Emerald Biosystems Wizard Crystallization Screen	0.2 M NaCl 0.1 M Hepes pH7.5 20 % PEG 3000
C	Hampton Research Index HT	0.2 M tri-sodium citrate 20 % PEG 3350
D	Qiagen Pact Suite	25 % PEG 1500 10 % succinate-phosphate-glycine
E	Qiagen Pact Suite	0.2 M NaCl 20 % PEG6000 0.1 M Tris pH8.0
F	Qiagen Pact Suite	0.2 M sodium malonate 20 % PEG 3350

Figure 5.14 *KpBPL* crystals could be obtained after incubation of the enzyme in the listed conditions above for several days at 4°C.

5.2.7. Modelling of AcBPL and PhBPL

AcBPL has around 40 % sequence similarity with other class I BPLs. Using PhBPL as a template (43.1 % sequence similarity), a model of AcBPL was constructed using SWISSMODEL (swissmodel.expasy.org). The GXGRXX motif found in other bacterial BPLs is not as conserved in AcBPL. The glutamine residue at position 59 of AcBPL is a highly conserved arginine in other BPLs, but like arginine, can still form hydrogen bonds with the carboxylic acid tail of biotin or the phosphate group of biotinyl-5'-AMP via its nitrogen group. In the model of AcBPL (**Figure 5.15**), the ABL is slightly longer than those found in other BPLs, and can form a protective lid over the adenylate group within its active site prior to biotinylation of BCCP, and hence may explain the slightly higher binding affinity that AcBPL has for ATP.

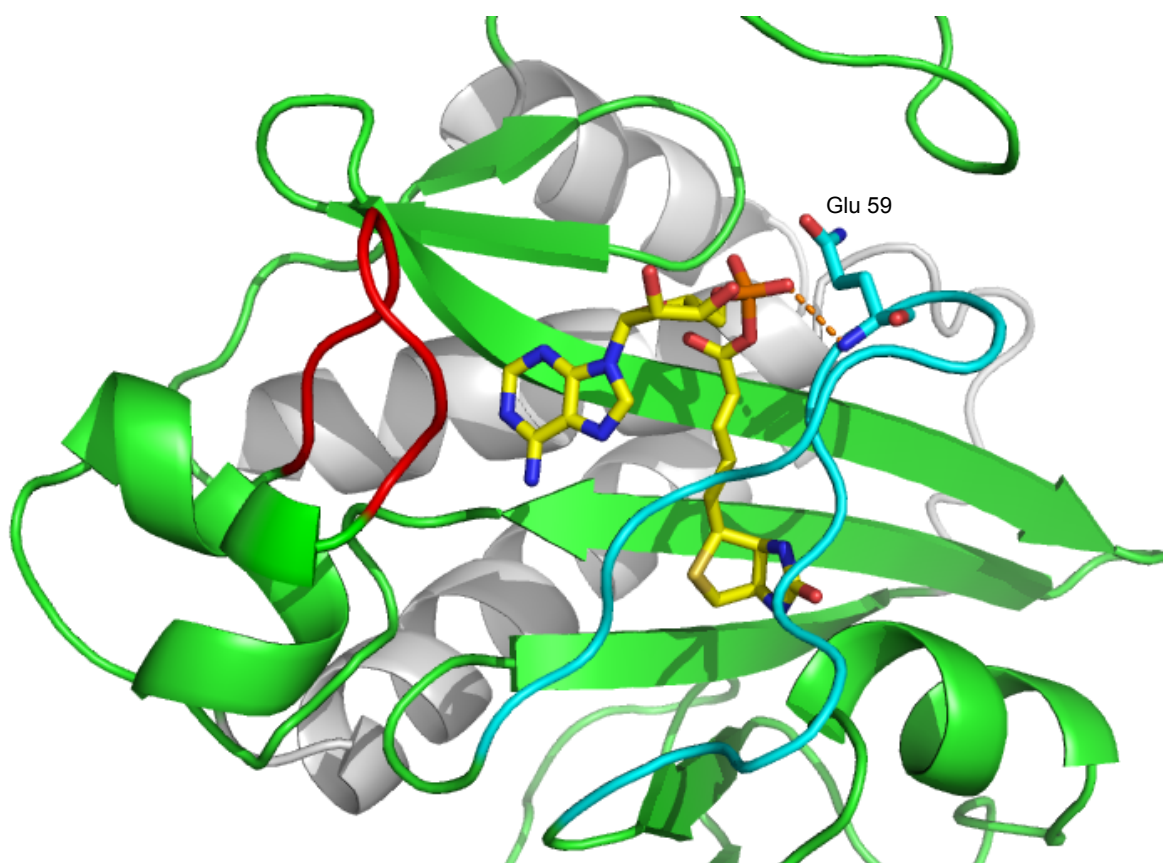


Figure 5.15 Homology model of AcBPL, with the ABL in red and the BBL in blue. Residue 59 is generally a conserved arginine in other BPLs, but is a glutamine in AcBPL

Another class II BPL from an ESKAPE pathogen is the BPL from *Pseudomonas aeruginosa* (PaBPL). Multiple attempts at purifying this protein was unsuccessful, and hence no further experiments were done on it. PaBPL has 23.5 % sequence identity with SaBPL, and 39.2 % sequence identity with BirA. A homology model of PaBPL constructed using SWISS-

MODEL using BirA as a template (**Figure 5.16**). The BBL of *Pa*BPL contains the same GRGRRGR residues, and other residues located in the biotin-binding site are fairly conserved, whilst the ABL and residues in the adenylate-binding site are not. The DNA-binding domain of *Pa*BPL is a few residues shorter than BirA, and based on the model, seems to be less structured compared to BirA due to the presence of a large flexible loop located at the N-terminus, and may be a reason why this protein is less stable in solution.

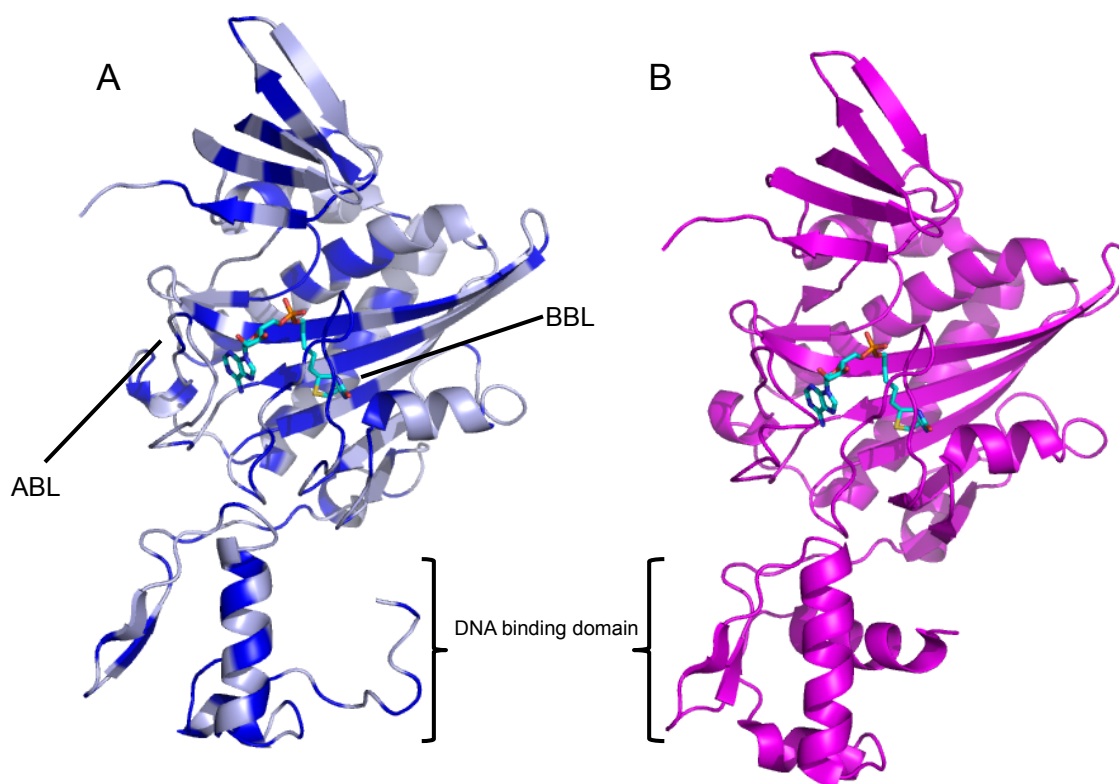


Figure 5.16 Model of (A) *Pa*BPL constructed with SWISS-MODEL using (B) BirA as a template. Dark blue residues on *Pa*BPL are those that are conserved between both *Pa*BPL and BirA, whilst light blue residues are different.

Discussion

The ESKAPE pathogens are bacteria which cause a variety of infections in hospitals, and are notoriously difficult to treat. Bacterial BPL is a good target for antibiotic design as it is essential for cell survival, and previous studies have shown that there is sufficient difference between bacterial and eukaryotic BPLs to design a drug specific to bacterial BPL (Chapter 3 and 4) (Ingaramo and Beckett, 2011, Konarev et al., 2003, Brunger, 1992) This chapter focuses on the expression, purification and analysis of the BPLS from three ESKAPE

pathogens, namely *K. pneumoniae*, *A. baumannii* and *P. aeruginosa* as an initial step to combat infections caused by these bacteria.

The structures of the ESKAPE BPL *S. aureus*, has been previously determined (Wood et al., 2006, Wilson et al., 1992, Konarev et al., 2003, Ingaramo and Beckett, 2011), hence we aimed to clone, express and purify the other ESKAPE pathogens. Instead of *A. baumannii* (which causes the majority of *Acinetobacter* infections), *A. calcoaceticus* was used instead for our study due to the difficulty of obtaining and working with *A. baumannii* cell cultures. A BLAST search on the genomes of *K. pneumoniae*, *A. calcoaceticus*, *Pseudomonas aeruginosa* and *Enterobacter faecalis* revealed the presence of BPLs which had high sequence homology to both BirA and SaBPL. Apart from AcBPL, all the other ESKAPE BPLs are class II BPLs that contain an N-terminal DNA-binding domain.

A first step in characterizing AcBPL and KpBPL was to examine their oligomerisation states. Our results show that the class I AcBPL was a monomer in both its apo and holo form, whilst KpBPL was a monomer in its apo form, but formed a homodimer when biotin and ATP was added to the protein. These results are consistent with previous studies done on other BPLs. In general, class II BPLs form a dimer when there is biotin or biotinyl-5'-AMP bound within the active site in order for the DNA-binding domain to bind to the BioO operon operator sequence to regulate biotin transcription, whilst class I BPLs are generally monomeric in both apo and holo form. An exception is the *Pyrococcus horikoshii* BPL which is a dimer in its apo and holo form, which may be useful for protein stability at the high temperatures at which *P. horikoshii* is found at (Bagautdinov et al., 2005a).

The formation of the reaction intermediate biotinyl-5'-AMP within the active site of class I and class II BPLs differ slightly. In class II BPLs, the binding of biotin and ATP happen in a sequential order, where biotin has to bind first prior to ATP binding. The unliganded biotin-binding site in bacterial BPLs consists of several β -sheets exposed to the solvent, and a disordered biotin-binding loop (BBL). Upon biotin binding, the BBL becomes ordered and closes over the solvent-exposed biotin binding site, to form hydrogen bonds between biotin and several residues located in the highly conserved GXGXXXR motif located in the BBL (**Figure 5.17**) (Tron et al., 2009, Bagautdinov et al., 2008, Wilson et al., 1992, Wood et al., 2006). The binding site for ATP in the class II BPL, BirA is formed only after biotin binds, with residues from the GXGXXXR motif contributing hydrogen bonds that can bind to the phosphate group of the adenylate, and residues which form the adenylate binding loop (ABL) disordered prior to ATP binding are ordered and covers the adenylate group (Wood et al., 2006, Wilson et al., 1992). In SaBPL however, there is evidence of a somewhat ordered

ABL (Pendini et al., 2013). In class I BPLs however, the ABL is ordered even in the absence of biotin binding, making a preformed ATP binding site, thus ATP and biotin binding in class I BPLs occur in a non-sequential manner (Tron et al., 2009, Bagautdinov et al., 2005a).

EcBirA	115	GRGRGRGR	121	} Class II BPL
KpBPL	115	GRGRGRGR	121	
SaBPL	119	GRGRFNR	125	
MtBPL	66	GRGRHGR	73	} Class I BPL
PhBPL	45	GHGRLLNR	51	
AcBPL	56	GRGQHQR	62	

Figure 5.17 Conserved GXGXXR motif located in the biotin-binding loop of BPLs. Sequence alignment of AcBPL against other bacterial BPLs of known structures show that it has a glutamine at position 59 as opposed to a highly conserved arginine found in other bacterial BPLs. Residues in green are conserved, whilst red residues are highly conserved.

KpBPL and AcBPL was able to biotinylate SaBCCP as indicated by a streptavidin-HRP western blot. An *in-vitro* biotinylation assay as described by Chapman-Smith *et al* was later used to determine the binding affinity of KpBPL and AcBPL for biotin or ATP (Chapman-Smith et al., 1999). The basis of the biotinylation assay involved the biotinylation of BCCP by either KpBPL or AcBPL. Instead of cloning and expressing BCCP from a biotin-dependent carboxylase of both *K. pneumoniae* and *A. calcoaceticus*, it was decided to use BCCP from *S. aureus* pyruvate carboxylase (SaBCCP) since it had been previously successfully expressed and purified. In general, known structures of BCCPs across organisms have a similar structure, and have a MKM motif located in a hairpin turn between two β strands, in which the lysine residue is biotinylated. An exception is the BCCP from *E. coli* acetyl-CoA carboxylase (EcBCCP) that has an extra “thumb” loop which aids in biotinylation and the transfer of CO₂ (Athappilly and Hendrickson, 1995, Roberts et al., 1999, Cronan, 2001). Stop-flow measurements showed that even though BPLs are able to biotinylate BCCPs from widely divergent organisms, the rate at which it biotinylates a non-cognate BCCP varies, and is dependent on the structures of both BPL and BCCP (Cronan, 1990, McAllister and Coon, 1966, Samols et al., 1988, Tissot et al., 1998, Lin and Cronan, 2011). For example, PhBPL is able to biotinylate PhBCCP, as well as EcBCCP and human BCCP, however, BirA is unable to biotinylate PhBCCP, and biotinylates human BCCP at a very slow rate. Human BPL is only able to biotinylate human BCCP, and has no effect on bacterial BCCPs (Lin and Cronan, 2011).

Bacterial BPLs generally bind to biotin with nanomolar affinity, whilst ATP binding is in the micromolar range (Chapman-Smith et al., 1999, Clarke et al., 2003, Purushothaman et al.,

2008, Daniels and Beckett, 2010). Results from the biotinylation assay show that *KpBPL* binds to ATP with a K_M of 580.5 μ M, whilst it binds to biotin with a K_M of 2 μ M, that is around 10 fold lower than other known bacterial BPLs. The concentration of biotin found in *E. coli* is estimated to be in the nanomolar range, and assuming that *K. pneumoniae* has similar intracellular biotin concentrations, the biotin concentration in *K. pneumoniae* cells is much lower than the binding affinity. This low binding affinity of *KpBPL* for biotin may be due to the fact that the genome of *K. pneumoniae* contains genes for synthesizing biotin, which have to be tightly regulated by *KpBPL* forming a homodimer (Rodionov et al., 2002).

EcBirA	211	MR-RV	ESV	VNQ	222
KpBPL	211	MR-RV	SDV	VNQ	222
MtBPL	161	QA-PE	VDP	DAT	172
PhBPL	134	NK-VP	NGAT	SMK	144
SaBPL	213	QQ-LE	NFA	AHRA	223
AcBPL	144	MPPVT	DS	QPI	155

Figure 5.18 Residues located in the Adenylate-binding loop of bacterial BPLs are unconserved, apart from the residues highlighted in green. This glutamate or asparagine in known bacterial BPL structures does not contact the adenylate group, but their hydrophilic tail group is exposed to the solvent instead. Grey residues are not part of the adenylate binding loop.

The binding of AcBPL for biotin is similar to other bacterial BPLs, however, its affinity for ATP ($K_M = 5.78 \mu$ M) is 10 fold higher than average. As mentioned above, the binding of ATP and biotin in class I BPLs is not a sequential process, likely due to the fact that they only play a role in biotinylating BCCP, and are not required for regulating biotin transcription. In the absence of either biotin or ATP, the *Aquifex aelicus* BPL (AaBPL) binds to each biotin or ATP with weak affinity, and binding of the ligand within the active site is a random process. However once biotin or ATP is bound within the active site, it promotes the binding of the other ligand (Tron et al., 2009). Unlike the biotin-binding loop that has a highly conserved sequence across BPLs (**Figure 5.17**), the adenylate-binding loop is not conserved, except for a glutamate or asparagine (highlighted in green in **Figure 5.18**) which does not come into contact with the adenylate, but exposes their hydrophilic tail group into the solvent, and may be important for structural stability. Sequence alignment of the ABL of AcBPL with other bacterial BPLs show that AcBPL does not resemble other BPLs in this region. *KpBPL* on the other hand has high sequence identity with BirA, but not SaBPL that is also a class II BPL. This large variation in the ABL suggest the binding of ATP within its active site is regulated differently amongst BPLs, and is not determined by the which class the BPL belongs to. The

different binding affinities of *KpBPL* and *AcBPL* for biotin or ATP should also take into account the difference the ability of these enzymes to cross react with *SaBCCP*.

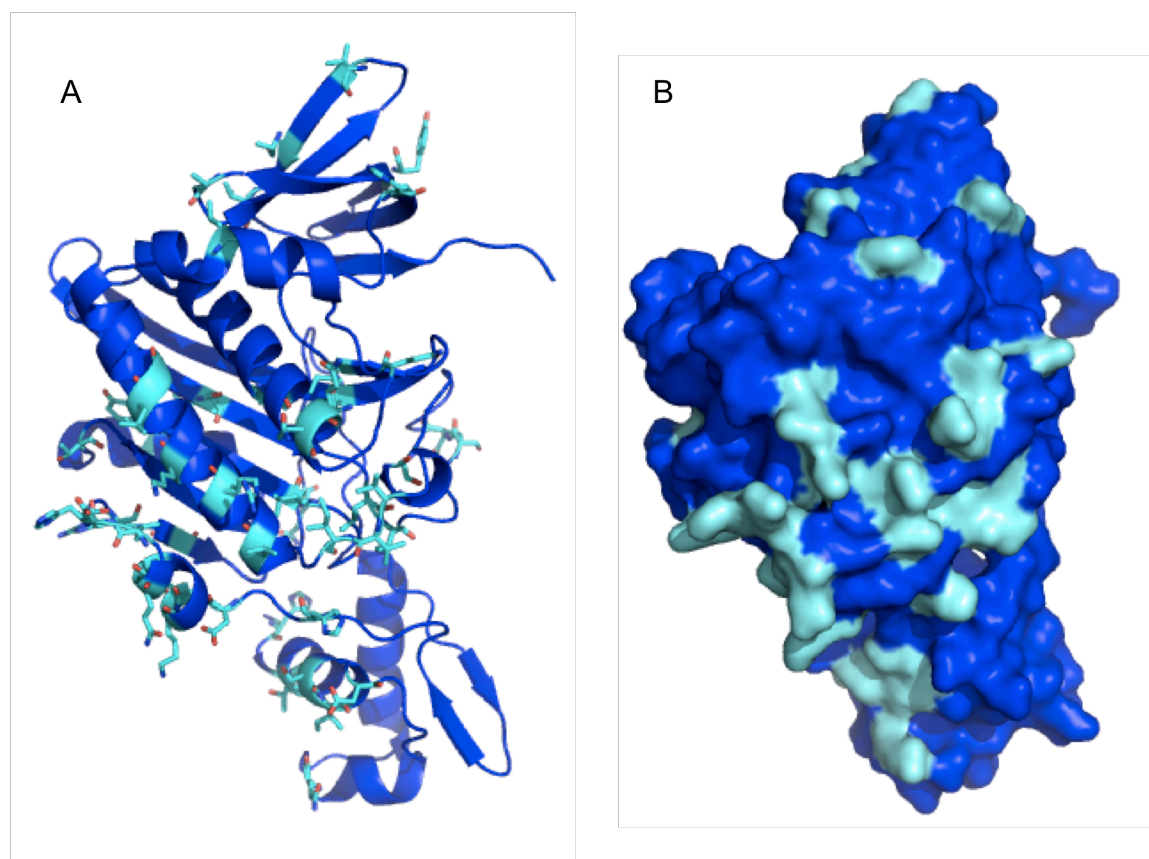


Figure 5.19 (A) Cartoon and (B) surface representation of *KpBPL* model with residues that are different from *EcBirA* highlighted in green. The majority of unconserved residues are located at the surface of the protein.

To date, the only class II BPLs with crystal structures that are available currently are *BirA* and *SaBPL* which have 39% sequence similarity. Despite obtaining protein crystals of *KpBPL* in several different crystallization conditions, no diffraction data could be obtained from these crystals. *KpBPL* is very similar to the *E. coli* *BirA*, with a 92.5% sequence similarity, and hence would be structurally similar. Sequence alignment of *KpBPL* and *EcBirA* shows that the majority of different residues are located on the surface of the protein, exposed to solvent, and away from the active site and the dimerisation interface (**Figure 5.19**). *K. pneumoniae* and *E. coli* are both Gram-negative enterobacteriaceae which encode the same genes required for biotin biosynthesis (*bioA*, *bioB*, *bioF*, *bioC*, *bioD* and *bioH*), and the *bioO* operon to which they bind to has the same sequence. *S. aureus* on the other hand, regulates a different set of biotin biosynthetic genes (*bioD*, *bioA*, *bioB*, *bioF*, *bioW* and *bioX*),

and the *S. aureus* bioO operon has a different sequence from that of *K. pneumoniae* and *E. coli* (Rodionov et al., 2002). SaBPL was purified with co-repressor bound within its active site, crystallographic studies show that the DNA-binding domain of SaBPL is positioned close to the catalytic active site. Unlike SaBPL, both BirA and KpBPL were first purified in their apo form. As the DNA-binding domain of BirA is placed further away from the active site compared to SaBPL, this allows the co-repressor to easily dissociate from BirA. As such, the active site of SaBPL is relatively more stable compared to BirA and KpBPL, providing tighter binding of the co-repressor within this region. SaBPL can also bind to its target DNA at micromolar concentrations, which will be further discussed in chapter 5.

Recently, inhibitors based on the structure of biotinyl-5'-AMP have been designed to inhibit SaBPL and MtBPL (Konarev et al., 2003, Ingaramo and Beckett, 2011, Brunger, 1992), and are active both in vitro and against their respective bacteria. Compounds which were chemically similar to biotinyl-5'-AMP but did not provide the same V-shape structure that biotinyl-5'-AMP forms whilst bound within the active site proved to be inactive, emphasizing the importance of accurate positioning of the compound within the active site. Interestingly, despite the high sequence and structural similarity found across the catalytic domain of BPLs, these inhibitors are selective against other bacteria and eukaryotic BPLs, and show low cytotoxicity against mammalian cell lines (Konarev et al., 2003, Ingaramo and Beckett, 2011, Brunger, 1992). As both KpBPL and AcBPL are potential targets for drug design, the non-hydrolysable analog of biotinyl-5'-AMP, biotinol-5'-AMP, was used for initial inhibitory studies. Biotinol-5'-AMP could inhibit KpBPL and AcBPL with nanomolar inhibition, which is unsurprising as it is structurally similar to the co-repressor. There are other inhibitors which have been designed against SaBPL, and it would be interesting to test the inhibitory effect that these compounds have against KpBPL and AcBPL, as well as to solve the crystal structure of KpBPL and AcBPL in complex with their natural ligands or an inhibitor to design a new generation of antimicrobials which can selectively inhibit KpBPL and AcBPL in order to treat deadly infections caused by *K. pneumoniae* and *Acinetobacter* species.

Chapter 6 Structural characterization of SaBPL in complex with DNA

Apart from playing a role in activating biotin-dependent metabolic enzymes through the heterodimerisation of SaBPL with SaBCCP, the homodimerisation of SaBPL regulates the synthesis of biotin biosynthetic genes through the repression of the biotin biosynthetic operon. To date, the structure of a class I bacterial BPL in complex with its target operon operator sequence has not been elucidated. This chapter focuses on the chapter consists of a recently published journal article (Pendini et al., 2013) that focuses on characterizing holo SaBPL in complex with its target biotin operon operator sequence, *bioO*, as well as its protein substrate, SaBCCP, using a combination of X-ray crystallography and small angle X-ray scattering.

Previous studies done on the *E. coli* BirA have showed that the apo enzyme only binds to *bioO* at millimolar concentrations. SaBPL on the other hand can bind to *bioO* with micromolar affinity. Included in this chapter is data that further supplements the results published in journal. Results in this chapter compare the binding of both apo and holo SaBPL with *bioO* using binding affinity assays, as well as SAXS. Crystallization trials of the SaBPL:*bioO* complex is also reported.

6.1. Contribution of publication

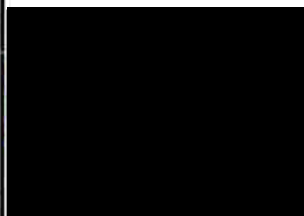
This chapter includes a journal article that has been published, in which my contribution includes the purification of both apo and holo forms of SaBPL, as well as the purification of SaBCCP. I then designed an EMSA experiment to determine that SaBPL could bind to its putative 44-mer *bioO* sequence. I further collected SAXS data of SaBPL and its binding targets, SaBCCP and *bioO*, as well as the SaBPL/*BioO* and SaBPL/SaBCCP complex at the Australian Synchrotron, and was involved in the analysis of the SAXS data. I also contributed to manuscript preparation of the published journal article.

Monash University

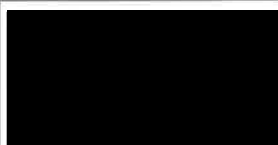

Declaration for Thesis Chapter 5: Structural characterization of SaBPL with its binding partners

Declaration by candidate:

In the case of Chapter 5, the nature and extent of my contribution to the work was the following:

Nature of contribution	Extent of contribution	Signature
<ol style="list-style-type: none">1. Expression and purification of SaBPL for SAXS2. Preparation of SaBPL:bioO and SaBPL:BCCP complexes for SAXS experiments.3. Analysis of SAXS data4. Performed EMSA assays and analysis5. Contributed towards manuscript preparation	45 %	

The following co-authors contributed to the work. Co-authors who are students at Monash University must also indicate the extent of their contribution in percentage terms:

Name	Nature of contribution	Signature
Nicole R. Pendini ^{1,2}	<ol style="list-style-type: none">1. Expression and purification of SaBPL for crystallography2. Crystallization of apo and holo SaBPL3. Collection of crystallographic data and analyzing and solving the structures of SaBPL4. Contributed towards manuscript preparation	
Steven W. Polyak ²	<ol style="list-style-type: none">1. Optimized protocol to purify SaBPL and performed biochemical assays.2. Contributed to manuscript preparation.3. Overall project direction	
Nathan P. Cowieson ^{1,3}	<ol style="list-style-type: none">1. Supervised the collection of SAXS data.2. Analysis of SAXS data	
Andrew Abell ⁴	<ol style="list-style-type: none">1. Contributed to manuscript preparation2. Overall project direction	
Grant W. Booker ²	<ol style="list-style-type: none">1. Supervised biochemical assays2. Contributed to manuscript preparation	
John C. Wallace ²	Contributed to manuscript preparation	
Jacqueline A. Wilce ¹	Contributed towards manuscript preparation	
Matthew C. J. Wilce ¹	<ol style="list-style-type: none">1. Analysis of SAXS data2. Contributed towards manuscript preparation3. Overall project direction	

1. School of Biomedical science, Monash University, VIC 3800, Australia

2. School of Molecular and Biomedical Science, University of Adelaide, Adelaide, South Australia, 5005, Australia
3. Monash Center for Synchrotron science, Monash University, VIC 3800, Australia
4. School of Chemistry and Physics, University of Adelaide, Adelaide, South Australia 5005, Australia

Declaration by co-authors:

- (1) the above declaration correctly reflects the nature and extent of the candidate's contribution to this work, and the nature of the contribution of each of the co-authors.
- (2) they meet the criteria for authorship in that they have participated in the conception, execution, or interpretation, of at least that part of the publication in their field of expertise;
- (3) they take public responsibility for their part of the publication, except for the responsible author who accepts overall responsibility for the publication;
- (4) there are no other authors of the publication according to these criteria;
- (5) potential conflicts of interest have been disclosed to (a) granting bodies, (b) the editor or publisher of journals or other publications, and (c) the head of the responsible academic unit; and
- (6) the original data are stored at the following location(s) and will be held for at least five years from the date indicated below:

Structural characterization of *Staphylococcus aureus* biotin protein ligase and interaction partners: An antibiotic target

Nicole R. Pendini,^{1,2} Min Y. Yap,¹ Steven W. Polyak,² Nathan P. Cowieson,^{1,3} Andrew Abell,⁴ Grant W. Booker,² John C. Wallace,² Jacqueline A. Wilce,¹ and Matthew C. J. Wilce^{1*}

¹Department of Biochemistry and Molecular Biology, School of Biomedical Sciences, Monash University, Victoria 3800, Australia

²School of Molecular and Biomedical Science, University of Adelaide, North Terrace, Adelaide, South Australia 5005, Australia

³Monash Centre for Synchrotron Science, Monash University, Victoria 3800, Australia

⁴School of Chemistry and Physics, University of Adelaide, North Terrace, Adelaide, South Australia 5005, Australia

Received 21 January 2013; Accepted 26 March 2013

DOI: 10.1002/pro.2262

Published online 5 April 2013 proteinscience.org

Abstract: The essential metabolic enzyme biotin protein ligase (BPL) is a potential target for the development of new antibiotics required to combat drug-resistant pathogens. *Staphylococcus aureus* BPL (SaBPL) is a bifunctional protein, possessing both biotin ligase and transcription repressor activities. This positions BPL as a key regulator of several important metabolic pathways. Here, we report the structural analysis of both holo- and apo-forms of SaBPL using X-ray crystallography. We also present small-angle X-ray scattering data of SaBPL in complex with its biotin-carboxyl carrier protein substrate as well as the SaBPL:DNA complex that underlies repression. This has revealed the molecular basis of ligand (biotinyl-5'-AMP) binding and conformational changes associated with catalysis and repressor function. These data provide new information to better understand the bifunctional activities of SaBPL and to inform future strategies for antibiotic discovery.

Keywords: biotin protein ligase; biotin-carboxyl carrier protein; DNA-binding; bacterial enzyme; biotinylation; small-angle X-ray scattering

Introduction

Biotin protein ligase (BPL) is a key enzyme in biotin biology that is responsible for specifically attaching the prosthetic group biotin onto biotin-dependent

enzymes. In some organisms, it also plays a role in the regulation of biotin biosynthesis. Biotin (Vitamin H or B7) is an important micronutrient found throughout the biosphere. All living organisms use

Abbreviations: BPL, biotin protein ligase; BCCP, biotin-carboxyl carrier protein; Btyl, biotinyl-5'-AMP; SAXS, small-angle X-ray scattering; ABL, adenosine-binding loop; BBL, biotin-binding loop; *bioO*, biotin biosynthetic operon operator; *BioY*, biotin transporter; HCS, human holocarboxylase synthetase.

Additional Supporting Information may be found in the online version of this article.

Nicole R. Pendini and Min Y. Yap contributed equally to this work

Grant sponsor: National Health and Medical Research Council (NHMRC) of Australia (application number 1011806). Grant sponsor: Adelaide Research and Innovation's Commercial Accelerator Scheme. Grant sponsor: BioInnovationSA's Commercial Development Awards.

*Correspondence to: Matthew C. J. Wilce, Department of Biochemistry and Molecular Biology, Monash University, Victoria 3800, Australia. [REDACTED]

biotin as a prosthetic group for a family of enzymes that perform carboxylation, decarboxylation, and transcarboxylation of substrates in metabolic pathways. For example, acetyl CoA carboxylase catalyzes the first committed step in fatty acid biosynthesis, and pyruvate carboxylase is required to replenish the tricarboxylic acid cycle with oxaloacetate. Biotin is particularly important in bacterial pathogenesis. During infection, bacteria have a high demand for the micronutrient, and respond by increasing the expression of proteins required for de novo biotin synthesis and uptake.^{1–5} There is thus great interest in understanding the metabolic adaption processes that allow bacteria to survive during infection, in particular, the role of BPL.^{6–8}

The ligation reaction that BPL catalyzes is well characterized,⁹ requiring biotin and ATP and proceeding through an adenylated intermediate, biotinyl-5'-AMP, before transfer of the biotin moiety to the biotin receiving enzymes at their biotin-carboxyl carrier protein (BCCP) domain. BPL isozymes fall into three structural classes. Class I enzymes are simple modules with the sole function of biotin attachment. High-resolution crystal structures have been reported for *Pyrococcus horikoshii* OT3 (PhBPL), *Aquifex aeolicus*, and *Mycobacterium tuberculosis*.^{10–12} These proteins exist as homodimers in both solution and in their crystallized forms. Other Class I enzymes, from both *M. tuberculosis* and *A. aeolicus*, have been reported to be monomeric, even in the presence of ligands.^{12,13} The two other classes contain the conserved catalytic module of Class I but differ in their N-terminal regions. Class II enzymes have an N-terminal DNA-binding domain, enabling dual functionality. Upon ligand binding, these BPLs homodimerize, facilitating a cooperative interaction with specific DNA sequences^{14,15} as exemplified by the *Escherichia coli* BPL (EcBPL, also known as BirA) (reviewed¹⁶). The dimers of Class I and Class II BPLs are structurally distinct as they use different surfaces for homodimerization. The Class III enzymes (which include human BPL) are monomeric and contain an N-terminal domain unrelated to the DNA-binding domain of Class II BPLs—the function of which has yet to be resolved. However, it has been shown to be required for substrate recognition during catalysis using a mechanism that is distinct from Class I and II enzymes.^{17–19} These key differences point to a plausible application for bacterial BPL as a target for novel antibiotics.

Bacteraemia caused by drug-resistant strains of *Staphylococcus aureus* is a major threat to health worldwide. Common bacterial infections are becoming more difficult and expensive to treat.^{20,21} To address this, research efforts have been devoted to identifying and validating novel drug targets. For example, pathways required for virulence, such as

biotin metabolism, provide an untapped source of potential new targets.^{4,22,23} We have recently provided the first data to demonstrate it is possible to selectively inhibit SaBPL over both EcBPL and their human counterpart, holocarboxylase synthetase (HCS).²⁴ Here, structural biology played an important role in the design of small molecule inhibitors with antibacterial activity against *S. aureus*. However, a greater understanding of how these inhibitors impact on SaBPL regulated pathways at the molecular and cellular level is required.

The BPL target in *S. aureus* (SaBPL) belongs to the bifunctional Class II enzymes. Genome annotation studies have revealed that it is required for the activation of two biotin-dependent enzymes, namely acetyl CoA carboxylase and pyruvate carboxylase. Additionally, it has been proposed that it functions as a transcriptional repressor of the biotin biosynthetic operon operator (*bioO*) and the biotin transporter *bioY*.²⁵ By combining biotin ligase and transcriptional repressor activity in a single protein, BPL is uniquely placed as the key regulator of biotin metabolism in *S. aureus*. How these two activities are co-ordinated by SaBPL is still unclear. However, through extensive genetic and biochemical studies of the closely related *E. coli* BPL (EcBPL) it has been proposed that the homodimerization and protein substrate binding interfaces on BPL are mutually exclusive.²⁶ Crystal structures of the EcBPL homodimer and PhBPL in complex with the BCCP subunit of methylmalonyl-CoA decarboxylase have been reported,^{27,28} providing some molecular detail for these protein:protein interactions. However, the Class I PhBPL enzyme does not undergo the monomer–dimer transition in response to biotin binding as seen with EcBPL,²⁹ and also uses a distinctly different surface for homodimerization. Furthermore, as the Class I enzymes lack DNA-binding activity they fail to provide enough detail to elucidate the complex lifecycle of the Class II BPLs. The absence of any structural data of a Class II BPL in complex with DNA has also restricted attempts to delineate this system further.

Here, we report three X-ray crystal structures of SaBPL (1) in complex with biotin, (2) with the adenylated reaction intermediate biotinyl-5'-AMP, and (3) apo-SaBPL. The holo-structures reveal the details of the dimer formation as facilitated by the binding of the biotinyl ligand. We also present a detailed investigation of the intermolecular interactions of SaBPL with binding partners SaBCCP and the biotin biosynthetic operon operator (*bioO*) that is the DNA target of SaBPL using small-angle X-ray scattering (SAXS). This analysis illustrates the mode of DNA binding of SaBPL and confirms that the two protein:protein interactions, that is, homodimer and heterodimer, indeed compete for a common surface on SaBPL. These data provide a

Table I. Data collection and refinement statistics (molecular replacement)

	apo-SaBPL	Biotin-SaBPL	Btyl-SaBPL
Data collection ^a			
Wavelength (Å)	0.95364	0.99810	1.5418 (Cu Kα)
Space group	<i>P</i> 2 ₁	<i>P</i> 4 ₂ 2 ₁ 2	<i>P</i> 4 ₂ 2 ₁ 2
Cell dimensions			
<i>a</i> , <i>b</i> , <i>c</i> (Å)	50.1, 51.4, 67.6	94.2, 94.2, 130.9	93.6, 93.6, 130.7
α , β , γ (°)	90, 108, 90	90, 90, 90	90, 90, 90
Resolution (Å)	35.0–2.1 (2.16–2.1)	40–3.2 (3.45–3.2)	20.0–2.6 (2.67–2.6)
<i>R</i> _{sym} or <i>R</i> _{merge}	11.3 (43.3)	5.2 (44.1)	5.7 (36.2)
<i>I</i> / σ <i>I</i>	8.8 (2.8)	11.1 (2.0)	12.7 (2.1)
Completeness (%)	96.1 (96.3)	98.7 (92.6)	98.3 (94.7)
Redundancy	3.8 (3.9)	4.6 (4.3)	4.1 (3.7)
Refinement			
Resolution (Å)	35.0–2.1	30–3.2	20.0–2.6
No. reflections	17,599	9929	18,509
<i>R</i> _{work} / <i>R</i> _{free}	19.6/24.9	19.2/23.9	19.9/25.7
No. atoms			
Protein	2484	2602	2602
Ligand/ion	0	16	38
Water	212	0	305
<i>B</i> -factors			
Protein	32.1	57.6	50.8
Ligand/ion	–	58.2	55.2
Water	36.8	–	65.2
R.M.S. deviations			
Bond lengths (Å)	0.019	0.015	0.022
Bond angles (°)	1.9	1.9	1.9
% in most favored regions of a Ramachandran plot	94.0	95.0	97.1

^a Diffraction data were collected from one crystal for each structure.

molecular mechanism that underlies the dual functions of this protein, paving the way for the development of a new class of antibiotics.

Results

Structural overview of apo- and holo-forms of SaBPL

To characterize the interaction between SaBPL and its native ligand biotinyl-5'-AMP, and its impact on SaBPL dimerization, we solved its crystal structure in apo-form, in complex with biotin alone (Bt-SaBPL) and in complex with biotinyl-5'-AMP (Btyl-SaBPL) (Table I). SaBPL was observed as a crystallographic dimer when either biotin or the reaction intermediate biotinyl-5'-AMP was bound to the catalytic site. In contrast, apo-SaBPL was a monomeric molecule with an overall fold analogous to the monomeric unit of dimeric SaBPL. Similarly to *E. coli* BPL the protein can be divided into three discrete domains [Fig. 1(A)]. The N-terminal domain (residues 1–61) forms a winged helix-turn-helix DNA-binding domain. The central catalytic domain (residues 68–274) forms an α – β structure containing eight β -sheets that form a major face of the catalytic site and seven α -helices that buttress against the β -sheet scaffold. The third, C-terminal domain (residues 282–323) is characterized by a fold similar to an SH3 domain³¹ and caps the catalytic site. Two

short random coil linkers (residues 62–67 and 275–281) link these three domains. In the case of apo-SaBPL only, no electron density is visible for the loop that forms over the bound ligand, known as the biotin-binding loop ([BBL] residues 118–129 [β 5– β 6 loop]) and residue 288, due to disorder in the absence of ligand.

Structural details of biotinyl-5'-AMP and biotin interactions in holo-SaBPL

Biotinyl-5'-AMP (abbreviated “Btyl” when SaBPL complex is referred to) binds with a tight “V” shape geometry and a buried surface area of 727 Å². Figure 1(B) shows the electron density around biotinyl-5'-AMP bound in the active site of SaBPL. The key interactions between SaBPL and biotinyl-5'-AMP are summarized in Figure 1(C). These interactions are consistent with those observed in the complex of SaBPL and a chemical analogue of biotinyl-5'-AMP, biotinol-5'-AMP (PDBID 3RKW²⁴). The biotin moiety is bound in a predominantly hydrophobic pocket of SaBPL with the carbon chain of the valeric acid group and the tetrahydrothiophene component of biotin surrounded by Gly121, Trp127, Trp 136, Gly208, Gly 190, Ile209, and Gly210. Hydrogen bonds stabilize the interactions with sidechains from Ser93, Thr94, Gln116, and mainchain hydrogen bonds from Arg120 to the polar ureido head group of biotin. The oxygen atom of the tetrahydrothiophene

is solvent exposed. The BBL is positioned over the biotin-binding pocket making multiple interactions with the ligand. The basic sidechains of Arg122 and Arg125 in the BBL interact with the carboxyl group of the valeric acid tail. The adenosine-binding site is formed by residues of β 10, including Lys187, Ser128, Asn212, and the loop between α 7 and α 8, including Ile224, Arg227, and Ala228 (known as the

adenosine-binding loop [ABL]), while Trp127 positions the adenylate moiety via π - π stacking interactions.

The Bt-*Sa*BPL structure (containing biotin only) was resolved to the moderate resolution of 3.2 Å. Although not providing details of the position of some sidechains, it does confirm that there are no major differences in the positions of the domains of *Sa*BPL between the holo-forms. The R.M.S.D. of the biotin-*Sa*BPL structure compared to Btyl-*Sa*BPL is 0.4 Å for 320 C α atoms. Further, the mainchain of the ABL loop is in the same position even in the absence of the adenosyl moiety (the sidechains of this loop were not defined in the electron density). These structures, together with a recently reported structure of *Sa*BPL with biotin-based ligands bound in the active site,³² show that any biotin ligand is sufficient to stabilize the BBL and to result in the formation of an *Sa*BPL dimer.

The dimerization interface of Btyl-*Sa*BPL

The dimerization interface of Btyl-*Sa*BPL consists of α 5-helix, the β 5- β 6 BBL, the β 10- β 11 loop including regions of these β -strands, the C-terminal end of the α 6-helix, and β 15- β 16 loop from the C-terminal domain [Fig. 2(A)]. Together these form a buried surface of 1028.9 Å².³⁴ Central to the dimer interaction is the antiparallel β -strand arrangement of the β 10-strand from one monomer to its counterpart on the other monomer to create an extended, albeit distorted, β -sheet joining the two monomers. The β 10- β 11 loop is juxtaposed against the opposing monomer and all the observed hydrogen bond and electrostatic interactions emanate from residues 194-203 to their partners on the opposing monomer. The α 5-helix contributes to dimer stability via an antiparallel interaction with the α 5-helix on the opposing monomer. The DNA-binding domains make no contact with each other and are spaced at their closest point (Lys3) 63.6 Å apart.

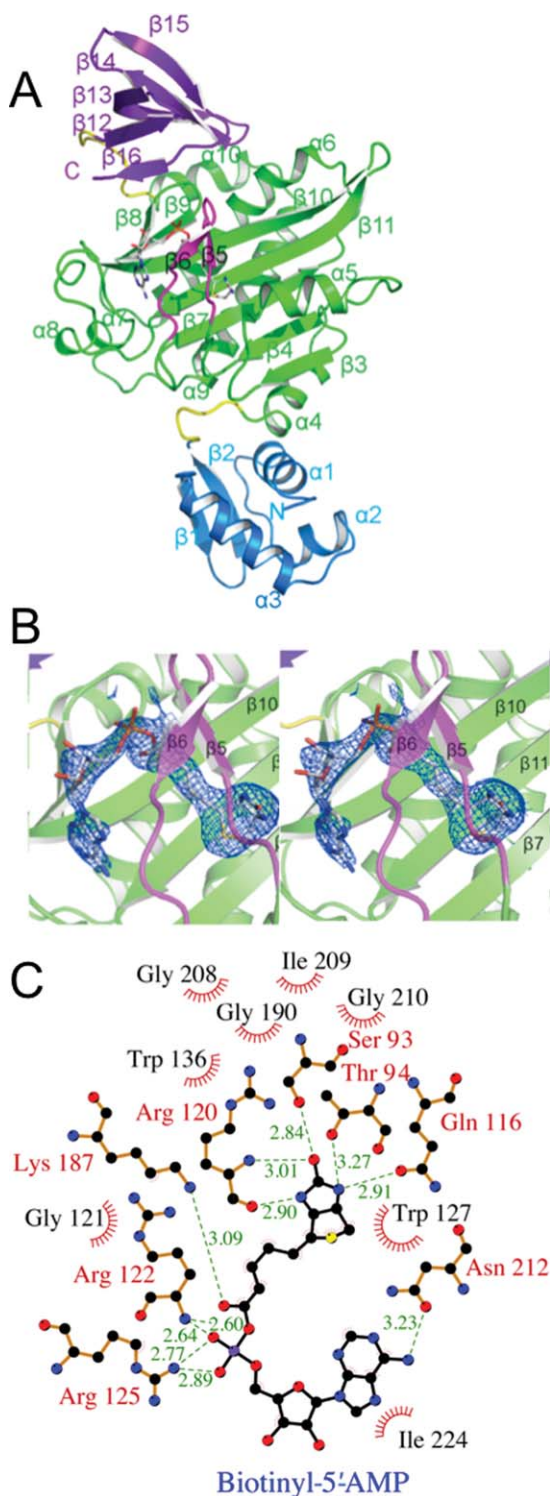


Figure 1.

Figure 1. Crystal structure of *Sa*BPL. (A) Cartoon schematic of Btyl-*Sa*BPL monomer showing the N-terminal DNA-binding domain, residues 2-60 (blue), the central catalytic domain residues 75-268 (green), and the C-terminal cap domain 282-323 (purple). The random coil linkers residues 62-67 and 275-281 that connect the domains are in yellow. The corepressor biotinyl-5'-AMP is shown in stick representation. The BBL is highlighted in pink. (B) Cartoon schematic of the catalytic site of Btyl-*Sa*BPL and the final 2F_o-F_c map (determined to 2.6 Å resolution and contoured at the 1 σ level) showing the positioning of biotinyl-5'-AMP (stick representation). (C) A schematic representation of contacts made to biotinyl-5'-AMP within the active site of *Sa*BPL made using LIGPLOT.³⁰ Residues involved in hydrogen bonding are annotated in red and hydrophobic interactions are annotated in black with red frays. Biotinyl-5'-AMP is shown with purple bonds and hydrogen bonding distance shown in Ångstroms by green dashed lines.

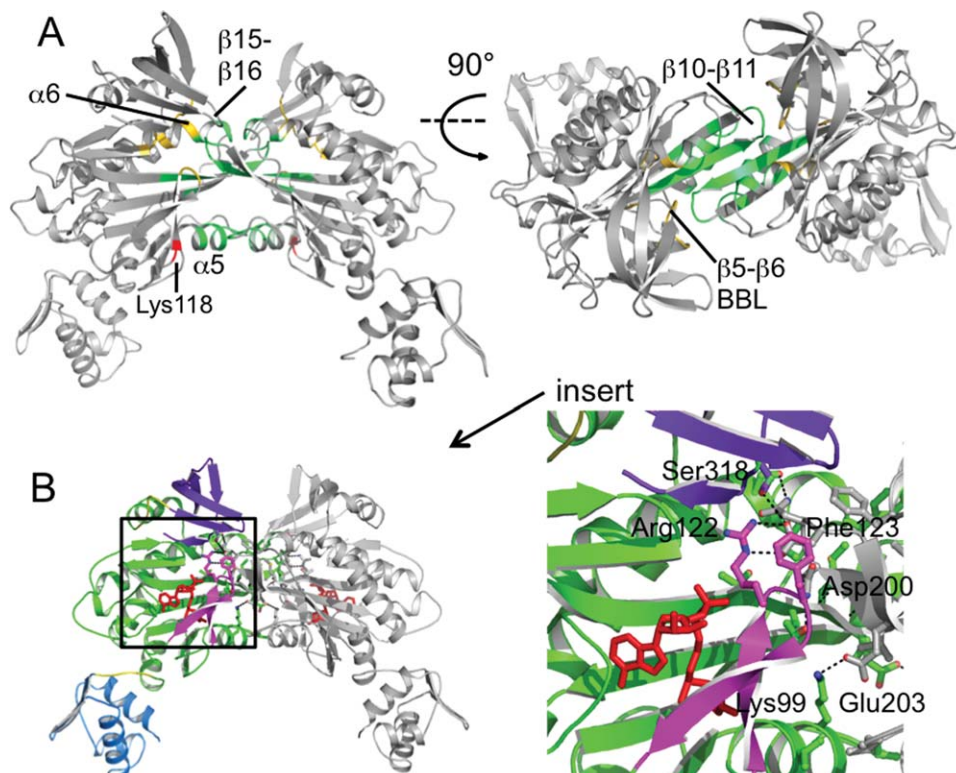


Figure 2. SaBPL dimer. Cartoon schematic of the holo-SaBPL dimer. (A) The regions of secondary structure involved in forming the dimer interface are colored according to the program PROFACE³³ and shown from two angles. The central cluster including $\beta 10$ – $\beta 11$, $\beta 15$ – $\beta 16$, and $\alpha 5$ are green and elements at the rim of the interface, including Lys118, $\alpha 6$, and the BBL loop, are colored red and yellow. (B) Contacts stabilized by the biotinyl-5'-AMP ligand are shown in context of the SaBPL dimer. One monomer is colored using the same scheme as in Figure 1, while the other monomer is gray. The ligand is in red stick figure representation. Residues involved in hydrogen bonding are shown in stick figure representation. Hydrogen bonds are indicated as dotted lines.

Of particular importance for its activity as a transcriptional repressor is the manner in which the dimer is stabilized by the bound biotin or biotinyl-5'-AMP ligand. Both the C-terminal domain and the BBL, which form direct contacts with the ligand, also make contact at the dimer interface. In particular, the $\beta 15$ – $\beta 16$ loop of the C-terminal cap domain (residues 317–319) and residues Arg122 and Phe123 of the BBL reside in the dimer interface [Fig. 2(B)]. Interestingly, residues from both of these elements (Ser318 from the C-terminal domain and Arg122 from the BBL) form a hydrogen bond with Asp200 emanating from the end of the $\beta 10$ – $\beta 11$ loop from the opposing monomer. Further, upon ligand binding and dimer formation, Asp320 forms a salt bridge with Arg125 in the catalytic core. This interaction appears to stabilize the loops between $\beta 5$ – $\beta 6$ and the cap domain that forms the biotinyl-5'-AMP binding site.

Comparison between apo and ligand bound SaBPL

A comparison of the monomeric apo-SaBPL structure and dimeric holo-SaBPL reveals the structural perturbations that take place concomitant with

ligand binding and the monomer–dimer transition. Apo- and holo-SaBPL structures display highly similar folds; the R.M.S.D of apo-SaBPL superposed with holo-SaBPL is 1.2 Å (between 302 C α atoms). Apo-SaBPL, however, occurs as a monomer, with the BBL completely undefined (residues 118–129 are not defined by electron density). This is in contrast with holo-SaBPL where the BBL is positioned through contacts with biotin in the catalytic site, forming an interaction surface for dimerization. Other small differences occur in the position of loops between $\beta 7$ – $\alpha 6$, $\beta 10$ – $\beta 11$, $\alpha 7$ – $\alpha 8$, and $\beta 12$ – $\beta 13$, respectively.

Structural analysis of SaBPL in complex with its target DNA

It has previously been predicted, but not shown, that dimeric SaBPL binds to the *S. aureus bioO*.²⁵ To verify this binding interaction, we identified a 44-bp sequence containing an imperfect inverted repeat, and tested binding to holo-SaBPL using electrophoretic mobility shift assay. Binding of holo-SaBPL to this sequence (and not to a control 44-bp dsDNA of an unrelated sequence) was confirmed (Supporting Information Fig. S2 and Supporting Information Methods). The affinity of holo-SaBPL

Table II. Structural parameters calculated from SAXS data and model of *SaBPL* and complexes

Molecule	R_g (Å) ^a (Guinier)	R_g (Å) ^b ($P(r)$)	D_{\max} (Å) ^c	χ^2 ^d	NSD ^e
<i>Holo-SaBPL</i>					
SAXS	30.7	30.2	97.0	0.78	0.89
Model (i)	30.7		99.8		
<i>Sa-bioO</i>					
SAXS	35.6	36.3	125.0	6.10	0.65
Model (ii)	36.7		145.0		
<i>Sa-bioO/SaBPL</i>					
SAXS	44	44.4	145	0.6	0.81
Model (iii)	40.7		153.0		
<i>Apo-SaBPL</i>					
SAXS	22.0	22.8	90	0.56	0.51
Model (iv)	22.3		86.3		
<i>SaBCCP</i>					
SAXS	16.9	16.7	57	0.77	0.60
Model (v)	16.7		54.1		
<i>SaBCCP/SaBPL</i>					
SAXS	22.5	22.8	75	0.98	0.69
Model (vi)	23.6		86.1		

^a R_g —radius of gyration given by Guinier approximation.

^b R_g —estimated from pair-wise distribution function.

^c D_{\max} —maximum molecular dimension from $P(r)$ function.

^d Goodness of fit of theoretical end experimental scattering curves calculated using FOXS.³⁵

^e Normalized spatial discrepancy for ab initio SAXS models calculated from DAMAVER.³⁶

for the *Sa-bioO* DNA sequence was approximated to be nanomolar ($K_D = 100$ nM) by EMSA titration.

To obtain structural information for this interaction, we subjected a complex of holo-*SaBPL* and the 44-bp DNA (henceforth referred to as *Sa-bioO*) to SAXS. SAXS data were collected for Btyl-*SaBPL*, the *Sa-bioO*, and the Btyl-*SaBPL/Sa-bioO* complexes. The experimental and calculated scattering curves are shown in Figure 3(A), the pair-wise distance distribution function, $P(r)$, is shown in Figure 3(B) and structural parameters are reported in Table II. The radius of gyration (R_g) for Btyl-*SaBPL* was determined by Guinier analysis to be 30.7 Å and the pair-wise distribution $P(r)$ for Btyl-*SaBPL* exhibits a bimodal distribution indicative of a dimer. The R_g and maximum dimension of the particle (D_{\max}) derived from the function ($P(r)$) profile were 30.2 and 97.0 Å, respectively. These values are consistent with those calculated from the crystal structure of Btyl-*SaBPL*. The D_{\max} derived from the $P(r)$ profile for *Sa-bioO* was 125 Å, and the $P(r)$ profile showed significant tailing towards a higher D_{\max} that is consistent with an elongated molecule such as dsDNA. Interestingly, this D_{\max} is shorter than the expected maximal dimension of an elongated 44-mer dsDNA (145 Å) suggesting that the dsDNA may be bent. This is possible as the *Sa-bioO* sequence contains a large number of A–T base pairs in its centre, which can increase the propensity of the dsDNA to bend. The $P(r)$ profile for the Btyl-*SaBPL/Sa-bioO* complex exhibited both a bimodal distribution as well as

tailing towards higher D_{\max} values. The D_{\max} of this complex was estimated to be 145 Å indicative of non-bent *Sa-bioO* upon binding of *SaBPL*.

Ab initio SAXS structures are displayed in Figure 3(C). Molecular models constructed from crystallographic structures are superimposed with the solution structure and the predicted scattering curve from this model was overlaid with the raw scattering data [Fig. 3(A)]. The ab initio SAXS structure for holo-*SaBPL* correlates remarkably well to the crystallographically determined *SaBPL* structure confirming the suitability of the system for SAXS analysis. In the case of *Sa-bioO*, the SAXS data indicate a solution structure that approximates the model based on extended B-form dsDNA [Fig. 3(C(ii))]. Third, an ab initio SAXS structure was calculated for the Btyl-*SaBPL/Sa-bioO* complex. Molecular coordinates were positioned into the SAXS structure using the program SITUS³⁷ which resulted in the recognition helices (residues 20–40) of the N-terminal domain of *SaBPL* positioned in adjacent major grooves of the DNA. This gave good consistency between the SAXS structure and the model [Fig. 3(C(iii))] with dimeric *SaBPL* straddled across the DNA at an approximately 45° angle.

Interaction of *SaBPL* with *SaBCCP*

SAXS was also used to further characterize the interaction between Btyl-*SaBPL* and *SaBCCP*. Data were collected for both apo-*SaBPL* and biotinylated-*SaBCCP* separately and together in a heterodimeric complex. The experimental and calculated scattering curves are shown in Figure 3(A), the $P(r)$ profiles shown in Figure 3(D) and structural parameters are reported in Table II. The apo-*SaBPL* SAXS data are in excellent agreement with the crystal structure. The R_g of 22.0 Å confirms the monomeric nature of this species. Likewise, the R_g and D_{\max} values for the biotinylated-*SaBCCP* are consistent with the size and shape expected, including a biotinyl-lysine group that is extended away from *SaBCCP*, in a conformation ideally suited for insertion into the intact carboxylase for catalysis. This is reflected in the $P(r)$ plot as a small shoulder on the high D_{\max} side. Notably, upon the addition of *SaBCCP* to BtOH-*SaBPL* (i.e., *SaBPL* in complex with biotinol-5'-AMP, a non-hydrolysable analogue of biotinyl-5'-AMP), the SAXS data indicate the absence of dimeric *SaBPL* and instead report a shape that is slightly larger than apo-*SaBPL*. The $P(r)$ plot closely resembles that of monomeric *SaBPL*; however, the Guinier R_g of 22.5 Å is slightly larger than that determined for apo-*SaBPL*.

The ab initio SAXS structure for apo-*SaBPL* is highly comparable to the crystallographically determined *SaBPL* monomer [Fig. 3(C(iv))]. The ab initio SAXS structure for the biotinylated-*SaBCCP* also accommodates the crystallographically determined

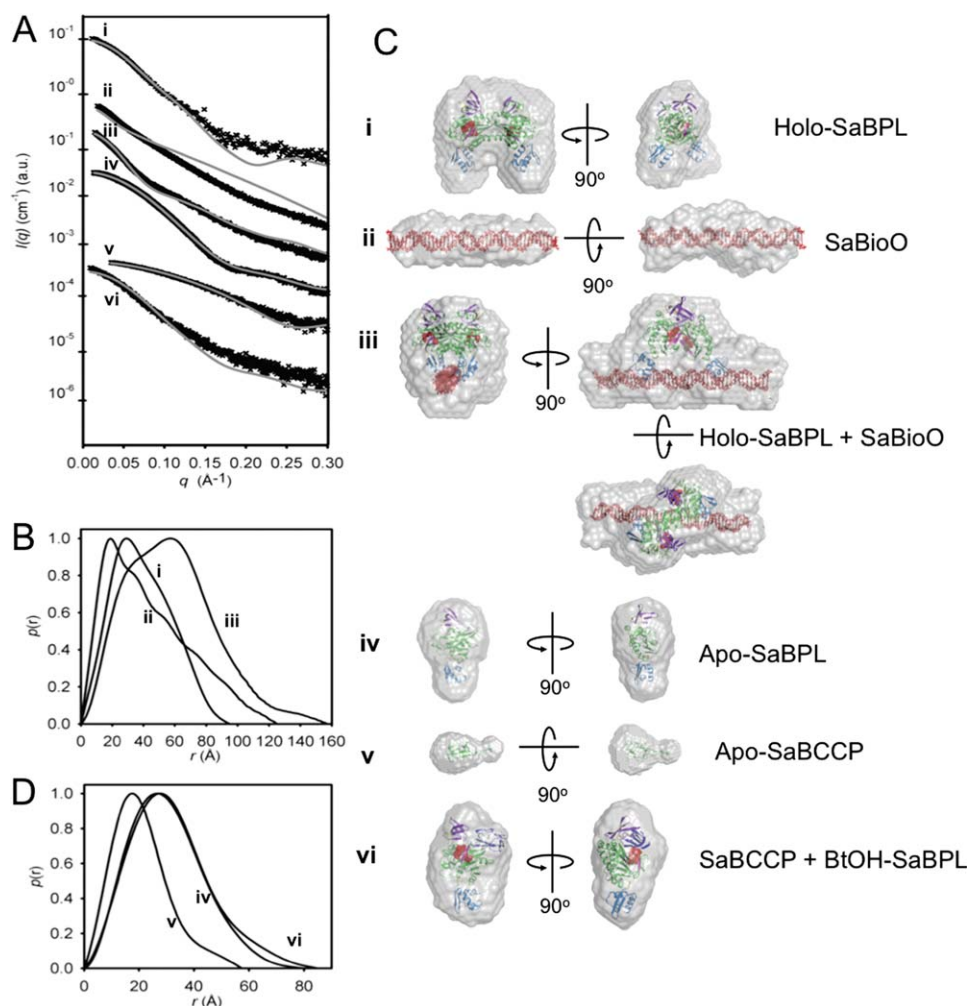


Figure 3. SAXS analysis of apo- and holo-SaBPL, SaBPL/DNA, and SaBPL/BCCP. (A) Scattering data for the six SaBPL, SaBioO, and SaBCCP samples (black crosses) with the predicted scattering curves (gray solid line) derived from models of these molecules and complexes (a.u. corresponds to arbitrary units). (B) Pair-wise distribution ($P(r)$) profiles for holo-SaBPL, SaBioO, and SaBPL/SaBioO complexes. (C) Ab initio reconstruction of the six samples overlaid with models derived from crystallographic structural data and modeling. (D) Pair-wise distribution ($P(r)$) profiles for apo-SaBPL, SaBCCP, and the SaBCCP/SaBPL complex. Note that each of the six scattering curves, $P(r)$ profiles, and ab initio models are correlated by a Roman numeral label.

SaBCCP structure (PDB ID: 3BG5) with an extrusion from one side that we suggest represents the biotinyl-lysine group [Fig. 3(C(v))]. A molecular model of SaBPL/BCCP was built using a monomer of holo-SaBPL in complex with the SaBCCP structure by analogy to the *P. horikoshii* BPL/BCCP complex (PDB ID: 2EJG). This required the repositioning of the C-terminal cap region of SaBPL relative to the catalytic domain by 5° , to open up the binding site to accommodate the SaBCCP (Supporting Information Fig. S3). The SaBPL/BCCP model is comparable to the ab initio SAXS structure [Fig. 3(C(vi))] although the fit of the scattering data calculated from this model with the experimental data was not ideal. This could have arisen from a number of sources. The juxtaposition of SaBCCP to the SaBPL could be subtly different to that observed for the *Pyrococcus* complex, and/or, the SAXS data may reflect the presence of small amounts of dimeric

SaBPL or free SaBCCP. Importantly, it is clear that the SaBCCP disrupted the dimeric SaBPL.

Comparison with human BPL

Together the X-ray crystallographic and SAXS data verify the interactions of SaBPL with its DNA and BCCP binding partners. With this understanding of the surfaces of SaBPL important for its function, we considered the potential for SaBPL to be targeted by specific inhibitors designed to inhibit SaBPL function. In particular, we compared the SaBPL molecular surface to that predicted for human BPL (also known as human HCS). Figure 4(A) illustrates the predicted surface similarity of SaBPL and HCS, based upon a sequence alignment of catalytic and C-terminal cap domains [Fig. 4(B)]. Although the ligand-binding site itself contains conserved residues that are involved in ligand binding [identical residues are colored blue in Fig. 4(A)], a significant

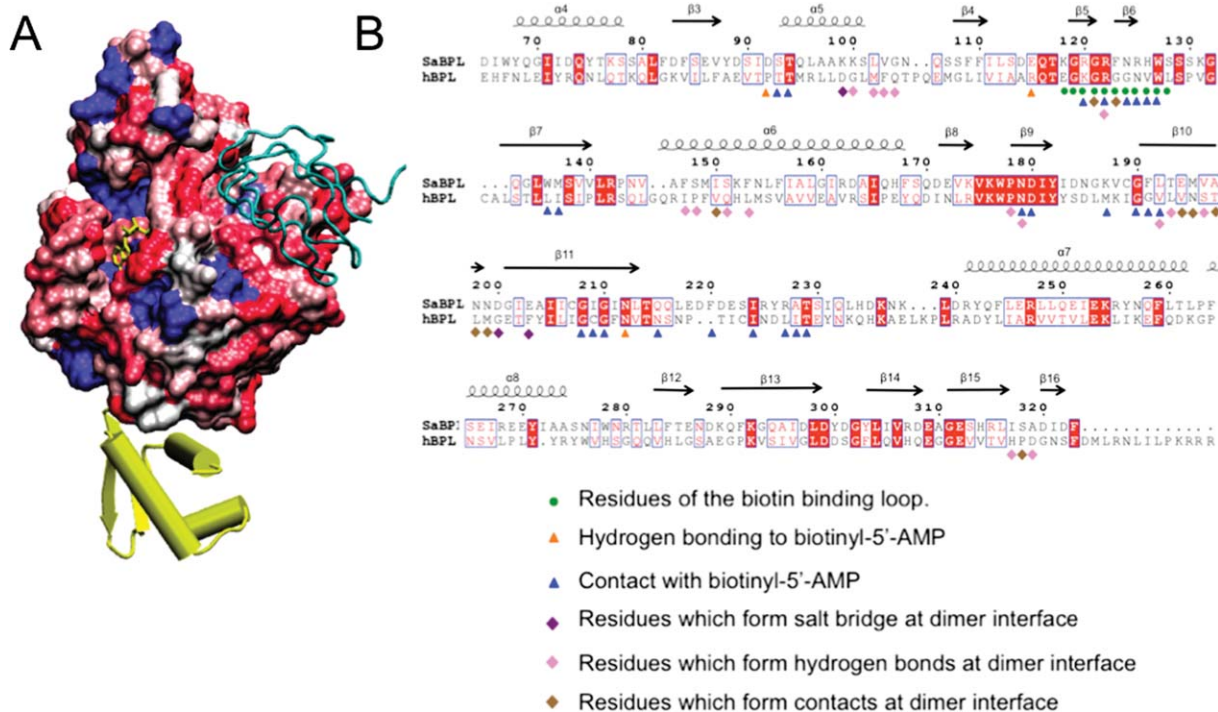


Figure 4. SaBPL as a potential drug target. (A) Similarity of surface amino acid residues of human BPL mapped to the surface of SaBPL. Identical amino acids are shown in blue. Sequence similarity is shown on a ramped scale from blue through white to red scored using the BLOSUM60 matrix where white indicates sequence similarity, pink and dark pink represent lesser similarity, and red represents the highest level of dissimilarity. The N-terminal DNA-binding domain is completely unrelated to the N-terminal domain of human BPL and is shown in yellow. SaBCCP modeled in its bound position is shown in cyan ribbons. (B) SaBPL sequence alignment with human SaBPL used for the surface comparison. Indicated are SaBPL amino acid residues involved at the catalytic site or the dimer interface of SaBPL.

number of residues that immediately surround the site show considerable variation. In particular, the adjacent ABL and BBL provide distinct side-chain functionalities that could form the basis of selectivity in inhibitor molecules targeted to the ligand-binding site. Additionally, the proposed BCCP binding site identified in this study also represents a region of poor sequence similarity that could be exploited in SaBPL inhibitor development.

Furthermore, the N-terminal domains of *S. aureus* and human BPL show no sequence homology at all. The N-terminal domains of eukaryotic BPLs are thought to perform an entirely different function that does not involve DNA binding.³⁸ Truncations and mutations to the N-terminal of human BPL render an inactive enzyme, indicating an underlying reliance on this region for catalytic function that is not seen for prokaryotic BPLs.^{9,19,38,39} Together, these key differences in the isozymes from *S. aureus* and human provide a structural basis for the selective inhibition of BPL for antibiotic discovery.

Discussion

We have investigated the molecular detail of BPL from the important human pathogen *S. aureus*. The crystallographically determined structures of apo-SaBPL and SaBPL in complex with biotin and

biotinyl-5'-AMP reveal that the enzyme undergoes a monomer to dimer transition upon ligand binding. Residues 118–129, that form the BBL, become ordered, as do specific loops creating part of the surface necessary for protein:protein interaction. Upon homodimer formation, the two N-terminal DNA binding domains are optimally positioned for an interaction with the major grooves at the inverted repeat sequences of the palindromic *Sa-bioO* DNA binding site.

This study confirms experimentally that SaBPL binds to the *Sa-bioO* DNA sequence and provides the first experimentally determined structure of the SaBPL/DNA complex using SAXS. By analogy to EcBPL, this complex will repress the transcription of genes containing the recognition motif in the promoter region. *E. coli* BPL controls expression of an operon containing the genes that encode the biotin biosynthetic enzymes, whereas in *S. aureus*, it is proposed that this operon as well as the gene encoding the biotin transport protein BioY are all regulated by BPL.²⁵ Our SAXS derived structure of the holo-SaBPL/Sa-bioO complex reveals the arrangement of SaBPL straddled across the dsDNA. The relative positioning of the molecules differs from previous models proposed for EcBPL bound to dsDNA.²⁷ This is due to slight differences in the dimer

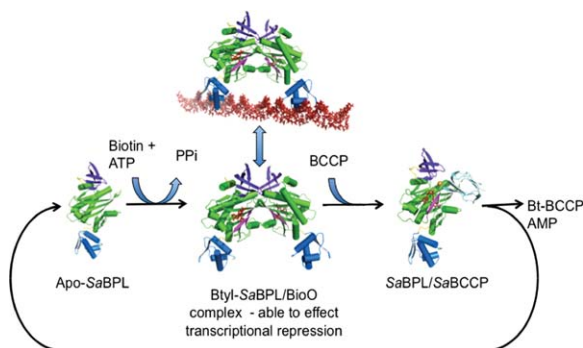


Figure 5. Schematic showing the regulation of SaBPL. The fate of SaBPL depends upon the availability of biotin for the conversion of apo-SaBPL to Btyl-SaBPL that is capable of effecting transcriptional repression and also the presence of BCCP that is able to compete for the SaBPL dimer surface becomes biotinylated resulting in the reformation of apo-SaBPL.

interface of holo-SaBPL and the positioning of the N-terminal domains revealed by X-ray crystallography compared to that of *EcBPL* (Supporting Information Fig. 4). Together these impact on their interaction at the major grooves of the DNA. Furthermore, the SAXS data reveal that the SaBPL dimer sits lower on the dsDNA than previous models have predicted, reflecting the highly complementary interface of the SaBPL dimer and target dsDNA.

This study also demonstrates that the presence of SaBCCP competes with SaBPL homodimer formation. SAXS data were consistent with the formation of a SaBPL/SaBCCP heterodimer, with no evidence of Btyl-SaBPL homodimer persisting in solution. This is consistent with a mutational study performed for *EcBPL* that tests the role of interface residues in homodimer and heterodimer formation.⁴⁰ The data also suggest that the SaBPL/SaBCCP heterodimer forms analogously to the crystal structure of the *P. horikoshii* BPL/BCCP complex⁴¹ and as modeled for the *EcBPL*/BCCP.²⁶ In our model of this complex, the reactive lysine of SaBCCP extends from the turn flanked between two β -strands. This strand-turn-strand structural element is positioned analogously to the β 10-turn- β 11 of the SaBPL partner in the dimeric form of SaBPL, albeit forming a parallel β -sheet interaction rather than antiparallel. This places the lysine towards the catalytic site where the biotin transfer can take place.

Together our data provide a molecular mechanism for biotin transfer in which the SaBCCP interacts at the dimer interface of holo-SaBPL (Fig. 5). Upon removal of the biotin from the catalytic site of SaBPL, the dimerization interface is destabilized—in particular by conformational changes to the BBL. This is predicted to free the biotinylated BCCP ready to perform its role in the biochemical pathway. In the absence of BCCP, holo-SaBPL forms a dimer

and, with two DNA-binding domains held in position, is able to form a complex with the *bioO* dsDNA resulting in transcriptional repression. This article is the first report containing structural data to support this mechanism for a complex Class II BPL. Furthermore, this study shows that, in the case of SaBPL, it is the presence of apo-BCCP that determines whether SaBPL acts in its biotin ligase role or as a transcriptional repressor. Even in the presence of a biotin ligand, BCCP outcompetes homodimer formation and thus interferes with repressor activity.

With the structural details for SaBPL, and its molecular interactions with binding partners, we have been able to assess the molecular surfaces of SaBPL and their suitability for the development of inhibitors. The biotinyl-5'-AMP binding site is clearly a critical site in SaBPL for the development of competitive inhibitors and, indeed, we have begun to exploit this site with the use of biotin analogues that bind tightly in the active site.²⁴ Here, we have shown that this site, while clearly conserved between species for binding to biotinyl-5'-AMP, possesses features that differ from human BPL that indicate the potential for the development of inhibitors specific for the bacterial BPL over the human form. Our work also confirms that the BCCP interface of SaBPL differs from that of human, suggesting it also as a site for potential inhibitor development. Third, the molecular details for the N-terminal domain of SaBPL that has no similarity at all to the N-terminal domain of human BPL may facilitate the development of yet another class of SaBPL inhibitor acting at the level of *bioO* derepression.

Because of the essential nature of BPL for survival, and *S. aureus* being one of the most clinically important pathogenic micro-organisms, our endeavor is to use the structural information reported here to target this protein for the development of new antibiotics. Targeting essential enzymes for which there are no pre-existing resistance mechanisms is a well-accepted strategy to combat the rise of drug-resistant bacteria. This data have provided a detailed understanding of the functional surfaces of SaBPL that will assist in the development of specific potent drugs against this class II BPL isoenzyme.

Materials and Methods

Preparation and crystallization of SaBPL

The cloning, purification, and crystallization of recombinant SaBPL have been previously reported.⁴² SaBPL was incubated with apo-BCCP for 1 h prior to final purification to ensure it was in the apo-form. Biotin or biotin+ATP+MgCl₂ was added to apo-SaBPL prior to sample use to form holo-SaBPL. Both the apo- and holo-SaBPL crystals were grown from similar conditions.⁴²

Preparation of SaBCCP

E. coli BL21 were transformed with a plasmid encoding GST-SaBCCP (residues 68–155 of acetyl-CoA carboxylase from *S. aureus*). The expression and purification of the biotin domain were performed as previously described.⁴³

Structure determination of SaBPL

X-ray diffraction data for crystals of biotinyl-5'-AMP/SaBPL (Btyl-SaBPL) were collected in-house using a Rigaku RUH2R rotating copper anode X-ray source equipped with Osmic confocal optics, an R-Axis IV detector. Diffraction data for crystals of biotin/SaBPL (Bt-SaBPL) and apo-SaBPL were recorded at the MX1 beamline at the Australian Synchrotron using a MAR research 165 CCD detector. All data were collected with cryo-cooling using an Oxford Cryosystems 700 Series cryostream at 100 K.

The diffraction data were integrated using MOSFLM⁴⁴ and the intensities were merged and scaled using the CPP4 suite of programs.⁴⁵ Initial phases were determined for the Btyl-SaBPL crystal structure by molecular replacement using PHASER⁴⁶ with the coordinates of the BPL from *P. horikoshii* OT3, PDB ID: 1WQ7, as the search model. The model was built with cycles of manual model building with COOT⁴⁵ and refinement with REFMAC.⁴⁷

The Btyl-SaBPL structure, with biotinyl-5'-AMP deleted, was used as the starting model for refinement of the Bt-SaBPL. Phases for the apo-SaBPL structure determination were determined by molecular replacement PHASER⁴⁵ using holo-SaBPL as the search model. The quality of the final models was evaluated using MOLPROBITY.⁴⁸ A final cycle of refinement was performed using the program PHE-NIX.⁴⁹ Statistics for the data and refinement are reported in Table I.

Preparation of dsDNA Sa-bioO sequence

DNA of sequence: 5'-CCTTAAATGTAACTTATTAATTATAAAAGTTTACATTTGGATT-3' and its complementary strand were purchased (Geneworks) as single-stranded oligonucleotides in gel purified form. The oligonucleotides were resuspended in Tris-EDTA buffer. The annealing reaction was performed by mixing equal volumes of both strands of DNA at equimolar ratio. The mixture was heated to 95°C for 3 min, and slowly cooled down to room temperature over 1 h. The annealed Sa-bioO was then stored at 4°C. The dsDNA concentration was determined spectrophotometrically at $\lambda = 260$.

Preparation of SaBPL/SaBCCP and SaBPL/DNA samples for SAXS experiments

The SaBPL/DNA complex was formed by adding SaBPL and the Sa-bioO DNA together at 2:1 molar (dimeric SaBPL/DNA) concentrations (200 μ M) in

50 mM Tris-HCl pH 7.0, 50 mM NaCl, 2 mM ATP, 2 mM biotin (or the nonhydrolysable analogue biotinol-5'-AMP), 10 mM MgCl₂, and 5% glycerol. The SaBPL/SaBCCP complex was formed by adding the proteins at equimolar concentrations (200 μ M) in presence of biotin and ATP (or biotinol-5'-AMP) in 50 mM Tris-HCl pH 7.0, 50 mM NaCl, and 5% glycerol. Just prior to the SAXS experiments all samples were buffer exchanged and concentrated in 3 K cut-off concentrators (Centricon) with the eluant used as the buffer blank. Sample concentrations were determined prior to complex formation spectrophotometrically at $\lambda = 280$ using experimentally determined extinction coefficients.

SAXS measurements and data reduction

SAXS was conducted for SaBPL and its complex with its cognate DNA (*bioO*) or SaBCCP as well as for the individual components of these complexes. SAXS measurements were made using the SAXS-WAXS beamline at the Australian Synchrotron, Melbourne, Australia, which is equipped with a Pilatus 1M-Detector. The scattering data were collected to provide an s range of 0.015–0.3 \AA^{-1} . Samples flowed past the X-ray beam in a 1.5 mm quartz capillary at room temperature during data collection. Scattering was collected over a range of concentrations, five concentrations between 0.2 and 2 mg/mL for each sample. The samples and matching buffer solutions were exposed to X-rays for 10 s, subdivided into 10×1 s exposures. The scattering images were integrated, averaged, and calibrated against water using software specific to the beamline. Scattering from the buffer and empty capillaries was subtracted after scaling scattering intensities to correspond to incident beam intensities. Data analysis was performed using the ATSAS suite of software. The program AUTOPOROD⁵⁰ was used to yield the pair-wise distribution function ($P(r)$) and to determine R_g (from the second moment of the $P(r)$ function) and D_{\max} . The R_g values calculated from the Guinier approximation and the $P(r)$ were favorably comparable. The radius of gyration (R_g) did not vary significantly over the concentrations ranges of each species of molecule and all Guinier plots were linear for $s.R_g$ 1.3.

Modeling of SAXS data

For each molecular species, the program DAMMIF⁵¹ was used to generate 20 ab initio dummy atoms models. These models were superposed, merged, and filtered using the program DAMAVER.³⁶ Theoretical scattering curves were calculated from the model coordinates and compared to the experimental data using FOXS.³⁵

Molecular figures and sequence/structure analysis

Figures were prepared using PYMOL.⁵² LIGPLOT³⁰ was used to generate Figure 1(C). The sequence

alignment [Fig. 4(B)] was made using ESPript.⁵³ Surface areas and contents were calculated using PISA.³⁴ The surface of SaBPL shown in Figure 4(A) was colored using MULTISEQ (part of VMD⁵⁴) according to sequence similarity based upon the BLOSUM60 matrix.

ACCESSION NUMBERS

Coordinates and structure factors have been deposited in the Protein Data Bank with accession numbers: BtYL-SaBPL PDBID = 3RIR, Bt-SaBPL PDBID = 3RKY, and, apo-SaBPL PDBID = 3RKX.

Acknowledgments

MCJW is an NHMRC Senior Research Fellow and acknowledges the support of the NHMRC and the Australian Research Council. NC was a Monash Centre for Synchrotron Science Fellow. Diffraction and scattering data were collected at the Australian Synchrotron MX1 and SAXS/WAXS beamlines. We also acknowledge the computer resources of the Victorian Partnership for Advanced Computing. We wish to thank Prof John Cronan (University of Illinois) for the kind gift of biotinol-5'-AMP.

References

- Chiang SL, Mekalanos JJ (1998) Use of signature-tagged transposon mutagenesis to identify *Vibrio cholerae* genes critical for colonization. *Mol Microbiol* 27:797–805.
- Lee JM, Zhang S, Saha S, Santa Anna S, Jiang C, Perkins J (2001) RNA expression analysis using an antisense *Bacillus subtilis* genome array. *J Bacteriol* 183:7371–7380.
- Sasseti CM, Rubin EJ (2003) Genetic requirements for mycobacterial survival during infection. *Proc Natl Acad Sci USA* 100:12989–12994.
- Bae T, Banger AK, Wallace A, Glass EM, Aslund F, Schneewind O, Missiakas DM (2004) *Staphylococcus aureus* virulence genes identified by bursa aurealis mutagenesis and nematode killing. *Proc Natl Acad Sci USA* 101:12312–12317.
- Bergman NH, Anderson EC, Swenson EE, Janes BK, Fisher N, Niemeyer MM, Miyoshi AD, Hanna PC (2007) Transcriptional profiling of *Bacillus anthracis* during infection of host macrophages. *Infect Immun* 75:3434–3444.
- Eisenreich W, Dandekar T, Heesemann J, Goebel W (2010) Carbon metabolism of intracellular bacterial pathogens and possible links to virulence. *Nat Rev Microbiol* 8:401–412.
- Becher D, Hempel K, Sievers S, Zuhlke D, Pane-Farre J, Otto A, Fuchs S, Albrecht D, Bernhardt J, Engelmann S, Volker U, van Dijk JM, Hecker M (2009) A proteomic view of an important human pathogen—towards the quantification of the entire *Staphylococcus aureus* proteome. *PLoS One* 4:e8176.
- Hecker M, Becher D, Fuchs S, Engelmann S (2010) A proteomic view of cell physiology and virulence of *Staphylococcus aureus*. *Int J Med Microbiol* 300:76–87.
- Pendini NR, Bailey LM, Booker GW, Wilce MC, Wallace JC, Polyak SW (2008) Microbial biotin protein ligases aid in understanding holocarboxylase synthetase deficiency. *Biochim Biophys Acta* 1784:973–982.
- Bagautdinov B, Kuroishi C, Sugahara M, Kunishima N (2005) Crystal structures of biotin protein ligase from *Pyrococcus horikoshii* OT3 and its complexes: structural basis of biotin activation. *J Mol Biol* 353:322–333.
- Gupta V, Gupta RK, Khare G, Salunke DM, Surolia A, Tyagi AK (2010) Structural ordering of disordered ligand-binding loops of biotin protein ligase into active conformations as a consequence of dehydration. *PLoS One* 5:e9222.
- Tron CM, McNae IW, Nutley M, Clarke DJ, Cooper A, Walkinshaw MD, Baxter RL, Campopiano DJ (2009) Structural and functional studies of the biotin protein ligase from *Aquifex aeolicus* reveal a critical role for a conserved residue in target specificity. *J Mol Biol* 387:129–146.
- Purushothaman S, Gupta G, Srivastava R, Ramu VG, Surolia A (2008) Ligand specificity of group I biotin protein ligase of *Mycobacterium tuberculosis*. *PLoS One* 3:e2320.
- Abbott J, Beckett D (1993) Cooperative binding of the *Escherichia coli* repressor of biotin biosynthesis to the biotin operator sequence. *Biochemistry* 32:9649–9656.
- Eisenstein E, Beckett D (1999) Dimerization of the *Escherichia coli* biotin repressor: corepressor function in protein assembly. *Biochemistry* 38:13077–13084.
- Beckett D (2009) Biotin sensing at the molecular level. *J Nutr* 139:167–170.
- Hassan YI, Moriyama H, Olsen LJ, Bi X, Zempleni J (2009) N- and C-terminal domains in human holocarboxylase synthetase participate in substrate recognition. *Mol Genet Metabol* 96:183–188.
- Ingaramo M, Beckett D (2009) Distinct amino termini of two human HCS isoforms influence biotin acceptor substrate recognition. *J Biol Chem* 284:30862–30870.
- Mayende L, Swift RD, Bailey LM, Soares da Costa TP, Wallace JC, Booker GW, Polyak SW (2012) A novel molecular mechanism to explain biotin-unresponsive holocarboxylase synthetase deficiency. *J Mol Med (Berl)* 90:81–88.
- Deleo FR, Otto M, Kreiswirth BN, Chambers HF (2010) Community-associated methicillin-resistant *Staphylococcus aureus*. *Lancet* 375:1557–1568.
- Turnidge JD, Kotsanas D, Munchhof W, Roberts S, Bennett CM, Nimmo GR, Coombs GW, Murray RJ, Howden B, Johnson PD, Dowling K (2009) *Staphylococcus aureus* bacteraemia: a major cause of mortality in Australia and New Zealand. *Med J Aust* 191:368–373.
- Liu CI, Liu GY, Song Y, Yin F, Hensler ME, Jeng WY, Nizet V, Wang AH, Oldfield E (2008) A cholesterol biosynthesis inhibitor blocks *Staphylococcus aureus* virulence. *Science* 319:1391–1394.
- Heras B, Shouldice SR, Totsika M, Scanlon MJ, Schembri MA, Martin JL (2009) DSB proteins and bacterial pathogenicity. *Nat Rev Microbiol* 7:215–225.
- Soares da Costa TP, Tieu W, Yap MY, Pendini NR, Polyak SW, Sejer Pedersen D, Morona R, Turnidge JD, Wallace JC, Wilce MC, Booker GW, Abell AD (2012) Selective inhibition of biotin protein ligase from *Staphylococcus aureus*. *J Biol Chem* 287:17823–17832.
- Rodionov DA, Mironov AA, Gelfand MS (2002) Conservation of the biotin regulon and the BirA regulatory signal in Eubacteria and Archaea. *Genome Res* 12:1507–1516.
- Weaver LH, Kwon K, Beckett D, Matthews BW (2001) Competing protein: protein interactions are proposed to control the biological switch of the *E. coli* biotin repressor. *Protein Sci* 10:2618–2622.
- Weaver LH, Kwon K, Beckett D, Matthews BW (2001) Corepressor-induced organization and assembly of the

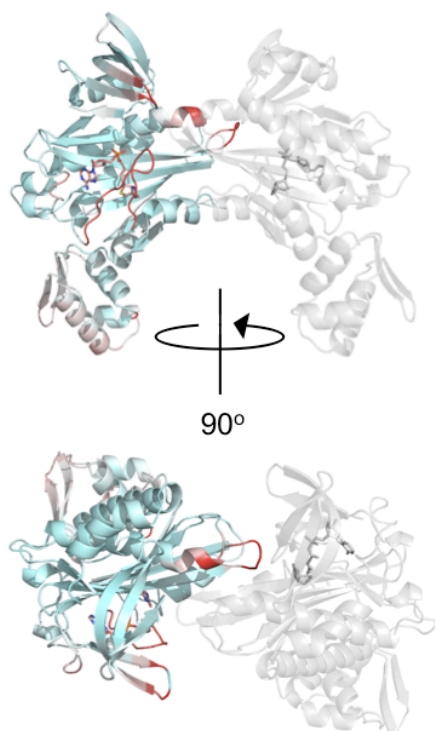
- biotin repressor: a model for allosteric activation of a transcriptional regulator. *Proc Natl Acad Sci USA* 98:6045–6050.
28. Bagautdinov B, Matsuura Y, Bagautdinova S, Kunishima N (2008) Protein biotinylation visualized by a complex structure of biotin protein ligase with a substrate. *J Biol Chem* 283:14739–14750.
29. Wood ZA, Weaver LH, Brown PH, Beckett D, Matthews BW (2006) Co-repressor induced order and biotin repressor dimerization: a case for divergent followed by convergent evolution. *J Mol Biol* 357:509–523.
30. Wallace AC, Laskowski RA, Thornton JM (1995) LIGPLOT: a program to generate schematic diagrams of protein-ligand interactions. *Protein Eng* 8:127–134.
31. Noble MEM, Musacchio A, Saraste M, Courtneidge SA, Wierenga RK (1993) Crystal structure of the SH3 domain in human Fyn—comparison of the 3-dimensional structures of SH3 domains in tyrosine kinases and spectrin. *EMBO J* 12:2617–2624.
32. Soares Da Costa TP, Tieu W, Yap MY, Zvarec OJ, Bell JM, Turnidge JD, Wallace JC, Booker GW, Wilce MC, Abell AD, Polyak SW (2012) Biotin analogues with antibacterial activity are potent inhibitors of biotin protein ligase. *ACS Med Chem Lett* 3:509–514.
33. Saha RP, Bahadur RP, Pal A, Mandal S, Chakrabarti P (2006) ProFace: a server for the analysis of the physicochemical features of protein-protein interfaces. *BMC Struct Biol* 6:11.
34. Krissinel E, Henrick K (2007) Inference of macromolecular assemblies from crystalline state. *J Mol Biol* 372:774–797.
35. Schneidman-Duhovny D, Hammel M, Sali A (2010) FoXS: a web server for rapid computation and fitting of SAXS profiles. *Nucleic Acids Res* 38:Suppl:W540–544.
36. Volkov V, Svergun D (2003) Uniqueness of ab initio shape determination in small-angle scattering. *J Appl Crystallogr* 36:860–864.
37. Wriggers W, Milligan RA, McCammon JA (1999) Situs: a package for docking crystal structures into low-resolution maps from electron microscopy. *J Struct Biol* 125:185–195.
38. Campeau E, Gravel RA (2001) Expression in *Escherichia coli* of N- and C-terminally deleted human holocarboxylase synthetase. Influence of the N-terminus on biotinylation and identification of a minimum functional protein. *J Biol Chem* 276:12310–12316.
39. Otsuka A, Abelson J (1978) The regulatory region of the biotin operon in *Escherichia coli*. *Nature* 276:689–694.
40. Adikaram PR, Beckett D (2012) Functional versatility of a single protein surface in two protein:protein interactions. *J Mol Biol* 419:223–233.
41. Bagautdinov B, Matsuura Y, Bagautdinova S, Kunishima N (2008) Protein biotinylation visualized by a complex structure of biotin protein ligase with a substrate. *J Biol Chem* 283:14739–14750.
42. Pendini NR, Polyak SW, Booker GW, Wallace JC, Wilce MC (2008) Purification, crystallization and preliminary crystallographic analysis of biotin protein ligase from *Staphylococcus aureus*. *Acta Crystallogr Sect F Struct Biol Cryst Commun* 64:520–523.
43. Chapman-Smith A, Turner DL, Cronan JE, Morris TW, Wallace JC (1994) Expression, biotinylation and purification of a biotin-domain peptide from the biotin carboxy carrier protein of *Escherichia coli* acetyl-CoA carboxylase. *Biochem J* 302:881–887.
44. Leslie AG (1999) Integration of macromolecular diffraction data. *Acta Crystallogr D Biol Crystallogr* 55:1696–1702.
45. (1994) The CCP4 suite: programs for protein crystallography. *Acta Crystallogr D Biol Crystallogr* 50:760–763.
46. Lopez G, Valencia A, Tress ML (2007) Firestar—prediction of functionally important residues using structural templates and alignment reliability. *Nucleic Acids Res* 35:W573–577.
47. Murshudov GN, Vagin AA, Dodson EJ (1997) Refinement of macromolecular structures by the maximum-likelihood method. *Acta Crystallogr D Biol Crystallogr* 53:240–255.
48. Lovell SC, Davis IW, Arendall WB, 3rd, de Bakker PI, Word JM, Prisant MG, Richardson JS, Richardson DC (2003) Structure validation by C α geometry: phi, psi and C β deviation. *Proteins* 50:437–450.
49. Adams PD, Afonine PV, Bunkoczi G, Chen VB, Davis IW, Echols N, Headd JJ, Hung LW, Kapral GJ, Grosse-Kunstleve RW, McCoy AJ, Moriarty NW, Oeffner R, Read RJ, Richardson DC, Richardson JS, Terwilliger TC, Zwart PH (2010) PHENIX: a comprehensive Python-based system for macromolecular structure solution. *Acta Crystallogr D Biol Crystallogr* 66:213–221.
50. Konarev P, Volkov V, AV S, Koch M, Svergun D. PRIMUS: a windows PC-based system for small-angle scattering data analysis. *J Appl Cryst* 36:1277–1282.
51. Franke D, Svergun DI. DAMMIF, a program for rapid ab-initio shape determination in small-angle scattering. *J Appl Cryst* 42:342–346.
52. The PyMOL Molecular graphics system (2002) (Version 1.5.0.2 Schrödinger, LLC.).
53. Gouet P, Robert X, Courcelle E (2003) ESPript/ENDscript: extracting and rendering sequence and 3D information from atomic structures of proteins. *Nucleic Acids Res* 31:3320–3323.
54. Humphrey W, Dalke A, Schulten K (1996) VMD—visual molecular dynamics. *J Mol Graph* 14:33–38.

SUPPLEMENTARY METHODS

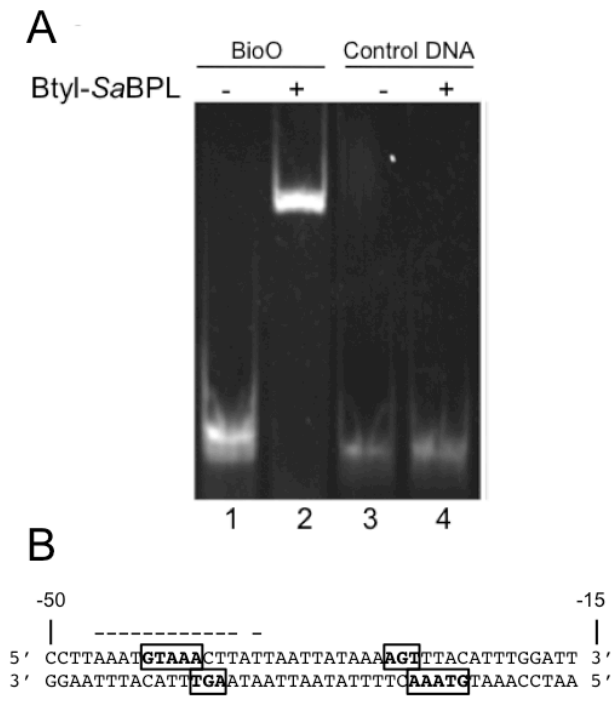
DNA binding interactions determined by EMSA - EMSA was used to measure the affinity of Btyl-SaBPL for the *Sa-bioO* DNA sequence and an unrelated DNA sequence control, pre-labeled with a 3' digoxigenin-11-ddUTP tag, using a DIG Gels Shift Kit (Roche Applied Science) according to manufacturers instructions. DNA:protein complexes were produced by incubating *Sa-bioO* (or control) with holo-SaBPL (concentrations encompassing 100 fold higher or lower than the predicted K_D) in the presence of 10 x molar excess ATP and biotin, in 50 mM Tris-HCl pH 7.0, 50 mM NaCl, 10 mM MgCl₂, and 5% glycerol, at room temperature for an hour. A TBE/10% acrylamide gel was loaded with and run for 20 minutes at 200 V, and scanned on an Alphaimager (Alpha Innotech). Quantitation of bands was carried out with IMAGEJ (<http://rsb.info.nih.gov/ij/>). The percentage of free DNA in each lane was determined by comparing the intensity of the band with the intensity of the band in the no-protein control lane.

Modelling of the SaBPL/Biotin Biosynthetic Operon and the SaBPL/BCCP complex - The region of the *bioO* repressor bound by SaBPL was delineated bioinformatically by Rodionov¹. Extension of this sequence allows for an imperfect inverted repeat: 5'-CCTTAAATGTAACTTATTAATTATAAAAGTTTACATTTGGATT-3'. Coordinates for B-form DNA were produced using the program Maestro (Schrodinger, NY USA). The SaBPL/SaBCCP model was produced as follows: the coordinates of BPL/BCCP complex from *P. horikoshii* (PDB ID: 2EJG) were superposed onto the structure of SaBPL. The SaBCCP was extracted from the *S. aureus* pyruvate carboxylase structure [PDB ID: 3BG5²], residues 1090-1170, and superposed on the BCCP domain. The program SITUS³ was used to assist in modelling the SaBPL/*Sa-bioO* complexes using the SAXS data. Briefly, the coordinates of *Sa-bioO* were fitted into the *ab initio* SAXS shape of the complex, then a

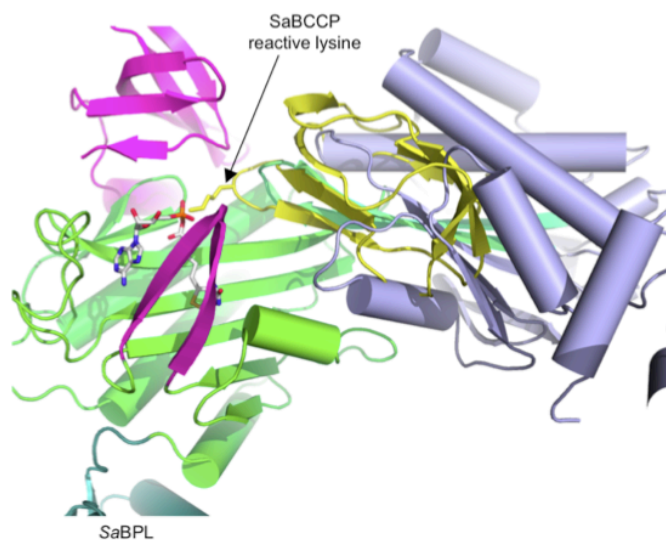
calculated envelope from the fitted *Sa-bioO* was subtracted away from the *ab initio* shape. The dimeric *SaBPL* coordinates were then fitted into the remaining envelope to produce the final complex.



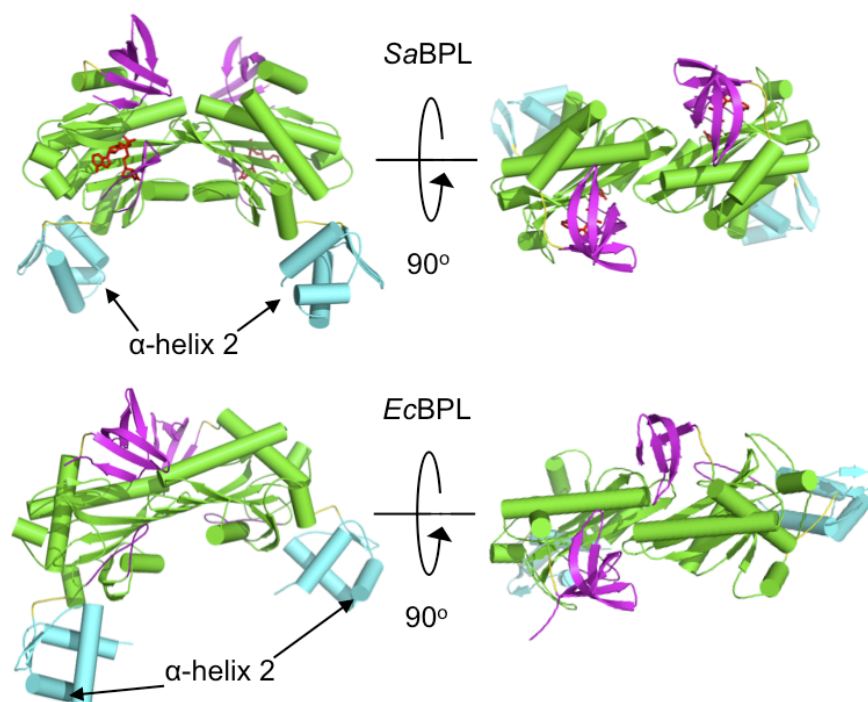
Supplementary Figure 1. Comparison of apo (monomeric) and holo (dimeric) *SaBPL*. The cartoon representation of the dimer is coloured according to the similarity of the apo and holo *SaBPL* structures. Blue indicates that the structures are similar ie. the RMSD C α atoms is less 2 Å. The colour is ramped through to red where the RMSD C α is greater than 4 Å.



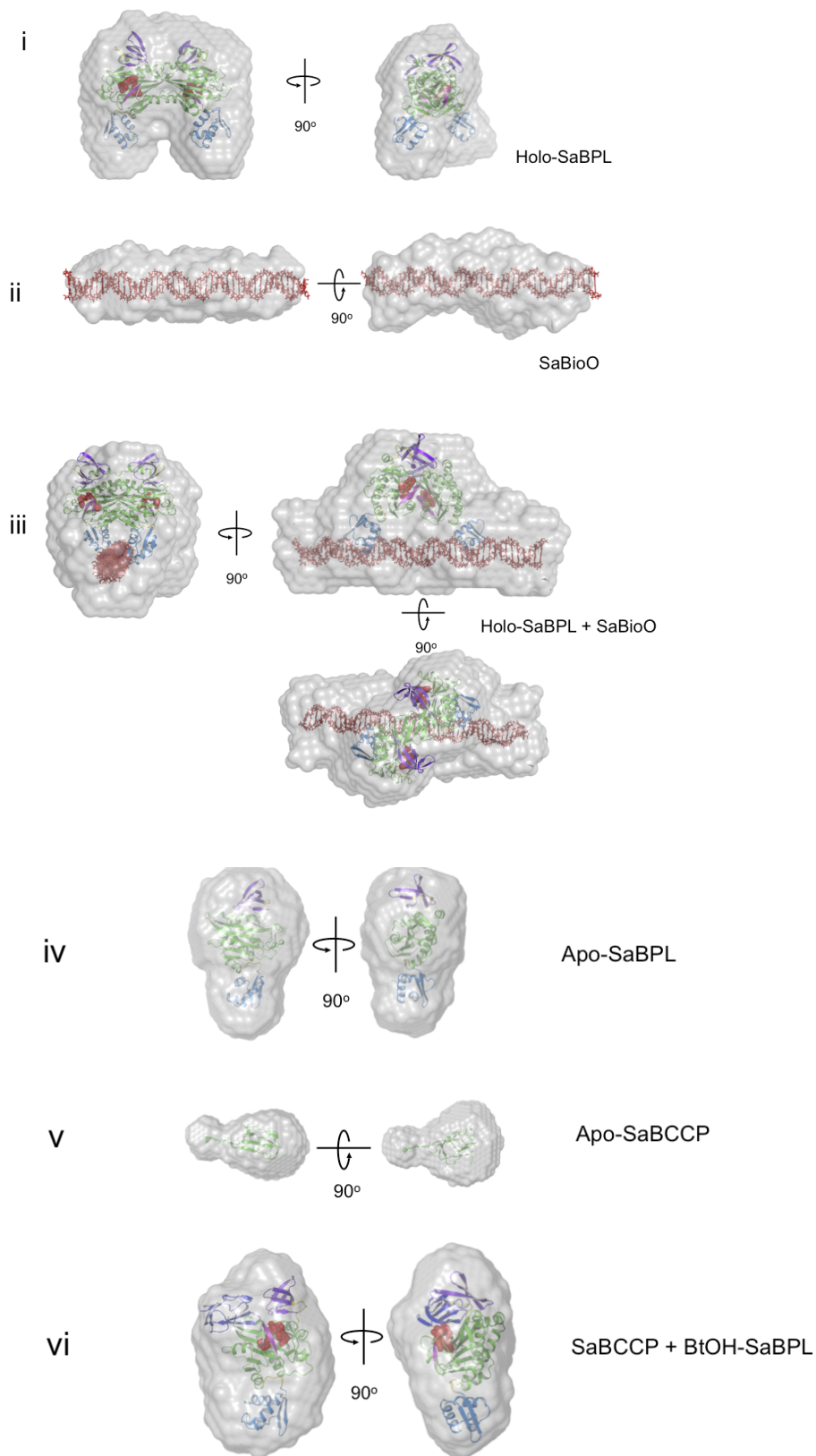
Supplementary Figure 2. Interaction of holo-SaBPL with the *S. aureus bioO* (*Sa-bioO*) DNA sequence. A) Electrophoretic mobility shift assay (EMSA) demonstrating that holo-SaBPL binds to the *Sa-bioO* DNA sequence but not to an unrelated dsDNA sequence. Lane 1: 0 μ M Btyl-SaBPL+ 0.29 μ M *Sa-bioO*; Lane 2: 0.29 μ M Btyl-SaBPL+ 0.29 μ M *Sa-bioO*; Lane 3: 0 μ M Btyl-SaBPL+ 0.292 μ M control non specific DNA; Lane 5: 0.29 μ M Btyl-SaBPL + 0.292 μ M control DNA. B) The region of the *Staphylococcus aureus* genome identified as *Sa-bioO*. Dashes are used to indicate the regions of the sequence that represent an inverted repeat and the bolded/boxed bases are the predicted regions of the sequence recognised by SaBPL.



Supplementary Figure 3. Model of the *Sa*BPL/BCCP complex. Cartoon representation of the *Sa*BCCP structure (PDB ID: 3BG5; coloured in yellow) positioned against one monomer of the *Sa*BPL dimer by analogy to the BPL/BCCP complex from *P. horikoshii* (PDB ID: 2EJG). This required that the C-terminal cap (coloured light pink) be slightly repositioned to avoid clashes. BCCP interacts at the BPL homodimer interface, as seen from its overlap with the second *Sa*BPL monomer (purple). Its reactive site lysine is positioned just above the BBL (dark pink) at the reactive site where biotin is transferred.



Supplementary Figure 4. Comparison of *SaBPL* dimer with *EcBPL*. *SaBPL* (top) and *EcBPL* (bottom: PDB ID: 1HXD) dimer structures are shown in cartoon representation. The *SaBPL* dimer interface differs from that of *EcBPL* resulting in a different angle of interaction of the catalytic domains (coloured green). Resultantly, the DNA binding domains (coloured light blue) are positioned differently in each model such that the α -helix 2 that binds at the major groove of target dsDNA are juxtaposed quite differently in the two models.



Supplementary Figure 5. SAXS analysis of apo- and holo-SaBPL, SaBPL/DNA and SaBPL/BCCP.) *Ab initio* reconstruction of the six samples overlaid with models derived from crystallographic structural data and modelling.

Note: Roman numeral labels are consistent with Figure 3.

REFERENCES

1. Rodionov DA, Mironov AA, Gelfand MS (2002) Conservation of the biotin regulon and the BirA regulatory signal in Eubacteria and Archaea. *Genome Res* **12**:1507-1516.
2. Xiang S, Tong L (2008) Crystal structures of human and *Staphylococcus aureus* pyruvate carboxylase and molecular insights into the carboxyltransfer reaction. *Nat Struct Mol Biol* **15**:295-302.
3. Wriggers W (2010) Using Situs for the integration of multi-resolution structures. *Biophys Rev* **2**:21-27.

6.2. Results

6.2.1. DNA-binding studies

6.2.1.1. Formation of the SaBPL-BioO complex

The biotin operon operator sequence (*bioO*) from the *S. aureus* genome was previously predicted to be the target of SaBPL in a bioinformatic study by Rodionov *et al* (Rodionov *et al.*, 2002). Based on these results, we identified a 44-bp sequence (*SaBioO*) that contained an imperfect inverted repeat for further EMSA studies (**Figure 6.1**).

```

5' - CCTTAAATGTAACTTATTAATTATAAAAGTTTACATTTGGATT - 3'
3' - GGAATTTACATTGAATAATTAATATTTTCAATGTAAACCTAA - 5'

```

Figure 6.1 The 44-mer *SaBioO* operon. The highlighted residues in red are the binding sites for the DNA-binding domain.

We have previously determined that holo SaBPL binds to the 44-mer *bioO* (Pendini *et al.*, 2013), and unexpectedly, apo SaBPL was also able to bind to the same sequence (**Figure 6.2A**). Two 22-mer sequences each containing one of the binding sites (HS1 and HS2) were also designed to determine if SaBPL requires both binding sites to be present. **Figure 6.2B** shows that the presence of both binding sites in *bioO* are needed for SaBPL to bind.

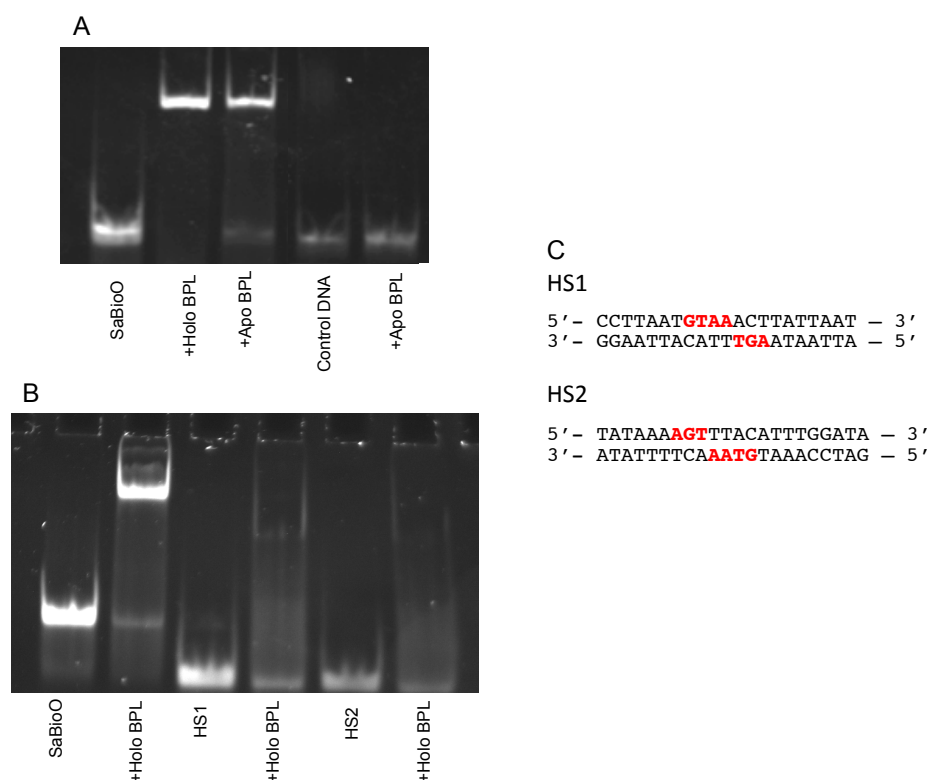


Figure 6.2 (A) EMSA was used to determine apo and holo SaBPL binding to *bioO*. Both forms of SaBPL can bind to the target DNA as indicated by the shift of the *bioO* band. (B) SaBPL requires both binding

sites to be present in the *bioO* sequence, as indicated by the lack of a band shift in the lanes containing HS1 and HS2. (C) the sequences of HS1 and HS2.

6.2.1.2. Binding affinity studies

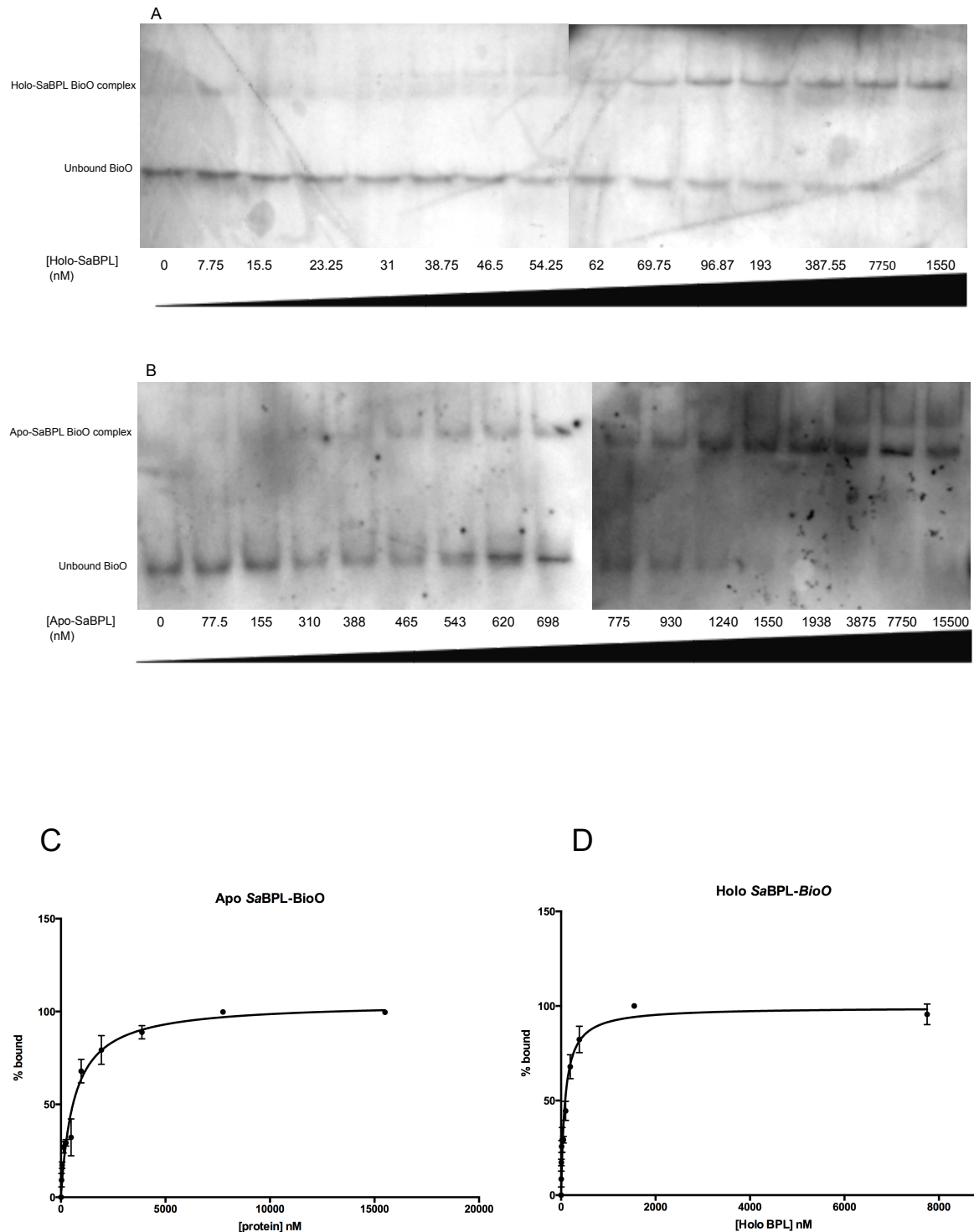


Figure 6.3. (A and B) DIG-labelled *bioO* EMSA of apo and holo SaBPL used to calculate the binding affinity of SaBPL for *bioO*. (C and D) Binding curves calculated from the percentage of bound DNA against concentration of protein used. The binding affinity of Apo SaBPL for *bioO* is 630.8 ± 68.7 nM, which is 10 fold lower than that of holo SaBPL, at 84.9 ± 10.6 nM.

In order to determine the binding affinity of SaBPL for *bioO*, DIG-labelled *bioO* was used in EMSAs due to its relative ease and safety in labeling double stranded DNA. Previous studies done on the well characterized *E. coli* BirA show that the apo form of BirA binds with very low affinity to its target DNA sequence compared to the holo protein (Xu and Beckett, 1997), hence we were interested in seeing how well both apo and holo SaBPL bound to the *bioO* sequence. 15.5 nM DIG-labelled *bioO* was incubated with increasing concentrations of holo (0 – 1550 nM) and apo (0 – 15500 nM) SaBPL. The intensity of DIG-labeled *bioO* could be quantitated using ImageJ, binding affinity analysed using Michaelis-Menten statistic on Graphpad Prism. Holo SaBPL had a binding affinity of 84.9 ± 10.6 nM for the target *bioO*, whilst the binding affinity that apo SaBPL had for *bioO* was 7.4 fold less (630.8 ± 68.8 nM) (Figure 6.3).

6.2.2. SAXS analysis of SaBPL-bioO complex

A

		R_g (Guinier)	R_g (P(r))	Dmax	NSD	χ^2
Holo-SaBPL	●	30.4	30.6	90	0.89	0.9
Holo-SaBPL/BioO	●	46.2	46.3	150	1.5	1.1
Apo-SaBPL/BioO	●	44.5	44.4	145	0.81	0.6
BioO	●	38.3	38.7	135	0.65	1.8

B

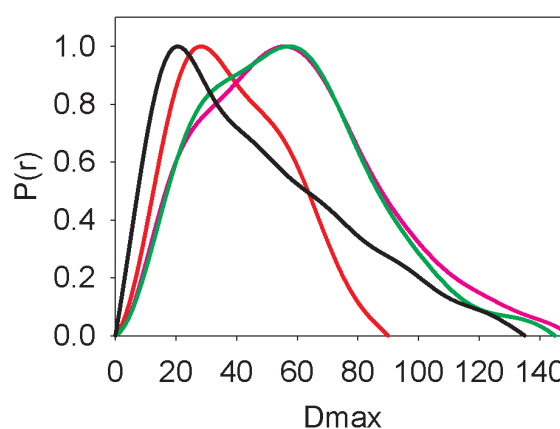


Figure 6.4 (A) Comparison of structural parameters calculated from SAXS data. R_g and D_{max} calculated from the models are provided in the paper by Pendini et al, 2013. (B) P(r) plot calculated from 4 different

SAXS experiments. In red: Holo-SaBPL, pink: Holo-SaBPL/*bioO*, green: Apo-SaBPL/*bioO* and black: *bioO* alone.

In order to verify the unexpected finding that apo SaBPL could bind to DNA in an EMSA assay, SAXS analysis was performed. **Figure 6.4A** shows the calculated results produced from 4 different SAXS experiment. The radius of gyration (R_g) and D_{max} calculated for both the apo and holo SaBPL-BioO complexes are similar, but greatly differ from that calculated from the scattering of holo-SaBPL or *bioO* alone. **Figure 6.4b** shows the different $P(r)$ produced from the SAXS experiment, which can give an indication of size and shape of a molecule. The $P(r)$ plot of holo SaBPL (in red) is a peak with a slight shoulder, and a short D_{max} , predicting a multimeric globular protein. *BioO* (in black) on the other hand, has a longer D_{max} , with multiple peaks, indicative of an elongated macromolecule. The SaBPL-*bioO* (pink and green) complexes on the other hand resemble an elongated macromolecule with multiple domains.

Ab initio SAXS structures of apo and holo SaBPL in complex with *bioO* are shown in **Figure 6.5**. The molecular coordinates of apo SaBPL in complex with *bioO* was created using the program SITUS as per the *ab initio* SAXS structure of holo SaBPL described by Pendini *et al* (Pendini et al., 2013). These *ab initio* models are in excellent agreement with the proposed model of the SaBPL binding DNA. Together these data are consistent with the EMSA findings showing that both apo and holo SaBPL can bind DNA.

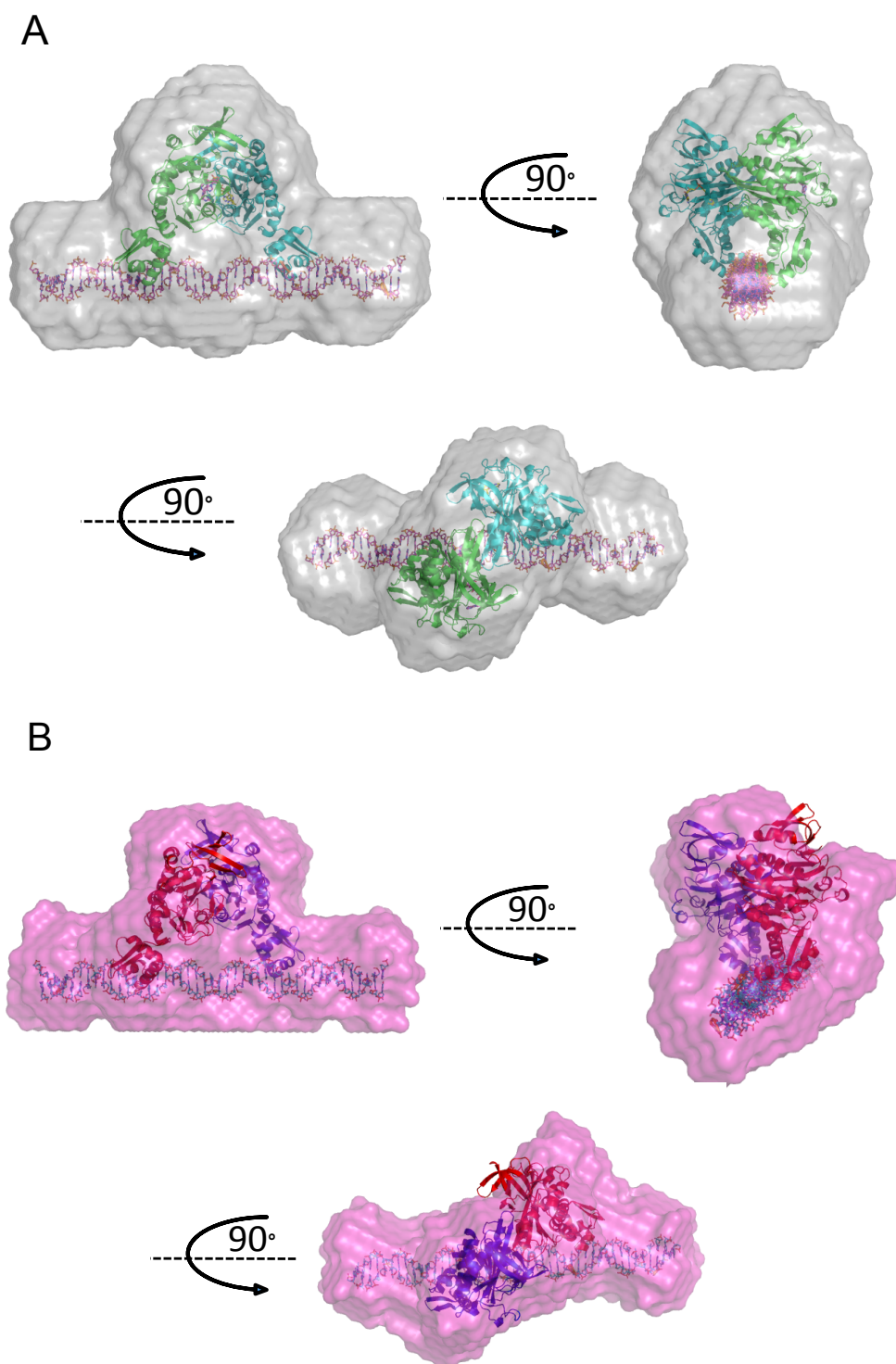


Figure 6.5 *Ab-initio* SAXS structures of (A) apo and (B) holo SaBPL in complex with bioO overlaid with models derived from crystallographic structural data and modeling.

6.2.3. Crystallization studies

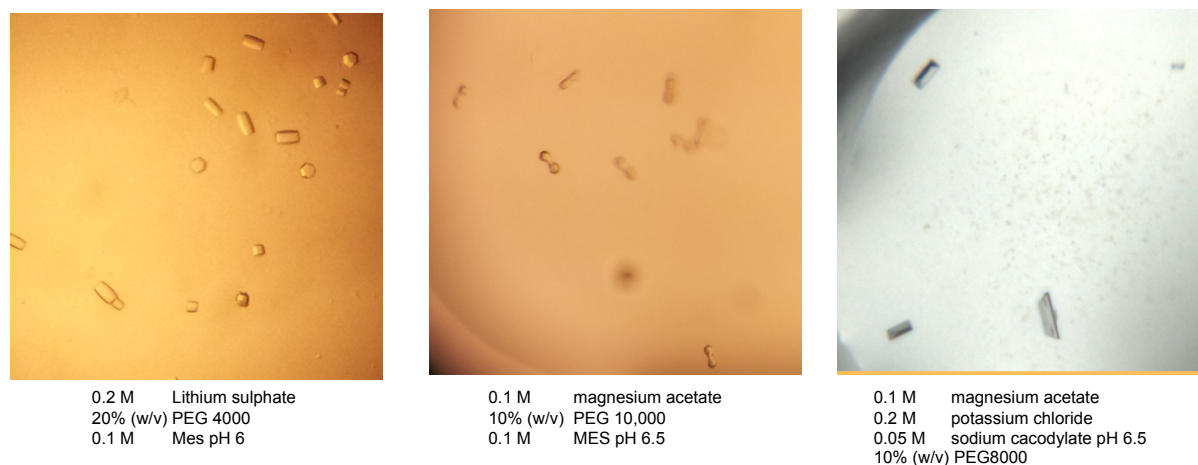


Figure 6.6 SaBPL + 44-mer *bioO* crystals.

To date, the crystal structure of a class II BPL complex with DNA has not been reported. Given the stability of the SaBPL dimer, it was decided to attempt crystallization of this enzyme in complex with the *bioO* sequence. After trialing hundreds of conditions from commercially available kits from Sigma, Hampton and Qiagen, only 3 conditions produced crystals, as listed in **Figure 6.6**. Further fine screening was performed by varying buffer pH, precipitant concentration and salt concentration to obtain crystals more suitable for X-ray diffraction experiments, however crystals that were grown using the 44-mer *bioO* had either weak or no diffraction. As the 44-mer *bioO* could potentially be preventing stable crystal contacts from forming due to its length, and hence the poor diffraction, shorter pieces of DNA were used instead to try to create crystals that were more stable. Either a single base pair or two base pairs were removed from both ends of the 44-mer to create a 42-mer and 40-mer *bioO*. After confirming that these sequences bound to SaBPL (**Figure 6.7**), broad screens of the 42-mer or 40-mer in complex with SaBPL was set up in the same method as the full length SaBPL-*bioO* complex. This proved to be unsuccessful, and hence other methods were trialed.

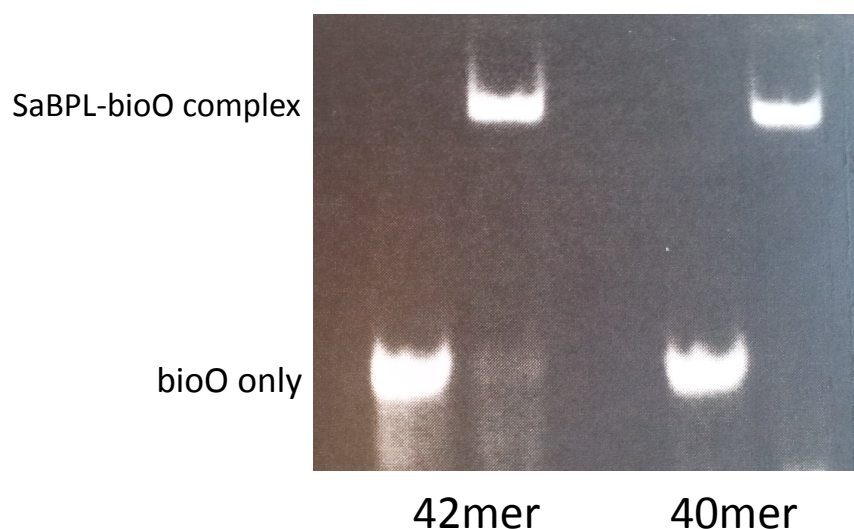


Figure 6.7 Holo SaBPL is able to bind to the 42-mer and 40-mer *bioO*

A different *bioO* sequence was then created so that there was a complementary overhang on either side of the DNA sequence (**Figure 6.8A**). This was again designed with creating more stable crystal contacts in mind. DNA probes containing the complementary overhangs were designed to promote concatamerisation, thereby potentially limiting the movement of the long DNA sequence, and promoting a crystal with stable crystal contacts to form. After confirming that the sequences containing overhangs could bind to SaBPL using EMSA (**Figure 6.8B**), the complex formed between the overhang *bioO* and SaBPL underwent crystallization trials. Again, several hundreds of conditions from commercially available crystallization kits from Sigma, Hampton and Qiagen were trialed, but only 2 conditions produced crystals, as listed in **Figure 6.6**. Fine screens of these two conditions were performed by varying buffer pH, salt concentration and precipitant concentration but crystals that formed had either weak or no diffraction (**Figure 6.9**).

A

BioO Overhang 1:

5' – CCTTAAT**GTAA**ACTTATTAATTATAAA**AGT**TTACATTTGGAT –3'
 3' – GAATTACATT**TGA**ATAATTAATATTTTCA**AATG**TAAACCTAG – 5'

BioO Overhang 2:

5' – CCTTAAT**GTAA**ACTTATTAATTATAAA**AGT**TTACATTTGGAT –3'
 3' – AATTACATT**TGA**ATAATTAATATTTTCA**AATG**TAAACCTAGG – 5'

B

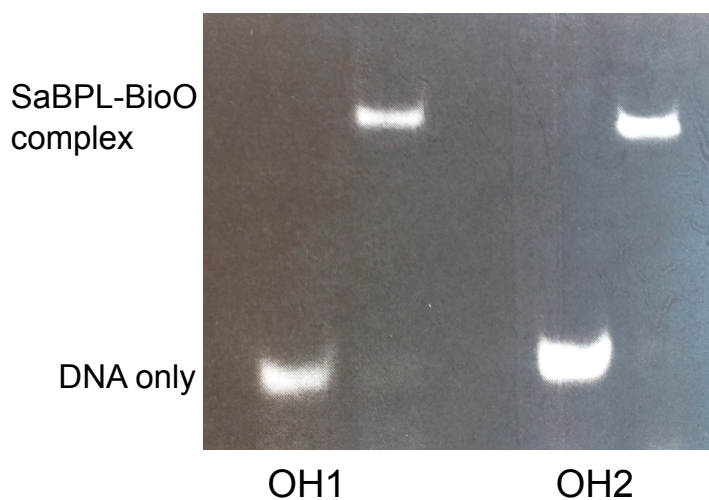


Figure 6.8 (A) *BioO* sequences with overhangs. Red residues indicate SaBPL binding sites. (B) EMSA showing that SaBPL can bind to the two overhang sequences.

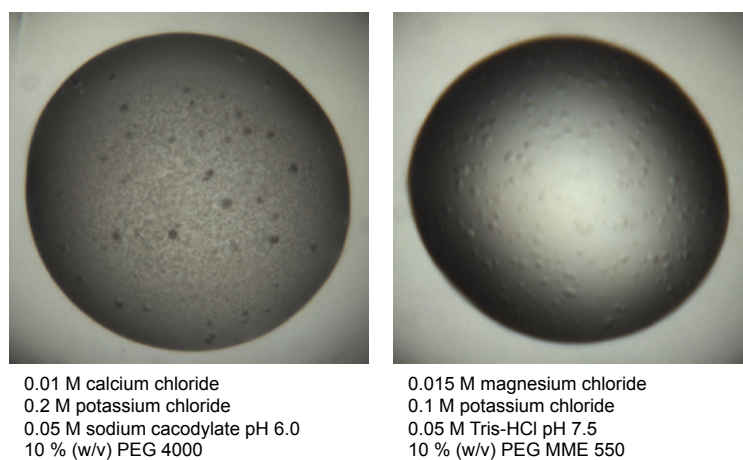


Figure 6.9 Crystals of SaBPL-*bioO* OH1 complex.

There are 7 extra nucleotide residues on either side of the two binding sites in *BioO* that could have high mobility after SaBPL binding to *bioO*, and could disrupt contacts between complex molecules from forming. Since these residues do not seem to play a role in binding to SaBPL, it was decided to remove them and try to crystallize this shorter construct (*BioO* 31-mer) in complex with SaBPL (**Figure 6.10A**). Removal of these extra residues had no effect on SaBPL binding (**Figure 6.10B**). Again, crystallization trials were performed, and although crystals formed in several different conditions, they were either too small despite attempts at refining the crystallization conditions, or had weak or no diffraction (**Figure 6.11**).

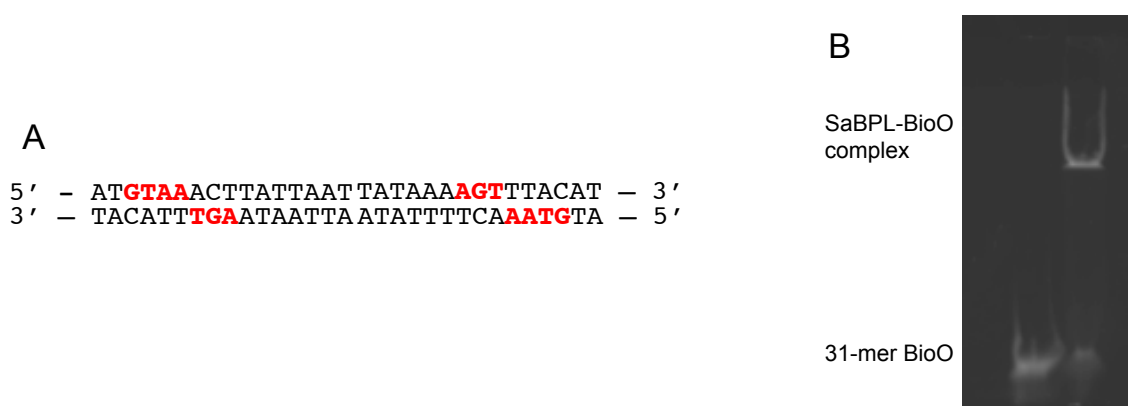


Figure 6.10 (A) *BioO* 31-mer (B) EMSA of 31-mer binding to SaBPL

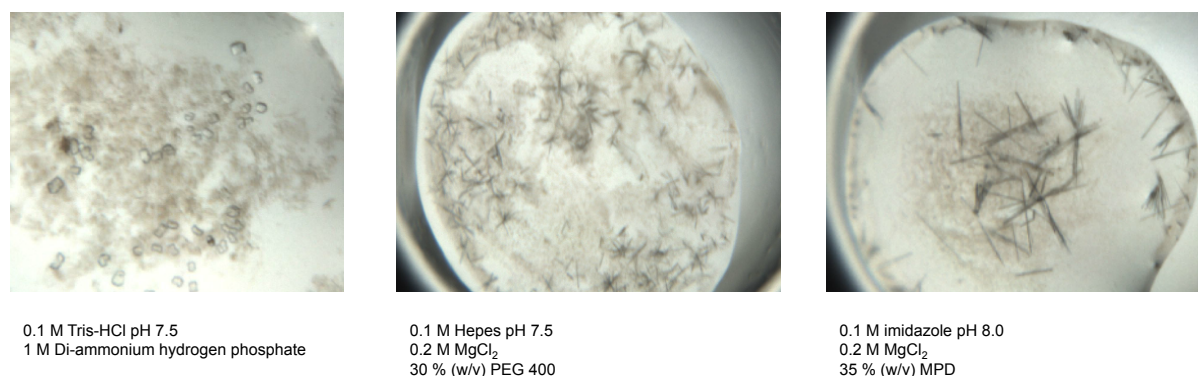


Figure 6.11 SaBPL-31mer complex crystals

6.3. Discussion

This chapter focuses on the dimerisation of SaBPL, and investigating its binding to the BioO operon using SAXS. Despite having structural similarity as the well characterized BirA, and participating in both the biotinylation of biotin-dependent carboxylases and the transcriptional repression of the *bioO* operon, both SaBPL and BirA have slight differences that are addressed in this chapter as well as through collaborative work done with researchers at the University of Adelaide.

Throughout this chapter, SAXS experiments were performed using purified recombinant protein. There are many excellent publications that go through the steps required for a successful SAXS experiment, however several problems regarding our SAXS experiment were encountered. Successful solvent subtraction could only be done by intense dialysis of the protein into the experimental buffer. As we initially encountered problems with protein aggregation appearing in the scattering data so dynamic light scattering was done on the sample prior to the experiment in order to determine monodispersity. Scattering from aggregation was further prevented by connecting a size exclusion chromatography column to the SAXS instrument and only collecting data from the expected peak.

Similar to BirA, crystallographic and kinetic experiments show SaBPL undergoes a monomer to dimer transition upon biotinyl-5'-AMP binding. SaBPL was initially purified as a biotinyl-5'-AMP bound homodimer, unlike BirA that was purified in its monomeric apo form. Analytical ultracentrifugation experiments (AUC) performed by our collaborators show that at micromolar concentrations, apo-SaBPL exists in equilibrium between its monomeric and dimeric states (Dr. Tatiana Soares da Costa, The University of Adelaide, unpublished data), with a K_D^{-1} of 29 μM in solution. This is in stark contrast to apo-BirA which is only dimeric in solution at millimolar concentrations (Streaker et al., 2002, Kwon et al., 2000, Zhao et al., 2009). Kinetic studies measuring the binding of BirA to its target BioO have shown that dimerisation of the protein precedes DNA binding (Streaker and Beckett, 2003), and that the affinity of apo or holo BirA has for *bioO* is dependent on how stable the dimer formed by the enzyme is (Streaker et al., 2002). As both the apo and holo forms of SaBPL can both form dimers at low concentrations, it is unsurprising to see that both enzymes can bind to BioO, with only a 7.4-fold difference in binding affinity. A SAXS experiment was done on both apo and holo SaBPL in complex with BioO using micromolar concentrations of protein. Similar P® plots could be calculated from the scattering data gathered from both the complexes, and *ab initio* models produced were identical as well, further supporting previous results: apo

SaBPL can form a dimer at micromolar concentrations, and bind to BioO. Our collaborators have identified a key phenylalanine amino acid (F123) in the dimerisation interface that forms a hydrophobic contact with the side chain of an aspartate residue at position 200 (D200) in the opposite SaBPL subunit (**Figure 6.12**). Of interest, the same residue in BirA is an arginine (R119), and when R119 was mutated to a phenylalanine, the apo-R119 F BirA mutant primarily formed a dimer when analysed using SEC-MALLs (Dr. Tatiana Soares da Costa, The University of Adelaide, unpublished data)

Class II BPLs are required for both biotinylation of biotin-dependent carboxylases and transcriptional repression of biotin biosynthetic genes. Regulation of these two roles in *E. coli* is fairly straightforward: *E. coli* bacteria only possess a single acetyl CoA carboxylase which is biotinylated, and a single BioO operon that requires transcriptional regulation. *S. aureus* on the other hand, needs to biotinylate both acetyl CoA carboxylase and pyruvate carboxylase, and has two different operons which are regulated by SaBPL (Rodionov et al., 2002), and presents a system which is more complex compared to that of *E. coli*. The ability of SaBPL to form a dimer and bind to the BioO operon irregardless of the absence or presence of ligand binding may allow for tighter control of gene expression, and potentially biotinylation of biotin-dependent carboxylases in *S. aureus* cells, and may allow the pathogen to quickly respond to any small changes in its surrounding environment.

The functions of the three domains of class II BPLs are not clear cut: removal of the DNA-binding domain not only obviously prevents transcriptional repression, but also affects the ability of the enzyme to synthesis biotinyl-5'-AMP despite being located away from the catalytic active site (Xu and Beckett, 1996), and mutations which are located away from the active site as well as the dimerisation interface can interfere with DNA binding (Chakravartty and Cronan, 2012). It is expected the formation of a class II BPL/BioO complex would result in significant structural changes of not just the DNA-binding domain, but that of the catalytic and cap domain as well. To date, there have been no reported crystallographic structures of a class II BPL in complex with its target DNA. Multiple attempts at trying to produce a crystal of the SaBPL-BioO complex have proved to be unsuccessful so far. The solubility and stability of the complex is unlikely to be an issue in this case, but the length of the DNA used for creating the complex potentially prevents stable crystal contacts from forming. Despite removing the unnecessary nucleotides at either end of the binding sites, there are still 16 nucleotides located between the binding sites that are unbound, and could be relatively flexible compared to the rest of the complex, preventing successful crystallization to occur.

The identification of superepressor BirA mutants that bind to BioO with a stronger affinity than the wild type enzyme may increase the potential of obtaining a crystal structure of the protein-DNA complex (Chakravartty and Cronan, 2012).

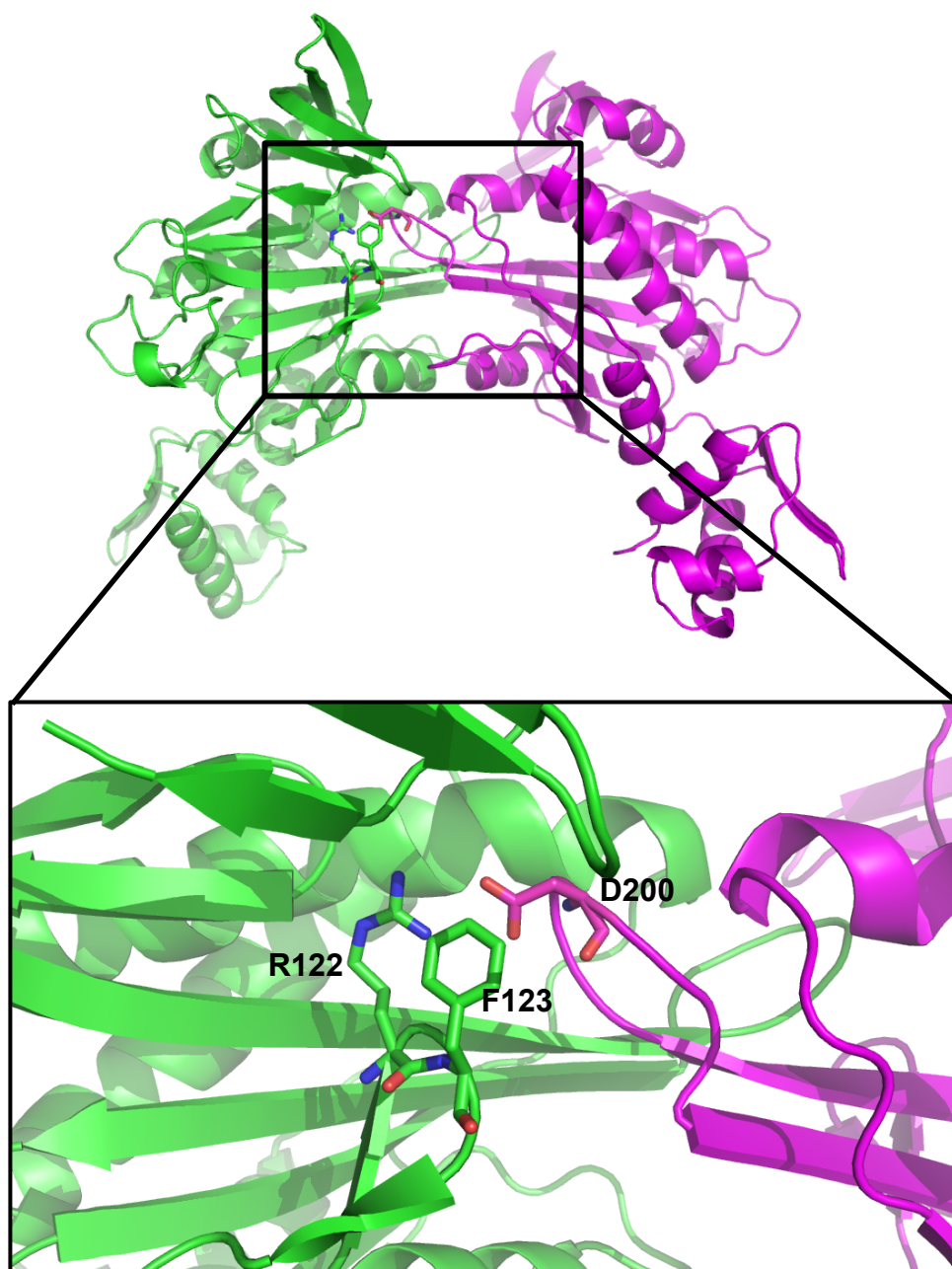


Figure 6.12 Dimeric structure of SaBPL. R122 and F123 of one subunit (green) can form contacts with D200 of the opposite subunit (magenta).

Chapter 7 Eukaryotic Biotin Protein Ligase

7.1. Introduction

Unlike bacterial BPL, of which there are several well characterized structures, there has been relatively little research investigating their eukaryotic counterparts. To date there are no known structures of any class III eukaryotic BPLs. Whilst all BPLs catalyse the same conserved biotinylation reaction, there are striking differences between the eukaryotic and prokaryotic homologues. Class I and class II BPLs generally range between 25 to 37 kDa in molecular weight. However, eukaryotic BPLs are larger; the full length human BPL (holocarboxylase synthetase, HCS) has molecular weight of 81 kDa, whilst the fungal BPLs from *Saccharomyces cerevisiae* (ScBPL) and *Candida albicans* (CaBPL) are 76.4 kDa and 73 kDa respectively (Leon-Del-Rio et al., 1995, Cronan and Wallace, 1995, Pendini et al., 2008a).

Eukaryotic BPL catalyse the same conserved biotinylation reaction as their bacterial counterparts, despite this, there are some important differences. First, many bacteria have the ability to synthesise their own biotin whereas eukaryotes are biotin auxotrophs, this means that higher order organisms such as yeast and humans need to control the use of biotin. Secondly, bacteria generally possess between 1-3 biotin requiring enzymes, whereas yeast and mammals must biotinylate a larger number of enzymes. There are 5 biotin-dependent enzymes which are found in humans, namely acetyl-CoA carboxylase-1 and 2 (ACC-1 and ACC-2), pyruvate carboxylase (PC), propionyl CoA carboxylase (PCC) and 3-methylcrotonyl CoA carboxylase (MCC), and each play important roles in fatty acid synthesis, amino acid catabolism and gluconeogenesis (Wolf, 1995, Brownsey et al., 2006, Thampy, 1989, Jitrapakdee and Wallace, 1999, Deodato et al., 2006, Baumgartner and Suormala, 1997). Up to six biotin-dependent enzymes are found in the yeast *Saccharomyces cerevisiae*: two isoforms of ACC, two isoforms of PC, urea amidolyase and the tRNA binding protein Arc1p (Hoja et al., 1998). Like *S. cerevisiae*, *Candida albicans* also contains urea amidolyase and Arc1p, but only contains a single PC and ACC (Pendini et al., 2008a). Thus, eukaryotic BPLs need a greater level of control so that exogenous biotin is used wisely.

Eukaryotic BPLs contain the same C-terminal cap domain and central catalytic domain that is found in bacterial BPL (*E. coli* BirA and HCS have 40 % sequence similarity in this region), but have an N-terminal domain which is largely unstructured, with several sites sensitive to proteolytic cleavage (Polyak et al., 1999, Mayende et al., 2012). Unlike class II BPLs,

eukaryotic BPLs do not form a homodimer, and the N-terminal domain of eukaryotic BPLs does not contain any known DNA-binding motifs, hence is unlikely to play a direct role in gene regulation. Limited proteolytic studies show that the ScBPL contains a 27 kDa N-terminal domain with a 50 kDa C-terminal region with a protease sensitive linker region connecting the two domains and it is thought that the juxtaposition of the domains change upon ligand binding within the active site (Polyak et al., 1999). In HCS, the first 159 amino acids of the N-terminal are sensitive to protease cleavage and highly unstructured, whilst residues 159 – 314 form a structured domain, and unlike ScBPL, the overall structure of HCS is not affected by ligand binding (Mayende et al., 2012). Like bacterial BPL, the C-terminal domain of eukaryotic BPLs participate in substrate recognition, whilst the catalytic domain is involved in ligand binding and biotinylation of the substrate protein (Hassan et al., 2009).

Although the N-terminal domain of human and yeast BPL contain some sequence similarity (24.9 % similarity between the N-terminal domain of HCS and CaBPL) (Cronan and Wallace, 1995), not much is known about the function of this domain. Unlike the class II bacterial BPLs, this domain does not seem to contain sequences that bind to DNA, and hence is unlikely to be required for gene regulation. Heteronuclear single quantum coherence NMR (HSQC-NMR) studies done on the N-terminal domain of HCS suggest that it is mainly random coil with some α -helical structure (Lee et al., 2010). Removal of the amino acids 1 – 159 of the N-terminus results in a HCS with reduced enzymatic activity, but could be fully reactivated by the re-addition of a protein consisting of residues 1- 159 (Lee et al., 2010). Residues 159 – 314 of the N-terminus form a structured domain, and mutations in this region reduce the affinity of HCS for BCCP (Mayende et al., 2012). Complementation assays done in *E. coli* using N-terminal deletion constructs of HCS showed that the various constructs had different abilities to biotinylate BCCP, suggesting that the N-terminal is required for biotin transfer (Campeau and Gravel, 2001). A yeast-2-hybrid assay also showed that the N-terminus was able to interact with BCCP, albeit with a weaker interaction compared to the catalytic C-terminal (Hassan et al., 2009). HCS mutations found in patients with MCD provided further evidence that the N-terminal domain is functionally important. Whilst mutations in the catalytic domain lead to a low K_M mutant that has decreased affinity for biotin but can be easily treated by biotin supplementations in patients with N-terminal mutations, Mayende *et al.* created several HCS variants that had mutations in the N-terminal that severely reduced enzyme activity. These mutant enzymes formed an unstable complex with BCCP that resulted in the dissociation of BCCP from the mutant before biotinylation could occur (Mayende et al., 2012).

Unlike many bacterial BPL that biotinylate BCCPs from a range of organism, the human enzyme has very low affinity for non-eukaryotic BCCPs (Lin and Cronan, 2011). This selectivity that HCS has may have arisen as to it has biotinylated 5 different carboxylases, and hence requires a method of controlling the biotinylation of multiple substrates. One mechanism by which cells can control biotinylation of different BCCPs could arise due to the multiple isoforms of HCS. The three known isoforms of HCS are translated from one mRNA that contains three translation start codons, namely Met1, Met7 and Met58 producing proteins that are 86 kDa, 82 kDa and 76 kDa in size respectively (Hiratsuka et al., 1998). The initiation codons for both Met1 and Met7 are both located on exon 6 within the HCS gene. The mechanisms that regulate differential expression of Met1 and Met7 are still under investigation. Met58 is located on exon 7, and expression of this isoform is thought to arise from alternative splicing of mRNA (Yang et al., 2001). All three isoforms are located in the cytoplasm, but Met58 is also found in the nucleus, suggesting that this isoform can be transported between the cytoplasm and nucleus (Bailey et al., 2010).

To date, the structure of eukaryotic BPLs has not been elucidated. This chapter describes preliminary results aimed at structurally characterizing HCS.

7.2. Results

7.2.1. Purification of FL-HCS

Overexpression of full-length HCS (80kDa) produced high levels of His-tagged protein. Large scale over-expression of the full length protein was performed by growing 12 Lt culture induced with 0.5 mM IPTG at 25 °C. After cell lysis and loading the supernatant onto a 5 mL nickel resin column, full-length HCS was eluted with 50 mM, then 100 mM imidazole. However, only small amounts of soluble protein were obtained, with the majority of the protein located in the insoluble cell pellet (see lane 12) (**Figure 7.1**). As the N-terminal domain of HCS is largely unstructured, it was decided to clone, express and purify the shortest isoform of HCS, or Met58-HCS for further experiments.

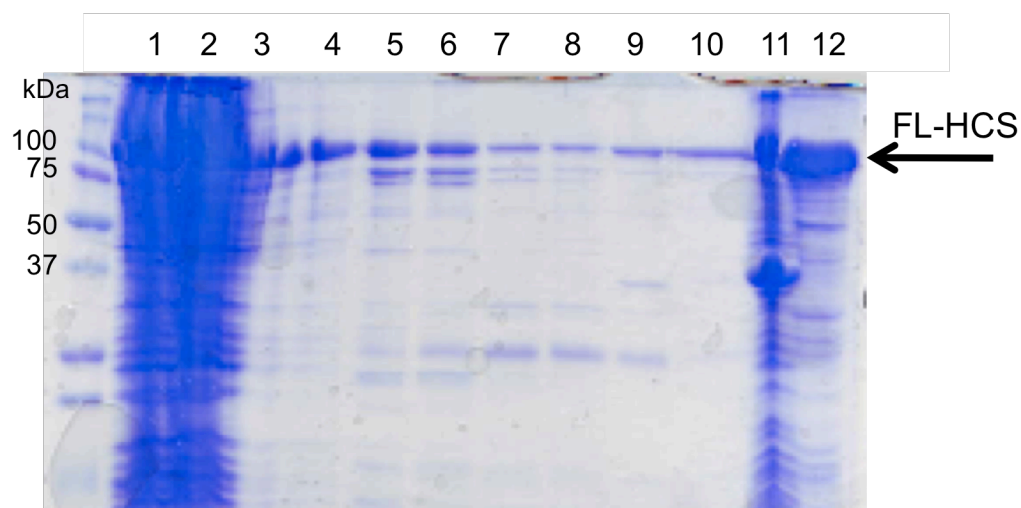


Figure 7.1 Nickel resin purification of FL-HCS. Lane 1: Load, 2: Flow through, 3: Wash, 4-6: 50 mM imidazole, 7-10: 100 mM imidazole, 11: nickel resin, 12: insoluble cell pellet. The arrow represents the expected size of full length HCS.

7.2.2.Expression and purification of Met58-HCS

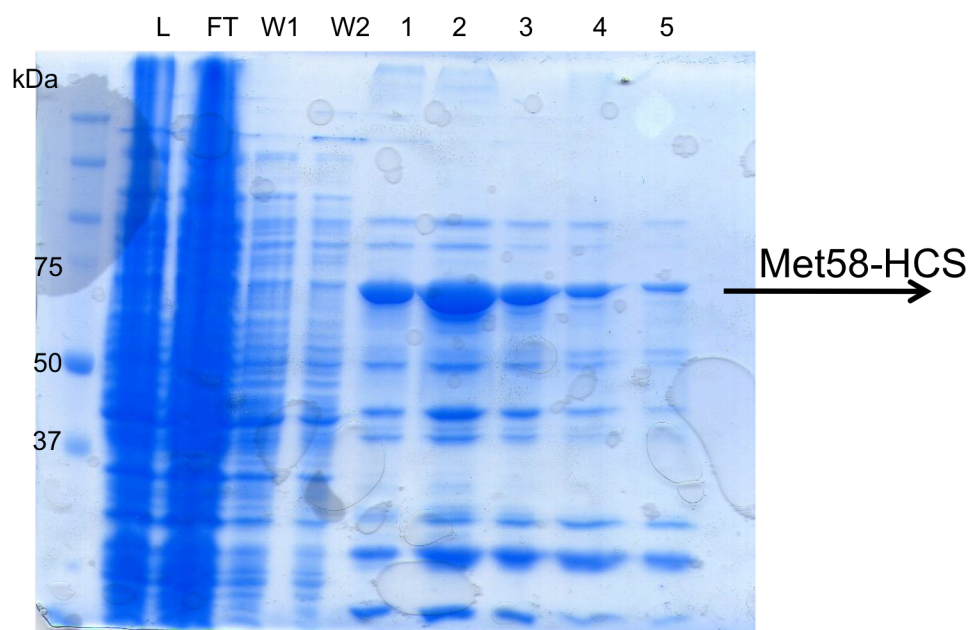


Figure 7.2 SDS-page analysis of Met58-HCS nickel purification. Lane L: Load, FT: Flow through, W1 and W2: Wash, 1-3: 50 mM imidazole, 4 - 5: 100 mM imidazole. The arrow represents the expected size of Met58-HCS

Met58-HCS was cloned into a pET15b His-Tag vector, and expressed in BL21 (DE3) plysS cells. Overexpression produced C-terminal His-tagged Met58-HCS that was first subjected to nickel-affinity chromatography. After binding to the nickel column and washing off the unbound protein with lysis buffer, Met58-HCS could be eluted off the column with 50 mM imidazole as analysed by SDS-PAGE (**Figure 7.2**). This also revealed that the samples

were not pure, thereby requiring another purification step. The eluted fractions were pulled and dialysed into SE buffer (Appendix II) for 3 hours, then overnight at 4 °C. Met58-HCS was further purified by loading onto a Q-sepharose anion exchange column using a gradient of 50 mM – 1 M NaCl over 5 column volumes (**Figure 7.3**). Further purification was done by size exclusion chromatography (**Figure 7.4**), and the final purified protein stored at – 80 °C.

Met58-HCS purified using size exclusion chromatography was not pure, and attempts at removing the smaller molecular weight contaminants were unsuccessful. Concentrating the protein to 2 mg/mL resulted in the protein precipitating out of solution. Diluted protein would also precipitate out of solution after several hours, even when stored on ice. In order to prevent this rapid precipitation, several changes were made during subsequent purification. First of all, 10 % glycerol was added to the lysis buffer prior to cell lysis. Tris-HCl at pH 7.5 in the SE buffer was replaced with either HEPES, pH 8.0 or MES, pH 6.5. The amount of NaCl in the SE buffer was also increased from 50 mM to 150 mM. However, these changes did not aid in preventing the precipitation of Met58-HCS. As high concentrations of protein were required for structural experiments, no further work was done using this protein due to time constraints, and it was decided to focus on the shorter catalytic domain instead.

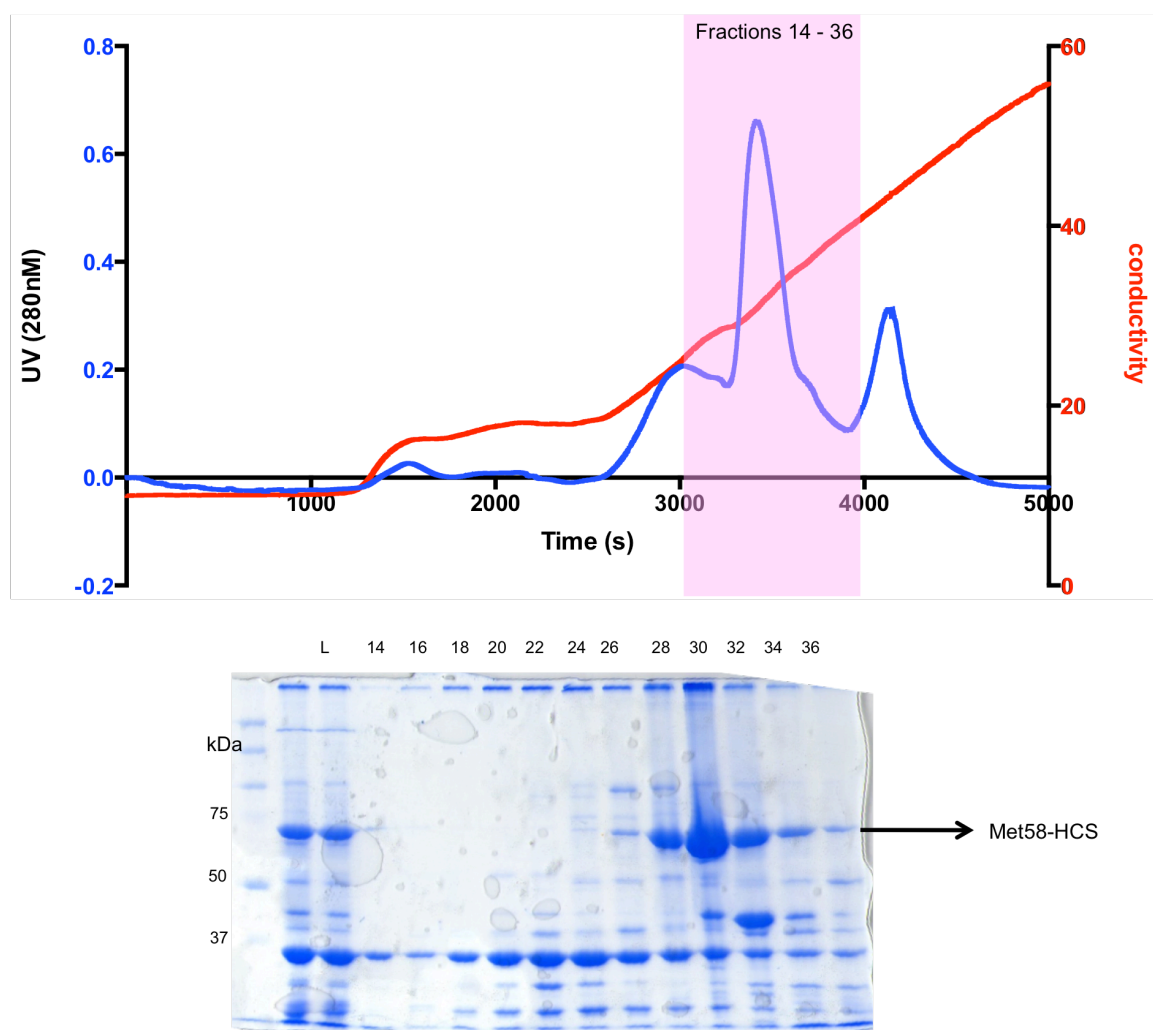


Figure 7.3 Met58-HCS anion exchange chromatography. Met58-HCS was eluted with 50 mM – 1M NaCl with a Q-sepharose column over 5 column volumes. The area shaded in pink on the chromatogram indicates the fractions analysed on a SDS-PAGE. The arrow on the SDS-PAGE indicates the expected molecular weight of Met58-HCS. Due to the presence of a large amount of contaminants present on the SDS-PAGE, a further step was required to purify the protein further.

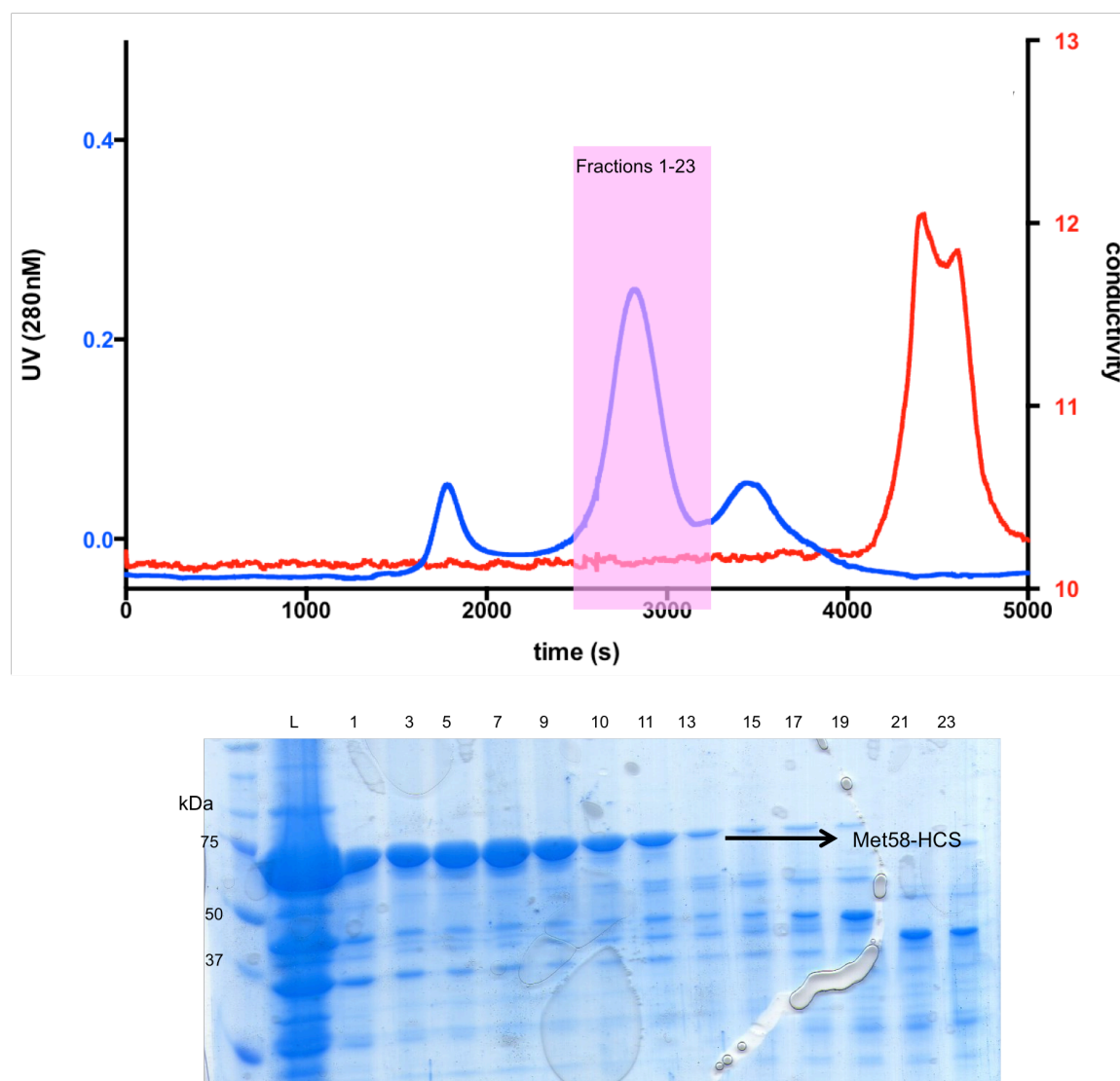


Figure 7.4 Met-58 HCS size exclusion chromatography. Fractions 1 – 23 which correspond to Met58-HCS (pink shaded area on chromatogram) were analysed on a SDS-PAGE. The low molecular weight contaminants could not be separated from Met58-HCS, and as the protein precipitated rapidly, no further work was done on Met58-HCS.

7.2.3.Expression and purification of CAT-GST

The catalytic domain of HCS was determined by aligning the full length HCS against *PhBPL* and *BirA*. It was determined via this sequence alignment that the catalytic domain of HCS used for cloning and expression should start from residue 459. After initially cloning the catalytic domain of HCS ranging from residues 459-717 (CAT) into a pET22b His-tag vector, and transforming into BL21 (DE3) *E. coli* cells, small scale over-expression trials showed that the His-tagged protein was insoluble. Hence it was decided to clone the same protein into a GST-vector with a thrombin cleavage site in order to aid in protein solubility. After cloning CAT into a pGex4t-2 vector (CAT-GST), the protein was transformed into BL21 (DE3) *E. coli* cells. Small scale over-expression trials of CAT-GST showed that this protein could be over-expressed at both 16 °C and 25 °C using 0.1 mM IPTG, 0.5 mM IPTG

and 1 mM IPTG (**Figure 7.5**). As all conditions produced similar levels of soluble protein, it was decided to produce the final protein by induction with 0.5 mM IPTG and growing at 16 °C for 18 hours.

However, when large-scale purification was attempted, the majority of sample was located in the insoluble pellet, and there was only a small amount of soluble protein located in the fractions eluted off the GST column with 10 mM reduced glutathione (**Figure 7.6**).

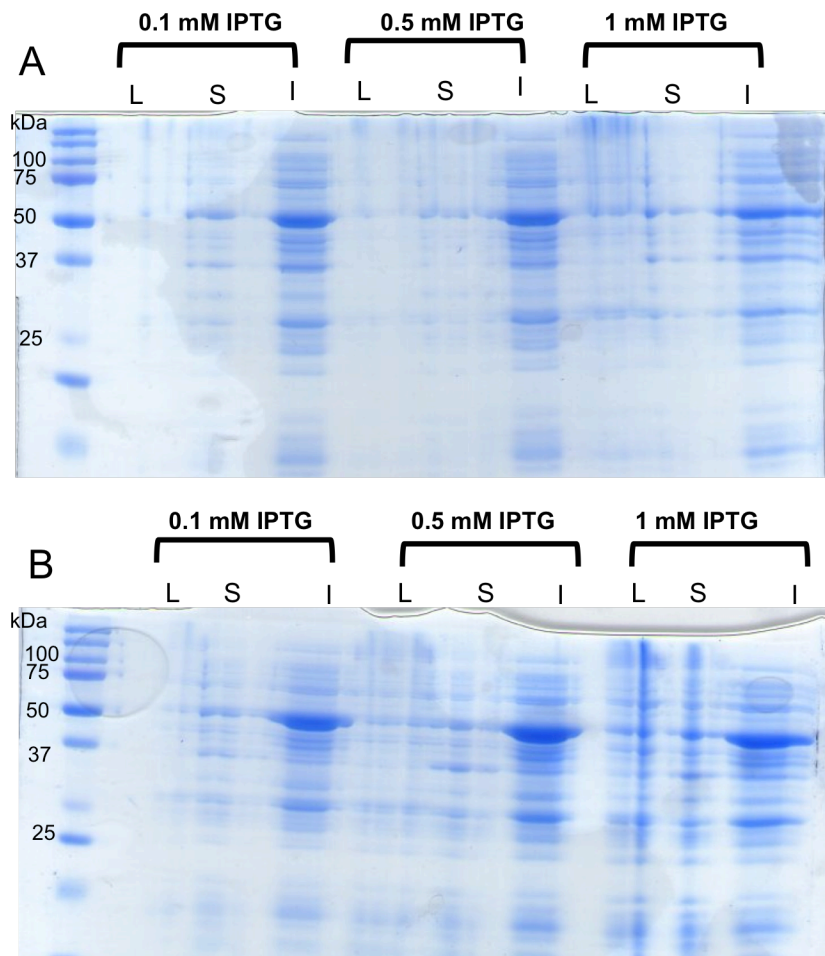


Figure 7.5 Small-scale over-expression of CAT-GST induced with 0.1 mM, 0.5 mM, and 1 mM IPTG at (A) 16°C and (B) 25°C. L: load, S: soluble protein, I: insoluble protein.

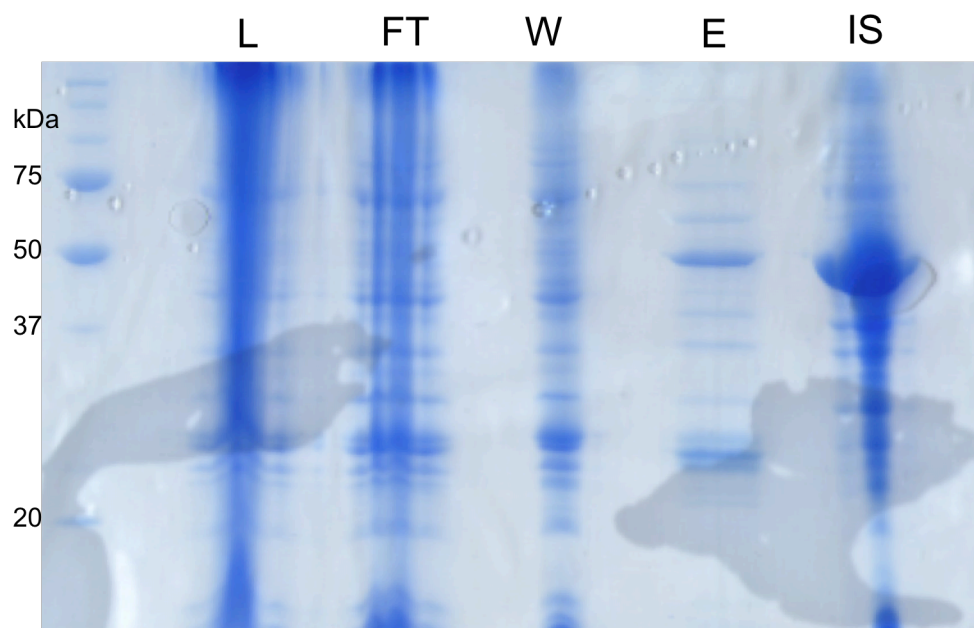


Figure 7.6 SDS-PAGE analysis of GST purification of Cat-GST. L: load, FT: flow-through, W: Wash, E: elution with 10 mM reduced glutathione, IS: insoluble

The plasmid containing cat-GST was then transformed into Rosetta 2 (DE3) competent *E. coli* cells as this strain was designed to increase the expression of the eukaryotic cat-GST by supplying tRNAs for several rare codons present in eukaryotic proteins, and potentially increasing the amount of soluble protein present. However, transformation of the CAT-GST pGEX-4t-2 plasmid into this cell line was not successful despite multiple attempts.

7.3. Discussion

In this chapter we have attempted to clone, express and purify the full-length HCS, the shorter isoform 58Met-HCS, as well as the catalytic domain of HCS to amounts suitable for SAXS and X-ray crystallographic studies, in order to gain an insight into the function and mechanism of the human BPL.

Prior to this study, there have been previous reports where HCS could be purified successfully for NMR and kinetic studies (Whitten and Trehwella, 2009, Lee et al., 2010). Lee *et al.* purified full-length recombinant HCS (FL-HCS) expressed in insect cells (Lee et al., 2010), whilst Ingaramo and Beckett expressed two HCS isoforms in *E. coli* cells as His₆-SUMO fusion proteins (Whitten and Trehwella, 2009). Our attempts at purifying significant amounts of His₆ fusion FL-HCS for structural studies were unsuccessful as the protein was unstable and precipitated rapidly. Due to time restraints, the His₆-SUMO construct was not cloned and expressed in our hands. As the N-terminal domain is large and unstructured, it was then decided to express and purify the shortest HCS isoform (Met58-HCS), but we were

unable to obtain the protein to the purity required for SAXS and X-ray crystallography. The catalytic domain of HCS was designed in a bid to obtain an enzyme that was stable enough for structural studies. The construct designed was based on a sequence alignment with *PhBPL*, and started from glutamate 464, however attempts at purifying the shorter, catalytic domain as a GST fusion protein were also not successful and hence no further work was done on these enzymes. A previous study done using a series of N-terminal deleted HCS constructs found that the catalytic domain alone was not catalytically active, and extra residues located in the N-terminal domain, with the shortest functional protein starting at lysine 378 (Campeau and Gravel, 2001). A mutant which started at leucine 460 was not active, and based on our inability to purify a stable protein, suggest that residues between L378 and L460 are required for structural stability of the catalytic domain. Hence, if the catalytic domain of HCS was to be used for future experiments, residues starting from L378 should be included in the design of the construct.

The function of the N-terminal domain in eukaryotic BPLs is still not entirely clear-cut, and may play other roles apart from aiding in the biotinylation of BCCP. A NCBI BLAST search of the N-terminal of HCS sequence and the BPLs from *S. cerevisiae* and *C. albicans* show that they have sequence similarity with members of the GAT-1 superfamily, which catalyses the removal of ammonia from glutamine onto a substrate. The three isoforms of HCS are located in both the nucleus and cytoplasm, and the N-terminal may aid in directing each isoform towards different locations in the cell (Ingaramo and Beckett, 2009). The structure of eukaryotic BPLs has not yet been determined, largely due to the protease sensitive N-terminus, and the instability of the protein in solution. As elucidation of the structure of these BPLs would help in providing insight into the function of the N-terminus, a method to purify large amounts of eukaryotic BPL would need to be optimised. We have used BL21(DE3) *E. coli* cells to express the full length HCS and the catalytic domain, whilst other researchers have used insect cells (Lee et al., 2010). Yeast cells, which require more time to express protein compared to bacterial cells, would be a reasonable alternative to purifying a eukaryotic protein. Another method would be to express HCS in mammalian cells, but due to time constraints, trialing the expression of HCS in yeast and mammalian cells was not attempted. The N-terminal domain of HCS was not cloned and expressed as a separate domain in our study, but has been previously expressed as a His₆ fusion enzyme in *E. coli* cells by other research groups, however the amount of protein that was purified was not reported (Lee et al., 2010). Due to the instability of the N-terminal domain, it is likely that amounts required for SAXS and X-ray crystallography would be difficult to obtain, and methods of producing this domain alone would need to be further optimized. It is likely that

the N-terminus requires residues of the catalytic domain for structural stability, and should be taken into account when designing a construct to be used for expression and purification.

Chapter 8 Final Discussion

Biotin protein ligase is a ubiquitous enzyme found in all organisms, playing an essential role in metabolism through the biotinylation of biotin-dependent carboxylases, and in some cases, transcriptional regulation. The *E. coli* BPL, BirA has been thoroughly studied, and has provided plenty of insight into the structure and function of BPLs. The crystal structure of PhBPL in complex with its substrate PhBCCP has also provided further information on the biotinylation process of BPL. Whilst there have been multiple publications focusing on bacterial BPLs, not much is known about eukaryotic BPLs, especially the function and structure of the N-terminal domain found in the human and yeast enzymes. Despite catalyzing the same biotinylation reaction, and containing a catalytic domain that is conserved throughout species, there are major differences between the different homologues. The results presented in this thesis focuses on the characterization of BPL from ESKAPE pathogens and eukaryotes in order to design drugs that can specifically target the catalytic active site of bacterial BPLs, and to gain a further understanding of the interaction of SaBPL with its target DNA and protein substrates.

The Center of Disease Control in the United States has identified a group of pathogens, collectively termed the ESKAPE pathogens, that is the cause of the majority of resistance problems in hospitals (Boucher et al., 2009). Given the rapid rate at which a great variety of human pathogens gain resistance to modern-day antibiotics (Boucher et al., 2009), there is a need to develop a novel antibiotic for which gain-of-resistance is unlikely. Enzymes or structures essential for bacterial cell survival and unique to bacteria have thus far been the obvious target (Volkov and Svergun, 2003, Schneidman-Duhovny et al., 2010, Kozin and Svergun, 2001), but the majority of antibiotics currently under development do not act on novel targets, with only 3 new classes of antibiotics developed in the past 35 years (Boucher et al., 2009). Bacterial enzymes with high sequence and structural identity with a mammalian homologue have traditionally been avoided due to potential toxicity issues, however the work produced in this thesis has suggested otherwise.

Infections caused by multi-drug resistant strains of *S. aureus* are a major problem worldwide, and as bacterial BPLs are essential for cell survival, SaBPL is a potential target for drug design (See Fig 8.1). The crystal structure of the apo, biotin-bound and Btyl-bound forms of SaBPL was solved, and served as a template for structure-based drug design. The biotin-binding site of BPLs is highly conserved, and relatively small in order to accommodate

the ureido and thiophene rings of biotin, and modifications made to these heterocycles rendered many biotin analogs unable to bind to BPLs (Slavoff et al., 2008), making this site unattractive in terms of designing a biotin analog inhibitor. However, the modification of the carbon chain of biotin with the addition of an alkyl or acetylene group produced molecules that could inhibit SaBPL, and provided new chemical scaffolds to which an adenine or adenine-like moiety could link to in order to target both the biotin and ATP binding site (Franke and Svergun, 2009). The ATP binding site of SaBPL has low sequence identity even with other bacterial BPLs, thus providing a potential region for developing selective anti-bacterials. The non-hydrolysable analog of Btyl, BtOH was initially found to be able to bind tightly to BirA, and had no affect on its ability to dimerise and bind to *bioO* and hence has been used in multiple structural and kinetic studies (Brown et al., 2004). The crystal structures of SaBPL and BirA in complex with BtOH show that despite the ability of BtOH to bind to both these isozymes, it does so in a different manner: the residues which come into contact with the ATP group of BtOH are different, and the hydrogen bonding network between the phosphodiester group of BtOH with BirA and SaBPL are not conserved. Based on the X-ray crystallographic structures of BtOH in complex with SaBPL, a series of molecules that retained the structure of the biotin element, but with a modified adenosyl moiety and phosphodiester linker were designed and synthesized in a bid to discover a new anti-microbial. The inhibitors that were designed contained a 1,2,3-triazole motif was used in place of the phosphodiester. The 1,2,3-triazole is a favourable isostere that can potentially form 3 different hydrogen bonds via its nitrogen molecules, as well as being able to participate in π - π interactions. The V-shaped conformation formed by both Btyl and BtOH when bound to the binding site of SaBPL was also retained by the triazole. This geometry was important as subtle changes in the conformation of the compound resulted in molecules that could not bind to SaBPL, highlighting the need for the exact positioning of the molecule within the binding site. Other key design features include removing the ribose sugar which was not required for binding (based on both structural and kinetic studies), and maintaining a 5-carbon linker between the triazole and biotin group. SPR was also used to determine binding affinity of these inhibitors to SaBPL, whilst X-ray crystallography was employed to establish the mode of binding of the complex formed between inhibitor and enzyme, as well as to provide a stepping-stone for the design of future generations of inhibitors.

As the active site of BPL is conserved throughout species, it was possible that this would pose a problem for drug selectivity. However, the 1,2,3 triazole that were discovered in our studies have been shown to have high selectivity for SaBPL over BirA and the human BPL. Several inhibitors also had anti-microbial activity against *S. aureus*, whilst showing no activity against *E. coli* cells, and no toxicity was found against HepG2 cells when treated with

these molecules. Through the successful development of inhibitory molecules that can selectively target the binding site of SaBPL presented in this thesis (Soares da Costa et al., 2012a, Soares da Costa et al., 2012b) together with the recent development of an inhibitor that selectively targets the ligand-binding site of the *M. tuberculosis* BPL (Duckworth et al., 2011), it has been demonstrated that bacterial enzymes that have a mammalian homologue with high structural and sequence identity still have the potential to be a candidate for drug design. The design of inhibitors that target the catalytic site of bacterial BPL is still in the early stages, and although methods of drug delivery are still to be conceived and performed, and further tests on animal models required, these inhibitors show promise as an interesting new class of antibiotic.

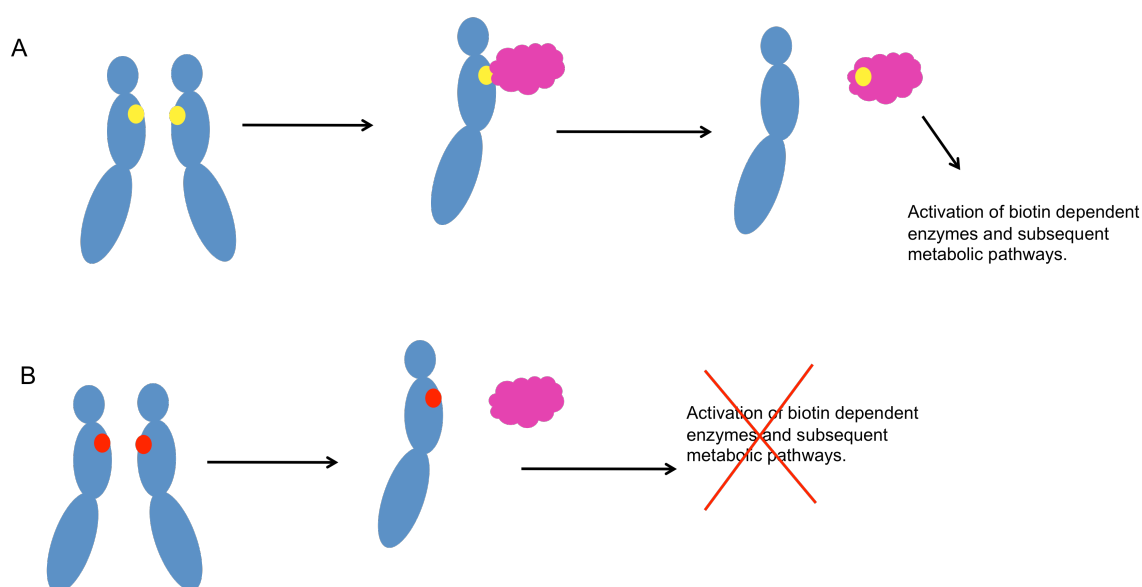


Figure 8.1 (A) In the presence of biotinyl-5'-AMP (yellow spot), SaBPL is able to form a heterodimer with BCCP (purple cloud) and biotinylates BCCP, thus activating biotin dependent enzymes and their subsequent metabolic pathways. **(B)** However, when an inhibitor (red spot) binds in the active site of SaBPL, biotinylation of BCCP does not occur, preventing the activation of important metabolic pathways and potentially inhibiting the growth of *S. aureus*.

Apart from SaBPL, the BPLs of other ESKAPE pathogens were also candidates for antibiotic design. *Kp*BPL and *Ac*BPL could be successfully purified, and both kinetic and structural work was attempted on these two proteins. The binding affinity of *Ac*BPL for ATP is around 10 fold higher compared to other bacterial BPLs, and may be attributed to differences in the ATP-binding site. The crystal structure of apo-BirA shows that both the biotin-binding loop (BBL) and the ATP-binding loop (ABL), as well as a number of other surface loops are unstructured, with biotin binding promoting the formation of the BBL and ABL, followed by ATP binding (Wood et al., 2006, Wilson et al., 1992). Known structures of bacterial BPLs on the other hand show that apart from the BBL, the ABL and other surface loops are preformed, and the binding of ATP and biotin occur in a random manner (Tron et al., 2009,

Bagautdinov et al., 2005b, Purushothaman et al., 2008). The length of the ABL varies amongst BPLs, and residues located in the ABL are not conserved even between bacterial BPLs, hence ATP binding may be regulated differently.

Unsurprisingly, both enzymes could also bind to BtOH, which can provide a starting point for drug design. Crystallisation of the apo and holo forms of *Kp*BPL and *Ac*BPL is underway in order to understand the mode of binding of BtOH or Btyl to these enzymes, and to see the major differences in binding compared to other known bacterial BPL structures. Due to the differences in the ATP-binding site, as well as non-conserved residues located within the active site itself, the inhibitors designed to target *Sa*BPL and *Mt*BPL have selectivity over *E. coli* BirA, and hence likely to have selectivity over *Kp*BPL and *Ac*BPL as well. To date, mutational studies in the ABL have only been reported in BirA (Naganathan and Beckett, 2007). Replacing residues located in the ABL of a class II BPL with those in a class I BPL could provide information on different modes of ATP binding, and from a drug design point of view, be used to design inhibitors that have both high affinity and specificity for a particular pathogenic BPL, without harming either the human homologue, or the normal flora present in the body.

Although the elucidation of the structures of several bacterial BPLs has been reported, the structure of their eukaryotic counterparts remains undetermined. This is mainly due to the large N-terminus that is largely unstructured and sensitive to proteolytic degradation. In order to elucidate the structure of HCS to determine the mode of binding of Btyl to the active site to aid in bacterial antibiotic design, the expression and purification of full length HCS, as well as the Met58 isoform and the catalytic domain of HCS (residues 459 – 717) was done in order to produce sufficient enzyme for X-ray crystallography. However, these enzymes were unstable in the buffer that was used for protein purification and formed precipitate. Future studies will need to focus on methods to express and purify large amounts of soluble eukaryotic BPL in order to proceed with structural studies. A mutant *Sa*BPL with residues in the catalytic site replaced with those found in the human enzyme has been expressed and purified by our collaborators at the University of Adelaide as biochemical and structural information of the humanized *Sa*BPL in complex with Btyl or BtOH in the absence of an active full-length HCS would be useful to identify the structural differences in ligand binding between HCS and bacteria, and crystallization trials of this enzyme is currently underway.

Removal of the N-terminal domain of HCS results in an enzyme that has reduced biotinylation activity, and NMR studies show that the N-terminus can interact directly with the substrate BCCP (Whitten and Trewella, 2009). Limited proteolysis studies done on

Saccharomyces cerevesiae BPL (ScBPL) show that in the absence of ligand binding, the linker region connecting both the N-terminal and catalytic domain was sensitive to protease cleavage, whilst ligand binding protected this linker region from protease digestion, with both domains interacting with each other due to a large structural change (Polyak et al., 1999). A similar study was performed on HCS, in this instance however, the human enzyme does not undergo ligand-induced conformational change (Oliva et al., 2004). Apart from providing structural information for drug-design studies, the structure of HCS would also increase our understanding of how the N-terminus aids the catalytic domain in biotinylation. As HCS (as well as other eukaryotic BPLs) is large, expressing and purifying each domain separately to use for crystal trials or NMR, and combining the structures of each domain using techniques such as SAXS or electron microscopy to position each domain in relation with each other would be a more rational approach, rather than to solve the structure of the full length enzyme.

SAXS was used combination with X-ray crystallography to model the complexes formed between SaBPL and its substrates (*bioO* and BCCP). Even though crystallography provides high atomic resolution structures of macromolecules, the packing of these molecules into a highly organised crystal lattice may lead to the formation of non-biologically relevant interactions within the molecule. A large amount of sample is required for crystal formation, and despite advances in crystallization methods and high-throughput structural analysis, some macromolecules simply cannot form crystals. Other methods to determine the 3-dimensional structure of macromolecules such as NMR and EM are limited by size, and extra effort to produce specialized samples for these experiments. In SAXS, X-rays are used to illuminate a monodisperse, purified sample in solution, and provides a scattering signal that comes from the rotational average of the molecules in solution (Jacques and Trewhella, 2010). Even though SAXS is only able to determine the low-resolution structure of a macromolecule, it is not limited by the molecular weight of the sample, and information about the size and shape can rapidly be obtained (Whitten and Trewhella, 2009). It is particularly useful in understanding systems with high flexibility, and aid in resolving the structure of multi-domain proteins and complexes when used in combination with X-ray crystallography or other structural methods, as well as structure validation (Putnam et al., 2007, Jacques and Trewhella, 2010). The biotin operon, *bioO*, is 44 nucleotides long, and is thought to be intrinsically flexible, thus potentially preventing the formation of a stable crystal lattice when attempting to crystallize the SaBPL/*bioO* complex. Attempts to crystallize the SaBPL/BCCP complex have also been unsuccessful, and so SAXS was used together with the known crystal structures of apo and holo SaBPL to create models of SaBPL and substrate complexes.

Like BirA, SaBPL undergoes a monomer to dimer transition upon ligand binding within its active site. The dimer formed by SaBPL is tighter than that compared to BirA, and SaBPL forms a dimer at micromolar concentrations even in its apo form. The apo form of BirA binds to its target DNA weakly (Streaker et al., 2002), whilst apo-SaBPL can bind to *bioO* with only a 10 fold weaker affinity compared to the holo enzyme. The ability of SaBPL to tightly dimerise may be linked to its more complex system: it has to biotinylate two carboxylases, and potentially regulates two different operons (Rodionov et al., 2002), and the tight dimerisation may allow for tighter control of the whole system. Dimerisation of class II BPLs leads to the binding of *bioO*, and we were able to use SAXS to model the complex formed between SaBPL and *SabioO*. However, SAXS is not able to detect small changes in the structure. The disordered surface loops of bacterial BPL become ordered upon ligand binding or homodimerisation (Kwon and Beckett, 2000, Adikaram and Beckett, 2012, Wood et al., 2006, Bagautdinov et al., 2005a, Tron et al., 2009), and the C-terminal domain undergoes structural changes upon BCCP binding (Bagautdinov et al., 2008). The DNA-binding domain, whilst located away from the catalytic active site, affects ligand binding when removed (Xu and Beckett, 1996), and residues located away from the DNA-binding domain affect *bioO* binding (Chakravartty and Cronan, 2012). All these indicate that the domains of bacterial BPL have to communicate with each other in order for successful ligand, BCCP and DNA binding to occur. There are reports of crystallization trials being done with super-repressor BirA and its target *bioO* (Chakravartty and Cronan, 2012), and we are attempting to crystallize SaBPL with *SabioO*. If successful, the structure of the BPL/*bioO* complex will not only provide information about the interactions formed between the protein and DNA, and small structural changes that occur which cannot be detected by SAXS, and may also provide further insight as to how a class II BPL can regulate both its roles.

The general model of the regulation mechanism by Class II BPLs suggests that apo-BCCP binds to a monomeric biotinyl-5'-AMP bound BPL and forms a heterodimer, and competes for heterodimer formation (Streaker and Beckett, 2006, Zhao and Beckett, 2008). Based on previous structural and biochemical studies, Weaver *et al.* constructed a model of BirA in complex with BCCP in which BCCP binds to BirA using the same dimerisation interface which is employed by the BirA homodimer (Weaver et al., 2001a). In a heteronuclear NMR spectroscopy experiment, two regions of BCCP which have the most extensive contacts in the model suggested by Weaver *et al.* are perturbed upon addition of BirA (Reche et al., 2000). To further support this model, a later crystal structure of the Class I BPL, PhBPL was shown to use this same interface to form a heterodimer with its cognate BCCP (Bagautdinov et al., 2008). However, Solbiati and Cronan have recently suggested that extensive protein-

protein interactions are not required for the regulation of the two roles of class II BPLs. Using short peptide sequences which are able to be biotinylated by BirA, they show that derepression of the BioO operon still occurs even in the presence of these short peptides despite binding to BirA in a different manner compared to BCCP, and postulate that BCCP binds to holo-BirA and rapidly dissociates after biotinylation and leaves BirA in its monomeric form and unable to bind to BioO (Solbiati and Cronan, 2010). Our SAXS experiment investigating the interaction of SaBPL and SaBCCP suggest that it is the former model that regulates the two roles of SaBPL: in the presence of SaBCCP, there is an absence of dimeric SaBPL, instead there is a molecule that resembles SaBPL in complex with SaBCCP, indicating that regulation of the two roles of class II BPLs requires competing protein-protein interactions. SaBPL mutants that cannot release BCCP after biotinylation were used to try to crystallise the SaBPL/BCCP complex, however this was unsuccessful. One potential method of crystallizing this complex is to crosslink SaBPL/SaBCCP together using glutaraldehyde or other chemical crosslinkers. There are multiple reports of crosslinking protein:protein complexes for crystallography trials (Andersen et al., 2009, Kudryashov et al., 2005) and this can be attempted to prevent the release of SaBCCP from SaBPL and capture the complex formed between SaBPL/SaBCCP and aid in crystallization.

The work done in this thesis has successfully paved the way for future drug design experiments that target bacterial BPL through the development of inhibitors that specifically target the Btyl binding site of SaBPL. Further biochemical and clinical studies are required to develop an inhibitor that not only has high affinity for the target BPL, but also high specificity due to the presence of an eukaryotic homologue with high sequence similarity in the catalytic domain. Evidence showing that intensive protein-protein interactions are required for the regulation of the dual roles of class II BPLs has also been presented, but elucidation of the structure of a class II BPL in complex with its cognate *bioO* or BCCP would provide additional proof to support this theory.

References:

- ABBOTT, J. & BECKETT, D. 1993. Cooperative Binding of the *Escherichia coli* Repressor of Biotin Biosynthesis to the Biotin Operator Sequence. *Biochemistry*, 32, 9649-9656.
- ADIKARAM, P. R. & BECKETT, D. 2012. Functional Versatility of a Single Protein Surface in Two Protein:Protein Interactions. *J Mol Biol.*, 419, 223-233.
- ALLISON, F. E. & MINOR, F. W. 1938. Coenzyme R requirements of rhizobia. *Soil Sci*, 46, 473-483.
- ANDERSEN, O. A., SCHONFELD, D. L., TOOGOOD-JOHNSON, I., FELICETTI, B., ALBRECHT, C., FRYATT, T., WHITTAKER, M., HALLETT, D. & BARKER, J. 2009. Cross-linking of protein crystals as an aid in the generation of binary protein-ligand crystal complexes, exemplified by the human PDE10a-papaverine structure. *Acta Crystallogr D Biol Crystallogr*, 65, 872-874.
- AOKI, Y., LI, X., SAKAMOTO, O., HIRATSUKA, M., AKAISHI, H., XU, L., BRIONES, P., SUORMALA, T., BAUMGARTNER, E. R., SUZUKI, Y. & NARISAWA, K. 1999. Identification and characterization of mutations in patients with holocarboxylase synthetase deficiency. *Hum Genet*, 104, 143-148.
- AOKI, Y., SUZUKI, Y., SAKAMOTO, O., LI, X., TAKAHASHI, K., OHTAKE, A., SAKUTA, R., OHURA, T., MIYABAYASHI, S. & NARISAWA, K. 1995. Molecular analysis of holocarboxylase synthetase deficiency: a missense mutation and a single base deletion are predominant in Japanese patients. *Biochem Biophys Acta*, 1272, 168-174.
- ARTYMIUK, P. J., RICE, D. W., POIRRETTE, A. R. & WILLET, P. 1994. A tale of two synthetases. *Nat Struct Biol*, 1, 758-760.
- ATHAPPILLY, F. K. & HENDRICKSON, W. A. 1995. Structure of the biotinyl domain of acetyl-coenzyme A carboxylase determined by Mad phasing. *Structure*, 3, 1407-1419.
- BAGAUTDINOV, B., KUROISHI, C., SUGAHARA, M. & KUNISHIMA, N. 2005a. Crystal structures of biotin protein ligase from *Pyrococcus horikoshii* OT3 and its complexes: structural basis of biotin activation. *J Mol Biol*, 353, 322-333.
- BAGAUTDINOV, B., KUROISHI, C., SUGAHARA, M. & KUNISHIMA, N. 2005b. Purification, crystallization and preliminary crystallographic analysis of the biotin-protein ligase from *Pyrococcus horikoshii* OT3. *Acta Crystallogr Sect F Struct Biol Cryst Commun*, 61, 193-195.
- BAGAUTDINOV, B., MATSUURA, Y., BAGAUTDINOVA, S. & KUNISHIMA, N. 2007. Crystallization and preliminary X-ray crystallographic studies of the biotin carboxyl carrier protein and biotin protein ligase complex from *Pyrococcus horikoshii* OT3. *Acta Crystallograph Sect F Struct Biol Cryst Commun*, 63, 334-337.
- BAGAUTDINOV, B., MATSUURA, Y., BAGAUTDINOVA, S. & KUNISHIMA, N. 2008. Protein biotinylation visualized by a complex structure of biotin protein ligase with a substrate. *J Biol Chem*, 283, 14739 - 14750.
- BAILEY, L., WALLACE, J. C. & POLYAK, S. W. 2010. Holocarboxylase synthetase: Correlation of protein localisation with biological function. *Archives of Biochemistry and Biophysics*, 496, 45-52.
- BARKER, D. F. & CAMPBELL, A. M. 1981a. The *birA* gene of *Escherichia coli* encodes a biotin holoenzyme synthetase. *J Mol Biol*, 146, 451-467.

- BARKER, D. F. & CAMPBELL, A. M. 1981b. Genetic and biochemical characterisation of the *birA* gene and its product : Evidence for a direct role of biotin holoenzyme synthetase in repression of the biotin operon in *Escherichia coli*. *J Mol Biol*, 146, 469-492.
- BAUMGARTNER, E. R. & SUORMALA, T. 1997. Multiple carboxylase deficiency - Inherited and acquired disorders of Biotin metabolism. *Int J Vit Nutr Res*, 67, 377-384.
- BERMAN, H. M., WESTBROOK, J., FENG, Z., GILLILAND, G., BHAT, T. N., WEISSIG, H., SHINDYALOV, I. N. & BOURNE, P. E. 2000. The Protein Data Bank. *Nucleic Acids Research*, 28.
- BOAS, M. A. 1927. The Effect of Desiccation upon the Nutritive Properties of Egg-white. *Biochem J*, 21, 712-724
- BOUCHER, H. W., TALBOT, G. H., BRADLEY, J. S., EDWARDS, J. E., GILBERT, D., RICE, L. B., SCHELD, M., SPELLBERG, B. & BARTLETT, J. 2009. Bad bugs, no drugs: no ESKAPE! An update from the Infectious Diseases Society of America. *Clin Infect Dis*, 48, 1-12.
- BROCKLEHURST, S. M. & PERHAM, R. N. 1993. Prediction of the three dimensional structures of the biotinylated domain from yeast pyruvate carboxylase and of the lipoylated H-protein from the pea leaf glycine cleavage system: A new automated method for the prediction of protein tertiary structure. *Protein Sci*, 2, 626-639.
- BROWN, P. H., CRONAN, J. E., GROTLI, M. & BECKETT, D. 2004. The biotin repressor: modulation of allostery by corepressor analogs. *J Mol Biol*, 337, 857-869.
- BROWNSEY, R. W., BOONE, A. N., ELLIOTT, J. E., KULPA, J. E. & LEE, W. M. 2006. Regulation of acetyl-CoA carboxylase. *Biochem Soc Trans*, 34, 223-227.
- BRUNGER, A. 1992. Free R value: a novel statistical quantity for assessing the quality of crystal structures. *Nature*, 355, 472-475.
- BURRI, B. J., SWEETMAN, L. & NYHAN, W. L. 1985. Heterogeneity of holocarboxylase synthetase in patients with biotin-responsive multiple carboxylase deficiency. *Am J Hum Genet*, 37, 326-337.
- CAMPEAU, E. & GRAVEL, R. A. 2001. Expression in *Escherichia coli* of N- and C-terminally deleted human holocarboxylase synthetase. Influence of the N-terminus on biotinylation and identification of a minimum functional protein. *J Biol Chem*, 276, 12310-12316.
- CAMPOREALE, G., ZEMPLINI, J. & EISSENBERG, J. C. 2007. Susceptibility to heat stress and aberrant gene expression patterns in holocarboxylase synthetase-deficient *Drosophila melanogaster* are caused by decreased biotinylation of histones, not of carboxylases. *J Nutr*, 137, 885-889.
- CHAKRAVARTTY, V. & CRONAN, J. E. 2012. Altered regulation of Escherichia Coli Biotin Biosynthesis in BirA Superrepressor Mutant Strains. *Journal of Bacteriology*, 194, 1113-1126.
- CHAPMAN-SMITH, A., MORRIS, T. W., WALLACE, J. C. & CRONAN, J. E., JR. 1999. Molecular recognition in a post-translational modification of exceptional specificity. Mutants of the biotinylated domain of acetyl-CoA carboxylase defective in recognition by biotin protein ligase. *J Biol Chem*, 274, 1449-1457.
- CHAPMAN-SMITH, A., MULHERN, T. D., WHELAN, F., CRONAN, J. E., JR. & WALLACE, J. C. 2001. The C-terminal domain of biotin protein ligase from *E. coli* is required for catalytic activity. *Protein Sci*, 10, 2608-2617.

- CHAUDHURI, R. R., ALLEN, A. G., OWEN, P. J., SHALOM, G., STONE, K., HARRISON, M., BURGIS, T. A., LOCKYER, M., GARCIA-LARA, J., FOSTER, S. J., PLEASANCE, S. J., PETERS, S. E., MASKELL, D. J. & CHARLES, I. G. 2009. Comprehensive identification of essential *Staphylococcus aureus* genes using Transposon-Mediated Differential Hybridisation (TMDH). *BMC Genomics*, 10, 291.
- CHEN, V., ARENDALL, W., HEADD, J., KEEDY, D., IMMORMINO, R., KAPRAL, G., MURRAY, L., RICHARDSON, J. & RICHARDSON, D. 2010. MolProbity: all-atom structure validation for macromolecular crystallography. *Act Crystallogr Sect D*, 66, 12-21.
- CHENG, J., MA, J., LIN, J., FAN, Z. C., CRONAN, J. E. & WANG, H. 2012. Only one of the five *Ralstonia solanacearum* long-chain 3-ketoacyl-acyl carrier protein synthase homologues functions in fatty acid synthesis. *Appl Environ Microbiol*, 78, 1563-1573.
- CHEW, Y. C., CAMPOREALE, G., KOTHAPALLI, N., SARATH, G. & ZEMPLINI, J. 2006. Lysine residues in N-terminal and C-terminal regions of human histone H2A are targets for biotinylation by biotinidase. *J Nutr Biochem*, 17, 225-233.
- CHOI-RHEE, E., SCHULMAN, H. & CRONAN, J. E. 2004. Promiscuous protein biotinylation by *Escherichia coli* biotin protein ligase. *Protein Sci*, 13, 3043-3050.
- CLARKE, D. J., COULSON, J., BAILLIE, R. & CAMPOPIANO, D. J. 2003. Biotinylation in the hyperthermophile *Aquifex aeolicus*. *Eur J Biochem*, 270, 1277-1287.
- CRONAN, J. E. 2005. Targeted and proximity-dependent promiscuous protein biotinylation by a mutant *Escherichia coli* biotin protein ligase. *J Nutr Biochem*, 16, 416-418.
- CRONAN, J. E., JR. 1990. Biotination of proteins in vivo. A post-translational modification to label, purify, and study proteins. *J Biol Chem*, 265, 10327-10333.
- CRONAN, J. E., JR. 2001. The biotinyl domain of *Escherichia coli* acetyl-CoA carboxylase. Evidence that the "thumb" structure is essential and that the domain functions as a dimer. *J Biol Chem*, 276, 37355-37364.
- CRONAN, J. E., JR. & WALLACE, J. C. 1995. The gene encoding the biotin-apoprotein ligase of *Saccharomyces cerevisiae*. *FEMS Microbiol Lett*, 130, 221-229.
- CRONAN, J. E. & LIN, S. 2011. Synthesis of the alpha,omega-dicarboxylic acid precursor of biotin by the canonical fatty acid biosynthetic pathway. *Curr Opin Chem Biol*, 15, 407-413.
- DANIELS, K. & BECKETT, D. 2010. Biochemical Properties and Biological Function of a Monofunctional Microbial Biotin Protein Ligase. *Biochemistry*, 49, 5358-5365.
- DARDEL, F., DAVIS, A. L., LAUE, E. D. & PERHAM, R. N. 1993. Three-dimensional structure of the lipoyl domain from *Bacillus stearothermophilus* pyruvate dehydrogenase multienzyme complex. *J Mol Biol*, 229, 1037-1048.
- DAVID, M. Z. & DAUM, R. S. 2010. Community-associated methicillin-resistant *Staphylococcus aureus*: epidemiology and clinical consequences of an emerging epidemic. *Clin Microbiol Rev*, 23, 616-687.
- DELEO, F. R., OTTO, M., KREISWIRTH, B. N. & CHAMBERS, H. F. 2010. Community-associated methicillin-resistant *Staphylococcus aureus*. *Lancet*, 375, 1557-1568.

- DEODATO, F., BOENZI, S., SANTORELLI, F. M. & DIONISI-VICI, C. 2006. Methylmalonic and propionic aciduria. *Am J Med Genet C Semin Med Genet*, 142, 104-112.
- DETITTA, G. T., EDMONDS, J. W., STALLINGS, W. & DONOHUE, J. 1976. Molecular structure of biotin: Results of two independent crystal structure investigations. *J Am Chem Soc*, 98, 1920-1926.
- DU VIGNEAUD, V., MELVILLE, D. B., FOLKERS, K., WOLF, D. E. & MOZINGO, R. 1942. The structure of biotin: A study of desthiobiotin. *J Biol Chem*, 146, 475-485.
- DU VIGNEAUD, V., MELVILLE, D. B., GYORGY, P. & ROSE, C. S. 1940. On the identity of vitamin H with biotin. *Science*, 92, 62-63.
- DUCKWORTH, B. P., GEDERS, T. W., TIWARI, D., BOSHOFF, H. L., SIBBALD, P. A., BARRY, C. E., SCHNAPPINGER, D., FINZEL, B. C. & ALDRICH, C. C. 2011. Bisubstrate adenylation inhibitors of biotin protein ligase from *Mycobacterium tuberculosis*. *Chemistry and Biology*, 18, 1432-1441.
- DUPUIS, L., LEON-DEL-RIO, A., LECLERC, D., CAMPEAU, E., SWEETMAN, L., SAUDUBRAY, J. M., HERMAN, G., GIBSON, K. M. & GRAVEL, R. A. 1996. Clustering of mutations in the biotin-binding region of holocarboxylase synthetase in biotin-responsive multiple carboxylase deficiency. *Hum Mol Genet*, 5, 1011-1016.
- EISENSTEIN, E. & BECKETT, D. 1999. Dimerization of the *Escherichia coli* biotin repressor: corepressor function in protein assembly. *Biochemistry*, 38, 13077-13084.
- EMSLEY, P., LOHKAMP, B., SCOTT, W. & COWTAN, K. 2010. Features and Development of Coot. *Acta Crystallogr D*, 66, 486-501.
- FORSYTH, R. A., HASELBECK, R. J., OHLSEN, K. L., YAMAMOTO, R. T., XU, H., TRAWICK, J. D., WALL, D., WANG, L., BROWN-DRIVER, V., FROELICH, J. M., C, K. G., KING, P., MCCARTHY, M., MALONE, C., MISINER, B., ROBBINS, D., TAN, Z., ZHU ZY, Z. Y., CARR, G., MOSCA, D. A., ZAMUDIO, C., FOULKES, J. G. & ZYSKIND, J. W. 2002. A genome-wide strategy for the identification of essential genes in *Staphylococcus aureus*. *Mol Microbiol*, 43, 1387-1400.
- FRANKE, D. & SVERGUN, D. I. 2009. DAMMIF, a program for rapid ab-initio shape determination in small-angle scattering. *J Appl Cryst*, 42, 342-346.
- FUCHSHUBER, A., SUORMALA, T., ROTH, B., DURAN, M., MICHALK, D. & BAUMGARTNER, E. R. 1993. Holocarboxylase synthetase deficiency: early diagnosis and management of a new case. *Eur J Pediatr*, 152, 446-449.
- GOULD, I. M., DAVID, M. Z., ESPOSITO, S., GARAU, J., LINA, G., MAZZEI, T. & PETERS, G. 2012. New insights into meticillin-resistant *Staphylococcus aureus* (MRSA) pathogenesis, treatment and resistance. *Int J Antimicrob Agents*, 39, 96-104.
- GYORGY, P., ROSE, C. S., HOFMANN, K., MELVILLE, D. B. & DU VIGNEAUD, V. 1940. A further note on the identity of vitamin H with biotin. *Science*, 92, 609.
- HALL, S. R., ALLEN, F. H. & BROWN, I. D. 1991. The Crystallographic Information File (CIF): a new standard archive file for crystallography. *Acta Crystallogr A*, 47, 655-685.
- HASSAN, Y., MORIYAMA, H., OLSEN, J., BI, X. & ZEMPLINI, J. 2009. N- and C-terminal domains in human holocarboxylase synthetase participate in substrate recognition. *Mol Genet Metab*, 96, 183-188.

- HIRATSUKA, M., SAKAMOTO, O., LI, X., SUZUKI, Y., AOKI, Y. & NARISAWA, K. 1998. Identification of holocarboxylase synthetase (HCS) proteins in human placenta. *Biochim Biophys Acta Prot Struct Mol Enzymol*, 1385, 165-171.
- HOJA, U., WELLEIN, C., GREINER, E. & SCHWEIZER, E. 1998. Pleiotropic phenotype of acetyl-CoA-carboxylase-defective yeast cells--viability of a BPL1-amber mutation depending on its readthrough by normal tRNA(Gln)(CAG). *Eur J Biochem*, 254, 520-526.
- INGARAMO, M. & BECKETT, D. 2009. Distinct amino termini of two human HCS isoforms influence biotin acceptor substrate recognition. *J Biol Chem*, 284, 30862-20870.
- INGARAMO, M. & BECKETT, D. 2011. Biotinylation, a Post-translational Modification Controlled by the Rate of Protein-Protein Association. *J Biol Chem*, 286, 13071-13078.
- INGARAMO, M. & BECKETT, D. 2012. Selectivity in post-translational biotin addition to five human carboxylases. *J Biol Chem*, 287, 1813-22.
- JACQUES, D. A. & TREWHELLA, J. 2010. Small-angle scattering for structural biology--expanding the frontier while avoiding the pitfalls. *Protein Sci*, 19, 642-657.
- JAMES, E. S. & CRONAN, J. E. 2004. Expression of Two Eschericia coli Acetyl-CoA carboxylase Subunits is Autoregulated. *J Biol Chem*, 279, 2520-2527.
- JI, Y., ZHANG, B., VAN, S. F., HORN, WARREN, P., WOODNUTT, G., BURNHAM, M. K. & ROSENBERG, M. 2001. Identification of critical staphylococcal genes using conditional phenotypes generated by antisense RNA. *Science*, 293, 2266-2269.
- JITRAPAKDEE, S. & WALLACE, J. C. 1999. Structure, function and regulation of pyruvate carboxylase. *Biochem J*, 340 (Pt 1), 1-16.
- KABSCH, W. 2010. XDS. *Acta Crystallogr D*, 66, 125-132.
- KNOWLES, J. R. 1989. The mechanism of biotin-dependent enzymes. *Ann Rev Biochem*, 58.
- KOGL, F. & TONNIS, B. 1936. *J Physiol Chem*, 242, 43.
- KONAREV, P. V., VOLKOV, V. V., SOKOLOVA, A. V., KOCH, M. H. J. & SVERGUN, D. I. 2003. PRIMUS - a Windows-PC based system for small-angle scattering data analysis. *J Appl Cryst*, 36, 1277-1282.
- KONDO, H., UNO, S., KOMIZO, Y. Y. & SUNAMOTO, J. 1984. Importance of methionine residues in the enzymatic carboxylation of biotin containing peptides representing the local bindyl site of *E. coli* actyl CoA carboxylase. *Int J Peptide Protein Res*, 23, 559-564.
- KOZIN, M. & SVERGUN, D. I. 2001. Automated matching of high- and low-resolution structural models. *J Appl Cryst*, 34, 33-41.
- KUDRYASHOV, D. S., SAWAYA, M. R., ADISETIYO, H., NORCROSS, T., HEGYI, G., REISLER, E. & YEATES, T. O. 2005. The crystal structure of a cross-linked actin dimer suggests a detailed molecular interface in F-actin. *Proc Natl Acad Sci U S A*, 102, 13105-13110.
- KUROISHI, T., RIOS-AVILA, L., PESTINGER, V., WIJERATNE, S. S. & ZEMPLENI, J. 2011. Biotinylation is a natural, albeit rare, modification of human histones. *Mol Genet Metab*, 104, 537-545.
- KWON, K. & BECKETT, D. 2000. Function of a conserved sequence motif in biotin holoenzyme synthetases. *Protein Sci*, 9, 1530-1539.

- KWON, K., STREAKER, E. D., RUPARELIA, S. & BECKETT, D. 2000. Multiple disordered loops function in corepressor-induced dimerization of the biotin repressor. *J Mol Biol*, 304, 821-833.
- LANE, M. D., ROMINGER, K. L., YOUNG, D. L. & LYNEN, F. 1964. The enzymatic synthesis of holotranscarboxylase from apo transcarboxylase and (+)-biotin. *J Biol Chem*, 239, 2865-2871.
- LEE, C., CHEONG, C. & JEON, Y. 2010. The N-terminal domain of human holocarboxylase synthetase facilitates biotinylation via direct interaction with the substrate protein. *FEBS Letters*, 584, 675-680.
- LEON-DEL-RIO, A. & GRAVEL, R. A. 1994. Sequence requirements for the biotinylation of carboxyl-terminal fragments of human propionyl-CoA carboxylase alpha subunit expressed in *Escherichia coli*. *J Biol Chem*, 269, 22964-22968.
- LEON-DEL-RIO, A., LECLERC, D., AKERMAN, B., WAKAMATSU, N. & GRAVEL, R. A. 1995. Isolation of a cDNA encoding human holocarboxylase synthetase by functional complementation of a biotin auxotroph of *Escherichia coli*. *Proc Natl Acad Sci USA*, 92, 4626-4630.
- LIN, S. & CRONAN, J. E. 2011. Closing in on complete pathways of biotin biosynthesis. *Mol Biosyst*, 7, 1811-1821.
- LISTER, P. D., WOLTER, D. J. & HANSON, N. D. 2009. Antibacterial-resistant *Pseudomonas aeruginosa*: clinical impact and complex regulation of chromosomally encoded resistance mechanisms. *Clin Microbiol Rev*, 22, 582-610.
- LOKANATH, N. K., SHIROMIZU, I., OHSHIMA, N., NODAKE, Y., SHUGAHARA, M., YOKOYAMA, S., KURAMITSU S., MIYANO M & N., K. 2004. Structure of aldolase from *Thermus thermophilus* HB8 showing the contribution of oligomeric state to thermostability. *Act Crystallogr Sect D*, 60, 1816-1823.
- LYNEN, F., KNAPPE, J., LORCH, E., RINGELMANN, E. & LACHANCE, J. 1961. Zur biochemischen Funktion des Biotins. 2. Reinigung und Wirkungsweise der beta-methyl-crotonyl-carboxylase. *Biochem Z*, 335, 123.
- MAYENDE, L., SWIFT, R., BAILEY, L., SOARES DA COSTA, T., WALLACE, J., BOOKER, G. & POLYAK, S. 2012. A novel molecular mechanism to explain biotin-unresponsive holocarboxylase synthetase deficiency. *J Mol Med*, 90, 81-88.
- MCALLISTER, H. C. & COON, M. J. 1966. Further studies on the properties of liver propionyl coenzyme A holocarboxylase synthetase and the specificity of holocarboxylase formation. *J Biol Chem*, 241, 2855-61.
- MORRONE, A., MALVAGIA, S., DONATI, M. A., FUNGHINI, S., CIANI, F., PELA, I., BONEH, A., PETERS, H., PASQUINI, E. & ZAMMARCI, E. 2002. Clinical findings and biochemical and molecular analysis of four patients with holocarboxylase synthetase deficiency. *Am J Med Genet*, 111, 10-18.
- MURSHUDOV, G., VAGIN, A. & DODSON, E. 1997. Refinement of Macromolecular Structures by the Maximum-Likelihood method. *ACTA Crystallogr D*, 53, 240-255.
- NAGANATHAN, S. & BECKETT, D. 2007. Nucleation of an allosteric response via ligand-induced loop folding. *J Mol Biol*, 373, 96-111.
- NARANG, M. A., DUMAS, R., AYER, L. M. & GRAVEL, R. A. 2004. Reduced histone biotinylation in multiple carboxylase deficiency patients: a nuclear role for holocarboxylase synthetase. *Hum Mol Genet*, 13, 15-23.

- NEYLON, C. 2008. Small angle neutron and X-ray scattering in structural biology: recent examples from the literature. *Eur Biophys J Biophys Lett*, 37, 531-541.
- NOBLE, M. E. M., MUSACCHIO, A., SARASTE, M., COURTNEIDGE, S. A. & WIERENGA, R. K. 1993. Crystal structure of the SH3 domain in human Fyn - Comparison of the 3-dimensional structures of SH3 domains in tyrosine kinases and spectrin. *EMBO J.*, 12, 2617-2624.
- NYHAN, W. L. 1987. Inborn errors of biotin metabolism. *Arch Dermatol*, 123, 1696-1698a.
- OLIVA, A., LLABRES, M. & FARINA, J. 2004. Applications of Multi-Angle Laser Light-scattering detection in the analysis of peptides and proteins. *Current Drug Discovery Technologies*, 1, 229-242.
- OTSUKA, A. J., ABELSON J., 1978. The regulatory region of the biotin operon in *Escherichia coli*. *Nature*, 689-693.
- PENDINI, N. R., BAILEY, L. M., BOOKER, G. W., WILCE, M. C., WALLACE, J. C. & POLYAK, S. W. 2008a. Biotin protein ligase from *Candida albicans*: expression, purification and development of a novel assay. *Arch Biochem Biophys*, 479, 163-169.
- PENDINI, N. R., POLYAK, S. W., BOOKER, G. W., WALLACE, J. C. & WILCE, M. C. 2008b. Purification, crystallization and preliminary crystallographic analysis of biotin protein ligase from *Staphylococcus aureus*. *Acta Crystallogr Sect F Struct Biol Cryst Commun*, 64, 520-523.
- PENDINI, N. R., YAP, M. Y., POLYAK, S. W., COWIESON, N. P., ABELL, A., BOOKER, G. W., WALLACE, J. C., WILCE, J. A. & WILCE, M. C. 2013. Structural characterisation of *Staphylococcus aureus* biotin protein ligase and interaction partners: An antibiotic target. *Protein Sci*.
- PESTINGER, V., WIJERATNE, S. S., RODRIGUEZ-MELENDEZ, R. & ZEMPLENI, J. 2011. Novel histone biotinylation marks are enriched in repeat regions and participate in repression of transcriptionally competent genes. *J Nutr Biochem*, 22, 328-33.
- POLYAK, S. W., CHAPMAN-SMITH, A., BRAUTIGAN, P. & WALLACE, J. C. 1999. Biotin protein ligase from *Saccharomyces cerevisiae*: The N-terminal domain is required for complete activity. *J Biol Chem*, 274, 32847-32854.
- POLYAK, S. W., CHAPMAN-SMITH, A., MULHERN, T. D., CRONAN, J. E., JR. & WALLACE, J. C. 2001. Mutational analysis of protein substrate presentation in the post-translational attachment of biotin to biotin domains. *J Biol Chem*, 276, 3037-3045.
- PRAKASH, O. & EISENBERG, M. A. 1979. Biotinyl-5'-adenylate: corepressor role in the regulation of the biotin genes of *Escherichia coli* K-12. *Proc. Natl. Acad. Sci*, 76, 5592-95.
- PURUSHOTHAMAN, S., GUPTA, G., SRIVASTAVE, R., RAMU, V. G. & SUROLIA, A. 2008. Ligand Specificity of Group I biotin Protein Ligase of *Mycobacterium tuberculosis*. *PLoS ONE*, 3, e2320.
- PUTNAM, C. D., HAMMEL, M., HURA, G. L. & TAINER, J. A. 2007. X-ray solution scattering (SAXS) combined with crystallography and computation: defining accurate macromolecular structures, conformations and assemblies in solution. *Q Rev Biophys*, 40, 191-285.
- RECHE, P., LI, Y. L., FULLER, C., EICHHORN, K. & PERHAM, R. N. 1998. Selectivity of post-translational modification in biotinylated proteins: the carboxy carrier protein of the acetyl-CoA carboxylase of *Escherichia coli*. *Biochem J*, 329 (Pt 3), 589-596.

- RECHE, P. & PERHAM, R. N. 1999. Structure and selectivity in post-translational modification: attaching the biotinyl-lysine and lipoyl-lysine swinging arms in multifunctional enzymes. *EMBO J*, 18, 2673-2682.
- RECHE, P. A. 2000. Lipoylating and biotinylating enzymes contain a homologous catalytic module. *Protein Sci*, 9, 1922-1929.
- RECHE, P. A., HOWARD, M. J., BROADHURST, R. W. & PERHAM, R. N. 2000. Heteronuclear NMR studies of the specificity of the post-translational modification of biotinyl domains by biotinyl protein ligase. *FEBS Lett*, 479, 93-98.
- ROBERTS, E. L., SHU, N. C., HOWARD, M. J., BROADHURST, R. W., CHAPMAN-SMITH, A., WALLACE, J. C., MORRIS, T., CRONAN, J. E. & PERHAM, R. N. 1999. Solution structures of apo and holo biotinyl domains from acetyl coenzyme A carboxylase of *Escherichia coli* determined by triple-resonance nuclear magnetic resonance spectroscopy. *Biochemistry*, 38, 5045-5053.
- RODIONOV, D. A., MIRONOV, A. A. & GELFAND, M. S. 2002. Conservation of the biotin regulon and the BirA regulatory signal in Eubacteria and Archaea. *Genome Res*, 12, 1507-1516.
- SAKAMOTO, O., SUZUKI, Y., AOKI, Y., LI, X., HIRATSUKA, M., YANAGIHARA, K., INUI, K., OKABE, T., YAMAGUCHI, S., KUDOH, J., SHIMIZU, N. & NARISAWA, K. 1998. Molecular analysis of new Japanese patients with holocarboxylase synthetase deficiency. *J Inherit Metab Dis*, 21, 873-4.
- SAKAMOTO, O., SUZUKI, Y., LI, X., AOKI, Y., HIRATSUKA, M., HOLME, E., KUDOH, J., SHIMIZU, N. & NARISAWA, K. 2000. Diagnosis and molecular analysis of an atypical case of holocarboxylase synthetase deficiency. *Eur J Pediatr*, 159, 18-22.
- SAKAMOTO, O., SUZUKI, Y., LI, X., AOKI, Y., HIRATSUKA, M., SUORMALA, T., BAUMGARTNER, E. R., GIBSON, K. M. & NARISAWA, K. 1999. Relationship between kinetic properties of mutant enzyme and biochemical and clinical responsiveness to biotin in holocarboxylase synthetase deficiency. *Pediatr Res*, 46, 671-676.
- SAMBROOK, J. & RUSSELL, D. 2001. *Molecular cloning: a laboratory manual*, Cold Spring Harbor, N.Y.: Cold Spring Harbor Laboratory.
- SAMOLS, D., THORNTON, C. G., MURTIF, V. L., KUMAR, G. K., HAASE, F. C. & WOOD, H. G. 1988. Evolutionary conservation among biotin enzymes. *J Biol Chem*, 263, 6461-6464.
- SCHNEIDMAN-DUHOVNY, D., HAMMEL, M. & SALI, A. 2010. FoXS: A Web server for Rapid Computation and Fitting of SAXS Profiles. *Nucleic Acids Research* 38, Suppl:W540-544.
- SCHUTTELKPF, A. W. & VAN AALTEN, D. M. F. 2004. PRODRG: a tool for high-throughput crystallography of protein-ligand complexes. *Acta Crystallogr D*, 60, 1355-1363.
- SHENOY, B. C. & WOOD, H. G. 1988. Effect of mutations at Met-88 and Met-90 on the biotinylation of Lys-89 of the apo 1.3S subunit of transcarboxylase. *FASEB J*, 2, 2396-2401.
- SLAVOFF, S. A., CHEN, I., CHOI, Y. A. & TING, A. Y. 2008. Expanding the substrate tolerance of biotin ligase through exploration of enzymes from diverse species. *J Am Chem Soc*, 130, 1160-1162.
- SOARES DA COSTA, T., TIEU, W., YAP, M. Y., PENDINI, N. R., POLYAK, S. W., PEDERSEN, D., MORONA, R., TURNIDGE, J. D., WALLACE, J. C., WILCE,

- M. C., BOOKER, G. & ABELL, A. 2012a. Selective inhibition of biotin protein ligase from *Staphylococcus aureus* *J Biol Chem*, 287, 17823-17832.
- SOARES DA COSTA, T. P., TIEU, W., YAP, M. Y., ZVAREC, O., BELL, J. M., TURNIDGE, J. D., WALLACE, J. C., BOOKER, G. W., WILCE, M. C., ABELL, A. D. & POLYAK, S. W. 2012b. Biotin analogues with antibacterial activity are potent inhibitors of biotin protein ligase. *ACS Med. Chem. Lett*, 3, 509-514.
- SOLBIATI, J. & CRONAN, J. E. 2010. The Switch Regulating Transcription of the *Escherichia coli* Biotin Operon Does Not Require Extensive Protein-Protein interactions. *Chemistry and Biology*, 17, 11-17.
- STANLEY, J. S., GRIFFIN, J. B. & ZEMPLIEN, J. 2001. Biotinylation of histones in human cells. Effects of cell proliferation. *Eur J Biochem*, 268, 5424-5429.
- STREAKER, E. D. & BECKETT, D. 1998. Coupling of site-specific DNA binding to protein dimerization in assembly of the biotin repressor biotin operator complex. *Biochemistry*, 37, 3210-3219.
- STREAKER, E. D. & BECKETT, D. 1999. Ligand-linked structural changes in the *Escherichia coli* biotin repressor. The significance of surface loops for binding and allostery. *J. Mol. Biol*, 292, 619-632.
- STREAKER, E. D. & BECKETT, D. 2003. Coupling of protein assembly and DNA binding: biotin repressor dimerization precedes biotin operator binding. *J Mol Biol*, 325, 937-948.
- STREAKER, E. D. & BECKETT, D. 2006. The biotin regulatory system: kinetic control of a transcriptional switch. *Biochemistry*, 45, 6417-6425.
- STREAKER, E. D., GUPTA, A. & BECKETT, D. 2002. The biotin repressor: thermodynamic coupling of corepressor binding, protein assembly, and sequence-specific DNA binding. *Biochemistry*, 41, 14263-14271.
- SUEDA, S., LI, Y., KONDO, H. & KAWARABAYASI, Y. 2006. Substrate specificity of archaeon *Sulfolobus tokodaii* biotin protein ligase. *Biochem Biophys Res Commun*, 344, 155-159.
- SUORMALA, T., FOWLER, B., DURAN, M., BURTSCHER, A., FUCHSHUBER, A., TRATZMULLER, R., LENZE, M. J., RAAB, K., BAUR, B., WICK, H. & BAUMGARTNER, R. 1997. Five patients with a biotin-responsive defect in holocarboxylase formation: evaluation of responsiveness to biotin therapy in vivo and comparative biochemical studies in vitro. *Pediatr Res*, 41, 666-73.
- SUZUKI, Y., YANG, X., AOKI, Y., KURE, S. & MATSUBARA, Y. 2005. Mutations in the holocarboxylase synthetase gene HLCS. *Hum Mutat*, 26, 285-90.
- SVERGUN, D. I., BARBERATO, C. & KOCH, M. H. J. 1995. CRY SOL - a Program to Evaluate X-ray Solution Scattering of Biological Macromolecules from Atomic Coordinates. *J Appl Cryst.*, 28, 768-773.
- SWEETMAN, L., SURH, L., BAKER, H., PETERSON, R. M. & NYHAN, W. L. 1981. Clinical and metabolic abnormalities in a boy with dietary deficiency of biotin. *Pediatrics*, 68, 553-558.
- THAMPY, K. G. 1989. Formation of malonyl coenzyme A in rat heart. Identification and purification of an isozyme of A carboxylase from rat heart. *J Biol Chem*, 264, 17631-17634.
- TISSOT, G., PEPIN, R., JOB, D., DOUCE, R. & ALBAN, C. 1998. Purification and properties of the chloroplastic form of biotin holocarboxylase synthetase from *Arabidopsis thaliana* overexpressed in *Escherichia coli*. *Eur J Biochem*, 258, 586-596.

- TOUMA, E., SUORMALA, T., BAUMGARTNER, E. R., GERBAKA, B., OGIER DE BAULNY, H. & LOISELET, J. 1999. Holocarboxylase synthetase deficiency: report of a case with onset in late infancy. *J Inherit Metab Dis*, 22, 115-122.
- TRON, C. M., MCNAE, I. W., NUTLEY, M., CLARKE, D. J., COOPER, A., WALKINSHAW, M. D., BAXTER, R. L. & CAMPOPIANO, D. J. 2009. Structural and functional studies of the biotin protein liase from *Aquifex aeolicus* reveals a critical role for a conserved residue in target specificity. *J Mol Biol.*, 387, 129-146.
- TURNIDGE, J. D., KOTSANAS, D., MUNCKHOF, W., ROBERTS, S., BENNETT, C. M., NIMMO, G. R., COOMBS, G. W., MURRAY, R. J., HOWDEN, B., JOHNSON, P. D. & DOWLING, K. 2009. *Staphylococcus aureus* bacteraemia: a major cause of mortality in Australia and New Zealand. *Med J Aust*, 191, 368-73.
- VOLKOV, V. V. & SVERGUN, D. I. 2003. Uniqueness of ab-initio shape determination in small-angle scattering. *J Appl Cryst*, 36, 860-864.
- WEAVER, L. H., KWON, K., BECKETT, D. & MATTHEWS, B. W. 2001a. Competing protein:protein interactions are proposed to control the biological switch of the *E coli* biotin repressor. *Protein Sci*, 10, 2618-2622.
- WEAVER, L. H., KWON, K., BECKETT, D. & MATTHEWS, B. W. 2001b. Corepressor-induced organization and assembly of the biotin repressor: a model for allosteric activation of a transcriptional regulator. *Proc Natl Acad Sci U S A*, 98, 6045-6050.
- WHITTEN, A. & TREWHELLA, J. (eds.) 2009. *Small-angle scattering and neutron contrast variation for studying bio-molecular complexes.*: Humana Press.
- WILDIERS, E. 1901. Nouvelle substance indispensable au developpement de la levure. *La Cellule*, 18, 313-316.
- WILSON, C. J., MYER, M., DARLOW, B. A., STANLEY, T., THOMSON, G., BAUMGARTNER, E. R., KIRBY, D. M. & THORBURN, D. R. 2005. Severe holocarboxylase synthetase deficiency with incomplete biotin responsiveness resulting in antenatal insult in samoan neonates. *J Pediatr*, 147, 115-118.
- WILSON, D. J., SHI, C., DUCKWORTH, B. P., MURETTA, J. M., MANJUNATHA, U., SHAM, Y. Y., THOMAS, D. D. & ALDRICH, C. C. 2011. A continuous fluorescence displacement assay for BioA: an enzyme involved in biotin biosynthesis. *Anal Biochem*, 416, 27-38.
- WILSON, K. P., SHEWCHUK, L. M., BRENNAN, R. G., OTSUKA, A. J. & MATTHEWS, B. W. 1992. *Escherichia coli* biotin holoenzyme synthetase/bio repressor crystal structure delineates the biotin- and DNA-binding domains. *Proc Natl Acad Sci USA*, 89, 9257-9261.
- WOLF, B. 1995. Disorders of biotin metabolism. In: SCRIVER, C. R., BEAVDER, A. L. & SLY, W. S. (eds.) *The metabolic and molecular basis of inherited diseases*. New york: McGraw-Hill.
- WOLF, B. & FELDMAN, G. L. 1982. The biotin-dependent carboxylase deficiencies. *Am J Hum Genet*, 34, 699-716.
- WOLF, B., GRIER, R. E., PARKER, W. D., JR., GOODMAN, S. I. & ALLEN, R. J. 1983. Deficient biotinidase activity in late-onset multiple carboxylase deficiency. *N Engl J Med*, 308, 161.
- WOOD, H. G. & BARDEN, R. E. 1977. Biotin enzymes. *Annu Rev Biochem*, 46, 385-413.

- WOOD, Z. A., WEAVER, L. H., BROWN, P. H., BECKETT, D. & MATTHEWS, B. W. 2006. Co-repressor induced order and biotin repressor dimerization: a case for divergent followed by convergent evolution. *J Mol Biol*, 357, 509-523.
- XU, Y. & BECKETT, D. 1994. Kinetics of biotinyl-5'-adenylate synthesis catalyzed by the *Escherichia coli* repressor of biotin biosynthesis and the stability of the enzyme-product complex. *Biochemistry*, 33, 7354-7360.
- XU, Y. & BECKETT, D. 1996. Evidence for interdomain interaction in the *Escherichia coli* repressor of biotin biosynthesis from studies of an N-terminal domain deletion mutant. *Biochemistry*, 35, 1783-1792.
- XU, Y. & BECKETT, D. 1997. Biotinyl-5'-adenylate synthesis catalysed by *Escherichia coli* repressor of biotin synthesis. *Methods Enzymol*, 279, 405-421.
- YANG, X., AOKI, Y., LI, X., SAKAMOTO, O., HIRATSUKA, M., KURE, S., TAHERI, S., CHRISTENSEN, E., INUI, K., KUBOTA, M., OHIRA, M., OHKI, M., KUDOH, J., KAWASAKI, K., SHIBUYA, K., SHINTANI, A., ASAKAWA, S., MINOSHIMA, S., SHIMIZU, N., NARISAWA, K., MATSUBARA, Y. & SUZUKI, Y. 2001. Structure of human holocarboxylase synthetase gene and mutation spectrum of holocarboxylase synthetase deficiency. *Hum Genet*, 109, 526-34.
- YAO, X., SODEN, C., SUMMERS, M. & BECKETT, D. 1999. Comparison of the backbone dynamics of the apo- and holo- carboxy terminal domain of the biotin carboxyl carrier subunit of *Escherichia coli* acetyl-CoA carboxylase. *Protein Sci*, 8, 307-317.
- YOKOI, K., ITO, T., MAEDA, Y., NAKAJIMA, Y., KURONO, Y., SUGIYAMA, N. & TOGARI, H. 2009. A case of holocarboxylase synthetase deficiency with insufficient response to prenatal biotin therapy. *Brain Dev*, 31, 775-778.
- ZHAO, H. & BECKETT, D. 2008. Kinetic partitioning between alternative protein-protein interactions controls a transcriptional switch. *J Mol Biol*, 380, 223-236.
- ZHAO, H., NAGANATHAN, S. & BECKETT, D. 2009. Thermodynamic and structural investigation of bispecificity in protein-protein interactions. *J Mol Biol*, 389, 336-348.

Appendix I - Abbreviations:

AaBPL	<i>Aquifex aeolicus</i> biotin protein ligase
AcBPL	<i>Acinetobacter calcoaceticus</i> biotin protein ligase
ABL	Adenosine binding loop
ACC	Acetyl CoA carboxylase
AMP	Adenosine monophosphate
APS	Ammonium persulphate
ATP	Adenosine 5'-triphosphate
BBL	Biotin binding loop
BCCP	Biotin carboxyl carrier protein
<i>bioO</i>	Biotin biosynthetic operon operator
BirA	<i>E. coli</i> biotin inducible repressor
BPL	Biotin protein ligase
BSA	Bovine serum albumin
BtOH	Biotinol-5'-AMP
Btyl	Biotinyl-5'-AMP
CDC	Centre of disease control
CSPD	Disodium 3-(4-methoxyspiro {1,2-dioxetane-3,2'-(5'-chloro)tricyclo [3.3.1.1 ^{3,7}]decan}-4-yl)phenyl phosphate
DIG	Digoxigenin
D _{max}	Maximal dimension
DNA	Deoxyribonucleic acid
EDTA	Ethylendiaminetetraacetic acid
EMSA	Electrophoretic mobility shift assay
GSH	Glutathione
GST	Glutathione-s-transferase
HCS	Holocarboxylase synthetase (human BPL)
HEPES	4-(2-hydroxyethyl)-1-piperazineethanesulfonic acid
HRP	Horseradish peroxidase
IC ₅₀	Half maximal inhibitory concentration
IPTG	Isopropyl β -D-thiogalactopyranoside
K _i	Inhibitory constant
K _m	Binding affinity
KpBPL	<i>Klebsiella pneumoniae</i> biotin protein ligase
MCD	Multiple carboxylase deficiency
MES	2-(N-morpholino)ethanesulfonic acid
MPD	2-Methyl-2, 4-pentanediol
MRSA	Multiple drug resistant <i>S. aureus</i>
MtBPL	<i>Mycobacterium tuberculosis</i> biotin protein ligase
NMR	Nuclear magnetic resonance
NSD	Normalized spatial discrepancy
P(r)	Pair-distance distribution function
PAGE	Polyacrylamide gel electrophoresis
PC	Pyruvate carboxylase
PCR	Polymerase chain reaction
PDB	Protein data bank
PhBPL	<i>Pyrococcus horikoshii</i> biotin protein ligase
pI	Isoelectric point
R _g	Radius of gyration
SaBPL	<i>Staphylococcus aureus</i> biotin protein ligase
SAXS	Small angle X-ray scattering

SDS	Sodium dodecyl sulphate
SPR	Surface plasmon resonance
TEMED	N,N,N',N'-tetramethylethylenediamine
TRIS	Tris(hydroxymethyl)aminomethane
v/v	Volume per volume
V_{\max}	Maximal velocity
w/v	Weight per volume
ϵ	Extinction coefficient
λ	Wavelength

Appendix II - List of buffers and media

2YT	1.6 % (w/w) Tryptone 1 % (w/w) Yeast extract 0.5 % (w/w) NaCl
2YT agar	1.6 % (w/w) Tryptone 1 % (w/w) Yeast extract 0.5 % (w/w) NaCl 1.5 % (w/v) agar
4 x Ni-NTA Buffer	500 mM Tris-HCl, pH 7.5 2 M NaCl
Lysis buffer	1 x Ni-NTA Buffer 10 mM imidazole 1 mM DTT 1 mM EDTA
Size exclusion buffer (SE buffer)	50 mM Tris-HCl, pH 7.5 50 mM NaCl 10 % (v/v) glycerol 1 mM DTT
Cation Exchange buffer (A)	50 mM NaPO ₄ , pH 8.0 10 % (v/v) glycerol 1 mM DTT
Cation Exchange buffer (B)	50 mM NaPO ₄ , pH 8.0 1 M NaCl 10 % (v/v) glycerol 1 mM DTT
Anion Exchange buffer (A)	50 mM Tris-HCl, pH 7.5 50 mM NaCl 10 % (v/v) glycerol 1 mM DTT
Anion Exchange buffer (B)	50 mM Tris-HCl, pH 7.5 1 M NaCl 10 % (v/v) glycerol 1 mM DTT
1 x PBS pH 7.4	137 mM NaCl 2.7 mM KCl 10 mM Na ₂ HPO ₄ 2 mM KH ₂ PO ₄

GST elution buffer	1 x PBS, pH 7.4 10 mM reduced glutathione
MonoQ buffer (A)	10 mM Hepes, pH 7.5 10 % (v/v) glycerol
MonoQ buffer (A)	10 mM Hepes, pH 7.5 1 M NaCl 10 % (v/v) glycerol
TBE	90 mM Tris-borate 2 mM EDTA
SDS-PAGE loading buffer	62.5 mM Tris-HCl, pH6.8 10 % (v/v) glycerol 5%(v/v) 2-mercaptoethanol 2 % (w/v) SDS 0.1 % (w/v) bromophenol blue
SDS-PAGE running buffer	125 mM Tris base 0.96 M glycine 0.1 % (w/v) SDS
SDS-PAGE coomassie blue staining solution	10 % (v/v) acetic acid 0.006 % (w/v) coomassie blue
SDS-PAGE destain solution	10 % (v/v) acetic acid 25 % (v/v) ethanol
TOWBIN transfer buffer	25 mM Tris 192 mM glycine 20 % (v/v) methanol

SDS-PAGE acrylamide gel

Stacking gel	10 % Separating gel	15 % Separating gel
4 % (w/v) acrylamide 125 mM Tris-HCl, pH 6.8 0.1 % (w/v) SDS 0.1 % (w/v) APS 0.1 % (w/v) TEMED	10 % (w/v) acrylamide 375 mM Tris-HCl, pH 8.8 0.1 % (w/v) SDS 0.1 % (w/v) APS 0.1 % (w/v) TEMED	15 % (w/v) acrylamide 375 mM Tris-HCl, pH 8.8 0.1 % (w/v) SDS 0.1 % (w/v) APS 0.1 % (w/v) TEMED

EMSA TBE gels

Stacking gel	8 % Separating gel
--------------	--------------------

4 % (w/v) acrylamide 1 x TBE	8 % (w/v) acrylamide 1 x TBE
---------------------------------	---------------------------------

Appendix III - Publications

Journal articles:

Structural characterisation of *Staphylococcus aureus* biotin protein ligase and interaction partners: an antibiotic target (2013)

Pendini, N., **Yap, M.Y.**, Polyak, S., Cowieson, N.P., Abell, A., Booker, G. W., Wallace, J.C., Wilce, J.A., Wilce, M.C.J.
Prot Sci.

Selective inhibition of biotin protein ligase from *Staphylococcus aureus* (2012)

Soares da Costa, T.P., Tieu, W., **Yap, M.Y.**, Pendini, N.R., Polyak, S.W., Sejer Pedersen, D., Morona, R. Turnidge, J.D., Wallace, J.C. Wilce, M.C.J., Booker, G.W. & Abell, A.D.
J Biol Chem. 2012 May 18;287(21):17823-32

Biotin analogues with antibacterial activity are potent inhibitors of biotin protein ligase (2012)

Soares da Costa, T.P. Tieu, W., **Yap, M.Y.**, Zvarec, O., Bell, J., Turnidge, J.D., Wallace, J.C., Booker, G.W., Wilce, M.C.J., Abell, A.D., Polyak, S.W.
ACS Med. Chem. Letts

Preparation and crystallization of the Grb7 SH2 domain in complex with the G7-18NATE nonphosphorylated cyclic inhibitor peptide (2010)

Yap M.Y., Wilce, M.C., Clayton, D.J., Perlmutter, P., Aguilar, M.I., Wilce, J.A.
Acta Crystallogr Sect F Struct Biol Cryst Commun. 2010 Dec 1; 66 (Pt12)

Conference proceedings:

Posters:

The characterization of *Klebsiella pneumoniae* and *Acinetobacter calcoaceticus* biotin protein ligase

Yap, M.Y., Polyak, S., Wilce, M.
2012 Monash University Biochemistry Postgraduate Research Conference

***Staphylococcus aureus* biotin protein ligase as a novel drug target**

Yap, M.Y., Soares da Costa, T.P., Tieu, W., Pendini, N.R., Polyak, S.W., Booker, G. W., Wallace, J.C., Abell, A, Wilce, J.A., Wilce, M.C.J.
26th Annual Symposium of The Protein Society (2012)

***Staphylococcus aureus* biotin protein ligase as a novel drug target**

Yap, M.Y., Soares da Costa, T.P., Tieu, W., Pendini, N.R., Polyak, S.W., Booker, G. W., Wallace, J.C., Abell, A, Wilce, J.A., Wilce, M.C.J.
37th Lorne Conference on Protein Structure and function (2012)

Structural analysis of *Staphylococcus aureus* biotin protein ligase using small angle X-ray scattering (SAXS) and crystallography

M. Y. Yap, N. R. Pendini, S. W. Polyak, G. W. Booker, J. C. Wallace, A. Abel, J. A. Wilce, M. C.J. Wilce
9th MPG Student Symposium (2010)

Structural analysis of Staphylococcus aureus biotin protein ligase using small angle X-ray scattering (SAXS) and crystallography

M. Y. Yap, N. R. Pendini, S. W. Polyak, G. W. Booker, J. C. Wallace, A. Abel, J. A. Wilce, M. C.J. Wilce

2010 Monash University Biochemistry Postgraduate Research Conference

Structural analysis of Staphylococcus aureus biotin protein ligase using small angle X-ray scattering (SAXS) and crystallography

M. Y. Yap, N. R. Pendini, S. W. Polyak, G. W. Booker, J. C. Wallace, A. Abel, J. A. Wilce, M. C.J. Wilce

10th International on Biology and Synchrotron Radiation Instrumentation (2010)

Staphylococcus aureus biotin protein ligase: A novel drug target

M. Y. Yap, N. R. Pendini, S. W. Polyak, N. Cowieson, G. W. Booker, J. C. Wallace, A. Abel, D. A.K. Traore, J. A.

Wilce, M. C.J. Wilce

35th Lorne Conference on Protein Structure and Function (2010)

Speaker:

Determination of bacterial biotin protein ligase (BPL) dimerisation using small angle X-ray scattering.

Yap, M.Y., Wilce, M

2011 Monash University Biochemistry Postgraduate Research Conference